Universität der Bundeswehr München
Fakultät für Elektrotechnik und Informationstechnik
Institute für Hoch – und Höchfrequenztechnik

Active Antennas with High Input Impedance Low Noise and Highly Linear Amplifiers

Ashraf Ramadan

Vollständiger Abdruck der von der Fakultät für Elektrotechnik und Informationstechnik der Universität der Bundeswehr München zur Erlangung des akademischen Grades eines

Doktor-Ingenieurs
(Dr.-Ing.)

genehmigten Dissertation

Universität der Bundeswehr München
Fakultät für Elektrotechnik und Informationstechnik
Institute für Hoch – und Höchfrequenztechnik
- Germany -

Active Antennas with High Input Impedance Low Noise and Highly Linear Amplifiers

By

Ashraf Ramadan

Vollständiger Abdruck der von der Fakultät für Elektrotechnik und Informationstechnik der Universität der Bundeswehr München zur Erlangung des akademischen Grades eines

Doktor-Ingenieurs
(Dr.-Ing.)

genehmigten Dissertation

Vorsitzender:	Prof. Dr.-Ing. U. Barabas
1. Berichterstatter:	Prof. Dr.-Ing. H. Lindenmeier
2. Berichterstatter:	Prof. Dr.-Ing. K. Fastenmeier

Die Dissertation wurde am 16. November 2004 bei der
Universität der Bundeswehr München
D-85577 Neubiberg, Werner-Heisenberg-Weh 39
Eingereicht und durch die Fakultät für Elektrotechnik
Am 13. January 2005 angenommen.

Tag der Promotion: 13. July 2005

To my dear beautiful mother and my dear decent father: Thank you for your continuous encouragement and deepest support. You are always my inspiration to do better.

To my late decent brother Dr.-Eng. Tamer: You left our life we live in, but you had never left my memory. I believe that the years of your encouragement, advices and learning from you were invaluable, I am forever grateful.

To my sister and my brothers: Thank you my dear sister, my dear brothers for supporting and understanding.

Acknowledgments

"How strange is a lot of us mortals! Each of us is here for a brief sojourn; for what purpose he knows not, though he sometimes thinks he senses it. But without deeper reflection one knows from daily life that one exists for other people-first of all for those upon whose smiles and well-being our own happiness is wholly dependent, and then for the many, unknown to us, to whose destinies we are bound by the ties of sympathy. A hundred times everyday I remind myself that my inner and outer life are based on the labours of other men, living and dead, and that I must exert myself on order to give in the same measure as I have received and am still receiving."

- Einstein, 1931

Wow! Maybe that says it all. I can remember when it took me by surprise to hear a colleague mention taking five years to complete the Ph.D.-five years after the Master's, that is. How little I knew then what deciding to continue beyond the Master's would entail for me. But I recall another colleague attributing his decision to stay for the Ph.D. program to thinking: "*It seemed like a pretty neat place to spend a few years.*" Albeit at a different location, and although "a few years" may have proven to been a euphemism, I still found his statement to hold throughout my time here. Attending a Dr.-Ing. Degree at a university like the University of Der Bundeswehr München in Germany is mostly about the people that it brings together, for this is what makes the experience so rewarding. But rather than implicating anyone, I would instead like to express my gratitude to each of you by mentioning some of your personal contributions which have meant so much to me. Therefore, here go my statements to you,

To Prof.Dr.-Ing. habil. Heinz Lindenmeier: During my past studying years for my Dr.-Ing. Degree under your supervision, and learning from your special scientific talent and experience, I was always indirectly reading in you the above golden lines written by Albert Einstein, so please Sir. Lindenmeier, here in my dissertation I repeated these golden lines, but directly. In all aspects, I would like to introduce my special thanks for your always-kind welcoming way and the wonderful invitations. I believe that thousands of words for thanking you will mean little, so please Sir, in summary I would like to say: You opened the door to a new world for me, I am grateful.

To Apl.Prof.Dr.-Ing. habil. Leopold Reiter: My special thanks for your excellent experimental and theoretical guidance during my work. Thank you too for your patience to read and correct the work manuscript, for the references you introduced and for the valuable technical discussions that we had. Additionally, I would like to thank you for your experimental tips which always led to impressive and excellent results.

To Apl.Prof.Dr.-Ing. habil. Jochen Hopf: Thank you for your efforts when I was a new guest in the university.

To Prof.Dr.-Ing. habil. Karl Fastenmeier: Thank you for the references you introduced and the discussions that we had.

To Prof.Dr.-Ing. habil. Stefan Lindenmeier: Thank you for giving me the chance to complete my Dr.-Ing. Degree at your new chair, and additionally, my special thanks for the software you introduced and the interesting technical discussions that we had.

To Dr.-Ing. Joachim Brose: I would like to introduce my special thanks for your always kind welcoming way and for taking from your time for the technical discussions that we had. Thank you too for the references you introduced and the scientific advices.

To Dr.-Ing. Tscharmi: Thank you for your efforts in settling every thing for the software I need during my research. My special thanks too for your support, help and advices on the personal level during my time in the university.

My special thanks to Frau Anja Reiter for her kind efforts and help in translating the thesis summary to the German language.

My thanks to my special colleague, the leader of the workshop and the gentle man Mr. Oliver Kindt, for his kindness and special personal help in a lot of situations through my time in Germany. I appreciate your help and advices during my time in the university too, in addition, I would like to introduce my thanks for the wonderful family invitations and your nice grilled chicken!

My thanks to my colleague Mr. Bernd Wahnschaffe for the nice jokes during the coffee break and in the university restaurant, specially the nice jokes about October Feast in Munich!

My thanks to my former colleague Dr.-Ing. Thomas Bechtler for the scientific materials and advices.

My thanks to my former colleague Dr.-Ing. Rainer Kronberger for the personal help and the scientific advices.

I am grateful to the rest of my colleagues in the Faculty of Electronics - High Frequency Institute - Universität der Bundeswehr München.

And finally, I am deeply grateful to my kind colleagues Mrs. Koppelt and Mrs. Inge Bajda for their supportive care, and the optimum way for help in every problem, in addition to their deep encouragement during my research.

Contents

Thesis Summary and Contributions

It has been common practice for several decades to fit commercial vehicles and private cars with radios to receive national broadcast programs. The performance of these radios has now become more critical in view of the demand for high fidelity audio, the increasing number of local radio stations and not least, the recent escalation in the electronic complexity of automobile information systems, which include the reception of Television, navigation, and traffic control data. Consequently, the well-known standard whip antenna used for car radios since the early 1950s is inadequate nowadays. The electrical performance of new types of car antennas, such as active window antennas make use of improved antenna structures; they profit from the progress in semiconductor technology and the dramatically reduced price of active elements: and they take advantage of much research done with respect to low noise and high linearity amplifier circuitry. A multitude of car antennas for TV, AM and FM reception with different principles of operation have been developed and implemented by German and Japanese car producers, whereas in Germany, some antennas have been developed at the institute for High-Frequency Techniques, University of the Bundeswehr Munich in cooperation with antenna producers and that are in mass production with several German Car producers. Generally, the typical problems in the design of modern car radio antennas are:(1) matching the antenna to the frequency range of 148KHz to 1606.5KHz (LW, MW) and the 49m – band (SW) for AM, TV for wide-frequency bands covering both VHF and UHF bands [73] ;(2) reduction of multipath fading in FM and TV broadcast reception; and (3) avoiding the reception of noise generated by the engine and electronic circuits installed in the car. In the AM frequency bands, exact impedance matching is impossible, since the antennas commonly used are electrically very small and thus have extremely small radiation resistance and very large reactance. This problem has been solved by placing an amplifier with low gain (about 2dB) close to the antenna terminals. The amplifier has high input impedance and output impedance matched to the receiver in order to reduce transmission losses due to mismatch. The same concept is applied to the design of antennas for AM broadcast reception that are printed on window glass [9], [10]. Ignition noise from the engine enters the antenna by both direct radiation and coupling to the vehicle. Digital electronic circuits in the car may also act as a source of interference. The current in digital circuits contains many harmonic frequency components in both FM and TV broadcast bands.

When either electromagnetic or electrostatic coupling exists between digital circuits and antenna or receiver circuits, digital currents may be induced on the antenna element, thus appearing in the AM, FM or TV receiver circuits and interfering with broadcast reception. Thus, the place to mount an antenna on the body of a car must be selected carefully in order to avoid noise interference. When a monopole element is used, the best place to mount it is often considered to be the rear fender. For an antenna printed on the window glass, the chosen location depends on the need to maintain unobstructed vision and the nature of the ambient noise interference. The windscreen antenna structure design is not the scope of this work but the reader can refer to [9] and [10] for a detailed design principles; however, the thesis places the emphasis on a new FM active antenna amplifier concept based high impedance GaAs FET input stage to be used with nowadays-modern car windscreen antennas as shown in Figure 1. Optimization, simulation, design and realization of the new amplifier for different FM windscreen antenna is the thesis main goal, whereas an evaluation based simulation and experimental measurements was done and compared to the standard industrial requirements.

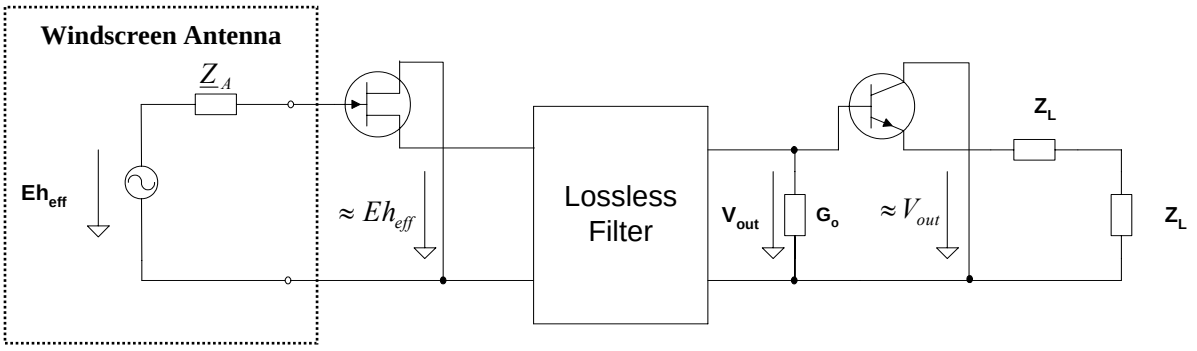

Figure 1: The New FM Active Antenna Amplifier

In the following pages, a summarized overview of the thesis is presented. It should be first remarked that the design evaluation through this work in general is based on the German industrial requirements according to the standards of the German Association of the Automotive Industry **VDA** (**Verband der Automobilindustrie**)[71], whereas for example, in case of an active antenna amplifier nonlinear performance, a minimum intermodulation distortion separation (denoted a_{K3}[dB] as will be explained later) of 65dB at the circuit output voltage of 100[dBμV] should be achieved with a total circuit noise figure lower than or equal to 6.3dB(NF≤ 6.3[dB]). **Chapter 1** is mainly divided to basic three sections. **Section I** reviews the state of the art of active antenna in modern cars whereas a short historical background is given in section 1.1. Section 1.2 introduces generally the vehicles antenna configurations and basic definitions, whereas the fundamental concepts behind the vehicles passive and active antenna structures are presented in sections 1.2.1 and 1.2.2 respectively.

Section 1.2.3 introduces an important concept for simulating the antenna-measured impedance with the amplifier circuitry, whereas a general matrix has been derived to transform the measured one-port antenna impedance data to a measured equivalent two-port data as shown in Figure 2. Such a transformation helps in designing active antenna amplifiers and simulating their linear and non-linear behaviour in presence of the antenna.

It should be remarked that with nowadays simulation and design software's, a lack of simulating or even optimizing an amplifier in presence of an antenna is available, and consequently the presented general matrix in section 1.2.3 can be used with any microwave simulation software when the one- port antenna impedance measurement is available. Section 1.2.4 presents the experimental measurement done in the University of der Bundeswehr Munich for vehicles active antenna amplifiers in free field.

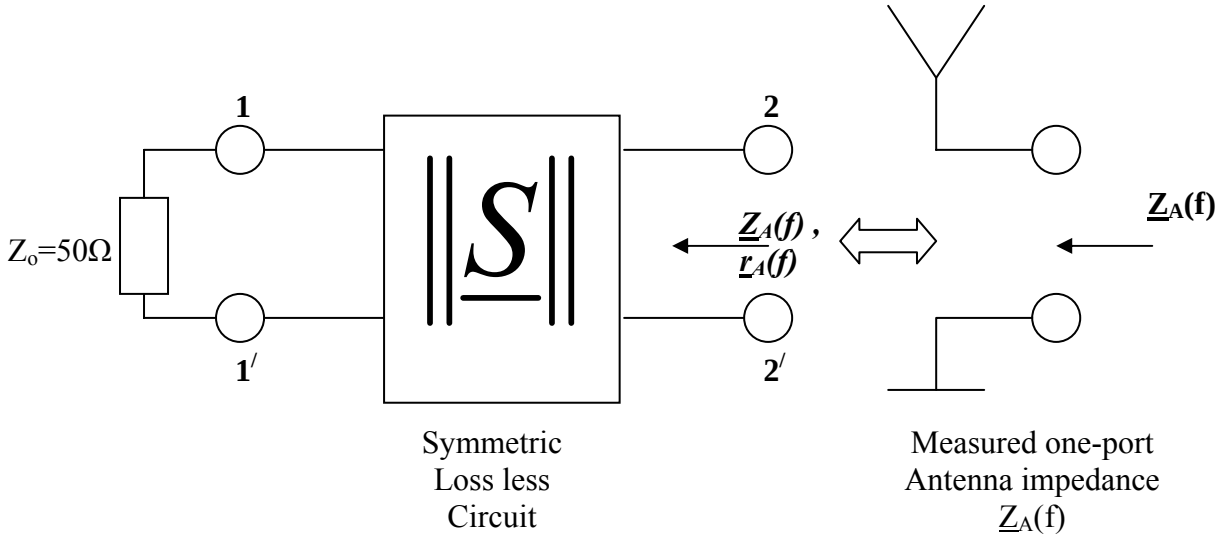

Figure 2: Antenna Measured Impedance Equivalent Two-port

Section II reviews shortly the different antenna transistor amplifiers for FM applications, whereas in section 1.3, the different three-terminal semiconductor devices used for active antennas are reviewed. Section 1.4 reviews the transistor modelling for active antennas, whereas the transistor S-parameters description and measurement setup is reviewed in section 1.4.1. Section 1.4.2 reviews shortly the noise sources in FET transistors and the general noise figure measurement setup. Section 1.4.3 explains the basic concept behind the transistor amplifiers third order intermodulation distortion and the experimental setup that will be used for evaluating the distortion of the realized amplifier through this work.

As shown in Figure 1, the source follower FET represents the first amplifier stage in the new design of this work, and consequently, **Section III** presents the important investigations (simulation and measurements) done for a design decision to trade-off between quality of JFET, HEMT and GaAs FET follower cells for FM active receiving antenna applications. A conclusion has been reached to use the GaAs FET transistor source follower for their superior intermodulation and noise performances compared to JFET and HEMT transistors as shown in Figures 3 and 4 respectively (intermodulation separation a_{K3}[dB] ≈ 80-85 dB at the circuit output voltage of 100dBµV which exceeds the requirements of **VDA** [71]). The noise figure simulation shown in Figure 4 assumes the noise model contribution of the transistor and a coil quality factor Q of 10. This is the typical factor of the actual available coil components. The simulated noise figure of the GaAs FET follower cell reaches ~ 1dB at 100MHz, whereas the measured values in the Laboratory was 1.4dB (not shown in Figure 4, but the noise figure measurements compared to simulation will be discussed in detail in chapter 2-Figure 2.32), which shows a good agreement between the measured and simulated values using practical components parameters. It should be noted, that assigning the actual components parameters and their parasitic is not always possible due to the samples variation. However such a noise figure simulation shows in principal a pictorial visualization of the transistor noise contribution with non ideal (e.g. a coil of quality factor Q = 10, this value is typical for most SMD -Surface Mounted Devices- coils available in the laboratory) circuit components.

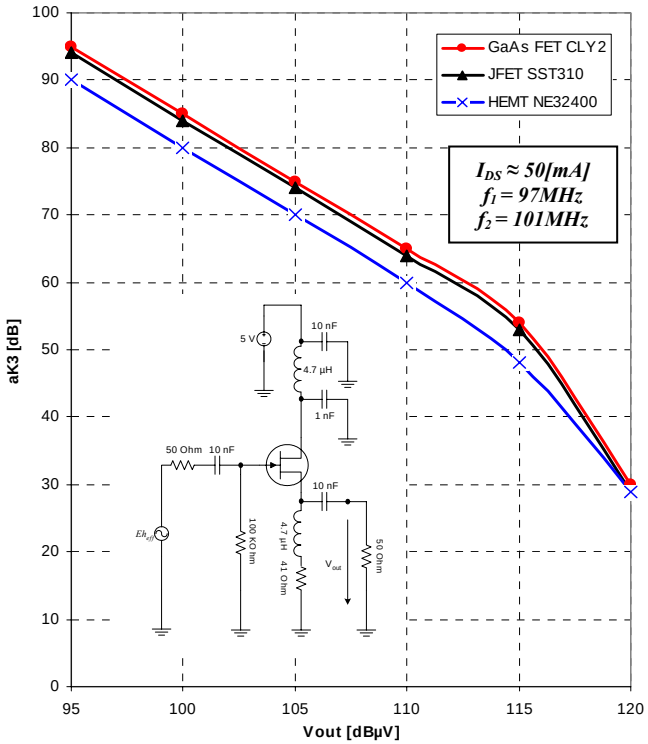

Figure 3: Simulated Third Order Intermodulation Distortion Performance of the JFET, HEMT and GaAs FET Follower Cells in a 50 OhmSystem

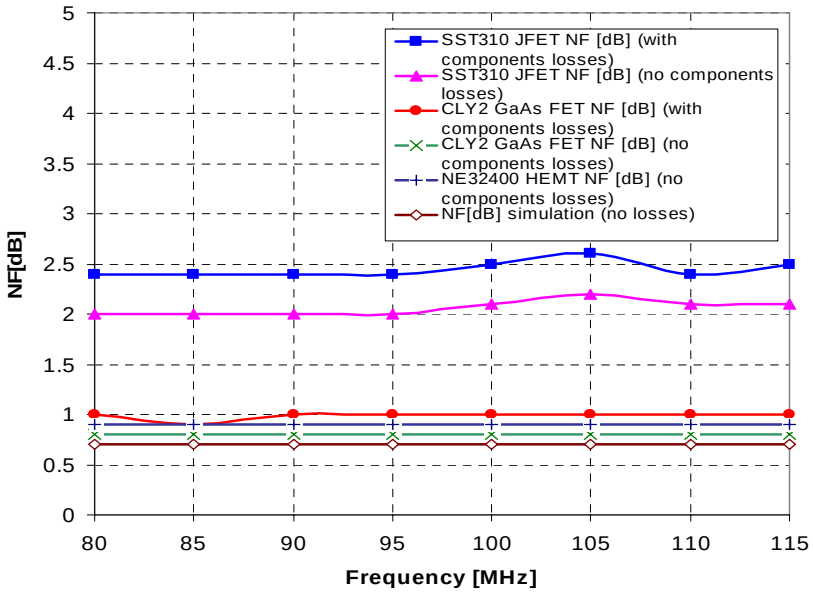

Figure 4: Simulated Noise Figure Performance (assuming ideal bias components once, and lossy components once) of the JFET, HEMT and GaAs FET Follower Cells in a 50 Ohm System

Chapter 2 presents the different design aspects of the new suggested low noise and high linearity FM active antenna amplifier shown in Figure 1. According to the standards of the German Association of the Automative Industry **VDA** (Verband der Automobilindustrie)[71] requirements, the noise evaluation of the new amplifier is presented in section 2.2. Sections 2.2.1 and 2.2.2 explains in detail the noise evaluation of active antennas compared to passive ones. For the new suggested active antenna FM amplifier, the effect of the antenna impedance (real and reactive parts) on the amplifier noise figure performance has been evaluated in section **2.2.3.A** as shown in Figure 5, whereas a conclusion has been arrived that the noise figure is approximately independent on the antenna impedance reactive part. The amplifier output signal to noise ratio has been evaluated in section 2.2.3 B for different antenna temperatures according to the **CCIR** recommendations [51]. Section 2.2.4 continued the evaluation of arbitrary antenna impedance on the FM amplifier third order intermodulation distortion performance as shown in Figure 6, whereas the same conclusion has been arrived that the intermodulation performance is approximately independent on the antenna impedance reactive part.

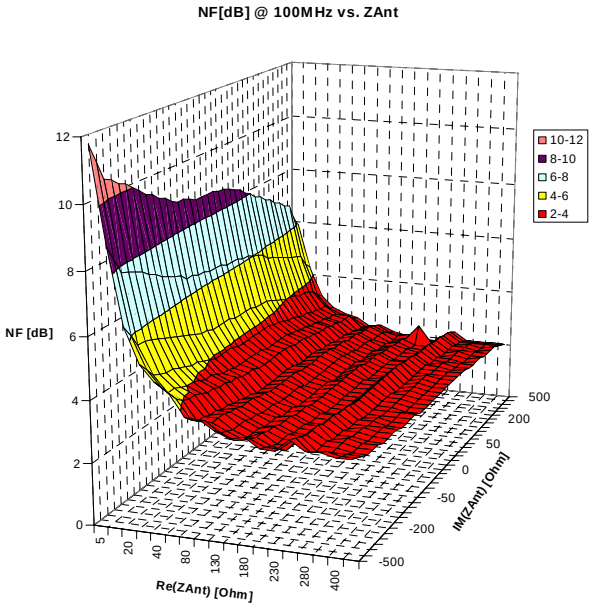

Figure 5: Noise Figure of the New Active Amplifier for Arbitrary Antenna Impedance

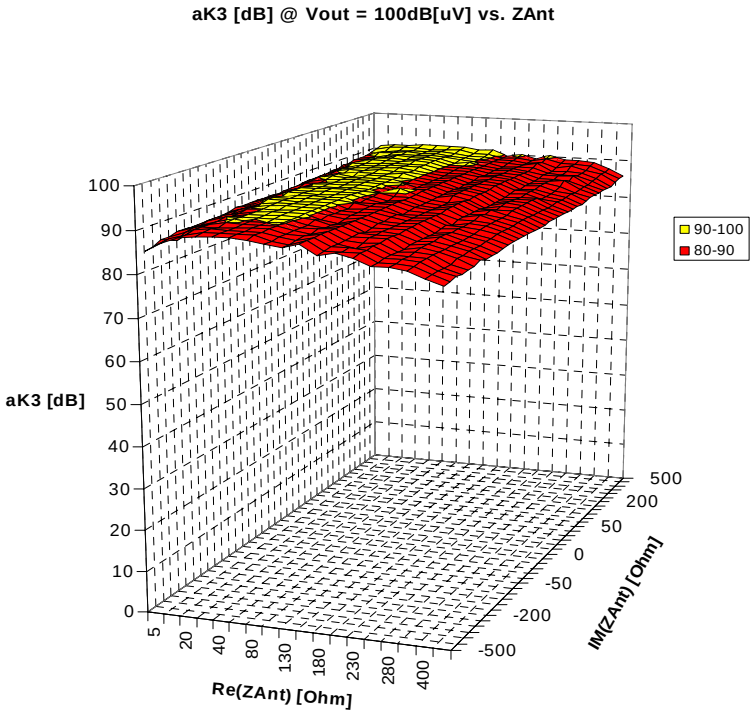

Figure 6: Intermodulation Distortion a_{K3} [dB] of the New Active Amplifier for Arbitrary Antenna Impedance

Section 2.2.5 provides in detail an approach for the design and optimization of the proposed active antenna new amplifier, whereas section 2.2.5.I (A) and (B) explained the optimization of the active antenna amplifier in case of a reference rod antenna and for the car window antenna structure. For the proposed amplifier shown in Figure 1, a design equation (2.45) has been derived, which shows the necessary optimization and design condition relating the antenna real part and the lossless filter input conductance. The importance and use of the derived design equation has been used in the design examples at the end of chapter two. The evaluation of the amplifier frequency response and the standard noise consideration requirements has been described in detail in section 2.2.5.II, whereas this section is ended by a derived evaluation equation (2.54) which showed the relation that should be satisfied between the amplifier power gain and the system noise figure according to the **VDA** industrial requirements. **Section 2.2.5.III** explains in detail the different aspects of the source follower GaAs FET cell stability problem. The section introduced a new concept of negatively biasing the source follower cell and its effect on the noise figure. However, due to the non-availability of negative supply in most cars, the cell stability problem using positive biasing has been solved by an experimental network reached at the institute laboratory as shown in Figure 7.

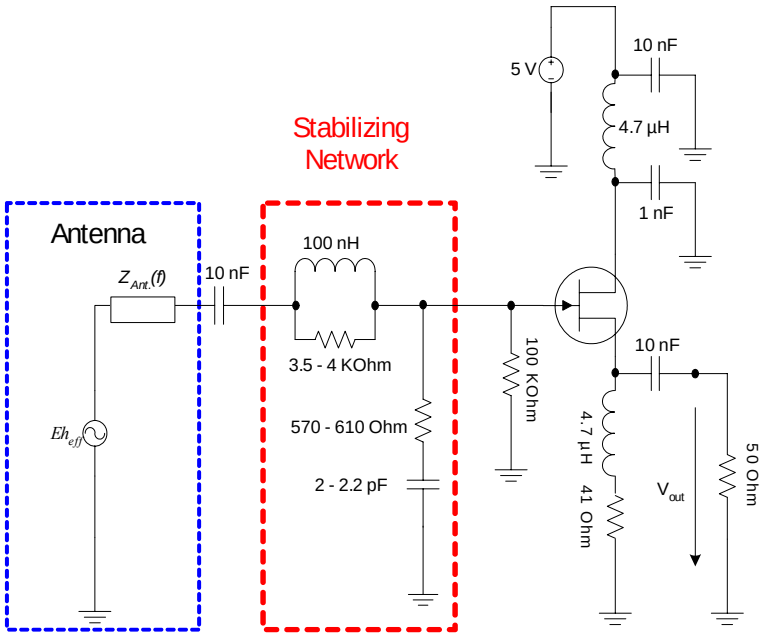

Figure 7: GaAs FET CLY2 Source Follower Cell Stabilizing Network

Section 2.2.6 considered a general design examples based on the possible three basic typical types of vehicles windscreen antenna impedances measured in the FM range as shown in Figure 8.

This section, in addition introduces a different realized amplifiers for each antenna with adopting the different stability techniques suggested in section 2.2.5.III.

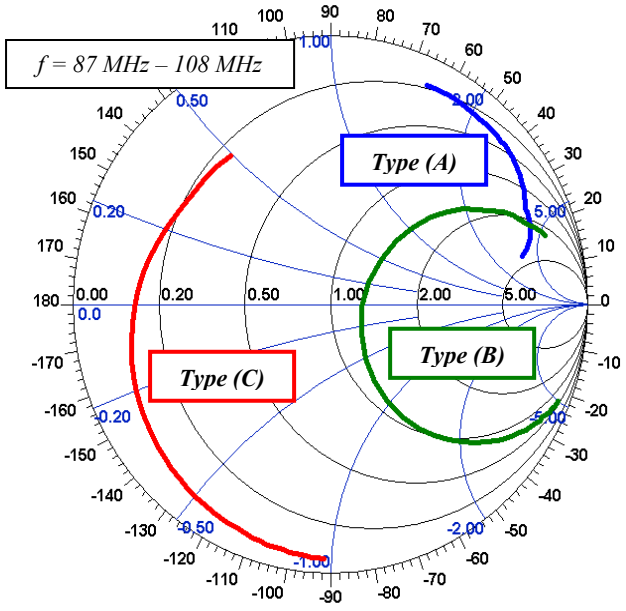

Figure 8: Basic Three Typical Vehicles Antenna Impedances Measured in the FM Range

Section 2.2.6.1 introduces a complete designed and realized amplifier example in case of possible typical high impedance antenna type, whereas in this example, the design equation 2.45 has been used once for optimizing the required lossless filter structure elements. Secondly, the same filter structure is directly optimized using the software optimizer. Finally the amplifier has been realized and stabilized by adopting the stability technique shown in Figure 7 which is explained in detail in section 2.2.5.III. **Section 2.2.6.2** considered the antenna impedance type (B) and a possible amplifier design, which is realized and measured experimentally, whereas another stability technique has been adopted. Finally, an antenna impedance type(C) has been introduced in section 2.2.6.3, whereas a possible amplifier has been realized and measured. Figure 9 and 10, shows a sample simulated and measured results of an amplifier realized in case of antenna impedance type (A) including ideal and non ideal components (this is referred in the thesis Figures as losses, e.g. as in Figure 4 and 9) . The rest of antenna types and their corresponding realized amplifiers are shown and discussed in detail through section 2.2.6.

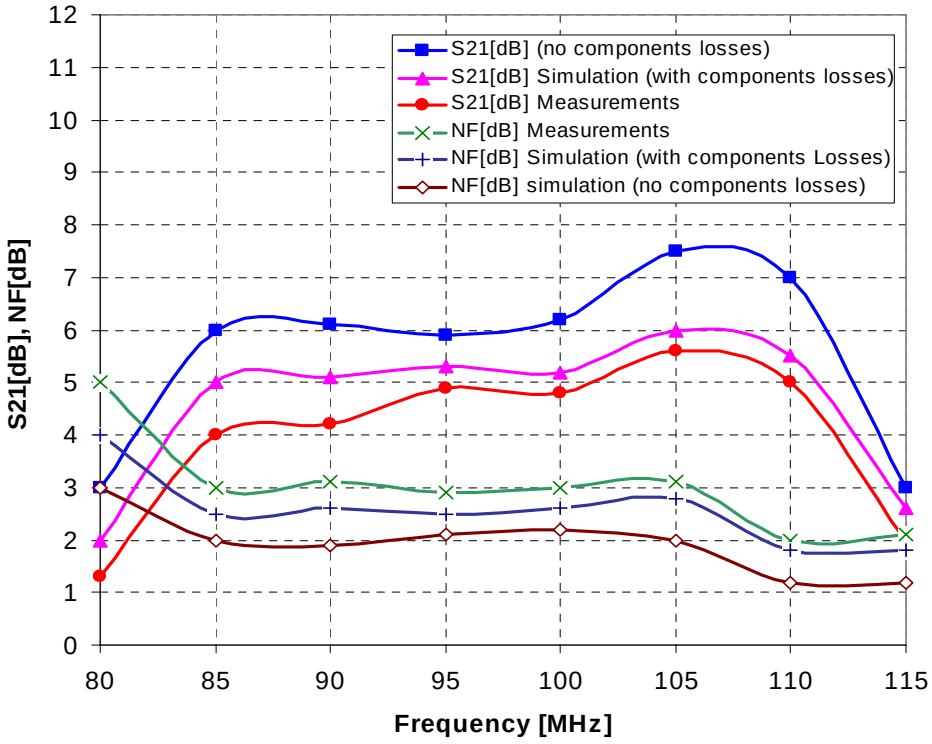

Figure 9: Measurements and Simulation Results of a Realized Active Antenna Amplifier for type (A) antenna Impedance

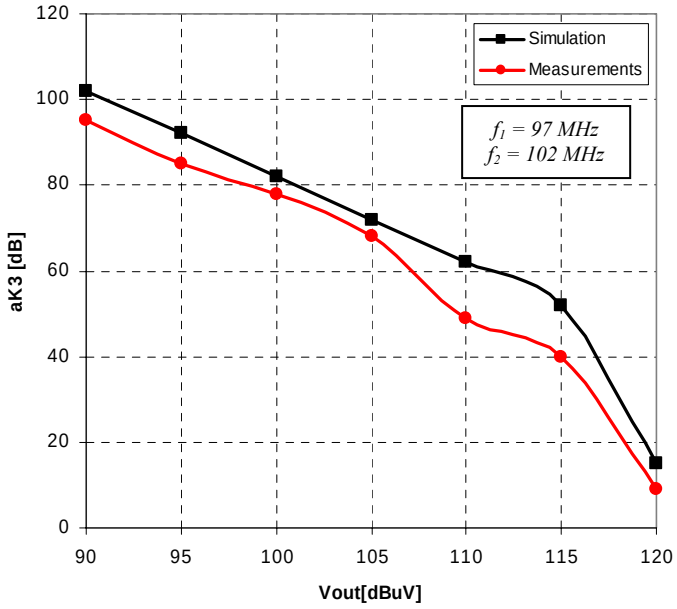

Figure 10: Measurements and Simulation Results of the Amplifier Third Order Intermodulation Distortion Performance (type (A) Antenna Impedance)

Section 2.2.7 addressed an important discussion about the possible amplifier intermodulation distortion variation in case of using different optimized filter structures. A general solution has been introduced to reach the amplifier best intermodulation distortion. The solution introduced is based on using a buffer amplifier bipolar transistor as shown in Figure 11, thus keeping the GaAs FET feedback impedance as high as possible for any optimized filter structure.

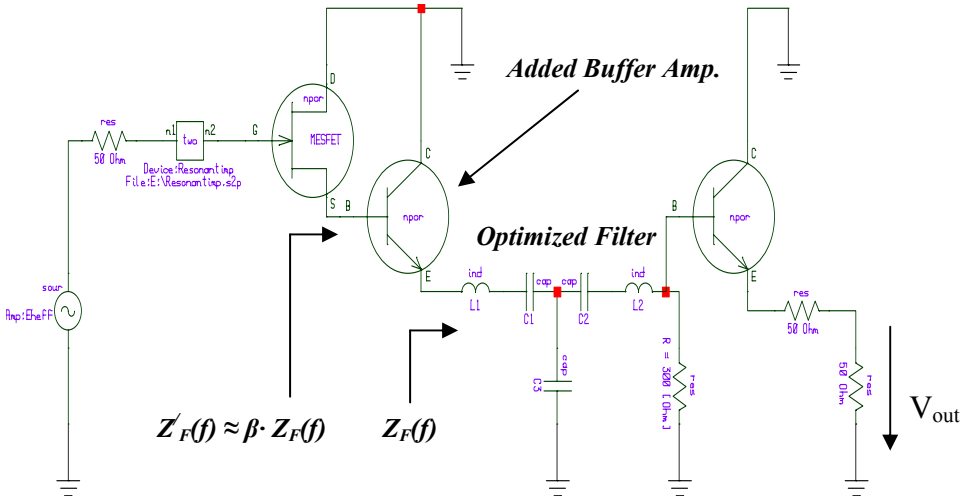

Figure 11: The FM Active Antenna Amplifier with Series Control Circuit Concept

Through section 2.2.7, a detailed study has been introduced for the possible use of JFET and Bipolar transistor amplifiers in place of GaAs FET. A conclusion has been reached that such transistors can be used for some antenna structures. A final conclusion is reached that JFET and Bipolar transistors can replace the GaAs FET in a 50 Ohm system, whereas the same noise figure and intermodulation distortion can be reached. **Section 2.2.8** introduces a design example of an active antenna amplifier (in a 50 Ohm system) based on the new concept highlighted in section 2.2.7.

Chapter 3 describes the realized control circuits for enhancing the non-linear performance of active antenna amplifiers in large signal environment. Through this chapter in sections 3.1 and 3.2, two basic possible control circuits shown in Figure 12 and 13 has been introduced and realized in case of a broadband source impedance amplifier. Section 3.3 described a possible modification of active antenna amplifiers control with AGC (Automatic Gain Control) at the input including High Input Impedance.

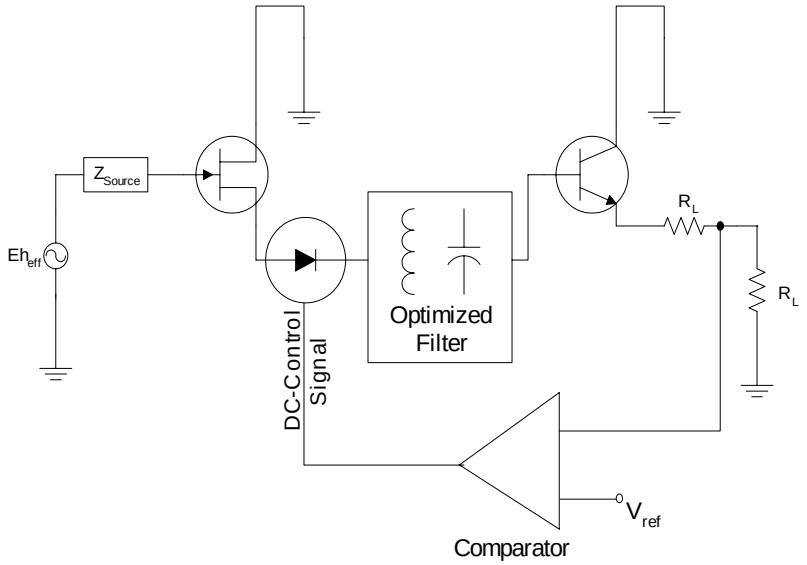

Figure 12: The FM Active Antenna Amplifier with Series Control Circuit Concept

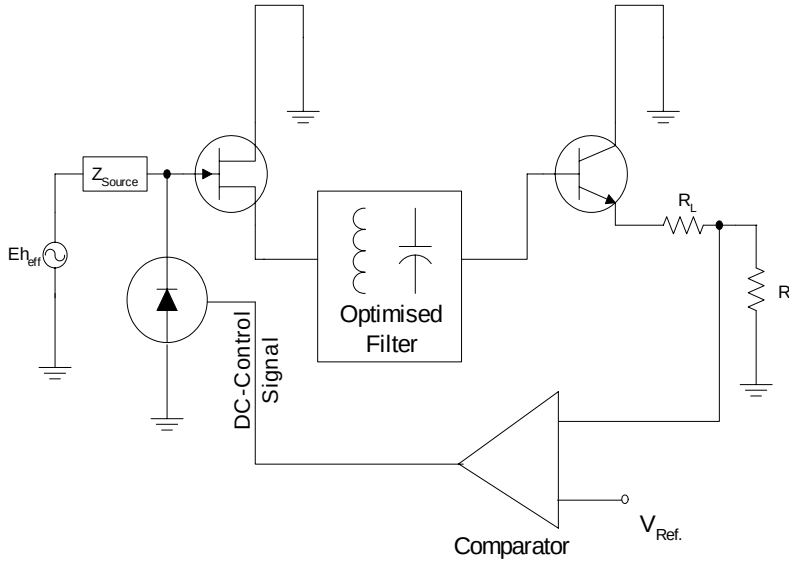

Figure 13: The FM Active Antenna Amplifier with Parallel Control Circuit Concept

Chapter 4 summarizes the concluded statements arrived through the thesis work and compares the performance between the CLY2 GaAs FET from TriQuint and a newly released NE2700 GaAs FET from NEC.

Finally, the reader can refer to appendix A for the acronyms used throughout the thesis. Appendix B contains some important variable definitions. The used Bibliography through this work is listed at the thesis end.

Chapter 1

I. State of The Art of Active Antennas In Modern Cars

INTRODUCTION

Active Antennas combine prominent features that make them usable for both military and commercial applications. The most important feature is that the antenna and the active device are treated as a single entity, and accordingly active antenna in its minimum configuration consists of a passive antenna, typically, a rod or a dipole and an integrated amplifying device allowing compactness, low cost, low profile, minimum power consumption, and multiple functionality. A typical active antenna consists of one or more electronic devices such as diodes (Gunn, IMPATT, Schottky, and varactor) and/or three terminal active devices (MESFET, HEMT, or HBT) integrated with planar antennas such as printed dipoles, microstrip patches, bowties, or slot antennas. To realize different functionalities, active antennas can be made frequency tunable injection locked, or mutually coupled [19]. Choosing the adequate configuration, multiple communication and sensor applications can be realized.

In the past, active antenna met little acceptance, and their development has been retarded by the fear that the problem of nonlinear distortions in a broadband active circuit might not be solvable. In the meantime, good improvements have been achieved with amplifiers with respect to third-order intermodulation distortion, which is the dominating nonlinear effect with FM reception. The performance of active antennas nowadays shows that nonlinearity must no longer be considered a problem in practice. This progress has been obtained by advanced circuitry and by better active elements. The suppression of nonlinear effects today is of even greater importance than some years ago due to the increased number of FM stations. Extreme demands arise in large cities where, typically, a multitude of FM stations is concentrated on radio towers.

This thesis extends the stated previous work and presents a theoretical and experimental new active antenna concept work done in the Institute of High Frequency at the University of der Bundeswehr Munich (Armed Force University-Munich)- Germany, which advances the state of the art in active antennas for microwave and modern automotive applications.

In this chapter, the state of the art in active antennas is presented starting from the history and definitions up to the actual published works. It also gives an overview of this thesis.

1.1 Historical Background

Copeland and Robertson demonstrated a mixer-integrated antenna using a tunnel diode,which they describe as an “antennaverter”. They also used a travelling wave antenna, together with tunnel diodes, to operate as a travelling wave amplifier, which they called an “antennafier” in 1961.

H. Meinke introduced thoughts about actual transistorized receiving antennas [1].

In 1971, H. Lindenmeier firstly addressed and described the integration of FET and antennas for reception [2], [3].

In 1976, H. Lindenmeier introduced the general theory behind the optimum bandwidth of signal-to-noise ratio of receiving systems with small antennas [6].

Automotive applications based active antennas has been studied and extended by H.Lindenmeier [4], [7].

Various car manufacturers have taken active antennas introduced by Lindenmeier, Meinke etal., [2], [3], [4], [5], [6] and [7] into series production since 1982.

1.2 Vehicles Antenna Configurations and Basic Definitions

1.2.1 Vehicles Conventional Passive Antenna Receiving System

A passive antenna structure is an electrical conductor or array of conductors that radiates (transmits and/or receives) electromagnetic waves. Electromagnetic waves are often referred to as radio waves. Most antennas are resonant devices, which operate over a relatively narrow frequency band. This work will focus on the receiving antennas. Figure 1.1 shows the conventional receiving system used for passive antennas [1], [57].

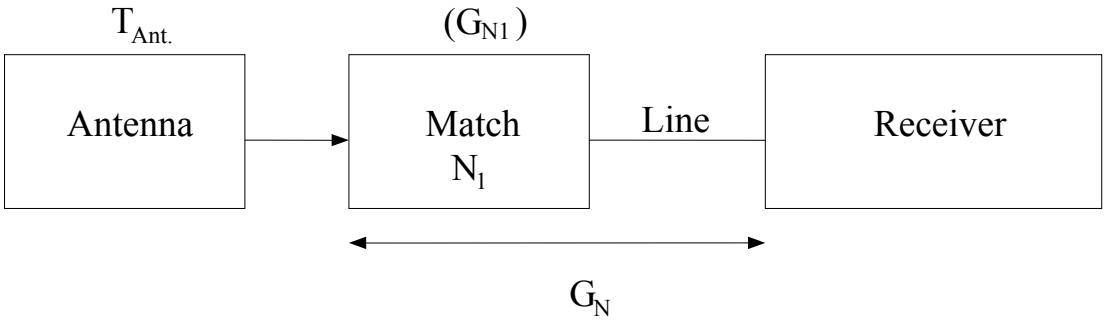

Figure 1.1: Passive Antenna Receiving System

In summary, the noise behaviour of this system can be expressed by its system noise-temperature T_S, which is approximately given by

$$T_S = T_{Ant.} + \frac{T_R}{G_N} \tag{1.1}$$

Where $T_{Ant.}$ is the antenna temperature of external noise, T_R the noise-temperature of the receiver and G_N is the available gain of the matching network N_1 and the line. As particularly at microwave frequencies G_N is generally much smaller than one, the additional noise temperature $T_S - T_{Ant.} = T_R / G_N$ is much higher than the additional noise temperature $T_{R,}$ as specified for the receiver alone. The first step done to improve this situation is by inserting a transistor amplifier at the output terminals of the matching network N_1 as shown in Figure 1.2. If the available gain of the transistor is sufficiently high, the influence of receiver noise on overall system noise-temperature may be omitted and we get:

$$T_S \approx T_{Ant.} + T_T / G_{N1} \tag{1.2}$$

T_T is the additional noise-temperature of the transistor and G_{N1} the available gain of the matching network N_1. Since $G_{N1} > G_N$ and by proper design $T_T < T_R$, T_S in the arrangement of Figure 1.2 is smaller than T_S with the conventional receiving system of Figure 1.1.

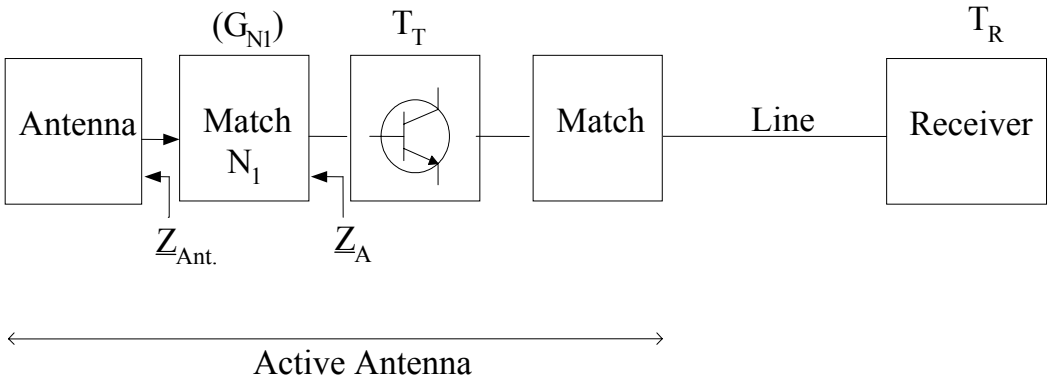

Figure 1.2: Basic Active Antenna Receiving System

It should be noted that T_T depends on the internal impedance $\underline{Z}_A$ that appears at the input terminals of the transistor. Referring to Figure 1.2, there is an optimum impedance $\underline{Z}_{opt}$ for which T_T becomes minimum $T_{Tmin.}$ As $\underline{Z}_{opt}$ does not coincide with the optimum impedance $\underline{Z}^*_A$ (complex conjugate of $\underline{Z}_A$) for power match, common pre-amplifiers do not give minimum system noise temperature. The absolute possible minimum of T_S with a given transistor is achieved by avoiding all additional matching networks and inserting the transistor at a gap in the antenna where the internal impedance is equal to Z_{opt}. By this way, we can get a noise match ($G_{N1} = 1$). The system noise temperature of this active antenna becomes:

$$T_S = T_{Ant.} + T_{T\min} \tag{1.3}$$

A detailed discussion about the effect of using transistorized antennas will be introduced in section 1.4.2. Figure 1.3 shows an example of a typical integrated multi antenna passive structures implanted in a car rear window for AM and FM reception (Only in the upper part of the antenna structure, above the uppermost heater, does a shunt with a comparatively high resistance reduce the heater current in the middle, but only to an insignificant extent). Both structures are printed onto the glass with the same technology as the heaters. Thus, both the heater and the antenna conductors can be in galvanic contact with the horizontal heater conductors. Since the connecting points between the antenna structure and heaters are arranged on equipotential lines, the defrosting of the rear window is not influenced. The AM structure is located in the free strip above the heaters without any galvanic contact with them. Therefore, The problems involved with antennas making use of the heaters for AM reception are avoided, since there is no need for broad band RF insulation by large coils (for up to 30A of heating current).

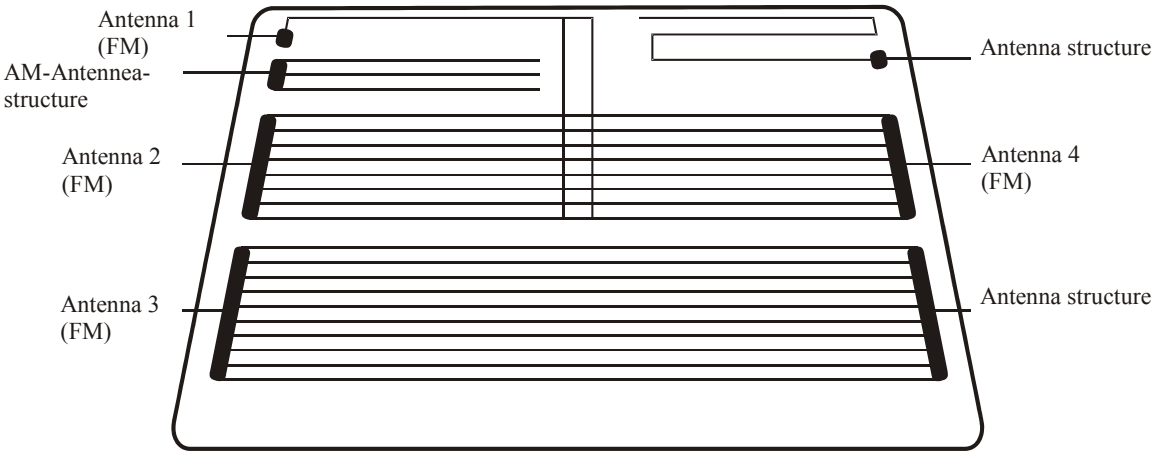

Figure 1.3: Receiving Antenna Structure Example implanted in a Car Rear Windscreen

However, with the expenditure of greater technical effort, an excellent antenna can be realized by using the heaters for AM too. This has been explained in detail in [10]. Generally, these typical antennas are designed at the Institute of High Frequency at the University of the Bundeswehr Munich [9]. Such a combination shown is used for diversity reception, whereas diversity improves signal reception with properly spaced antennas.
One receiving antenna from Figure 1.3, itself can be modelled with its equivalent circuit as shown in Figure 1.4.

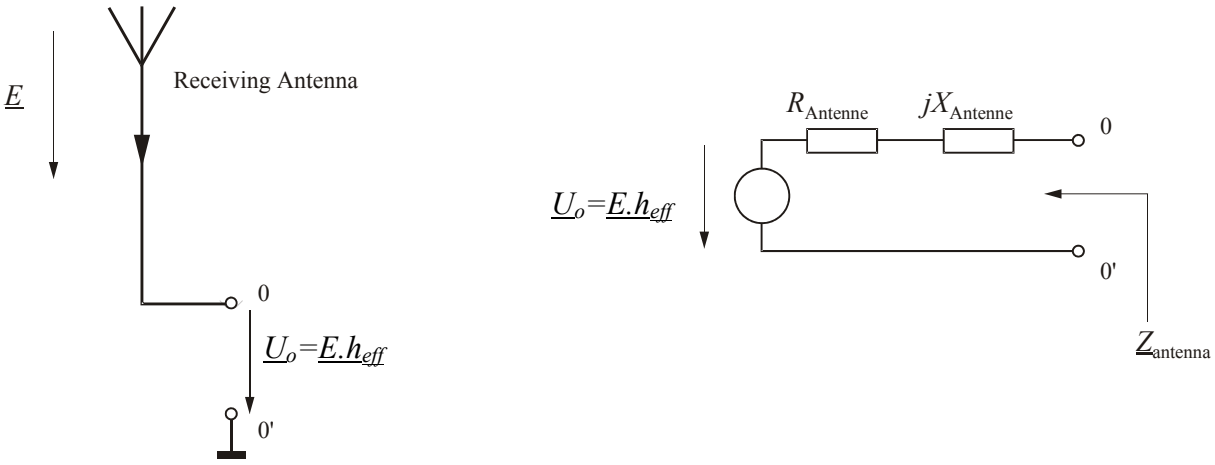

Figure 1.4: Receiving Antenna Model and Circuit Representation

As shown in Figure 1.4, the antenna acts as a source that generates an open circuit voltage U_O. The electric field strength E generates this voltage which is called Electro magnetic force **EMF** that can be determined from $\underline{U_O} = \underline{E}.h_{eff}$, where h_{eff} is the effective height of the receiving antenna [10]. The antenna has a real part which is the equivalent antenna resistance $R_{Antenna}$ and an equivalent inductive / capacitive effects which can be modelled as a reactance as shown in the antenna circuit model. The antenna resistance is the combination of the radiation resistance R_{rad} plus the ohmic and dielectric losses R_{loss} in the conductors and the insulators (and in some cases the loss in a ferromagnetic core) which make up the antenna structure. The antenna impedance $\underline{Z}_{Antenna}$ is frequency dependent and can be simply modelled to be

$$\underline{Z}_{Antenna}(f) = R_{Antenna}(f) + jX_{Antenna}(f) = \left[R_{rad} + R_{loss}\right](f) + jX_{Antenna}(f) \tag{1.4}$$

In the present work, the antenna real part resistance $R_A(f)$(will be written R_A for simplicity) , will directly mean $R_{Antenna}(f)$ which represents the combination of both the radiation and loss resistances respectively. However, since R_{loss} represents the actual resistances or resistive effects, it can be represented as a source of thermal noise power by including a mean-square noise-voltage or noise current generator (as will be explained in chapter 2) into the antenna circuit model. This thermal noise source is often important when the model of the antenna is used to describe a receiving antenna, but this is usually not considered when describing a transmitting antenna [45]. Regarding the antenna reactive part notation, $X_A(f)$ will represents $X_{Anttenna}(f)$ and for simplicity will be written X_A.

An important antenna characteristic to be measured is its radiation pattern, which is often described as antenna directivity [45]. In summary, the antenna directivity describes the radiation pattern and the ability of an antenna to focus energy in a particular direction when transmitting or to receive energy better from a particular direction. Figure 1.5 and 1.6 shows an antenna (connected to a car) pattern examples in the spherical coordinates (r, φ, θ), for a whip antenna once and a windscreen antenna once simulated in the FM range, whereas the measured pattern can be represented by [20]:

$$\underline{C}(\varphi,\theta) = \frac{\underline{V}_{\varphi}(\varphi,\theta)}{\underline{V}_{\varphi\max}(\varphi,\theta)} \tag{1.5}$$

Where, $\underline{V}_{\varphi}(\varphi,\theta)$ is the received signal voltage [Volt], θ is the elevation angle (set to be 90° in case of FM reception) and φ is the azimuth angle ($0^\circ \le \varphi \le 360^\circ$).

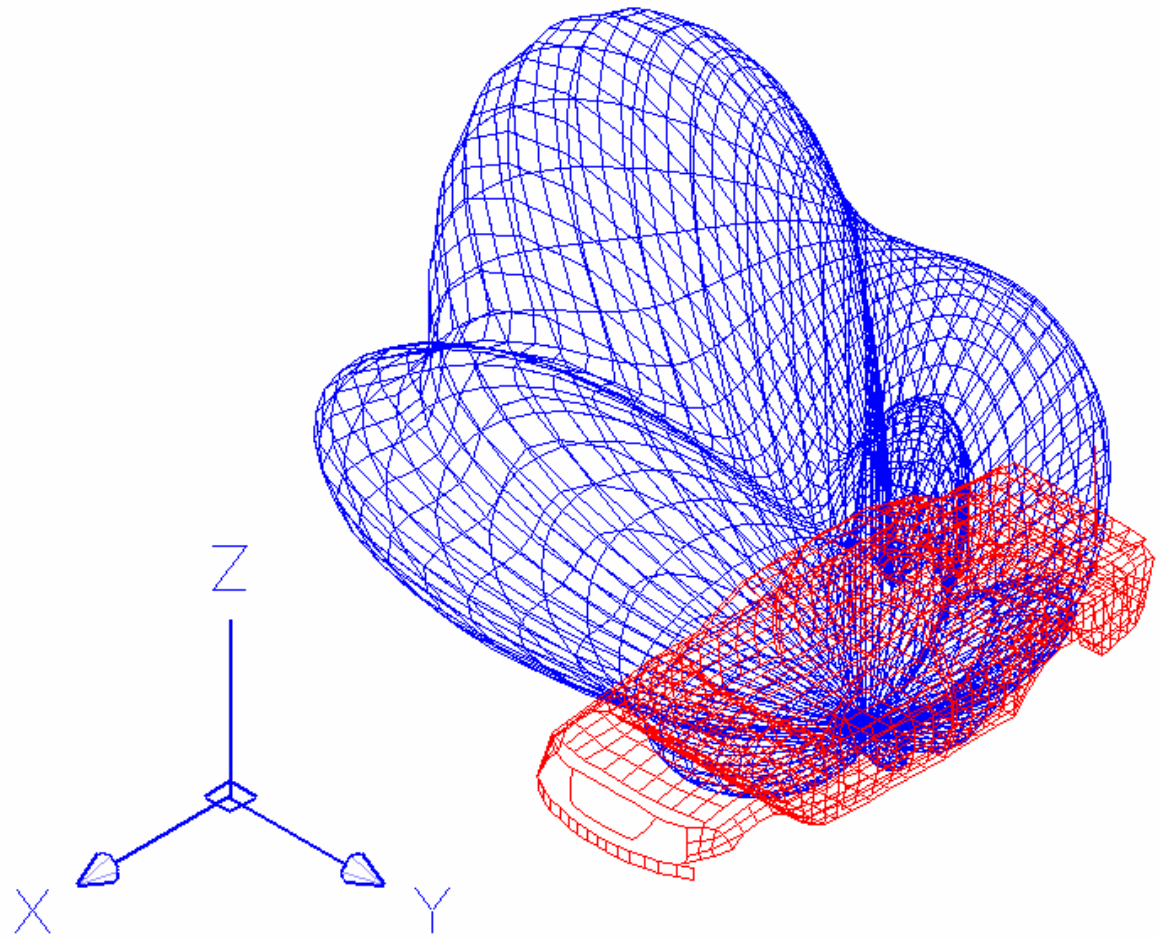

Figure 1.5: An Example of a whip Antenna Pattern Simulated at 100 MHz [11].

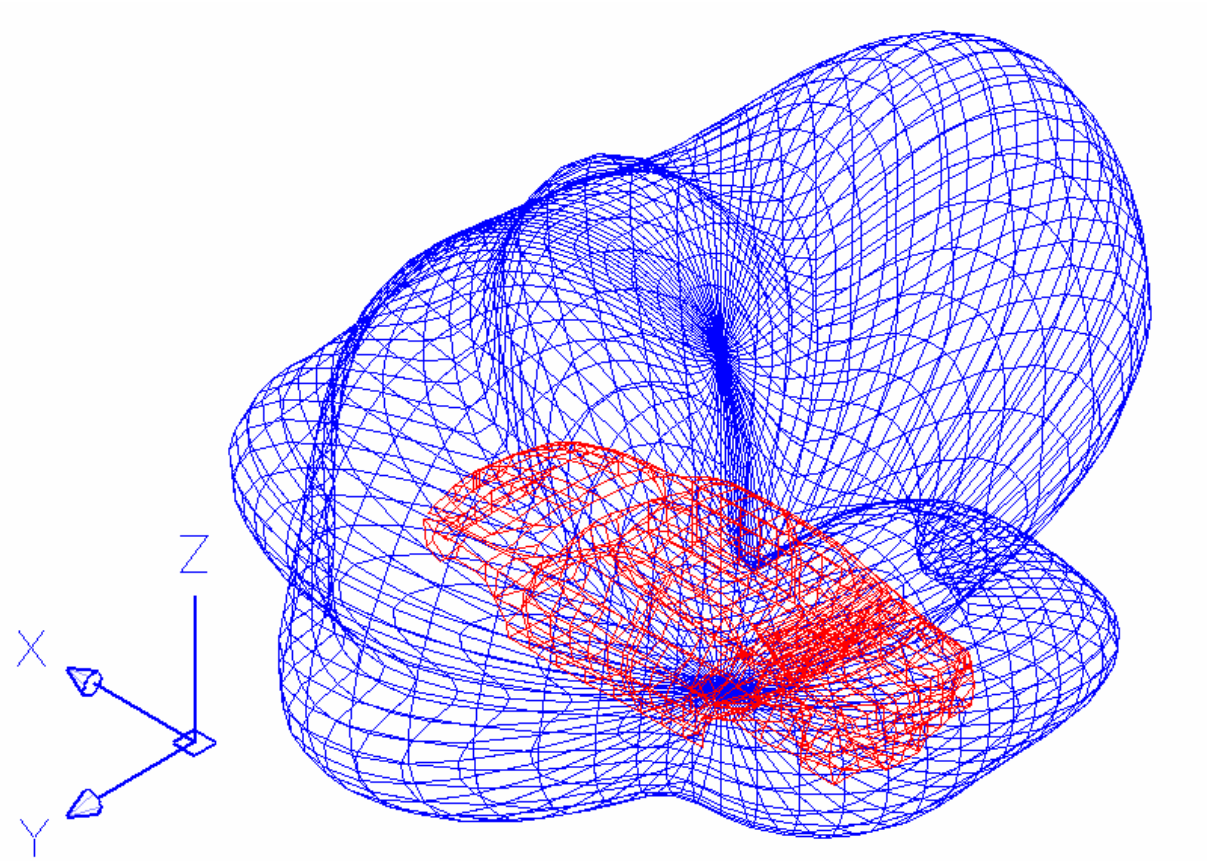

Figure 1.6: An Example of a windscreen Antenna Pattern Simulated at 100 MHz [11].

Nevertheless, due to the multiple passive antenna structures implanted in a car rear window (Figure 1.3), the pattern shown in Figure 1.6 may be influenced due to the correlation coupling between the different antenna elements. The coupling exists between all antennas and all of them affect each other. For more information, experimental and theoretical references are in [10], [11].

1.2.2 Vehicles Active Antenna Structure

Following the basic definition described in section 1.2.1, an antenna has to be understood as a two-port that transforms the free space wave to the transverse electromagnetic (TEM) wave delivered to the coaxial output cable as shown in Figure 1.7. Consequently, if the antenna two-port includes active elements, it is an active two-port and an active antenna respectively. This definition will help in simulating the antenna when it is incorporated with an amplifier circuit using any simulation software, whereas the antenna can be represented by its two-port S-parameters matrix as will be derived in the following section.

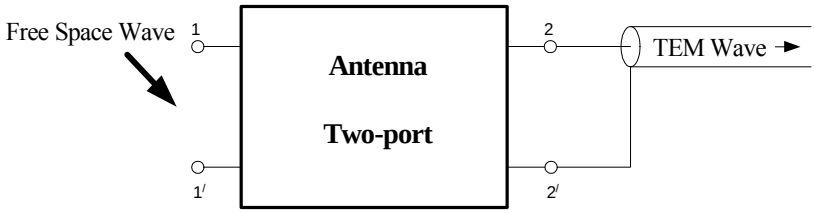

Figure 1.7: Basic definition of an antenna: An antenna is a two-port transforming the free-space wave into the TEM wave or vice versa.

In 1977, Lindenmeier and Meinke [7] stated that if a cable of lengths 1-5 m connected between the antenna and the amplifier, the antenna systems will lie under the passive category as shown in Figure 1.8 (a). For the term active antenna, it could be taken to mean any antenna in which the power source or amplifier is very closely associated with the radiating or receiving element. The term seems most appropriate when the active component is coupled directly to the element without an intervening match (or mismatch) to any sort of transmission line as shown in Figure 1.8 (b).

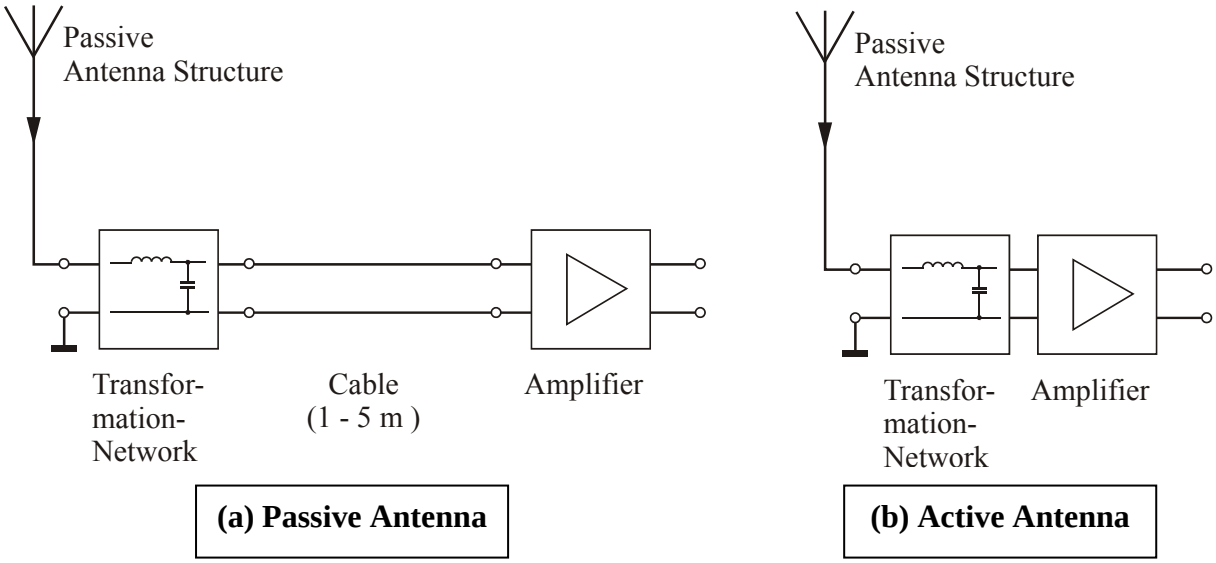

Figure 1.8: Passive and Active Antenna Detailed Definition

According to the above discussion, a car active windscreen antenna can be as shown in Figure 1.9, and actually, this is the basic implemented active antenna in most of nowadays cars, whereas a transformation network is implemented between the windscreen antenna and the amplifier. The mostly used active device for active antennas realization was and still the bipolar transistor.

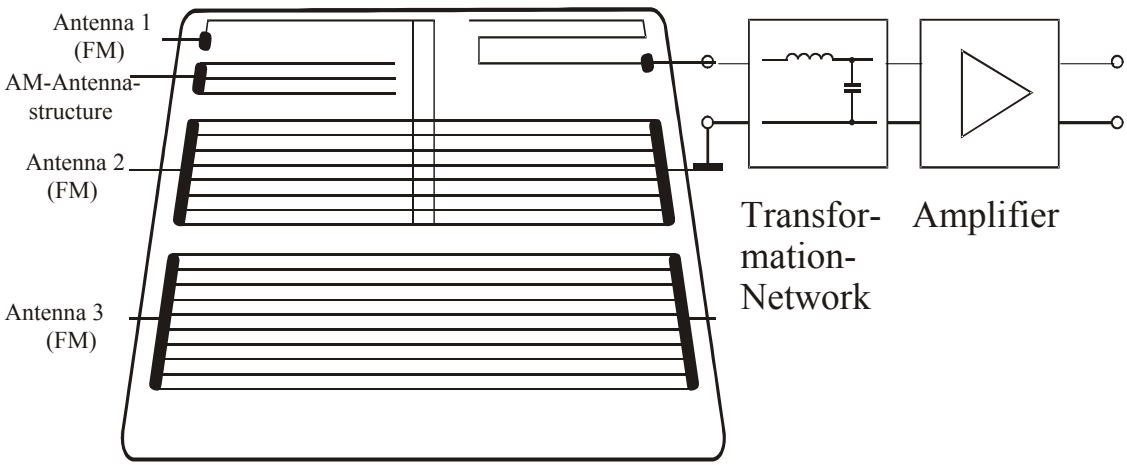

Figure 1.9: Example of an Active Windscreen Antenna

Due to nowadays-extra requirements of electronic implementations inside the cars, a noticeable noise effects appeared in TV pictures when a TV is used in a car. The reason is the switching noise when an automatic switching is working to select the best antenna from the different antennas implemented inside the car windscreen. Consequently, the bipolar transistor associated with its matching network cannot handle such a switching noise due to its limited high ohmic input impedance. A research started by Lindenmeier , Bechteler [20] in 2001, for implementing a better transistor from the high ohmic input impedance point of view, and the conclusion was to use a source follower based GaAs FET transistor directly connected to the windscreen antenna, thus reducing the prescribed switching noise effects due to the superiority of GaAs FET characteristics [13],[14],[22],[32] and [52]. The use of high input GaAs FET facilitates cancelling the use of the matching networks with their design problems as it was not an easy design task to find a suitable match for every amplifier connected to different antenna structure. By using the source follower GaAs FET cell, good intermodulation distortion behaviour of the total system can be achieved (~ 81 to 84dB third order intermodulation separation reached experimentally in a 50 Ohm system [20] at 50mA GaAs FET drain bias current) , thus a low noise and high linearity vehicles active antenna amplifier can be reached.

The main purpose in this dissertation is to extend and generalize the vehicles FM active antenna concept proposed in [20] by introducing an extended new design suitable for different antenna structures and have the capability of providing low noise high linearity active antenna system.

The expected advantages to be obtained with this new active antenna concept based GaAs FET connected directly to the windscreen antenna can be summarized as follows:

1- No RF power extracted from the windscreen, thus no RF losses.

2- The input GaAs FET acts as a probe.

3- Switching in front of the active element is also possible.

4- Frequency separation for FM and TV application is possible after the GaAs FET amplifier input stage.

5- Switching for FM has no effect on TV and vice versa.

6- For any antenna structure, the design rules available in situation of any amplifier realization.

1.2.3 The Vehicle Windscreen Antenna Impedance General Matrix For Active Antennas Simulation

At this stage, it should be noted that when simulating or even deriving an active antenna model, it must be considered that the active antenna consists of two fundamental different parts that have to be treated separately. The active device can be modelled based on measured parameters (behavioural) or a large-signal (physical) model can be used. The embedding windscreen antenna structure can be described on the circuit level (behavioural) or based on full-wave simulations (physical). For the simulation purposes, we will derive a suitable general-purpose matrix for the antenna structure measured impedance data independent on the simulation software used. The matrix will be used through our presented work design examples.

In this section, for complete design and simulation of an active antenna amplifier, a suitable general-purpose matrix will be derived for the windscreen antenna structure measured impedance data. The matrix will be used in the subsequent chapters.

Pictorial Description of the New Approach for one-port antenna emulation using an equivalent symmetric loss-less two-port network

Usually the antenna available data is its frequency dependent impedance as shown in Figure (1.10).

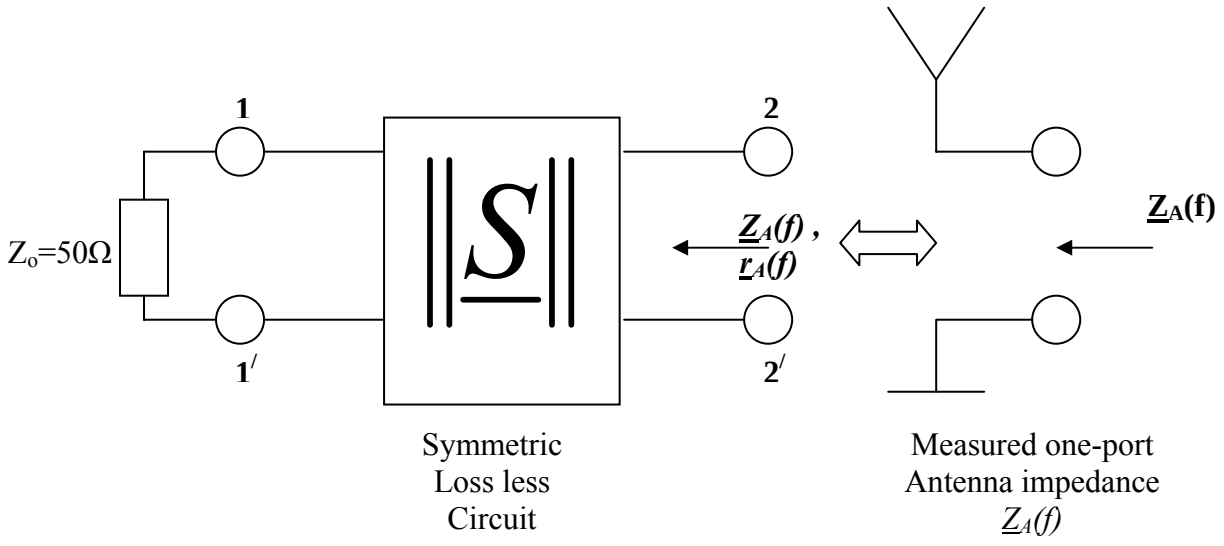

Figure 1.10: Antenna Measured Impedance Equivalent Two port

From Figure 1.10, assume that the antenna will be realized by a symmetric loss-less circuit model, so the reciprocal two-port S-parameter matrix applies, and then we have

$$\left\|\underline{S}\right\| = \begin{vmatrix} S_{11}e^{j\phi_{11}} & S_{12}e^{j\phi_{12}} \\ S_{21}e^{j\phi_{21}} & S_{22}e^{j\phi_{22}} \end{vmatrix} \tag{1.7}$$

Whereas the reflection coefficient vector $\underline{r}_A = r_A e^{j\phi_A}$, which represents the normalized impedance vector: $\underline{r}_A(f) = \dfrac{\underline{Z}_A(f) - Z_o}{\underline{Z}_A(f) + Z_o}$

Here, note that the available antenna impedance measurements is simply the matrix component, $S_{11}e^{j\phi_{11}}$ so the main goal now is to derive an expression of each matrix component ($S_{ij}e^{j\phi_{ij}}$) as a function of the measured antenna impedance.

The matrix elements derivation:

Applying the two-port loss-less conditions for a two-port network:

Condition (1): $$S_{11}^2 + S_{12}^2 = 1 \tag{1.8}$$

But simply $S_{11} = r_A$, so, we have:

$S_{12} = \sqrt{1 - r_A^2}$, and since $S_{11} = S_{22}$, then accordingly, we have: $S_{21} = \sqrt{1 - r_A^2}$

Condition (2): $$S_{11} \cdot S_{12} \cdot e^{j(\phi_{11} - \phi_{12})} + S_{21} \cdot S_{22} \cdot e^{j(\phi_{21} - \phi_{22})} = 0 \tag{1.9}$$

But since a symmetric circuit model is assumed to represent the antenna network, then we have: $S_{11} = S_{22}$ and $S_{12} = S_{21}$, so substituting in *condition (2)* and dividing both sides by $S_{11} \cdot S_{12}$, then condition (2) will be reduced to:

$$e^{j(\phi_{11} - \phi_{12})} = -e^{j(\phi_{12} - \phi_{22})} \quad \Rightarrow \quad e^{j(\phi_{11} - \phi_{12})} = e^{\pm j\pi} \cdot e^{j(\phi_{21} - \phi_{22})} = e^{j(\pm\pi + \phi_{21} - \phi_{22})}$$

$$\Rightarrow \phi_{11} - \phi_{12} = \pm\pi + \phi_{21} - \phi_{22} \qquad \text{Phase Identity} \tag{1.10}$$

The symmetric circuit model representing the antenna network, will in addition leads to: $\phi_{11} = \phi_{22}$ and $\phi_{12} = \phi_{21}$, and noting that the available measured ϕ_A is simply ϕ_{11}, so one can solve the phase identity (1.7) for ϕ_{12}, then we have: $\phi_{12} = \phi_{11} \pm \pi/2 = \phi_A \pm \pi/2$

Therefore, the elements of the completely emulated two-port matrix components as a function of the measured one–port antenna impedance are:

$$\|\underline{S}\| = \begin{vmatrix} r_A e^{j\phi_A} & \sqrt{1-r_A^2} \cdot e^{j(\phi_A \pm \pi/2)} \\ \sqrt{1-r_A^2} \cdot e^{j(\phi_A \pm \pi/2)} & r_A e^{j\phi_A} \end{vmatrix} \tag{1.11}$$

Based on the assumption of two-port symmetric loss-less circuit model, which will represent the one-port measured antenna impedance (but this does not mean at all that a symmetric circuit should model the antenna practically.).

So, simply the following system shown in Figure 1.11 can be reached which represents any active antenna. It can be used with any simulator, since it represents a direct transformation for any frequency dependent source impedance circuit (connected to an amplifier or any two port system) to a 50[Ohm] output-input system.

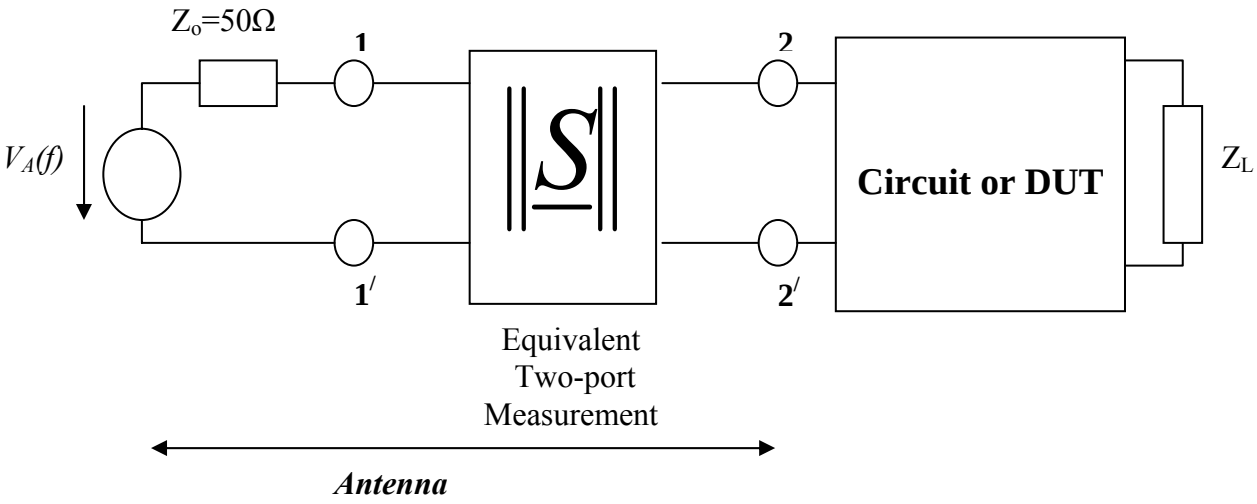

Figure 1.11: System representation for subsequent simulation

1.2.4 Measuring the Vehicles Active Antenna Amplifiers in Free Field

This section presents a summary for the measurement place and system used to evaluate the vehicles active antennas. For the necessary measurements of the different developed cars windscreen antenna structures patterns and evaluating the automotive active antenna amplifier systems, a measurement place developed at the Institute of High Frequency – University of der Bundesweh Munich – Germany as shown schematically in Figure 1.12.

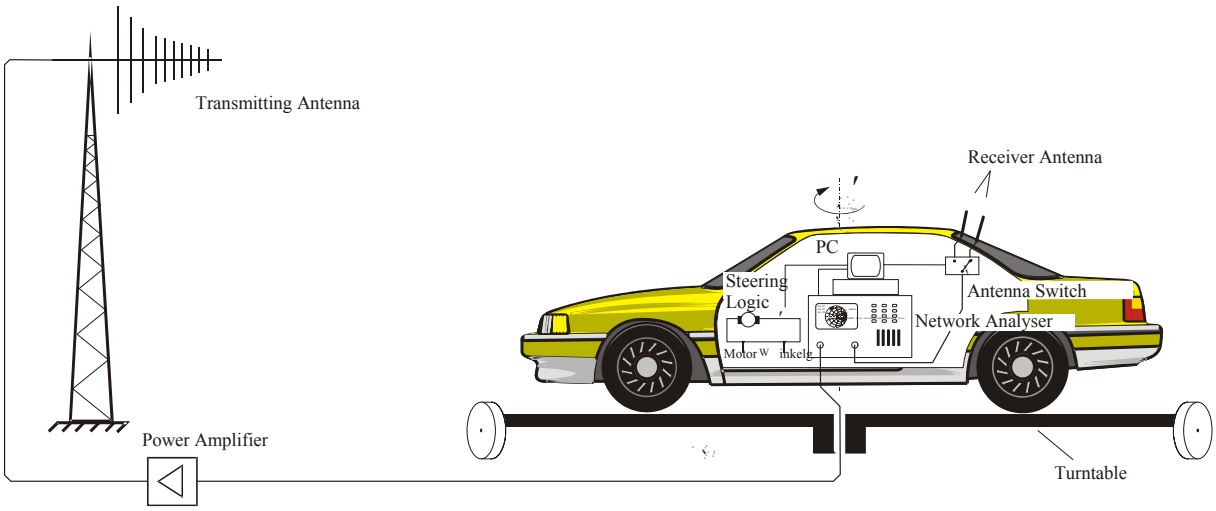

Figure 1.12: Car Antenna Measurement Place System

The system composed of a transmitter and a radom room inside which the car antenna performance to be measured as shown in Figure 1.13(a). The radom room is far way from the antenna at around 50 m distance. The system includes sender antenna of a logarithmic periodic type, control unit with computer and network analyzer. An actual picture (taken in winter 2003, which illustrates the actual implemented system in the university) is shown in Figure 13(a). Figure 1.13(b) shows the car (vehicle) inside the radom room for measurements. For the necessary active antenna evaluation measurements, the first step is a connection of a reference *rod antenna* as shown in Figure 1.13(b), followed by rotating the vehicle (from $0^{\circ} to 360^{\circ}$) in 5° (azimuth angle) steps using the turntable shown and the angle of elevation is a fixed degree of 85°.

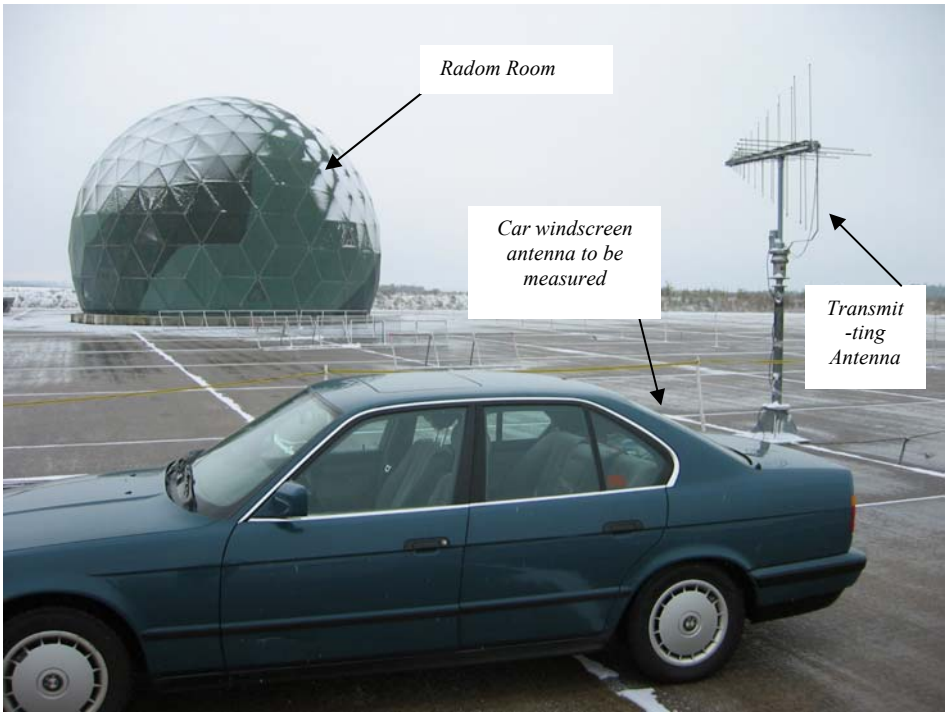

Figure 1.13(a): Antenna Measurement Place at the Armed Force University in Munich

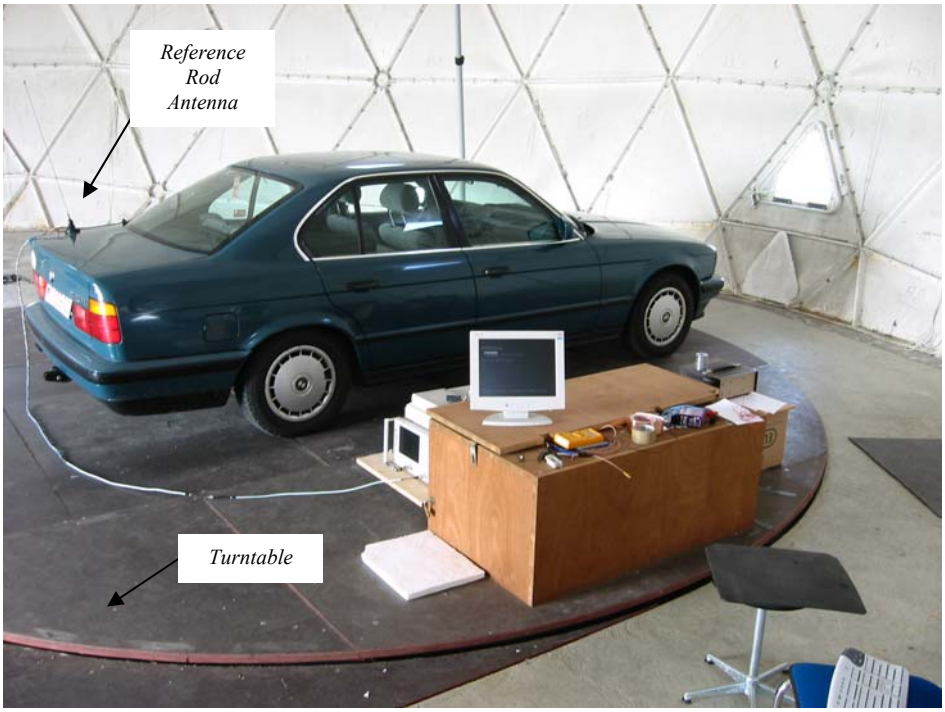

Figure 1.13(b): The Car inside the Radom Room with a Reference Rod Antenna connected to the Measurement system

Then recording the Network analyzer results and the antenna patterns using the software implemented in the PC. The second and final step incorporates removing the reference rod antenna and connecting the designed active antenna amplifier to the suggested windscreen and repeating the described procedure previously.

Figure 1.14, shows an example of typical obtained measured results from the described previous steps. Diagrams of the antenna impedance, horizontal pattern and the antenna and or the amplifier relative frequency responses respectively can be displayed. Such diagrams help in enhancing the antenna structure if the active antenna results are not satisfactory according to the application [69], [70].

Until this stage, a summarized introductory of the active antennas used in modern cars generally has been introduced. The next section will focus on the antenna transistor amplifiers for active receiving antennas, as they constitute the heart of the active antenna, in addition that they determine final evaluation performance of the active antenna in general.

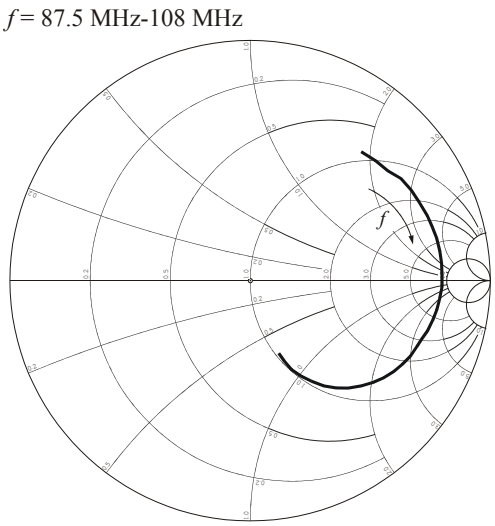

(a) Antenna Impedance Example

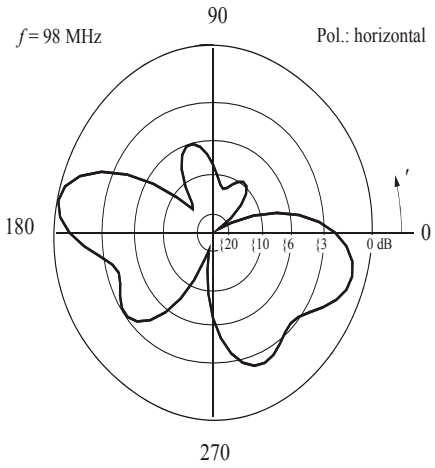

(b) Antenna Gain Pattern Example

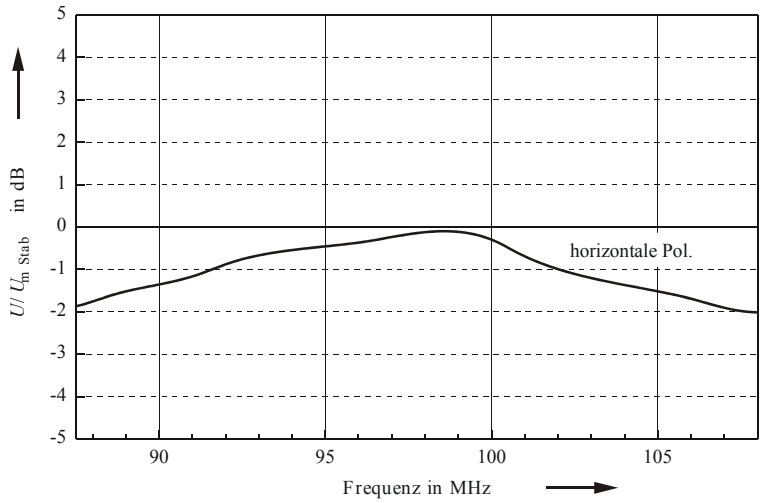

(c) Antenna Frequency Response Example

Figure 1.14: Characterization Measured Example of a Vehicle Windscreen FM Antenna

II. Antenna Transistor Amplifiers for FM Active Receiving Antennas

INTRODUCTION

As described before, the active antenna in its minimum configuration consists of a passive antenna and an integrated amplifying device. The question that may be arises, which integrated amplifying device should be used if different semiconductor devices like bipolar, FET, MOSFET, GaAs MESFET, etc. transistors are available.

In the early work of [1], a suggestion has been made to use a FET transistor at the input stage due to their low noise performance. Recently in 2001 in [20], the GaAs FET has been adopted for modern vehicles FM Active antenna amplifiers due to their superior low noise figure (around 0.8-0.9dB in the FM range) and excellent third order intermodulation (for a follower cell, a 81-84dB @ drain current of 50mA can be reached at output voltage level of 100 dBμV) performances. However, the GaAs FET transistor cost is still high, so this work additionally considered a research about the possibility to design active antenna with different cheaper semiconductor device like JFET transistor or similar equivalent HEMT transistor for comparison to show their universal nature possibility to replace the GaAs FET.

In this section, the semiconductor three terminal devices will be reviewed briefly. The theory behind the different transistors or even models in the presented active antenna amplifier of this workis not the scope of this dissertation.

1.3 Semiconductor Three-Terminal Devices for Active Antennas

1.3.1 Junction Field Effect Transistors

The simplest type of FET is the JFET, or Junction Field-Effect Transistor. It consists of a long channel of semiconductor material, either P or N doped, with a contact on each end, labeled source and drain respectively. The third control terminal, called the gate, is placed to contact the edges of the channel, and is doped opposite to the polarity of the channel. When a voltage is applied between source and drain, current flows. The current flow can be modulated by applying a voltage between the gate and source terminals. When this occurs, the electric field applied effectively narrows the channel, and the flow of current is restricted.

JFETs have several advantages over the historically important BJT (Bipolar Junction Transistor). They do not require any input current to function, which makes them useful for circuits requiring high input impedance. However, their gain is usually relatively low in comparison. They are used in low-noise, low-signal level analogue applications, and sometimes used in switching applications [46].

1.3.2 High Electron Mobility Transistors

HEMT stands for High Electron Mobility Transistor. A HEMT is a MESFET [44] with a junction between two materials with different band gaps (i.e. a heterojunction) as the channel instead of a n-doped region. A commonly used combination is GaAs with AlGaAs. The effect of this junction is to create a very thin layer where the Fermi energy is above the conduction band, giving the channel very low resistance (or to put it another way, "high electron mobility"). This layer is sometimes called a two-dimensional electron gas. As with all the other types of FETs, a voltage applied to the gate alters the conductivity of this layer. Ordinarily, the two different materials used for a heterojunction must have the same lattice constant (spacing between the atoms). An analogy - imagine pushing together two plastic combs with a slightly different spacing - at regular intervals, you will see two teeth clump together. In semiconductors, these discontinuities are a kind of "trap", and greatly reduce device performance. A HEMT where this rule is violated is called a PHEMT or pseudomorphic HEMT. This feat is achieved by using an extremely thin layer of one of the materials - so thin that it simply stretches to fit the other material. This technique allows the construction of transistors with bigger bandgap differences than otherwise possible. This gives them better performance. To the best of the author's knowledge, PHEMTs and related devices are the fastest transistors available. They can be used to make amplifiers which work at over 200 GHz. Applications are similar to MESFETs - microwave and millimetre wave communications, radar, and radio astronomy.

1.3.3 Metal-Semiconductor Field Effect Transistors

MESFET stands for Metal-Semiconductor Field Effect Transistor. It is quite similar to a JFET in construction and terminology. The difference is that instead of a using a p-n junction for a gate, a Schottky (metal-semiconductor) junction is used. MESFETs are usually constructed in GaAs or InP (never silicon), and hence are faster but more expensive than silicon-based JFETs or MOSFETs. MESFETs are used up to approximately 30GHz, but building a computer processor using them will probably not be economic for some time. MESFETs are commonly used for microwave frequency communications and radar[46].

1.4 Transistor Modelling for Active Antennas

For linear (behavioural) modelling of the active device, measured S-parameters are typically used. The device is described as a black box containing measured two-terminal or analytically calculated three-terminal S-parameters. Sometimes, a small model is derived from the measured parameters. Large-signal characterization (physical modelling) is an important requisite since it is only under this operation condition that the power producing amplification of the active antenna will reach a stable limit circle. The derivation of a large-signal model for the active device such that they provide a realistic estimation of the nonlinear performance is a subject of intense research. The linear transistor model is reviewed briefly here for design purposes. Since the nonlinear transistor models varieties are a subject of intense research, a refer to the basic transistor circuit model will be presented if necessary and the reader can refer to [13], [18], [26], [34], [46], [47] and [52] for details. In this work, different nonlinear transistor models available from the simulation software *Serenade Harmonica Software version 8.7* will be used. (This software simulator is produced from Ansoft [54]).

1.4.1 S-Parameter Description

The transistor (three-terminal device) is generally characterized by its two-port S-parameters with one of its ports grounded and the others are assumed to be terminated with the port characteristic impedance, usually 50Ω. Typically, these parameters are measured in a common source configuration using a network analyzer as shown in Figure 1.13.

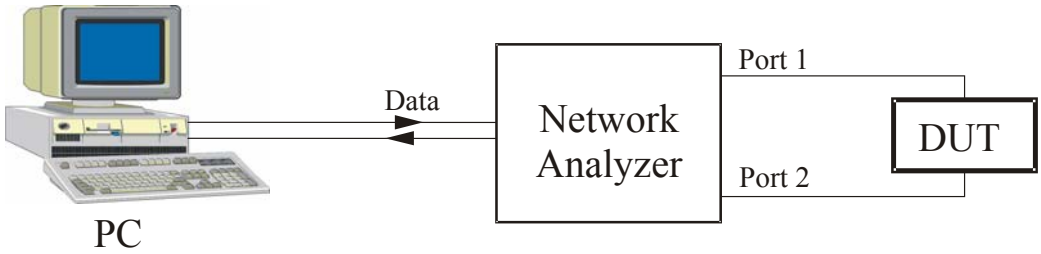

Figure 1.13: Measurement Setup for a two Port Network

Figure 1.14 shows a description of the transistor as a two-port device. This configuration is used for two-port S-parameter measurements. The two-port S-parameter matrix of the transistor can be written as[43]:

$$\begin{bmatrix} b_1 \\ b_2 \end{bmatrix} = \begin{bmatrix} S_{11} S_{12} \\ S_{21} S_{22} \end{bmatrix} \cdot \begin{bmatrix} b_1 \\ b_2 \end{bmatrix} \tag{1.12}$$

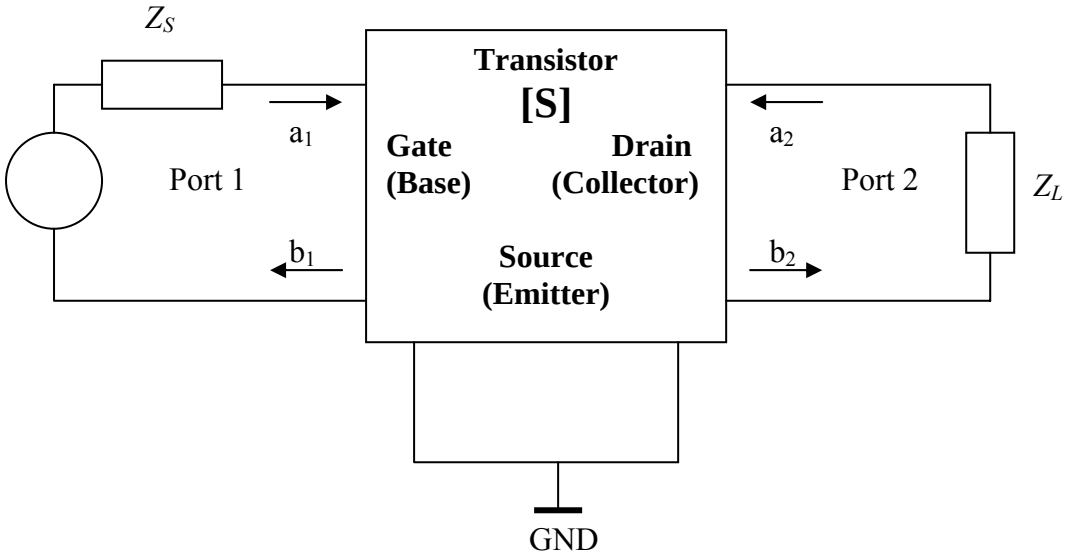

Figure 1.14: Transistor as a two-port Device

The following basic definitions in 50 Ohm system will frequently be used through this present work [44],

$S_{11} = \left.\frac{b_1}{a_1}\right|_{a_2=0}$ = Input reflection coefficient with the output port terminated by a matched load

(Z_L=Z_o sets $a_2 = 0$)

$S_{22} = \left.\frac{b_2}{a_2}\right|_{a_1=0}$ = Output reflection coefficient with the input terminated by a matched load

(Z_S=Z_O sets source voltage = 0)

$S_{21} = \left.\frac{b_2}{a_1}\right|_{a_2=0}$ = Forward transmission (insertion) gain with the output port terminated in a matched load.

$S_{12} = \left.\frac{b_1}{a_2}\right|_{a_2=0}$ = Reverse transmission (insertion) gain with the input port terminated in a matched load.

The Amplifier Amplification will defined to be *V*, where V in dB is

$$V[dB] = 20 \cdot \log_{10}|S_{21}| \tag{1.13}$$

The Amplifier isolation will be defined to be *I*, where I in dB is

$$I[dB] = 20 \cdot \log_{10}|S_{12}| \tag{1.14}$$

In contrast to low frequency modelling, S-parameters are used at microwave frequencies rather than equivalent circuit models because the number of fitted parameters (including all parasitic) is very large. It is therefore difficult to derive a good model. For large-signal (time-domain) analysis, there is no option, and therefore large-signal modelling is needed, however this is not the scope of this work and we are willing to depend on the models implemented in our simulation software Serenade Harmonica ver.8.7 from Ansoft [54].

1.4.2 Noise In Transistors for Active Antennas

In order to describe the RF noise of a JFET, HEMT or GaAs FET in case of using one of them for active receiving antenna, one has to determine the parameters of the noise model in addition to the small-signal equivalent-circuit elements taking into account that generally, the sensitivity of a receiving antenna is determined by its noise behaviour. The receiving system noise temperature T_S with transistorized antenna (Figure 1.2) can be expressed by [4]

$$T_S = T_{Ant.} + T_T + \frac{T_R}{G} \tag{1.15}$$

Where $T_{Ant.}$ is the antenna noise temperature due to the external noise, T_T is the transistor noise temperature, G is the transistor power gain and T_R is the receiver noise temperature. For

optimum performance, T_S should be as low as possible [4]. For passive antenna (whereas no transistor is connected), T_T is equal to zero and G is unity, thus

$$T_S = T_{Ant.} + T_R \tag{1.16}$$

Equation 1.16 shows that for possible minimum T_S, one should note that $T_{Ant.}$ can't be influenced and a minimum T_{Smin} is a function of the receiver noise temperature T_R which is 1000^oK for a very sensitive receiver (Noise figure of $F_R = 2 = 3$[dB]) [10]. For an active antenna (transistorized antenna as in Figure 1.2) we get

G>>1 which leads to $T_R / G << 1$ thus we have

$$T_S \approx T_{Ant.} + T_T \tag{1.17}$$

Equation (1.17) shows the advantage of using a transistorized antenna, where a minimum T_{Smin} can be achieved by using a good low noise transistor with low T_T, which is definitely lower than 1000^oK (case of passive antennas). In [2], [5], Lindenmeier introduced a new conclusion regarding the transistor temperature T_T, whereas it was found that T_T is dependent on the internal impedance of the signal source feeding the transistor. This internal impedance has an optimum value, which depends on the transistor and on the frequency. Inserting the transistor at a gap in an antenna, where the antenna impedance is equal this optimum value[6], then T_T equals to 120^oK which shows the good improvement in the system noise temperature compared to a passive antenna. However, it should be noted that as the antenna impedance varies with frequency, exact noise match could only be obtained at one single frequency. In order to visualize the noise effects in transistors connected to antennas for an active antenna realization, consider the receiving antenna system arrangement shown in Figure 1.15 once with passive load and second with amplifier network.

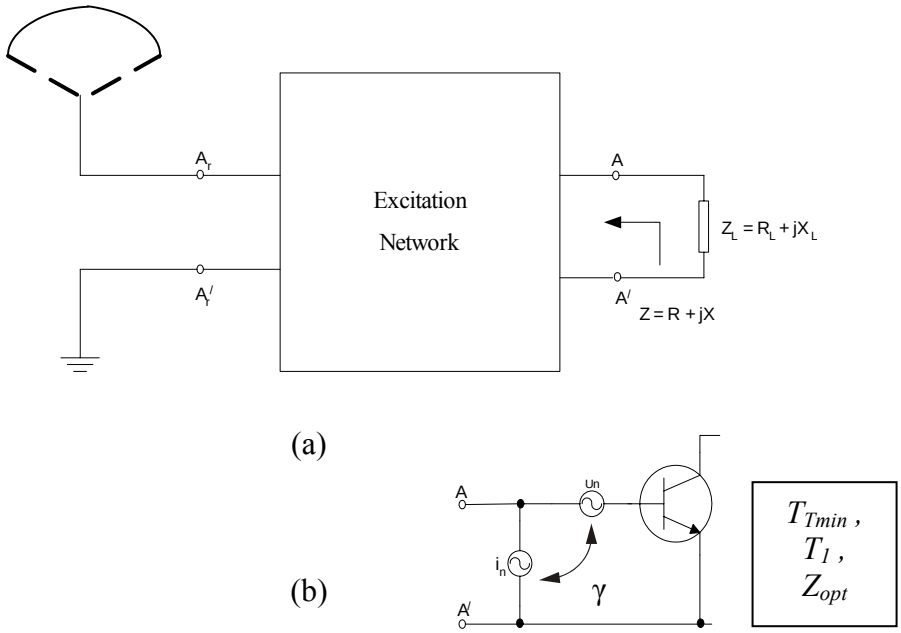

Figure 1.15: Receiving Antenna System with (a) passive load, (b) amplifier network

In Figure 15 (a), the radiator and excitation network form a unit representing the antenna with its terminals A and A$^{/}$. In many cases, the radiator and its excitation network can be separated neither spatial nor as far as its electrical performance is connected. This means that this network may be distributed over the interior of the sphere, which is partly true with many antennas of more complicated shape than a single classical dipole. Thus A_r and $A_r^{/}$ are imaginary terminals, which are introduced only to achieve a distinct representation. Define the arbitrary antenna impedance between the terminals A_r-$A_r^{/}$ to be $\underline{Z}_{Ant.}$,($Z = R + jX = Z_{Ant.} = R_A + jX_A$), then the maximum power in the receiving or transmitting condition with the antenna arrangement in Figure15 (a) is obtained when the antenna impedance Z_A equals the optimum impedance $\underline{Z}_{opt}$ that means

$$Z_{Ant.} = R_A + jX_A = Z_L^* = Z_{opt} = R_{opt} + jX_{opt} \tag{1.18}$$

Where $\underline{Z}_L^*$ is the conjugate complex of $\underline{Z}_L$ which is either a load impedance or in the transmitting condition the internal impedance of a generator. It is well known that the normalized power in case of receiving antenna or either radiating one may be calculated as follows [6]

$$\frac{P_{re}}{P_{re-\max}} = \frac{P_{ra}}{P_{ra-\max}} = \left(1 + \frac{1}{4}\frac{\left|Z_{Ant.} - Z_{opt}\right|^2}{R_A \cdot R_{opt}}\right)^{-1} \tag{1.19-A}$$

Where; $P_{re}/P_{re\text{-}max}$ is the normalized received power (denote: $P_{received} = P_{re}$, $P_{received\text{-}maximum} = P_{re\text{-}max}$) and $P_{ra}/P_{ra\text{-}max}$ is the normalized radiated power (denote: $P_{radiated} = P_{ra}$, $P_{radiated\text{-}maximum} = P_{ra\text{-}max}$).

Then if equation (1.18) has been achieved ($\underline{Z}_{Ant.} = \underline{Z}_{opt}$), then the received power will arrive to its maximum value ($P_{re} = P_{re\text{-}max}$), however this can be achieved within the receiving antenna bandwidth. To illustrate this point, consider the complex impedance plane of a passive antenna as shown in Figure 1.16 [4], whereas $\underline{Z}_{Ant.}$ is arbitrary frequency dependent antenna impedance. The frequency range wherein the second term of the sum in Eqn. (1.19-A) is less than one gives the 3-dB power bandwidth [6]. A boundary circle as in the impedance plane in Figure 1.16 describes those impedance values with which $P_{re} / P_{re\text{-}max} = P_{ra} / P_{ra\ max} = ½$. Thus the impedance curve $\underline{Z}_{Ant.}$ delivers the normalized power bandwidth around the centre frequency f_o ($b_p = (f_{2p} - f_{1p})/f_o$).

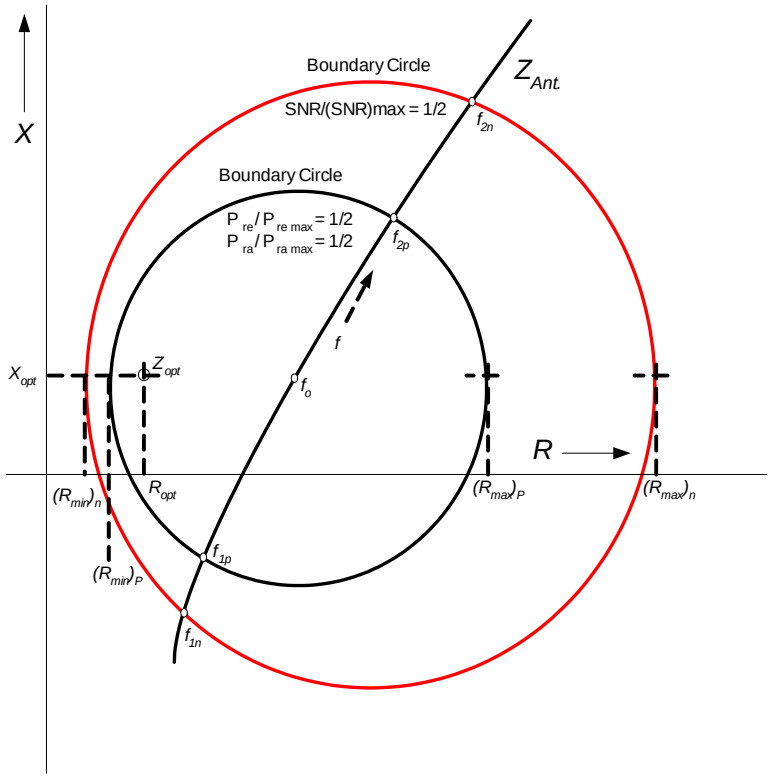

Figure 1.16: Circles of Constant Normalized Power and SNR respectively in the Antenna Impedance Plane; $\underline{Z}_{opt}$ impedance for optimum power and optimum SNR respectively, $\underline{Z}_{Ant.}$ curve of Antenna Impedance. ($f_{2p} - f_{1p}$) and ($f_{2n} - f_{1n}$) are the widths of the power transmission band and the SNR transmission band respectively.

In Figure 1.16,

The normalized diameter δ_P of the boundary circle for power matching is a constant defined in [6] to be

$$\delta_P = \frac{(R_{\max})_P - (R_{\min})_P}{R_{Opt}} = 4\sqrt{2} \tag{1-19-B}$$

Whereas the boundary circle for SNR considerations at lower frequencies is much greater than that with power considerations. The normalized diameter δ_n reads as follows [6]

$$\delta_n = \frac{(R_{\max})_n - (R_{\min})_n}{R_{Opt}} = \frac{T_{Ant.}/T_{N\min} + 1}{T_1/T_{N\min}} \sqrt{1 + \frac{4 \cdot T_1/T_{N\min}}{T_{Ant.}/T_{N\min} + 1}} \tag{1-19-C}$$

Moreover, the SNR bandwidth is obtained from $(f_{2n}\text{-}f_{1n})/f_o$.

Replacing the passive load between A-A$'$ in Figure 1.15 (a) by an active network shown Figure 15 (b), whereas $T_{T\text{-}min}$ represents the active network minimum noise temperature, T_1 is the active device characteristic temperature and recall that [6] may express the normalized signal-to-noise ratio after analogy of the normalized power given in Eqn. (1.19), thus the normalized signal to noise ration will be

$$\frac{SNR}{SNR_{\max}} = \frac{T_{S\min}}{T_S} = \left(1 + \frac{T_1/T_{T\min}}{T_{Ant.}/T_{T\min} + 1} \cdot \frac{\left| \underline{Z}_{Ant.} - Z_{opt} \right|^2}{R_A \cdot R_{opt}} \right)^{-1} \tag{1.20}$$

The noise characteristic of the active network is given by its minimum noise temperature T_{Tmin} at optimum source impedance, also called $\underline{Z}_{opt} = R_{opt} + jX_{opt}$, and its characteristic temperature T_1 [6]. $T_{Ant.}$ is the antenna noise temperature due to the received noise and T_S represents the noise temperature the minimum of which is obtained with $Z = Z_{opt}$ and reads as follows

$$T_{S-\min} = T_{Ant.} + T_{T-\min} \tag{1.21}$$

Thus, a minimum system noise temperature has been arrived. The connection of the active network shown in Figure 1.15(b) to the antenna, will result in a system as shown in Figure 1.17, whereas α_r is the a noise ratio factor falls between the numerical values 0.25 and 0.5 (as defined in [6] and [10], α_r is the ratio between the transistor characteristic temperature T_1 and the active network minimum noise temperature $T_{T\text{-}min}$) .

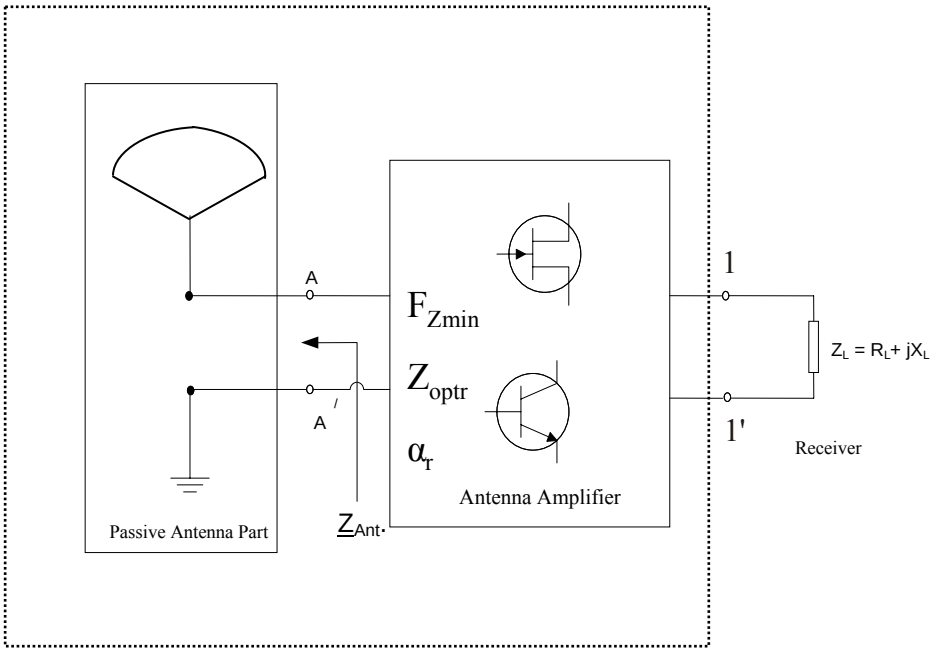

Active Antenna

Figure 1.17: General Principle of Active Antenna

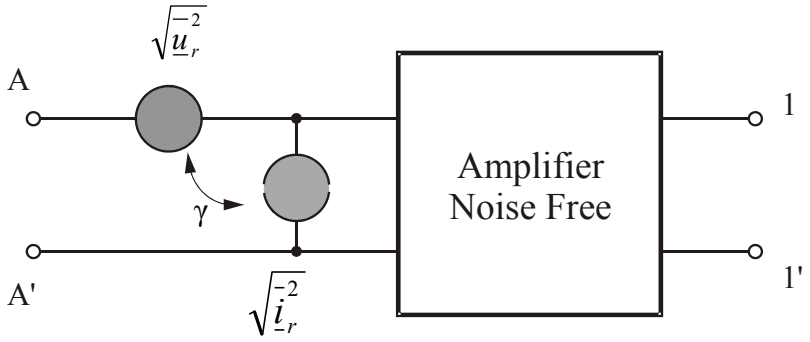

Figure 1.18: General Form of Noisy Linear Amplifier

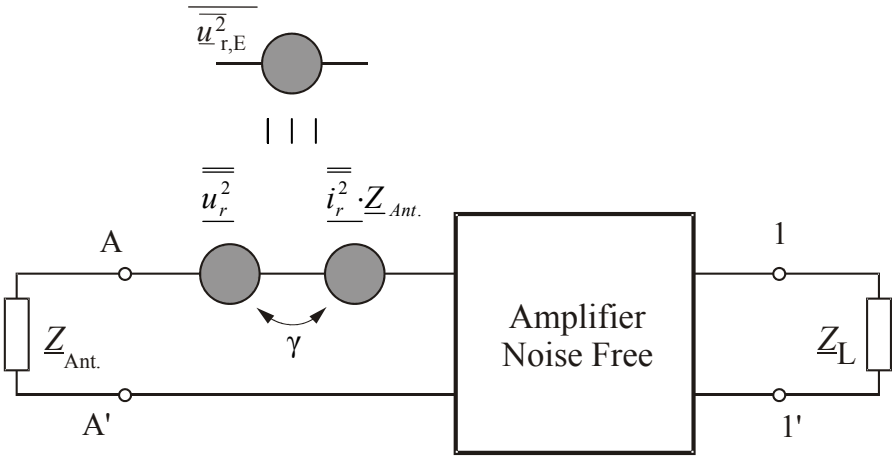

Figure 1.19: General Form of Noisy Linear Amplifier connected to source and load impedances

Figures 1.18 and 1.19 summarize the noise sources in the general intrinsic FET equivalent circuit [10]. For a detailed theory and information about the theory behind the noise in linear amplifiers, the reader can refer to [56] in addition. In Figure 1.17, the antenna impedance seen at the terminals A-A$^{/}$ is represented by the antenna impedance $\underline{Z}_{Ant.}$ connected to the transistor amplifier as shown in Figure 1.19. Briefly, the noise sources associated with an amplifier can be described at the amplifier input by the average noise voltage and current source $\overline{\underline{u}_r^2}, \overline{\underline{i}_r^2}$ respectively correlated with a correlation facto $\underline{\gamma}$ as shown in Figure 1.18.

Refer to Figure 1.19, in case of an amplifier terminated by a source and load impedances of $\underline{Z}_A$ and $\underline{Z}_L$ respectively. Let the input noise voltage to be $U_{r,E}$ and assuming that the amplifier power amplification factor is V, then the output effective noise voltage $U_{r,A}$ at the load in a 50-Ohm system will be

$$U_{r,A} = U_{r,E} \cdot V \tag{1.22}$$

Define the additional noise figure of an antenna transistor to be F_Z, then its dependence in case of an antenna impedance $\underline{Z}_A$ is [10]

$$\frac{F_Z}{F_{Z\min}} = 1 + \alpha_r \cdot \frac{\left|\underline{Z}_{Ant.} - \underline{Z}_{optr}\right|^2}{R_A \cdot R_{optr}} \tag{1.23}$$

Whereas F_{Zmin} is the minimum, additional noise figure that can be reached using a good transistor with minimum noise temperature T_{Tmin} as discussed in section 1.2. From [9], and by analogy Equation (1.23) can be re-written as

$$\frac{T_T}{T_{T\min}} = 1 + \alpha_r \cdot \frac{\left|\underline{Z}_{Ant.} - \underline{Z}_{optr}\right|^2}{R_A \cdot R_{optr}} \tag{1.24}$$

From which one can conclude that the transistor noise temperature T_T will be minimum (equals to T_{Tmin}) when $\underline{Z}_{Ant.} = \underline{Z}_{optr}$, and consequently the additional noise figure F_Z will reach its minimum value $F_{Z\text{-}min}$. It should be noted that the noise ratio factor α_r in Equations (1.23) and (1.24) is of importance, whereas as explained in[10], it is lying between the numeric values of 0.25 until 0.5.

A full correlation between the voltage and current noise sources at the transistor input is present when α_r takes the value of 0.25, which means that the magnitude of the correlation factor $\underline{\gamma} = 1$.

When α_r takes the value of 0.5, then the magnitude of the correlation factor $\underline{\gamma}$ = zero, which means that the two noise voltage and current source are de-correlated. It should be noted that a de-correlation between the voltage and current noise sources is an important aim to be reached for active antenna design, since simply this will mean a minimum system noise temperature and thus minimum noise figure can be reached.

An important remark is that the antenna impedance varies with frequency, so exact noise match can only be obtained at one single frequency, and consequently an exact noise match all over the antenna bandwidth is not possible. A solution has been suggested and concluded by Lindenmeier in [5] that in case of directly connecting bipolar transistor to the antenna for a broadband active antenna applications design (for example, from f_1 to f_2), it is favourable to design the antenna so that its impedance curve forms a loop around the optimum impedance $\underline{Z}_{opt}$ as shown in Figure 1.20.

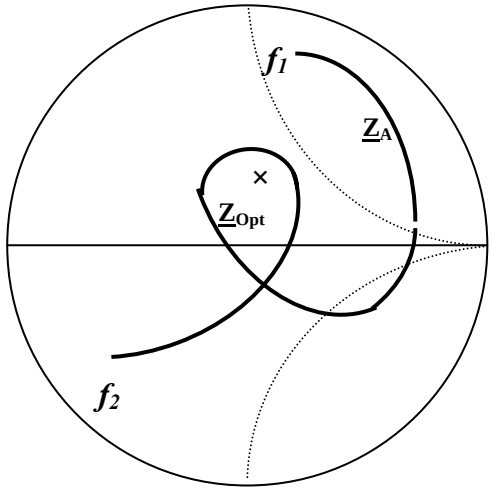

Figure 1.20: The Antenna impedance curve forms a Loop around $\underline{Z}_{opt}$ for Broad Band Applications Design using Bipolar Transistor.

Moreover, in case of connecting FET to the antenna, the antenna impedance can be of general design characteristic as concluded [5]. Figure 1.21 shows the circles of constant normalized power and SNR respectively in the Antenna Impedance Plane. $\underline{Z}_{opt}$ is the optimum impedance for optimum power and optimum SNR respectively, $\underline{Z}_{Ant.}$ curve of Antenna impedance. In [5], Lindenmeier concluded that as the antenna impedance frequency points (like f_1, f_2, f_3 shown in Figure 1.21) lies inside the boundary SNR circles, then no matching network is needed, and the antenna can directly be connected to the FET. Otherwise, a matching network should be optimized in case of antenna impedance frequency points outside the SNR boundary circles.

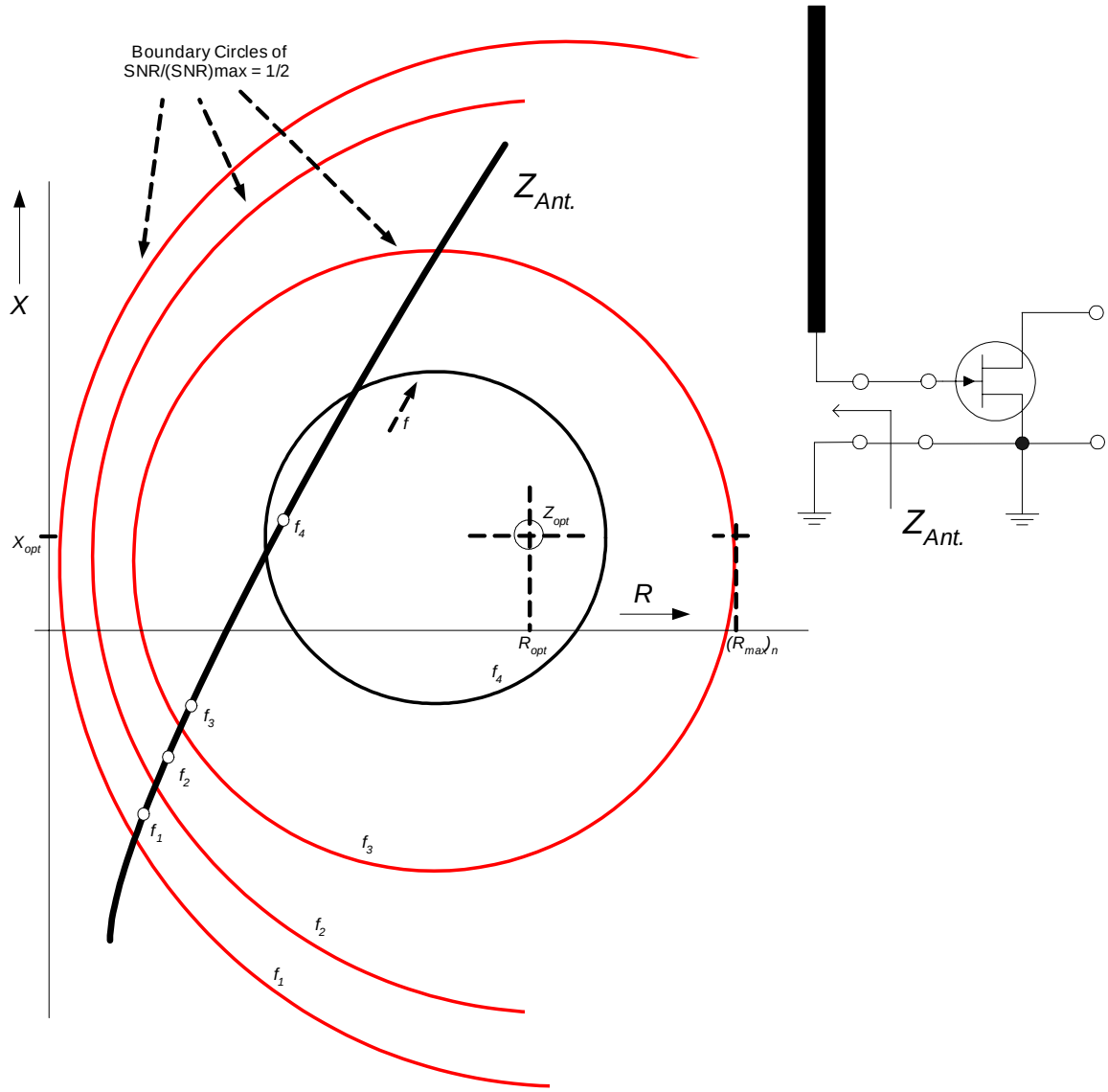

Figure 1.21: Antenna impedance Z_A curve design characteristics directly connected to FET Transistor

In the presented work, a general design examples has been considered based on the possible three typical types of vehicles windscreen antenna impedances measured in the FM range as shown in Figure 1.22, which achieves the broad band design requirements explained before in case of using FET. The design examples will be discussed in detail in Chapter 2.

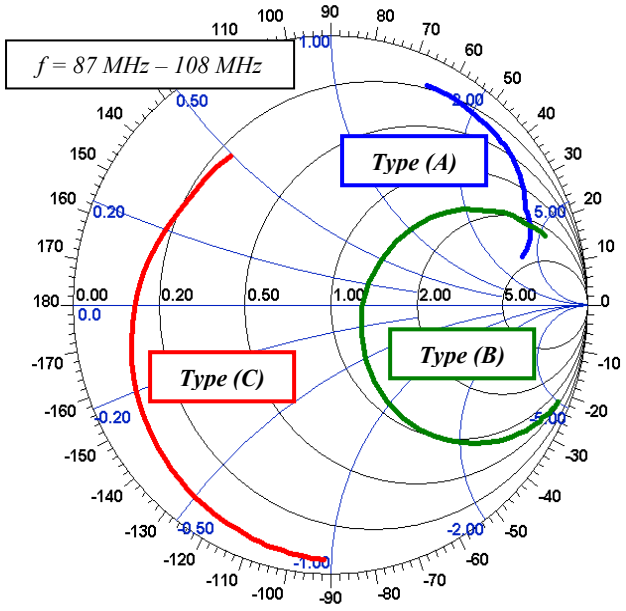

Figure 1.22: Typical Three Possible Antenna Impedances Measured in the FM Range

Noise Figure Measurement of Active Antenna Amplifiers

The loaded two-port network amplifier noise figure is

$$F[dB] = 10 \cdot \log_{10}\left[\frac{(S/N)_Q}{(S/N)_L}\right] = 10 \cdot \log\left[\frac{U_{r,A}^2}{kT_O BR_Q \cdot V}\right] \qquad (1.25)$$

Where,

$U_{r,A}$ …….. the effective value of the output noise voltage [V]
k ……. Boltzmann constant (1.38×10^{-23}W/K)
T_O …. Reference Temperature [Kelvin] (300^{o}K)
B … Measurement Bandwidth [Hz] (*120 KHz in case of FM measurements*)
R_Q source resistance at the input port 0-0/ port [Ohm]
V …. Amplifier power amplification factor

Practically the active antenna amplifier amplification is frequency dependent, and consequently, equation 1.24 that will be measured is modified to be

$$F[dB] = 10 \cdot \log_{10}\left[\frac{(S/N)_Q}{(S/N)_L}\right] = 10 \cdot \log\left[\frac{U_{r,A}^2(f)}{kT_O BR_Q \cdot V(f)}\right] \tag{1.26}$$

One possible measurement setup to measure the noise figure F[dB] is shown in Figure 1.22.

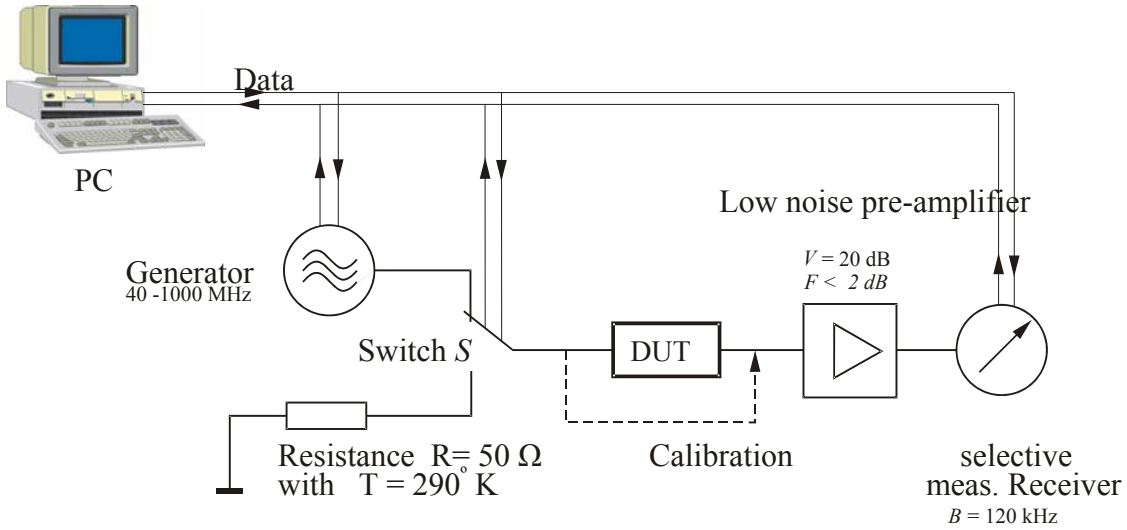

Figure 1.22: Noise Figure Measurement Block Diagram

1.4.3 Third Order Intermodulation Distortion In Transistor Amplifiers

Intermodulation distortion is another type of noise that is generated in a transistor or the active device as a function of the input signals [49]. Detailed theory and analysis has been presented in [10], [13], [18], [46] and [47], which will not be repeated here. Figure 1.23 summarizes the amplifier third order intermodulation distortion concept, whereas the amplifier nonlinearity generates unwanted intermodulation frequencies $2f_2 - f_1$ and $2f_1-f_2$ at the amplifier output, so the amplifier design should meet a high value of the a_{k3} separation. The harmonics are $n{\cdot}f_1$ and $m{\cdot}f_2$, $n,m \in \Re$ (the real numbers domain).

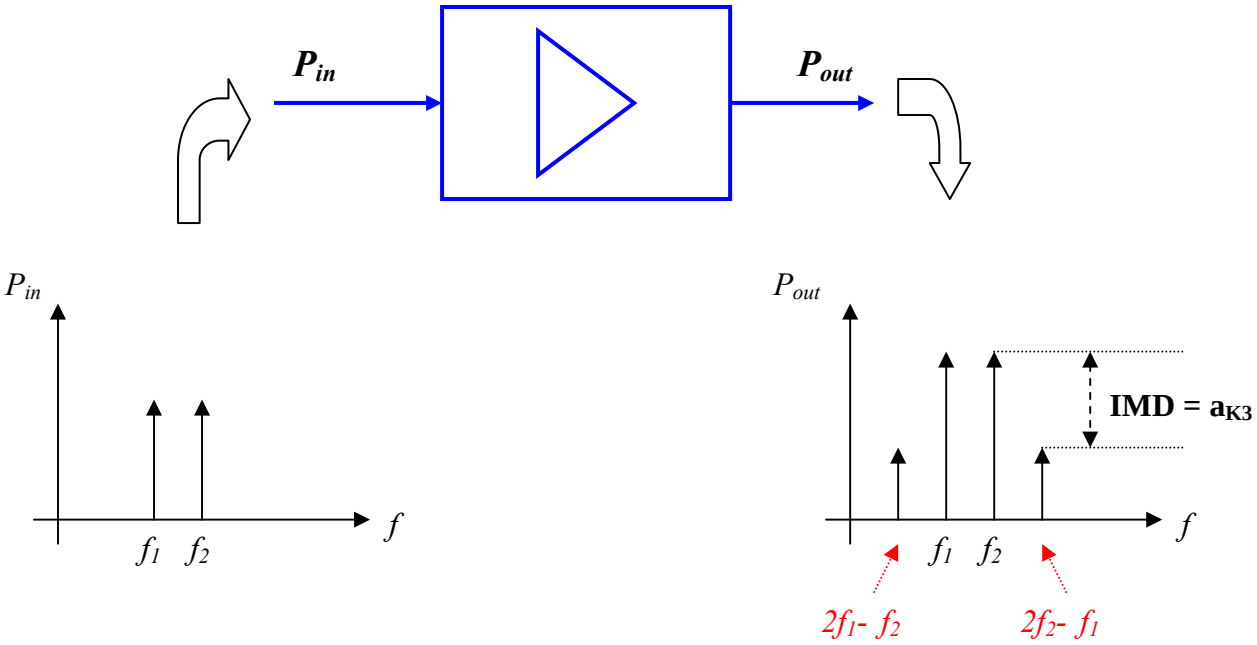

Figure 1.23: Amplifier Third Order Intermodulation Distortion

In the present work, a research evaluation will be presented of different FET source follower cell third order intermodulation distortion for FM applications. The evaluation will depend on simulations and measurements of different amplifier cells realized in the laboratory of the High Frequency Institute at the University of der Bundeswehr Munich as will be presented in the next sections. Figure 1.24 shows the measurement setup for observing the intermodulation distortion separation (denoted IMD = a_{K3}). The difference between the desired and undesired power level (in dBm) at the output port is a_{K3} in dB; that is,

$$a_{K3}[dB] = P_{out}(f_2)[dBm] - P_{out}(2f_2 - f_1)[dBm] \qquad (1.27)$$

Equation (1.27) will be used for evaluating the different amplifier cells intermodulation distortion.

Measurement Setup of Active Antenna Amplifiers Intermodulation Distortion

Figure 1.24 shows the measurement setup used in the lab for evaluating the amplifier intermodulation distortion.

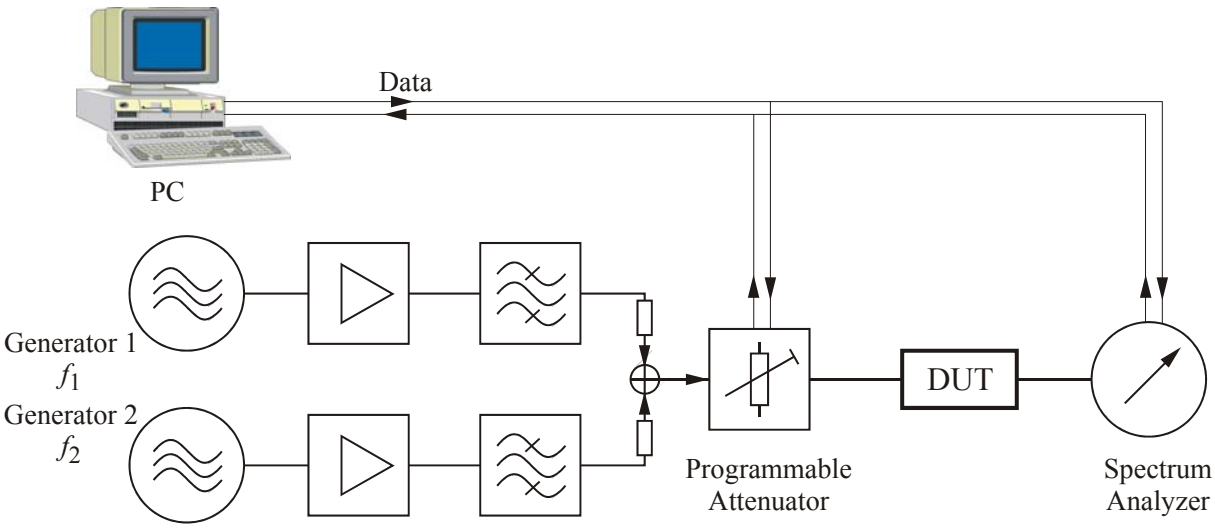

Figure 1.24: Measurement setup of Intermodulation Distortion of a FET Amplifier (DUT)

III. Trade-off between Quality of JFET, HEMT and GaAs FET Follower Cells for FM Active Receiving Antenna's Applications

INTRODUCTION

Though active antenna amplifiers can be realized with any three-terminal transistor devices, the active antenna developed in this work is based on the GaAs FET (CLY2 from TriQuint) transistors due to their better intermodulation distortion and noise figure performances [13],[20] and [33]. This work considered both junction field effect transistors JFETs (SST310 from Philips) and the high electron mobility transistors HEMTs(NE32400 from NEC) for testing their possible use, and what is optimum for vehicles active antenna requirements and why is the answer of this section. Active antenna amplifiers with different semiconductor devices are designed, fabricated, and compared to show the final universal nature of the design subsequent procedures. The goal of this section is to show the general steps done for testing different follower cell amplifiers based JFET, HEMT and GaAs FET to be used in Active antennas. Such a general research procedure allows the designer to arrive to a suitable decision regarding the optimum active device to be used for achieving low noise and high linearity active antenna amplifiers. The design evaluation through this work in general is based on the German industrial requirements according to the standards of the German Association of the Automative Industry **VDA** (**Verband der Automobilindustrie**)[71], whereas for example, in case of an active antenna amplifier nonlinear performance, a minimum intermodulation distortion separation (denoted a_{K3}[dB] as will be later explained) of 65dB at the circuit output voltage of 100[dBμV] should be achieved with a total circuit noise figure lower than or equal to 6.3dB(NF≤ 6.3[dB] as will be derived in Chapter 2, section 2.2.2-Figure 2.8).

1.5 Source Follower Cell Noise Figure and Third Order Intermodulation Performances

Consider the source follower general circuit cell shown in Figure 1.25 that will be used in the simulation and design study in this work. In this figure, R_{source} represents the antenna real part source impedance. R_{Load} represents the receiver input resistance (In the following, primarily study, the 50 Ohm system will used which means that $R_{source} = R_{Load} = 50$[Ohm], and a general complex source antenna impedance will be extended in Chapter 2).

The cell noise figure and power gain will be simulated in the FM range (87MHz – 108 MHz) and measured in different cases. The generator and load resistances variation effects on the follower cell third order intermodulation performance will be studied by varying the generator resistance once, and for the effect of load variation, a series resistance connected with the receiver $R_{L\text{-}series}$ is added to be varied. R_{Source} can be selected according to the necessary operating point. In the following study, for the allowable requirement of different FET power consumption [33], [53], a bias design value of $I_{DS} \approx 50[mA]$ is chosen for all cells based JFET, HEMT and GaAs FET respectively.

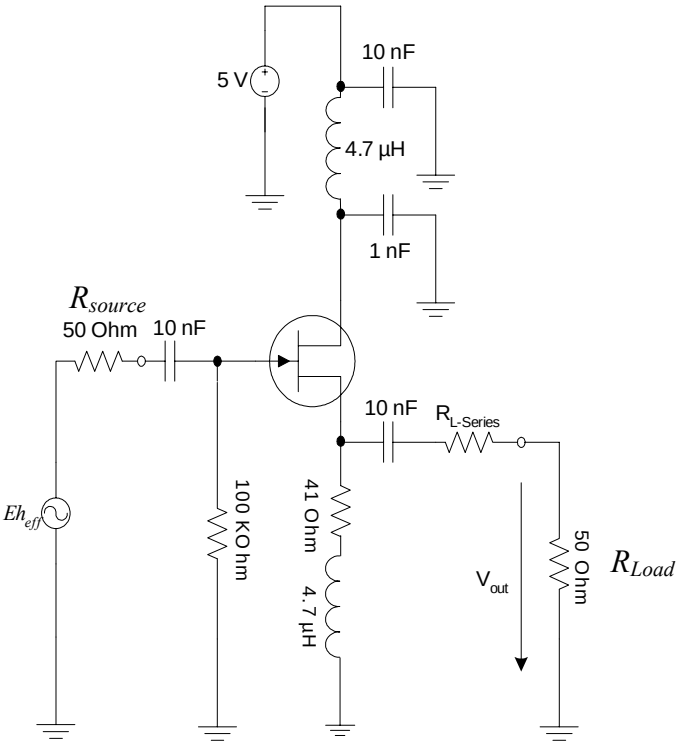

Figure 1.25: General FET Source Follower Cell

1.5.1 Noise Figure and Power Gain Performances

Figures 1.26, and 1.27 shows the simulation comparison results of the different selected transistors in the 50 Ohm system at a selected drain current of $I_{DS} \approx 50[mA]$. It is clear that the JFET transistor suffers from the high noise figure (NF[dB]@100MHz ≈ 2 dB without the circuit components losses, but with low quality RF coils of typical quality factor Q = 10(the NF gets higher and reaches 2.5dB) in addition to the JFET low power gain in the FM range (S_{21}[dB]@100MHz ≈ 0.5dB dB) compared to both HEMT and GaAs FET transistors.

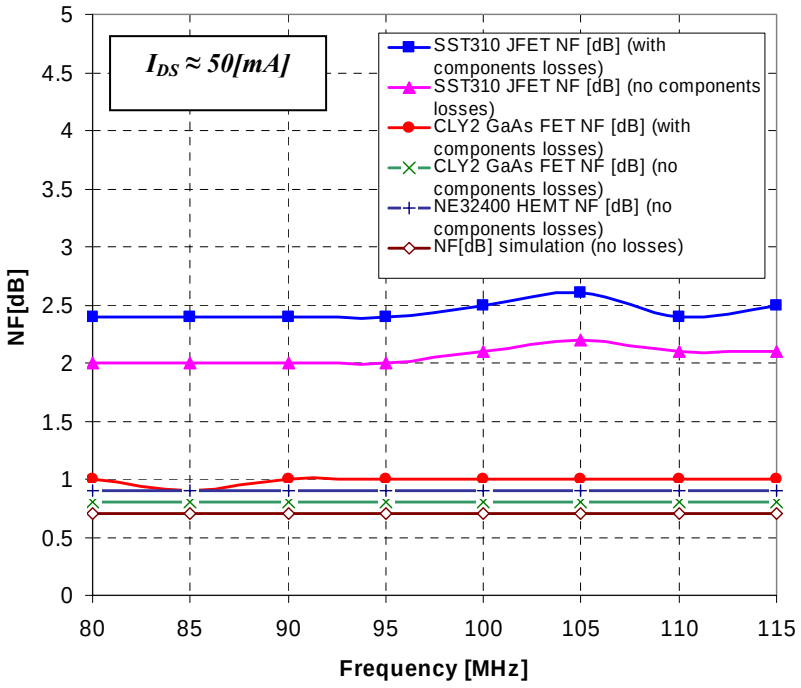

Figure 1.26: Simulated Noise Figure Performance of the JFET, HEMT and GaAs FET Follower Cells in a 50 Ohm System

However for the JFET high noise figure, it can be reduced to ~1.5dB with a parallel connection (Gate to Gate, Drain to Drain and Source to Source) of the same JFET transistor.

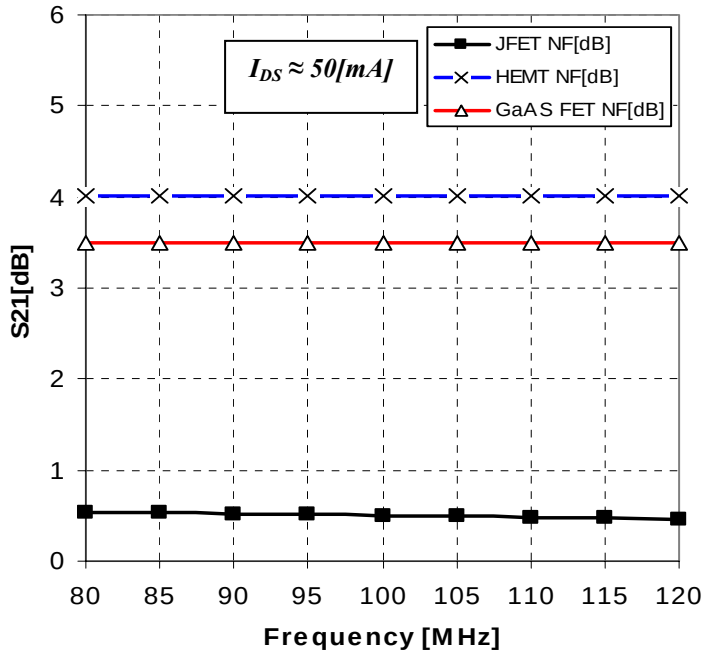

Figure 1.27: Simulated Power Gain Performance of the JFET, HEMT and GaAs FET Follower Cells in a 50 Ohm System

Finally, it should be noted that the HEMT has a slight better power gain and low noise figure (S_{21}[dB]@100MHz ≈ 4dB dB and NF[dB]@100MHz ≈ 0.9dB assuming components losses) performances compared to the GaAs FET transistor(S_{21}[dB]@100MHz ≈ 3.5dB dB and NF[dB]@100MHz ≈ 1 dB with taking the circuit components losses into account).

1.5.2 The Follower Cell Third Order Intermodulation Performance

The third order intermodulation behaviour is evaluated using Equation 1.27 presented before for computing a_{K3}[dB]. Figures 1.28, compares the simulation results of the intermodulations distortion separation $a_{K3}[dB]$ versus the circuit output voltage $Vout[dB\mu V]$ for the different selected transistors in a 50 Ohm system at the selected drain current of $I_{DS} \approx 50[mA]$. It is quite interesting to conclude that the JFET and GaAs FET share the same intermodulation distortion behaviour *(a_{K3}*[dB]@V_{out}=100$dB\mu V$ ≈ 84.5dB*)* and in addition better than the HEMT transistor *(a_{K3}*[dB]@V_{out}=100$dB\mu V$ ≈ 80.2dB*)*.

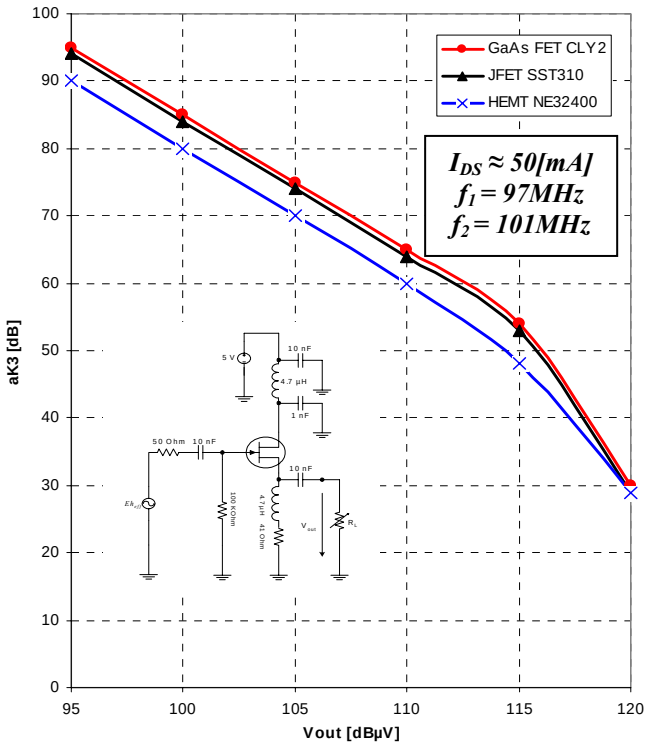

Figure 1.28: Simulated Third Order Intermodulation Distortion Performance of the JFET, HEMT and GaAs FET Follower Cells in a 5OhmSystem

1.5.2.1 Effect of Generator Resistance on the Follower Cell Third Order Intermodulation Distortion Performance

For active antennas applications, the amplifier cell should have a constant third order intermodulation distortion behaviour independent on both source and load impedance possible variations (the variation is simply a representation of variable antenna impedance real part). The following Figure summarizes the simulation results done for the different selected transistors, which helps to select the optimum transistor for vehicles FM active antenna application. In Figure 1.29, a JFET intermodulation distortion performance degradation is noticed as the source resistance varied which declares that the JFET *has no stable high input impedance*.

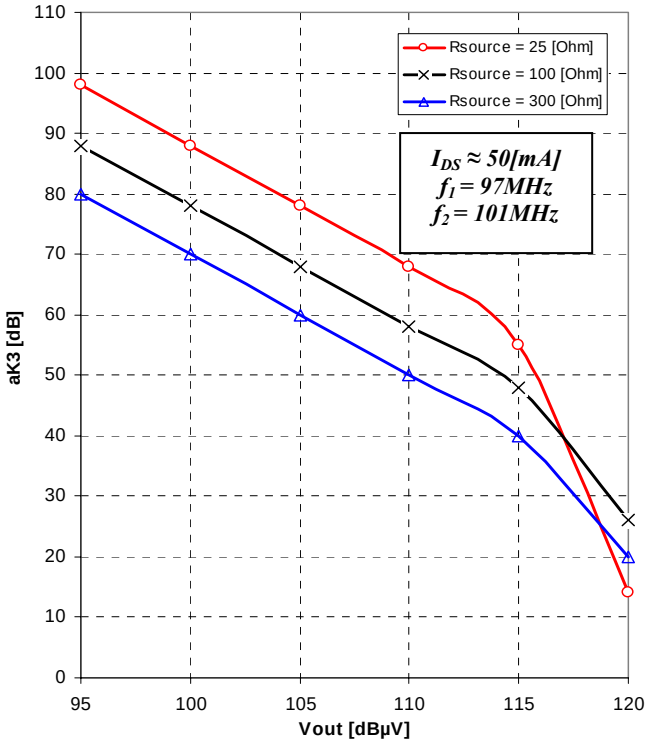

Figure 1.29: JFET Cell Simulated Distortion Performance at different variable source Resistance

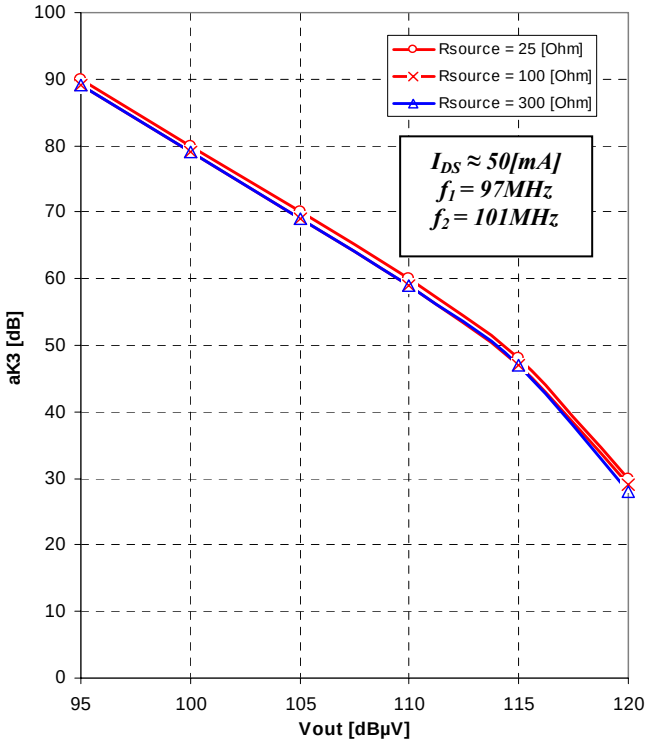

Figure 1.30: HEMT Cell Simulated Distortion Performance at different variable source Resistance

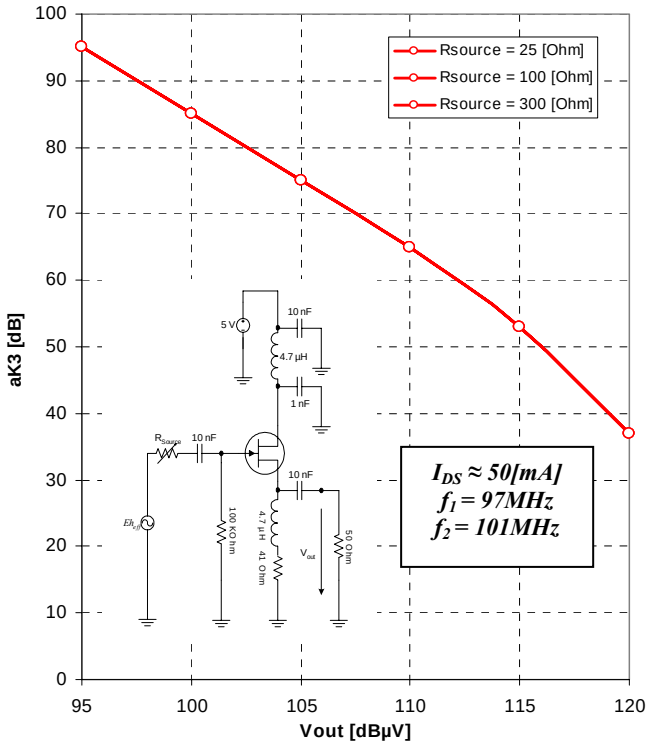

Figure 1.31: GaAs FET Cell Simulated Distortion Performance at different variable source Resistance

From Figures 1.30 and 1.31, it is clear that the HEMT and GaAs FET intermodulation distortion is approximately constant and independent on the source impedance possible variations. Consequently, the HEMT and GaAs FET can be used for FM active antennas applications, however since the GaAs FET has a better intermodulation distortion behaviour, one can conclude that the GaAs FET is the optimum transistor for FM active antennas applications. In the next sub-section, a study will show the effect of variable load impedance on the GaAs FET intermodulation distortion behaviour.

1.5.2.2 Effect of Load Resistance variation on the GaAs FET Follower Cell Third Order Intermodulation Distortion Performance

Referring to the follower cell in Figure 1.25, for $R_S = R_L = 50$Ohm system, a series resistance $R_{L\text{-series}}$ is connected between the GaAs FET source terminal and load for maximum power transfer. Finding an optimum value of $R_{L\text{-series}}$ that should be chosen so that not to degrade the cell intermodulation distortion behaviour begins by investigating its variation and then evaluating the Follower cell intermodulation distortion. An optimum value of 50 Ohm is reached which kept the GaAs FET third order intermodulation distortion approximately constant $(a_{K3}[\text{dB}]@V_{out}=100dB\mu V \approx 80\text{dB}$ compared to the 84dB reached in Figure 1.31. The results are shown in Figure 1.32 investigation, whereas the $R_{L\text{-series}}$ is varied from 50-600Ω. The increase of $R_{L\text{-series}}$ far away from the optimum value (50Ohm) results in the circuit power gain reduction, which in turn reduces the total circuit intermodulation separation a_{K3}.

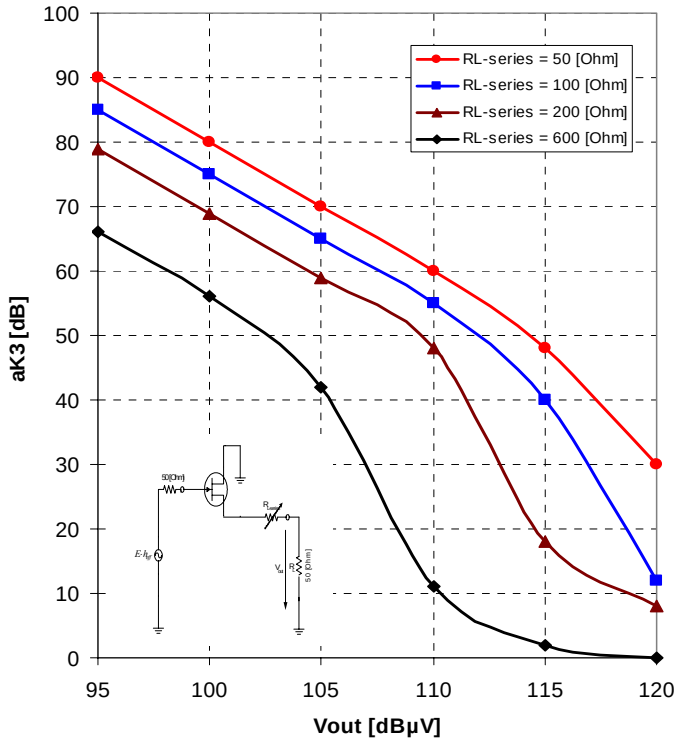

Figure 1.32: GaAs FET Follower Cell Simulated Distortion Performance for Different Load Series Resistance $R_{L\text{-series}}$
(It should be remarked here, that the reduction of a_{K3} is a result of the reduction of the circuit power gain S_{21}).

An important investigation done for the design purposes that will be introduced in chapter 2, is the effect of load resistance R_L variation on the whole Follower cell intermodulation distortion within the FM band. For a source resistance of R_S = 50 Ohm and $R_{L\text{-series}}$ = Zero Ohm, the value of R_L is varied from 50Ω-5KΩ, and then the third order intermodulation separation a_{K3} is evaluated via simulations as shown Figure 1.33.

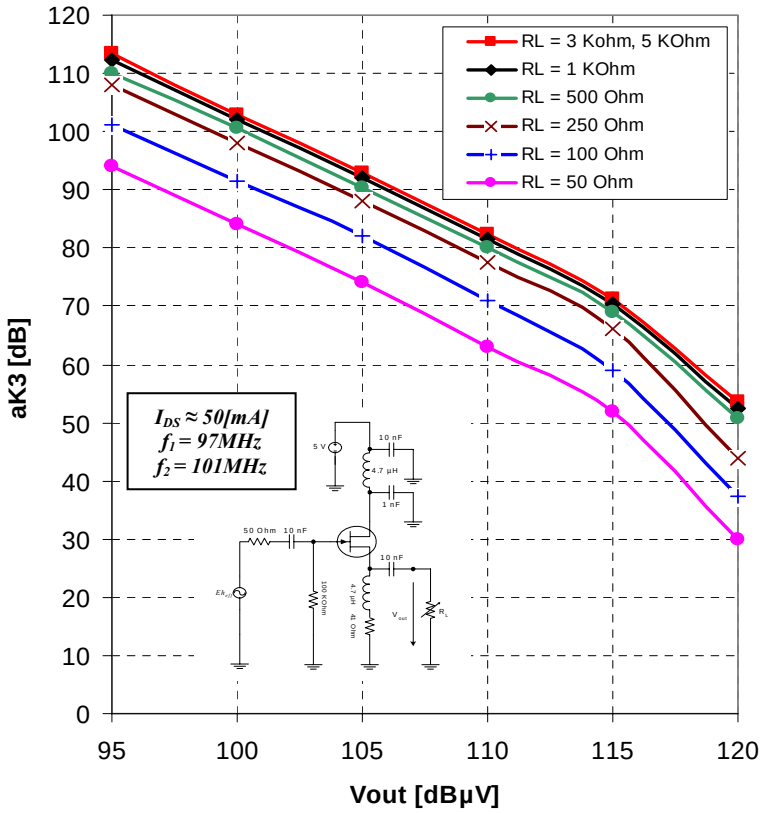

Figure 1.33: Simulation of GaAs FET Follower Cell Distortion Performance for Variable Load Resistance R_L

Figure 1.33, shows that the intermodulation distortion separation reached a maximum value of 103dB for an output voltage of 100dBµV at R_L = 5KOhm. It should be noted that load resistance R_L in principle functions as a feedback for the source follower, and according to the investigation done in Figure 1.33, one can conclude that the feedback impedance should be high enough for maximum intermodulation separation, which is the basic design requirement in active antenna amplifiers. This generally means that when the follower cell is loaded by a passive network (lossless filter for example for selecting the FM band of interest), the passive network should fulfil the high input impedance requirement in the FM band of interest to guarantee a maximum third order intermodulation separation. Such a passive network can be a T-filter structure which fulfils the high input impedance design requirement for example as in [20] proposed design. Design examples in chapter two, will show such a design concept based T-filter structure and other possible filter structures. The different structures effect on the amplifier intermodulation distortion will be studied in detail through Chapter 2.

1.5.2.3 Effect of Drain Current Bias on the Follower Cell Third Order Intermodulation Distortion Performance

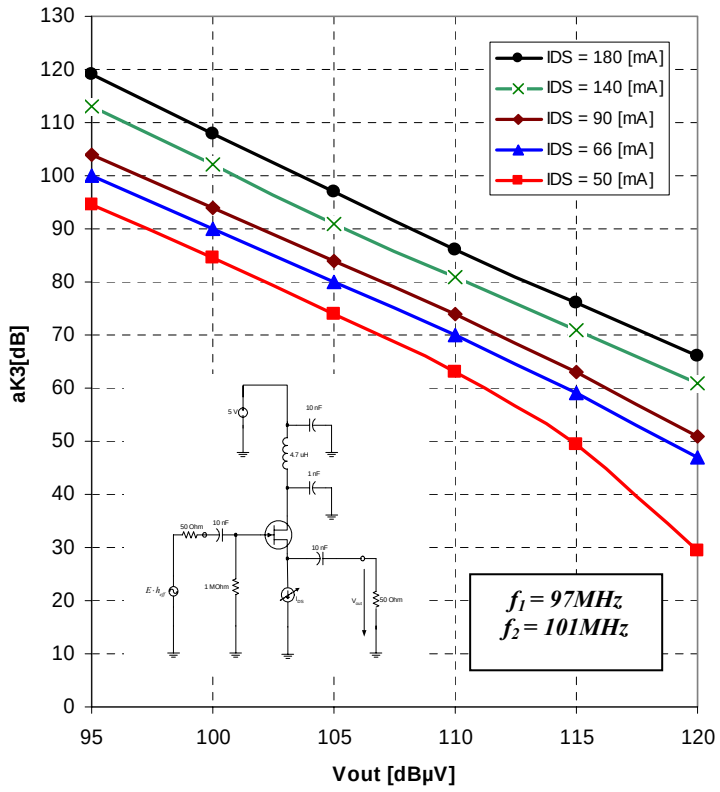

Figure 1.34: GaAs FET Follower Cell Simulated Distortion Performance at different Bias Current

Figure 1.34 shows that the follower cell introduces a considerable enhancement of the intermodulation distortion separation for higher currents, whereas a variable current source value is varied for the necessary simulation requirement ; however, the transistor limits the follower circuit performance power consumption [14], [18]. Consequently, a drain current of $I_{DS} \approx 50$ [mA] (at which a_{K3}[dB] ≈ 84.5[dB]) will be chosen for the GaAs FET follower cell design in the present work. The follower circuit shown in Figure 1.20 has been realized for $R_{Lseries}$ = Zero Ω and R_L = 50 Ω. Figure 1.35 shows the cell measured performance in the laboratory. A good agreement between the measurements and simulation is achieved (~ 4 dB difference).

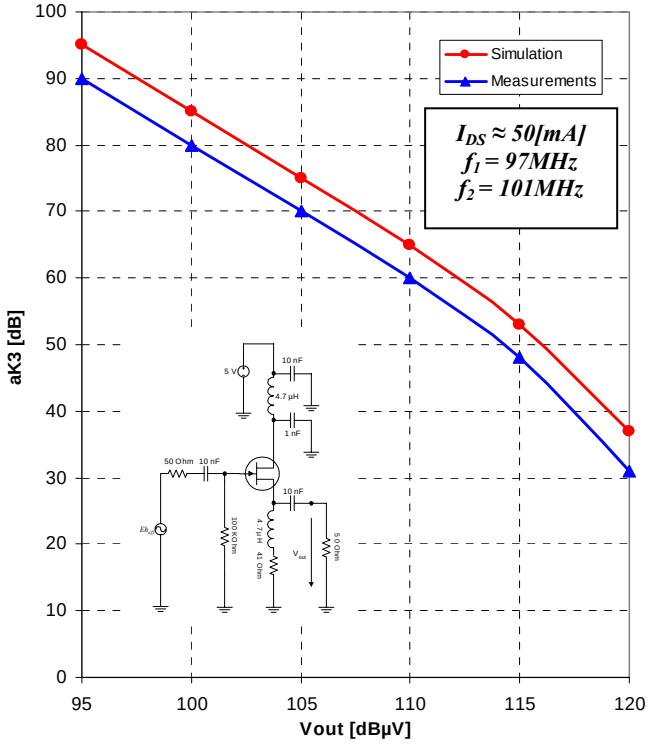

Figure 1.35: Simulation and Measurements of GaAs FET Follower Cell Distortion Performance

The previous presented study illustrated the general different factors influencing the FET follower cell performance *(Noise, Power Gain and Third Order Intermodulation Distortion),* and it can be considered as a general study procedure for any suggested transistor in the future. According to the introduction introduced in this chapter regarding the industrial requirements according to the **VDA** standards, the JFET may look to achieve the **VDA** requirements, whereas NF < 6.3dB (a 2.5-3dB as in Figure 1.26) and a_{K3} > 65dB (more than 80 dB can be reached as shown in Figure 1.28) in addition to its cheap price compared to the GaAs FET. One should importantly recognise that from figure 1.29, a serious problem appeared with JFET transistors, which is the non-stable intermodulation performance with variable source resistance. This shows that the JFET has no stable input impedance if an antenna connected directly to it. Unfortunately, the no-stable JFET performance limits its application in FM active antennas in general. But regarding the GaAs FET as shown in Figure 1.31, it enjoys a constant intermodulation performance with variable source impedance. This reveals a constant intermodulation performance if an antenna connected directly to the GaAs FET.

Thus apart from the different transistors JFET market cheap prices or even the high prices of the GaAs FET transistors, *a scientific conclusion can be reached at this stage*, *that the GaAs FET is the optimum transistor for FM active receiving antennas achieving the industrial requirements* suggested by the **VDA** [71] since it enjoys a stable performance in case of variable source and/or load resistance (a variable source impedance will be considered in Chapter 2).

In the following chapter, a new concept for FM active antenna amplifier will be introduced. The design will be based on the reached conclusion, i.e. using the GaAs FET. However, the possible different other available transistors (e.g. JFET, Bipolar) will be considered in addition to show their possible use in the FM active antenna amplifiers.

Chapter 2

The New Low Noise - High Linearity FM Active Antenna Amplifier

INTRODUCTION

As introduced in chapter one, the active antenna in its minimum configuration consists of a passive antenna, typically, a rod or a dipole and an integrated amplifying device. In evaluating and analyzing the output of these antennas, there are different components to consider like the transistor noise contribution, the amplified noise generated by external sources (man-made or galactic), and the signal voltage at the operating frequency….etc.

Generally, when designing an active antenna amplifier for a specific application, there are many constraints to be met and decisions to be made. These include gain, bandwidth, impedance levels, feedback, stability, cost, and, as expected, noise. The amplifier designer can elect one of two paths. Typically he worries about the gain and bandwidth first and later in the design process he checks for noise. The present work design and analysis philosophy strongly urge the reverse approach, with initial emphasis on noise performance. First, the input stage is considered (as done in Chapter 1), discrete or IC, bipolar or FET. The operating point is then selected. If preliminary analysis shows that the noise specification can be met, a circuit configuration can be selected and the amplifier designed to meet the remainder of the circuit requirements. A critical noise specification can be one of the most serious limiting factors in design; it is best to meet the most stringent requirement head-on. This chapter presents the new *Active Antenna Amplifier* design concept and analysis in view of the above stated evaluation points and according to the standards of the German Association of the Automotive Industry **VDA** (Verband der Automobilindustrie)[71] as stated earlier in Chapter one. Through this chapter, the primary goals will be focused on calculations and numerical evaluations of the new amplifier Noise Figure, power gain, SNR…etc. performances based on the **VDA** standards to show how close or far the new amplifier performance from these industrial standards. A design condition(s) for the new amplifier will be derived.

The Follower cell stability investigations will be discussed in detail by different measurements and new suggested solutions. Finally, the amplifier Noise, Linearity and stability will be discussed by simulated and measured realized example(s) in the laboratory to show its general performance in the FM range.

2.1 Block Diagram Description of the new Amplifier

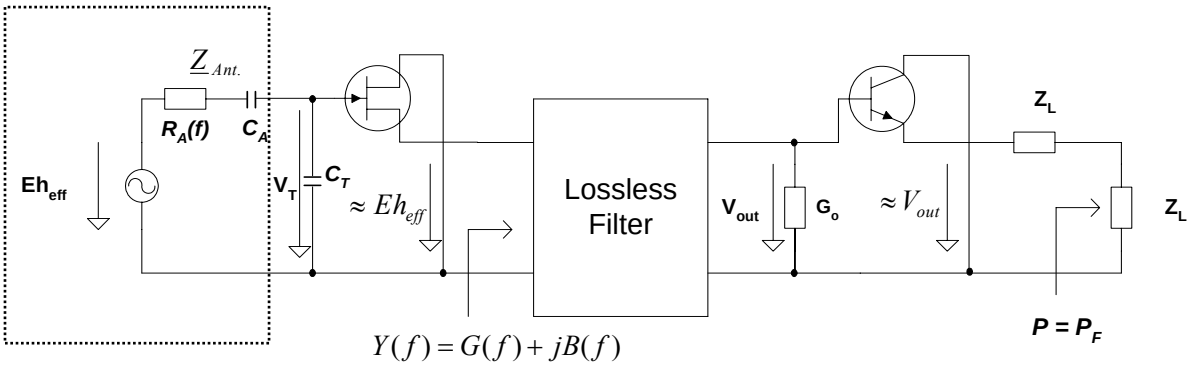

Figure 2.1: The New FM Active Antenna Amplifier

Figure 2.1 illustrates the new RF amplifier circuit diagram. The car windscreen FM antenna is directly connected to the input of a source follower field effect transistor (in the realized examples the will be presented later, the FET will be CLY2 GaAs FET from TriQuint). As shown in this Figure, the antenna acts as a source that feeds the transistor. The electric field strength E generates a voltage (*EMF*) that can be determined from $V_a = E \cdot h_{eff}$. Assume that the FM antenna has a capacitance C_A, while the transistor has an input capacitance C_T.
These two capacitances form a capacitive voltage divider. Generally, the signal voltage that drives the GaAs FET transistor is then

$$\underline{V}_T = \frac{\left(1/\omega C_T\right)}{\underline{Z}_{Ant.} + \left(1/\omega C_T\right)} \cdot E \cdot h_{eff} \tag{2.1}$$

Where $\underline{Z}_{Ant.} = R_A + jX_A$ is the antenna impedance (with X_A resulting from C_A and with negligible value of R_A).

For electrically short car window antennas, the voltage $\underline{V}_T$ is nearly independent of frequency. Therefore, the active antenna presented here has a wide bandwidth [2]. The gain-bandwidth product of such a device can be computed from the performance of the field effect transistor in Figure 2.1. It will reproduce at the output the input voltage as long as its cut-off frequency is high enough.

In Figure 2.1, Additional reactance's (Lossless Filter) is used to intentionally limit the bandwidth of the active antenna and to be optimized according to the desired FM range. Finally, the output signal from the filter is fed to a buffer Bipolar amplifier (in the presented design, the bipolar BFG196 from Siemens will be used) to allow connecting similar receiver impedance at its emitter terminal, so simply a matching for maximum power transfer can be achieved with the desired receiver load. As long as the noise voltage generated by the transistor at the amplifier output is less than the wide band noise picked up by the antenna, the system is capable of supplying the same signal-to-noise ratio as an optimized passive antenna for the same specific frequency. In the following section, the noise performance of the new design based on the **VDA** standards [71] will be evaluated.

2.2 Noise Evaluation of the new Active Antenna Amplifier

As a fixture in RF and microwave receivers, the low-noise amplifier (LNA): provides an impedance match to the antenna to enhance signal reception, amplifies the incident RF signal before it encounters higher noise receiver circuitry, and helps isolate the antenna from local oscillator tones and unwanted mixing products generated in the receiver chain. Being commonly-employed and fulfilling requirements in wireless systems that are difficult to circumvent with cars window architectural innovations, Active Antenna LNAs make for an interesting study from a technology perspective. The realization of an active antenna LNA pushes fundamental limits in device speed, noise, and power consumption in ways that can be addressed in only a very limited fashion by circuit techniques, and thus the design of these amplifiers yields an interesting point of comparison between semiconductor processes as well as valuable insight into the continued development of active antennas RF technologies. The specific goals for an active antenna LNA will always be application dependent, but the design focus in future active antenna wireless systems will shift toward extracting the maximum capability from the RF link in terms of bandwidth, dynamic range, and power consumption. A key concept in next-generation RF links will be adaptive performance; in the context of an active antenna LNA, the question is weather power can be trade off for sensitivity and gain in a manner that does not unduly compromise system operation. Performance should be evaluated in terms of the best possible noise figure that can be achieved while reasonable gain, linearity, isolation, power dissipation, and impedance matching are all maintained. The discussion in this section focuses primarily on the new active antenna amplifier noise compared to the equivalent passive rod antenna because the noise is the more fundamental problem in that it cannot be circumvented with circuit techniques or added power consumption. The noise evaluation will be built according to the German Association of the Automotive Industry **VDA** (Verband der Automobileindustrie).

2.2.1 Noise Evaluation of Active Antenna Compared to a Reference Passive Antenna

(A) Passive Antenna Connected Directly to the Receiver

In this section, an evaluation of the additional noise figure added by the receiver will be presented. Consider first the case of a passive antenna connected directly to the receiver input. According to the German Association of the Automotive Industry **VDA**, the noise voltage level at the receiver input should not be greater than -11dBμV measured in a noise bandwidth of 120 KHz when it is directly connected to the passive antenna structure[71]. Referring to Figure 2.2, define the receiver equivalent noise voltage to be $\overline{U_{RE}^2}$ and the antenna equivalent noise voltage generated from the antenna real part to be $\overline{U_{RA}^2}$ (the antenna reactive part is neglected since it is not responsible of any noise increase assuming ideal antenna reactive components).

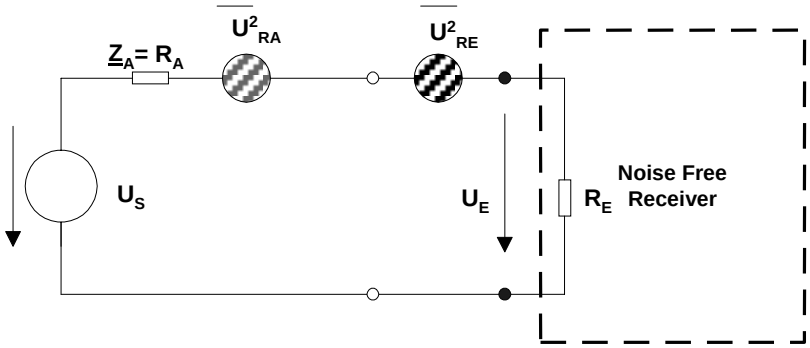

Figure 2.2: Noise Evaluation of a passive antenna structure connected to the receiver

The acceptable noise voltage at the receiver input U_E = -11dBμV, from which we have $U_E = 10^{\frac{U_E dB\mu V}{20}} [Volt] \rightarrow U_E = 2.818 \times 10^{-7} V$. To evaluate the receiver additional noise figure, define F_E to be the receiver noise figure, and F_{ZE} to be the receiver additional noise figurer. From [8],[13], the relation between the receiver noise figure F_E and the additional noise figure F_{ZE} is

$$F_E = 1 + F_{ZE} \tag{2.2}$$

From Figure 2.2, in a matched system $R_A = R_E = Z_o$, the receiver additional noise figure [8] can directly be evaluated to be

$$F_{ZE} = \frac{[2 \cdot U_E]^2}{4 \cdot k \cdot T_o \cdot B \cdot Z_o} \tag{2.3}$$

Where,

k is Boltzmann's constatnt (1.38×10^{-23} J/K), T_o is the standard effective temperature in Kelvin, B is noise bandwidth in Hertz and Z_o is the reference impedance of 50 Ohm.

Assuming a reference noise temperature of 300K, let us determine the receiver additional noise factor by substituting into Equation 2.3, we have $F_{ZE} = 3.31 \rightarrow F_{ZE}[dB] = 5.2$. This additional receiver noise figure F_{ZE} is the standard value in case of a passive antenna structure that will be taken as a reference for the comparison with the new active antenna amplifier design.

(B) Active Antenna Circuit Connected to the Receiver

Before evaluating the new active antenna amplifier presented in Figure 2.1, let us calculate the tolerable additional noise figure according to the **VDA** of the receiver when it is connected to an active amplifier as shown in Figure 2.3.

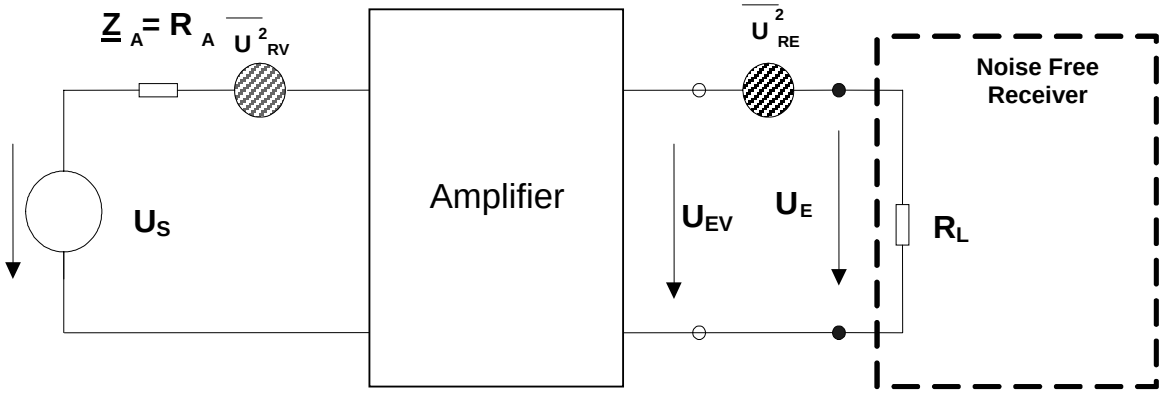

Figure 2.3: Noise Evaluation of an active antenna structure connected to the receiver

Referring to Figure 2.3, Assume a matching between the receiver input impedance and the amplifier output and according to the **VDA standards** [71], the permissible noise voltage value at the receiver input is counted to be -7.5dBµV. Define the receiver noise voltage in case of FET connection as shown above to be $U_{EV,}$ Then the calculation of the permissible receiver noise figure proceeds as follows, $U_{EV}\left[dB\mu V\right] = -7.5 \rightarrow U_{EV} = 4.217 \times 10^{-7} Volt$ at $Z_O = 50$ [Ohm]. Define the additional noise figure in case of connecting an amplifier as shown in Figure 2.2 to be F_{ZVt}, then using Equation (2.3), one can evaluate the additional noise figure in this case to be $F_{ZVt} = (2 \cdot U_{EV})^2 / 4 \cdot k \cdot T_o \cdot B \cdot Z_O = 7.41 \rightarrow F_{Vt}\left[dB\right] = 8.7$. This additional receiver noise factor F_{ZVt} is the standard tolerable value in case of an active antenna connected to the receiver.

Now the noise performance of the suggested new design (Figure 2.1) will be evaluated in view of the permissible standards assigned by the **VDA** [71].

2.2.2 Noise Evaluation of the new Active Antenna design

Consider the circuit diagram shown in Figure 2.4, whereas the lossless filter to be designed and optimized has been replaced by an ideal transformer of turns ratio 1:Ü, so that to extract the linear performance of the whole circuit, thus facilitating to set a condition(s) on how should the filter voltage gain be optimized in combination with an arbitrary antenna impedance to achieve the lowest noise figure performance. From Equation 2.3, one can conclude that the additional noise figure is proportional to the noise voltage, thus it can be a representative for the antenna, and amplifier and receiver input voltages. Consequently the additional noise figure will be used to represent the circuit different noise sources as shown in Figure 2.4.

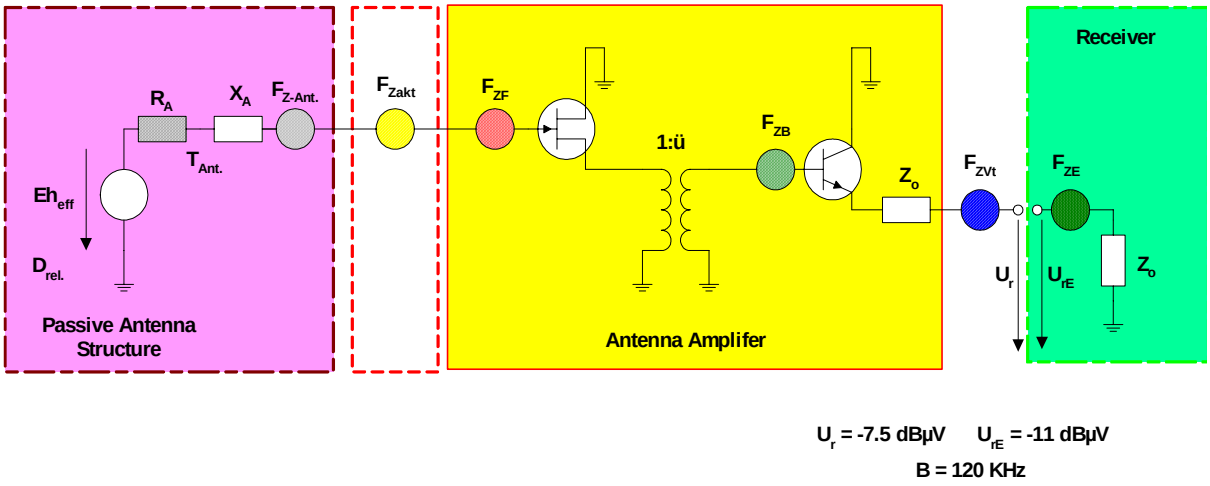

Figure 2.4: Noise Evaluation of the New Active Antenna Amplifier

In the following discussion, the term *noise figure* is equivalent to the *total noise figure*; whereas the term *additional noise figure will be announced in advance as* F_Z (the subscript Z in the German language is a representation for the word additional, then when we write for example F_{ZK}, the Z starting subscript means additional, thus F_{ZK} means; the additional noise figure related to the source or symbol K).
(Note that: *Total Noise Figure(OR equivalently Noise Figure) = 1 + Additional Noise Figure* [8]).

The additional noise figure representation of a noise voltage can be re-explained as follows:
Assuming that a noisy resistance additional noise figure is *F*, then the average noise voltage can be expressed by [13],[47]

$$\overline{u}_n^2 = 4 \cdot k \cdot T_o \cdot Z_o \cdot B \cdot F_{Z_O} \tag{2.4}$$

Consequently, the additional noise figure F_{Zo} is proportional to the noise voltage u_n which means that F_{Zo} can be a representative of the noise voltage.
In Figure 2.4, the antenna real and imaginary parts are labelled as R_A and X_A respectively. It is known that the antenna real part is responsible of the antenna noise voltage [1], thus there is no noise contribution of the reactive part X_A. Therefore, as shown in the figure, the antenna noise contribution from the real part R_A will be considered. The antenna noise voltage will be represented by the antenna additional noise figure F_{ZAnt}(the same colour as R_A to show that R_A is responsible for the noise voltage expressed by $F_{ZAnt.}$). The antenna relative directivity will be defined to be D_{rel} [8]. Additionally in Figure 2.4, the standard **VDA** effective values of the amplifier and receiver noise voltages are defined to be U_r and U_{RE} respectively.

The subsequent analysis will be based on the low noise GaAs FET used from TriQuint **CLY2** and the low noise bipolar transistor **BFG196** from Siemens. Experimental transistor parameters and values will be substituted to show the real expected noise performance of the new active antenna amplifier under study. As explained before and shown in Figure 2.4, the additional noise figure of the car window antenna passive structure is defined to be $\mathbf{F_{ZAnt}}$, and the active part composed of the antenna amplifier (*composed of the CLY2 GaAs FET, Transformer and the BFG196 Bipolar*) additional noise figure will be defined to be $\mathbf{F_{Zakt}}$. Now, a general mathematical expression will be derived for evaluating the additional noise figure of the proposed active antenna F_{Zakt}.

Define the passive antenna relative real part to be

$$R_{Ar} = \frac{R_A}{Z_o} \tag{2.5}$$

This is the unit-less antenna relative real part in the 50 Ohm system (represented by Z_O, whereas Z_o = 50[Ohm]) will generate an additional noise figure F_{ZA} (in this case $F_{ZAnt.}$ don't hold any more as it is related to the antenna real part R_A[Ohm]), so an expression should first be derived to show the relation between the antenna additional noise figure $F_{ZAnt.}$ generated from R_A[Ohm] and the additional noise figure F_{ZA} generated from the antenna relative real part R_{Ar} which is unit less (it is a ratio between resistances). This is shown in Figure 2.5 which summarizes the additional noise factor at each specific point of the new active antenna amplifier that will be used in the subsequent circuit noise analysis.

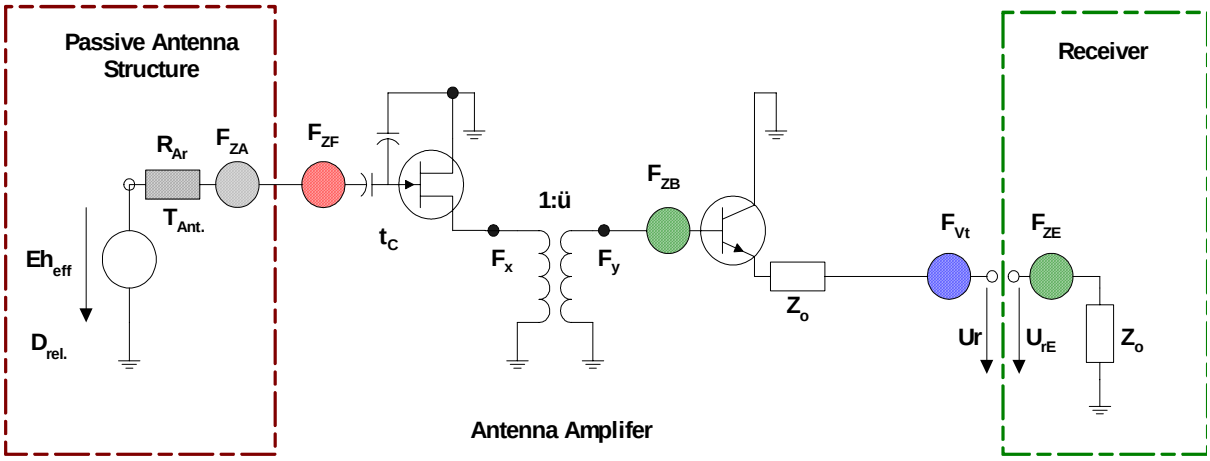

Figure 2.5: Noise Evaluation of the New Active Antenna Amplifier

Define the following: The additional noise figures of GaAs FET and Bipolar transistor to be $\mathbf{F_{ZF}}$ and $\mathbf{F_{ZB}}$ in the 50 Ohm system (or equivalently in the Z_o system, since Z_o= 50 [Ohm]) respectively. Due to the presence of the GaAsFET input capacitances, the FET source voltage is less than the gate voltage by the voltage capacitive coupling factoring $\mathbf{t_C}$, and for simplicity, assume that the Bipolar follower is ideal and its coupling factor is one. The additional noise figure of the antenna amplifier is defined to be $\mathbf{F_{ZVt}}$ whereas the receiver additional noise figure is $\mathbf{F_{ZE}}$. According to Figure 2.5, we have

The antenna noise voltage u_n generated from R_A is[12]

$$u_n = \sqrt{4 \cdot k \cdot T_{Ant.} \cdot B \cdot R_A} \tag{2.6}$$

To derive an expression for the antenna additional noise figure F_{ZA} generated from the antenna relative real part R_{Ar}, one can rewrite the Equation 2.6 as follows (knowing that the antenna additional noise figure is [8], $F_{ZAnt.} = T_{Ant.}/ T_o$)

$$u_n = \sqrt{4 \cdot k \cdot T_{Ant.} \cdot B \cdot R_A} = \sqrt{4 \cdot k \cdot \left(\frac{T_{Ant.}}{T_o} \cdot T_o \right) \cdot B \cdot \left(\frac{R_A}{Z_o} \cdot Z_o \right)}$$

$$= \sqrt{4 \cdot k \cdot T_o B \cdot Z_o \cdot \left(\frac{T_{Ant.}}{T_o} \cdot \frac{R_A}{Z_o} \right)} = \sqrt{4 \cdot k \cdot T_o B \cdot Z_o \cdot \left(\frac{T_{Ant.}}{T_o} \cdot R_{Ar} \right)} \tag{2.7}$$

$$= \sqrt{4 \cdot k \cdot T_o B \cdot Z_o \cdot \left(F_{ZAnt.} \cdot R_{Ar} \right)}$$

$$= \sqrt{4 \cdot k \cdot T_o B \cdot Z_o \cdot \left(F_{ZA} \right)}$$

From Equation 2.7, the additional noise factor F_{ZA} can be easily defined to be

$$F_{ZA} = \frac{T_{Ant.}}{T_o} \cdot R_{Ar} = F_{ZAnt.} \cdot R_{Ar} \tag{2.8}$$

This formula can be evaluated for different antenna temperature $T_{Ant.}$ ($T_{Ant.} = T_o$, $2 \cdot T_o$, $3 \cdot T_o$, ..Etc.). Assume that the antenna temperature $T_{Ant.} = T_o$, thus $F_{ZAnt.} = 1$, which means that $F_{ZA} = R_{Ar}$.

Now, the aim is to find the transformer ratio dependence on the antenna real part. Adopting the assumption of $T_{Ant.} = T_o$ and from Figure 2.5, then the additional noise figure at point *x* is F_x:

$$F_x = \left(F_{ZA} + F_{ZF} \right) \cdot t_C^2 = \left(R_{Ar} + F_{ZF} \right) \cdot t_C^2 \tag{2.9}$$

Where, $F_{ZA} = R_{Ar}$ at $F_{ZAnt.} = 1$

Consequently the additional noise figure at point y is F_y:

$$F_y = \left(R_{Ar} + F_{ZF} \right) \cdot t_C^2 \cdot \ddot{u}^2 \tag{2.10}$$

And since the additional noise figure of the resistance Z_o is $F_{Zo}=1$ [8], then F_{Vt} can directly be evaluated of the total amplifier system at output. Thus we have

$$F_{Vt} = 1 + \left(R_{Ar} + F_{ZF} \right) \cdot t_C^2 \cdot \ddot{u}^2 + F_{ZB} \tag{2.11}$$

By solving the equation 2.11 for ü, we have

$$\ddot{u}(R_{Ar}) = \sqrt{\frac{F_{Vt} - 1 - F_{ZB}}{(R_{Ar} + F_{ZF}) \cdot t_C^2}} \tag{2.12}$$

This represents an important design equation relating the different additional noise figures through the circuit and will help for selecting or maximizing the transformer ratio to achieve a certain noise figure, as will be shown in the subsequent discussion.

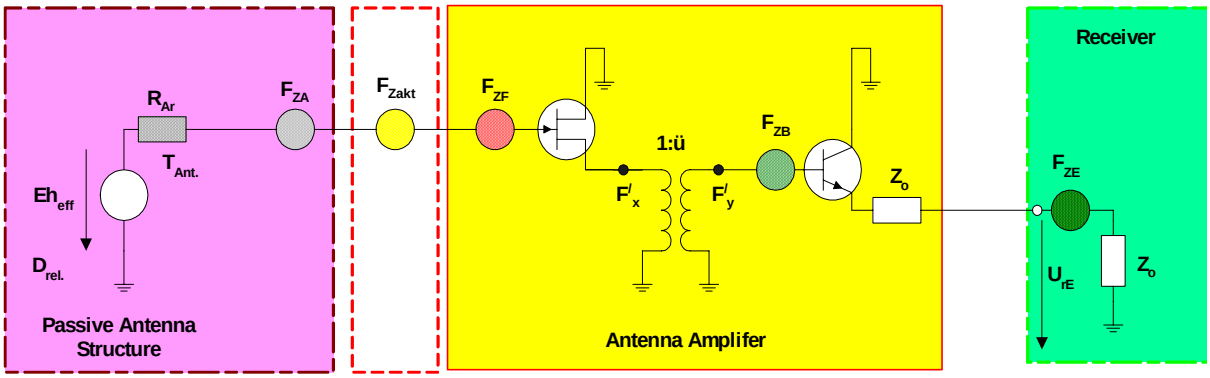

Figure 2.6: Noise Factor Evaluation of the proposed Active Antenna

Now, connecting the receiver to the antenna amplifier output as shown in Figure 2.6, the active antenna additional noise figure F_{Zakt} can be evaluated as follows,

According to Figure 2.6, knowing that F_{ZO} =1, the additional noise factor at point y', will be

$$F_{y'} = (F_{ZE} + 1 + F_{ZB}) \tag{2.13}$$

The additional noise figure at point x' is simply

$$F_{x'} = \frac{F_{y'}}{[\ddot{u}(R_{Ar})]^2} \tag{2.14}$$

Directly, the additional noise figure of the proposed active antenna is

$$F_{Zakt.}(R_{Ar}) = \frac{1}{R_{Ar} \cdot t_C^2} \cdot \left[F_{ZF} + F_{x'}\right] \tag{2.15}$$

Substituting from (2.13) and (2.14) into (2.15), the additional noise figure can be formulated to be

$$F_{Zakt.}(R_{Ar}) = \frac{1}{R_{Ar} \cdot t_C^2} \cdot \left[F_{ZF} + \frac{1}{\left[\ddot{u}(R_{Ar})\right]^2} \cdot (1 + F_{ZB} + F_{ZE}) \right] \tag{2.16}$$

In dB notation, the noise figure of the active antenna $F_{akt.}$ ($F_{akt.} = 1 + F_{Zakt.}$) will be

$$F_{akt.}(R_{Ar})[dB] = 10\log(1 + F_{Zakt.}(R_{Ar})) \tag{2.17}$$

Equation 2.17 is an important design equation since it shows the new active antenna additional noise figure dependence on an arbitrary antenna resistance real part (which represented here by the relative real part $R_{Ar} = R_A/Z_o$), GaAs FET additional noise figure, the Bipolar transistor additional noise figure and the necessary filter voltage gain ratio (emulated by the transformer ratio $\ddot{u}(R_{Ar})$) that should be chosen for achieving a minimum system additional noise figure . This equation will be evaluated for different arbitrary real part antenna R_{Ar} to show how close the new amplifier to the assigned standards by **VDA** ($F_{Vt}[dB] = 8.7$ in case of active antenna as explained in section 2.2.1 B). Let us first evaluate the transistors additional noise figures F_{ZF} and F_{ZB} in the $Z_o = 50$[Ohm] system by simulating the different circuits using the practical Library model from Siemens implemented in Serenade Harmonica 8.7 Software [54] which is the used simulation software through this work as stated earlier in Chapter one.

Figure 1.20 in chapter one showed a schematic of the CLY2 source follower GaAsFET that will be used to evaluate the FET additional noise factor in a 50 Ohm system at a GaAs FET drain current of $\mathbf{I_{DS}=50mA}$, and drain to source voltage of $\mathbf{V_{DS}= 2.9V}$.
The simulation of the source follower circuit in figure 1.20, results in a circuit total noise figure read by the simulator **NF = 0.8dB** at *f = 100MHz* (Note that the simulator symbol for the total noise figure is announced to be **NF[dB]** which we will call F [dB], and F_F will mean the total noise figure of the GaAs FET, so the subscript F stands for FET), from which the total noise figure as a number F_F can be calculated to be $F_F = 10^{\frac{NF[dB]}{10}} = 1.2$, accordingly the CLY2 GaAsFET input equivalent series noise resistance at the reference temperature T_O will be $R_{nF} = (F_F - 1) \cdot 50\Omega = (1.2 - 1) \cdot 50 = 10Ohm$, so the additional noise figure of the CLY2 GaAsFET

can be calculated to be $F_{ZF} = \frac{R_{nF}}{Z_O} = \frac{10}{50} = 0.2$ (note that the GaAs FET total noise figure F_F is $F_F = 1 + F_{ZF}$, F_{ZF} is the additional noise figure of the GaAs FET). The GaAs FET capacitive coupling factor voltage division can be calculated, by simulating the circuit voltage gain, which resulted in a $t_C = 0.9$.

Figure 2.7 shows the schematic of the BFG196 Bipolar from Siemens that will be used to evaluate the Bipolar additional noise factor in a 50 Ohm system at a collector current of $\mathbf{I_C}$ = **25.8mA**, and collector to emitter voltage of $\mathbf{V_{CE}}$ **= 4.34V**.

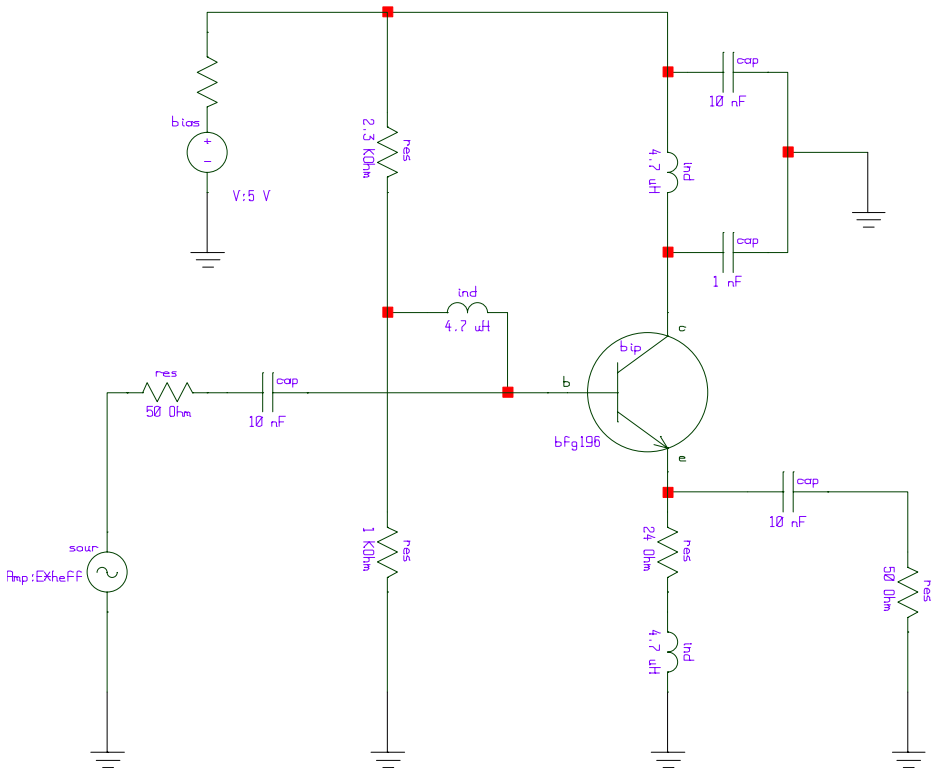

Figure 2.7: Additional Noise Factor Evaluation of the BFG196 NPN Bipolar

The simulation of the Bipolar circuit shown, results in a circuit total noise figure of **NF = 1.4dB** read at $f = 100MHz$, from which the total Bipolar noise figure as a number F_B (here B is for Bipolar)can be calculated to be $F_B = 1.38$, accordingly the BFG196 NPN Bipolar input equivalent series noise resistance at the reference temperature T_O will be $R_{nB} = (F_B - 1) \cdot 50\Omega = (1.38 - 1) \cdot 50 = 19Ohm$, so the additional noise factor of the NPN BFG196 Bipolar can be calculated to be $F_{ZB} = {R_{nB}}/{Z_O} = {19}/{50} = 0.38$

As stated in section 2.2.1 A), that in a matched case to the receiver (as in the case of Figure 2.6), the standard additional receiver noise figure calculated according to the **VDA** is F_{ZE} = 3.31, therefore the receiver noise figure is $F_E = (1 + 3.31) = 4.31 = 6.3$ dB which is the acceptable standard **VDA** limit, so substituting from the above calculations into Equation 2.16 and 2.17 to evaluate the new active antenna noise figure as a function of an arbitrary passive antenna structure real part R_{Ar} and comparing the generated values to the standard requirements implied by the **VDA**. Combining Eqn.(2.12) and (2.17), The additional noise figure $F_{akt.}$ in dB notation of the proposed active antenna therefore is

$$F_{akt.}(R_{Ar})[dB] = 10\log\left[1 + \frac{1}{R_{Ar}\cdot t_C^2}\cdot\left[F_{ZF} + \frac{(R_{Ar} + F_{ZF})\cdot t_C^2}{(F_{Vt} - 1 - F_{ZB})}\cdot(1 + F_{ZB} + F_{ZE})\right]\right] \qquad (2.18)$$

The evaluation results of Equation 2.18 in dB compared to standard requirements implied by the VDA for an arbitrary passive antenna real part R_A is shown in Figure 2.8.

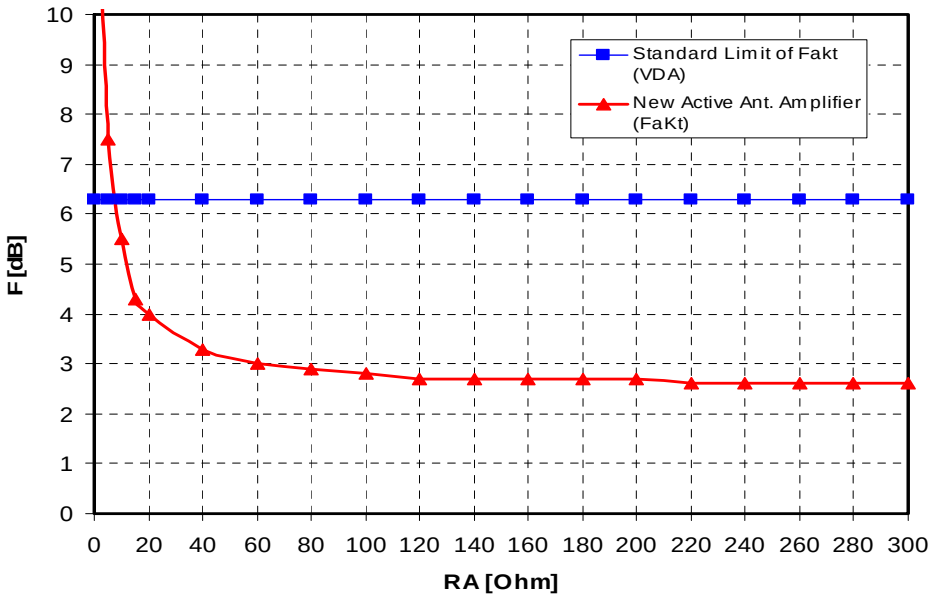

Figure 2.8: Additional Noise Factor Evaluation of the New Active Antenna Compared to the Standard VDA requirements

From Figure 2.8, one can conclude that the proposed new active antenna design concept fulfils the additional noise figure requirements proposed by the **VDA ($F_{Zakt.VDA\text{-}standard}$ < 6.3dB)** with a good extent, which can be reached if the antenna real resistance R_A greater than or equal to 8 Ohm. The value sets the first design condition and limitation use of the new presented concept. This condition can be formulated by the following inequality

$$For \quad F_{Zzakt.VDA-s\,\tan dard} < 6.3dB \rightarrow \quad The\ antenna\ real\ part\ should\ be: \left|R_A\right|_{\min} \geq 8\Omega \qquad (2.19)$$

Until now, the antenna impedance real part (R_A) noise contribution was considered, assuming a negligible noise contribution from the losses of the antenna imaginary part (X_A) assuming ideal antenna reactive part(which be represented by lossless reactive components). In the following section, we shall present a simulation study done to show the effect of the whole antenna impedance *($\underline{Z}_A = R_A + jX_A$)* on the presented amplifier noise performance.

2.2.3 A. Effect of Antenna Impedance on the new Amplifier Noise Performance

In a quest to realize gain and controlled impedances in a low noise and low power framework, the design of an active antenna LNA brings together a number of poignant technology issues. Investigating a range of circuit topologies and possibilities of developing techniques to circumvent limitations are important steps in determining the extent to which these issues represent fundamental barriers in amplifier noise performance. A detailed noise study done on transistors noise performance [23] followed by a lot of work on the issue of the low noise amplifier design [13], [29], [30], [31] and [49]. In [33], the different Field effect transistors considered, and an application conclusion built about how both HEMT and GaAs FET can be used for low noise applications in the frequency range of 10GHz up to 100GHz. In a recent study done in [20], a minimum value of the antenna impedance real part reached for a low noise figure application based GaAs FETs.

In all of the above publications, however the effect of the antenna on the amplifier noise performance for the 100MHz applications is not studied, or even simulated. In addition that the case of variable source arbitrary impedance was not considered or even simulated. In this section, the performance of the presented new active antenna design has been investigated by simulating the circuit total noise figure performance in the FM range. Nevertheless, before embarking on such an investigation, a means of representing and considering the circuit to be simulated is explained for its importance for the active antenna low noise amplifiers (LNAs) in general and specifically in RF and microwaves systems. The amplifier circuit noise performance to be evaluated is shown in Figure 2.9, whereas a GaAs FET bias current of 50mA and a bipolar collector current of 25mA will be used.

A transformer emulates the antenna real part, with transformation ratio of $1/\sqrt{R_{Ar}}$, where R_{Ar} represents the relative antenna real part as defined before in Eqn. 2.5. The reactive part of the antenna is simulated by a general variable reactance (jX_A). As explained in section 2.2.2, a transformer is implemented between the GaAs FET and the bipolar transistor to extract the circuit linear behaviour, whereas the ratio of this transformer is selected to be $1/ü(R_{Ar})$, so that in this ratio, $ü(R_{Ar})$ is adjusted for maximum noise voltage delivery to the receiver. The value of $ü(R_{Ar})$ is evaluated using Equation (2.12). The receiver noise voltage source, is represented by an ac *noise source* (denoted to be V_{nscr}, where nscr means noise source) in series with a noise free receiver, thus complete receiver simulation modelling is achieved. The value of the receiver noise source can be computed using the following equation:

$$V_{nscr} = \sqrt{4 \cdot k \cdot T_o \cdot B \cdot Z_o \cdot F_{ZE}} \qquad (2.20)$$

Where, Z_o is the noise free receiver reference impedance of 50 Ohm, and F_{ZE} (= 3.31) is the receiver additional noise factor computed in section 2.2.1 (A). With the help of Equation (2.12),(2.20) and by substituting the different GaAs FET CLY2 and Bipolar BFG196 parameters derived and explained in section 2.2.2, then the presented new amplifier circuit shown in Figure 2.9 can be easily simulated. In this figure, the antenna real part is emulated by a linear transformer, whereas the reactive part is varied and simulated by connecting a variable reactive jX_A element available by the simulator as shown in the figure. By selecting different values for the antenna real impedance real part (R_{Ar}) and varying the reactive part, a noise figure dependence on the antenna impedance plane (three-dimensional graph) can be generated as done in Figure 2.10.

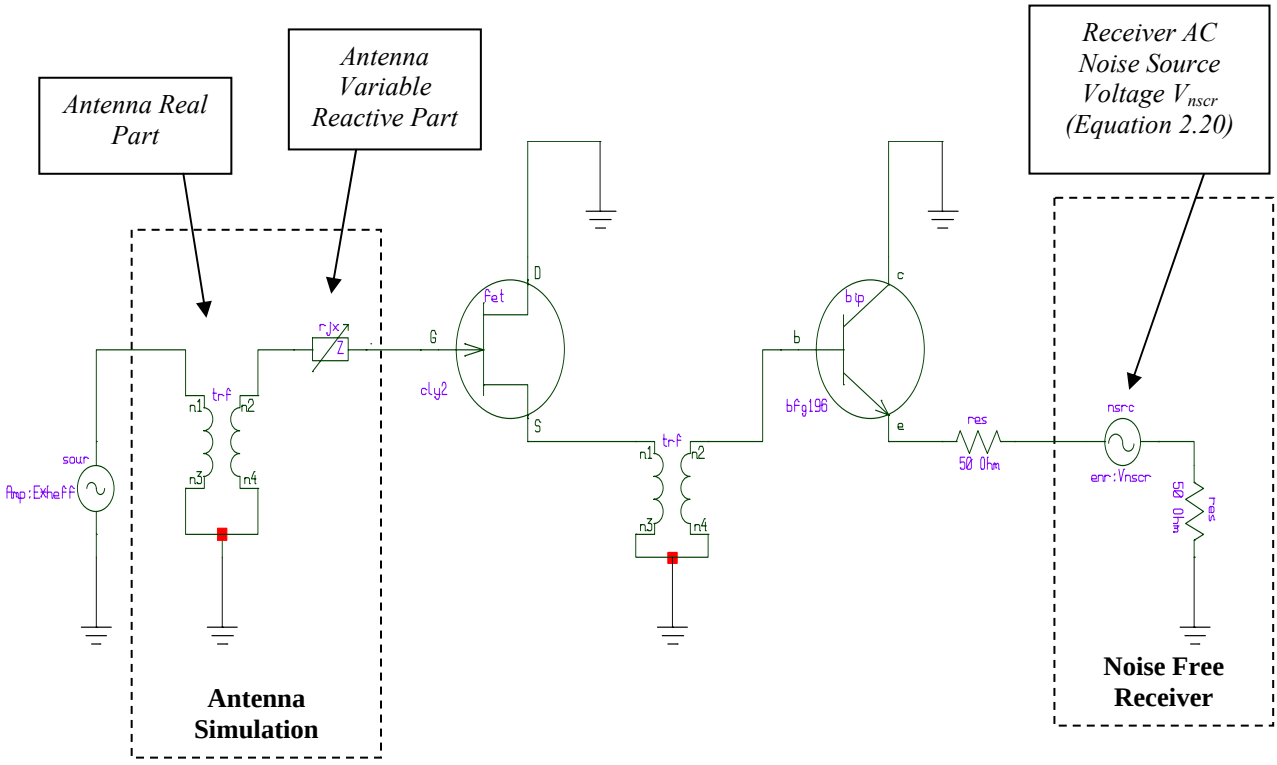

Figure 2.9: RF Circuit of Noise Figure Evaluation of the New Active Amplifier for Arbitrary Antenna Impedance

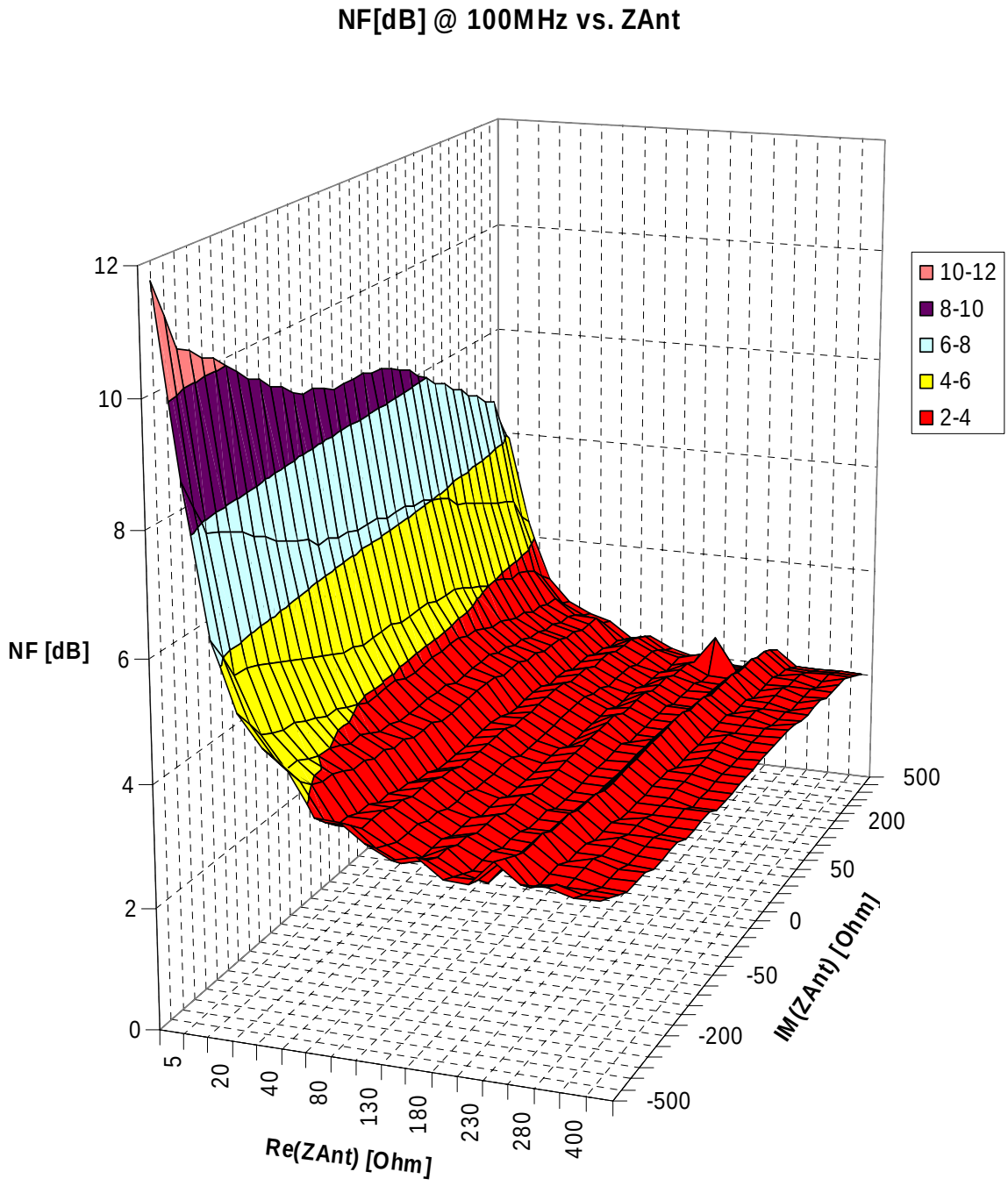

Figure 2.10: Noise Figure of the New Active Amplifier for Arbitrary Antenna Impedance

It is quite clear the special advantage of using a GaAsFET transistor in front of an antenna, which showed (Figure 2.10) the noise figure approximate independence on the antenna impedance reactive part. According to this conclusion, the effect of the antenna reactive part can be ignored, and the output signal to noise ratio of presented active antenna amplifier system can easily be evaluated.

By Referring to Figure 2.11 (a), (b), consider a reference rod antenna represented by its impedance real part connected to the receiver once and the presented active antenna connected to the same receiver, whereas the antenna window structure is represented as a passive antenna structure.

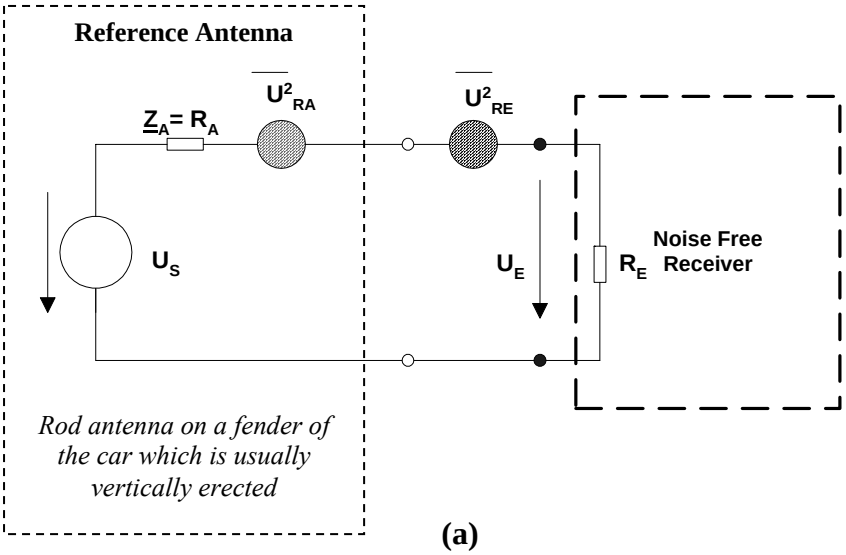

(a)

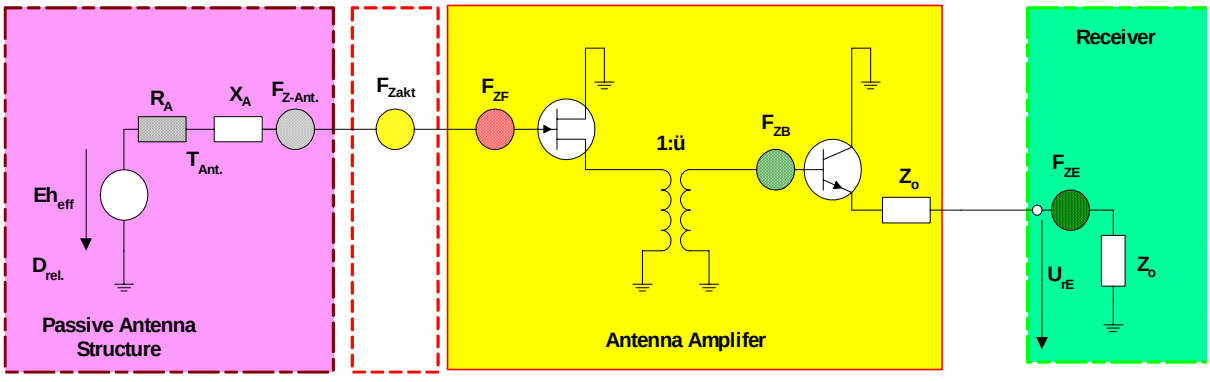

(b)

Figure 2.11: Signal to Noise Ratio Evaluation in Case of: (a) Reference Rod Antenna connected to the Receiver. (b) The Active Antenna Connected to the Receiver

2.2.3 B. Active Antenna Output Signal to Noise Ratio Evaluation

Now, comparing the two systems shown in Figure 2.11, the Antenna relative directivity $D_{relative}$ can be defined to be [9], [10]:

$$D_{relative} = \frac{P_{Passive}}{P_{reference}} \tag{2.21}$$

Where,
$P_{passive}$ is the average power delivered to the receiver (case of window structure), $P_{reference}$ is the average power delivered to the receiver (case of reference rod Antenna).

From [8], the system relative output signal to noise ratio is defined to be

$$SNR_{relative} = \frac{SNR_{Active-Antenna}}{SNR_{Rod-Antenna}} \tag{2.22}$$

From Figure 2.11 and Equation 2.21, the relative output signal to noise ratio can be directly formulated to be

$$SNR_{relative} = D_{relative} \cdot \frac{F_{ZAnt.} + F_{ZE}}{F_{ZAnt.} + F_{Zakt.}(R_{Ar})} \tag{2.23}$$

In dB notation, Equation 2.23 will be

$$\begin{aligned} &SNR_{relative}(R_{Ar}, D_{relative})[dB] = \\ &D_{relative}[dB] - 10 \cdot \log(F_{ZAnt.} + F_{Zakt.}(R_{Ar})) + 10 \cdot \log(F_{ZAnt.} + F_{ZE}) \end{aligned} \tag{2.24}$$

Equation 2.24 shows the proposed system output relative signal to noise ratio, and its dependence on the whole system different parameters. Since the antenna additional noise figure $F_{ZAnt.}$ can be defined to be [6],[8], and [13]

$$F_{ZAnt.} = \frac{T_{Ant.}}{T_o} \tag{2.25}$$

Where, $T_{Ant.}$ is the fictitious effective input noise temperature of the antenna, which in principle depending on the atmospheric, galactic and man-made-noise according to the CCIR [51], and T_o is the reference noise temperature of 300ºK, thus Equation (2.24) can be reformulated to be

$$SNR_{relative}(R_{Ar}, D_{relative})[dB] = D_{relative}[dB] - 10 \cdot \log(\frac{T_{Ant.}}{T_o} + F_{Zakt}(R_{Ar})) + 10 \cdot \log(\frac{T_{Ant.}}{T_o} + F_{ZE}) \quad (2.26)$$

Equation (2.26) shows in addition, the system output signal to noise ratio temperature dependence which emulates the car window temperature variation at different temperature conditions. By evaluating Equation 2.26 (with the help of Equation 2.16), then the variation of the relative signal to noise ratio of the proposed active antenna can be displayed as shown in Figures 2.12 and 2.13 for $T_{Ant.} = T_o = 300^oK$, and $T_{Ant.} = 3 \cdot T_o = 900^oK$ respectively. The equation has been evaluated for frequently measured directivity values [10] of the reference Rod Antenna ($D_{rel} = 0[dB]$ *case*) and a car window structure directivities of -1.5 dB and -3.5 dB respectively. From Figures 2.12, and 2.13, we can conclude that at higher temperature values ($T_{Ant..} = 3 \cdot T_o = 900^oK$), the system relative signal to noise ratio at different frequently measured directivities varies from the nominal values at ($T_{Ant.} = T_o = 300^oK$) *within* 1dB to 1.5 dB which can be considered to be accepted temperature dependence suggested by the CCIR recommendations [51].

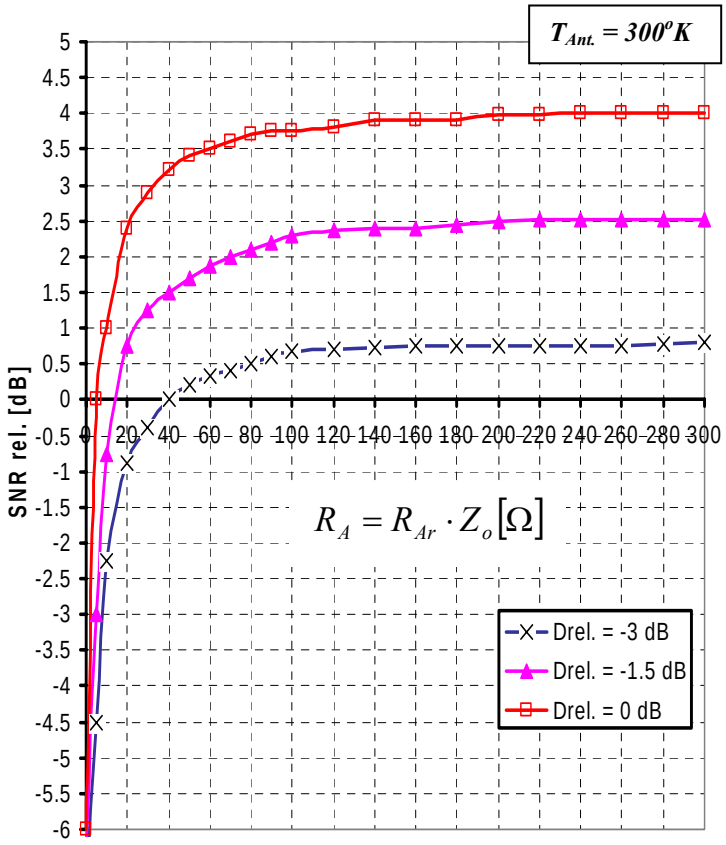

Figure 2.12: Relative Signal to Noise Ratio Evaluation at $T_{Ant.} = 300^oKelvin$ According to (2.26) formula

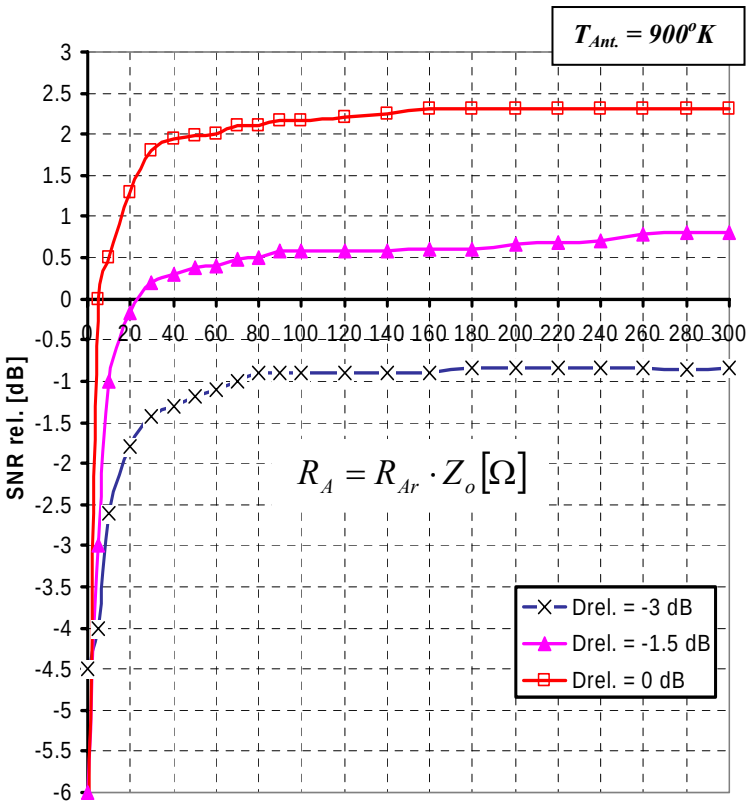

Figure 2.13: Relative Signal to Noise Ratio Evaluation at $T_{Ant.} = 900^{o}Kelvin$ According to (2.26) formula

2.2.4 Effect of Antenna Impedance on the new Amplifier Intermodulation Distortion

As stated earlier in chapter one, the intermodulation distortion is another type of noise that is generated in the transistor or the active device as a function of the input signals [49]. In the past, active antenna met little acceptance, and their development has been retarded by the fear that the problem of nonlinear distortions in a broad band active circuits might not be solvable [9]. In the meantime, good improvements have been achieved with amplifiers with respect to third-order intermodulation distortion, which is the dominating nonlinear effect with FM reception [9],[20].The active antenna, therefore, is best described by assigning to it: a) A frequency range, b) A minimum sensitivity which we determined by the noise figure in the last section, c) A dynamic range which is determined by the second, third, and higher-order intercept points, and d) Polarization(horizontal or vertical) [10].

In [20], a study has been introduced and a conclusion has been reached that the source impedance can affect the Intermodulation behaviour of the amplifier system.

In this section, the simulation results for evaluating the third order intermodulation distortion of the proposed new active antenna amplifier in the FM range (87MHz – 108MHz) will be presented for arbitrary antenna impedance. Figure 1.24 presented in chapter one, summarized the experimental procedure which will be adopted for simulation whereas, a two un-modulated harmonic signals of slightly different frequencies will be fed to the input of the proposed amplifier and the third order intermodulation distortion separation (denoted IMD = a_{K3}) will be computed at the output according to Equation 1.27 presented in chapter one.

The proposed amplifier circuit to be simulated is as presented in principle in Figure 2.9, whereas in the intermodulation distortion evaluation case, the circuit will be fed with a two frequency independent RF sources each of 97MHz and 101MHz respectively. The GaAs FET bias current of I_D = 50 mA and a collector current of I_C = 25 mA will be used. Using the same procedure described in section 2.2.4, and using Equation 1.27 definition, a three dimensional graph of a_{K3} versus the antenna impedance plane is generated as shown in Figure 2.14. The IMD values are evaluated at a circuit output voltage of $V_{out} = 100dB\mu V$ which is the standard value assigned by the **VDA**.

For the proposed amplifier circuit, it is quite clear that the intermodulation distortion is quite independent on the whole antenna impedance plane (the antenna impedance real and imaginary parts) generally and the impedance imaginary part specifically, which indicates a high linearity amplifier behaviour.

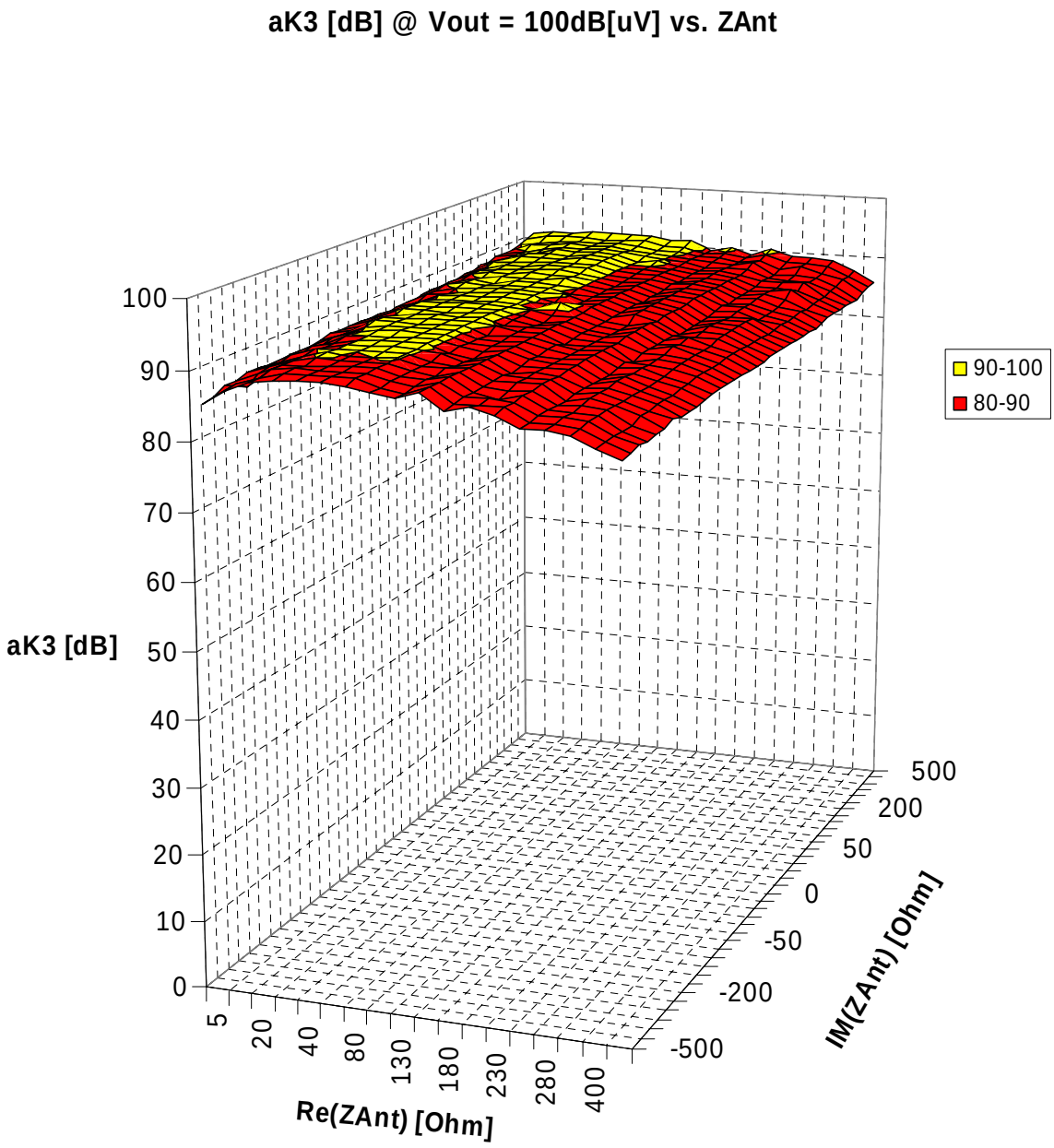

Figure 2.14: Intermodulation Distortion a_{K3}[dB] the New Active Amplifier for Arbitrary Antenna Impedance

2.2.5 Design and Optimization Approach of the Proposed Active Antenna New Amplifier

Until now, the performance evaluation of the proposed new active antenna amplifier has been introduced. In the following sub sections, the necessary design conditions that should be fulfilled for optimizing the amplifier-required frequency response and noise performance for arbitrary antenna impedance before its practical realization will be derived. In the following derivations, a rod antenna will be used as a reference, whereas it will be connected to the car once and the nowadays-used active antenna amplifiers once so that to extract the design new conditions in view of the already used active antennas. This will show the expected advantages of the presented new amplifier design. Finally the amplifier stability problem will be discussed from both simulation point and experimental point of views.

2.2.5. I. Optimization of the Active Antenna Amplifier Frequency Response

Figure 2.15 shows a rod antenna connected to the car and other test windscreen antenna. Starting with a rod antenna connection, we have the following case (A) as follows

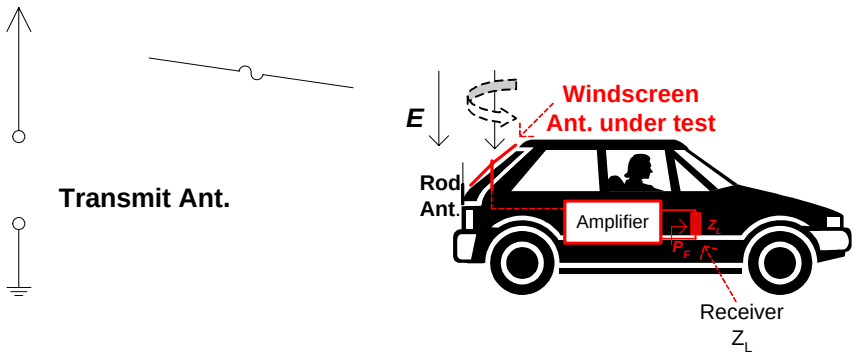

Figure 2.15: Transmit and Car receive antenna

(A) The Reference Rod Antenna and an actual Amplifier:

Assume that the reference antenna is a Rod Antenna, and define the effective area of the rod Antenna to be A_r. The average maximum received power P_r to the load can be formulated in the following two cases I, II will illustration in Figures 2.16 and 2.17 respectively.

I. For a Passive Load:

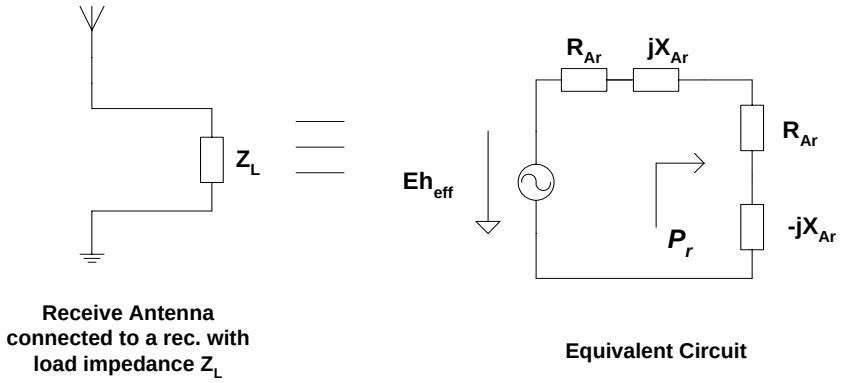

Figure 2.16: Loaded Antenna Model

$$P_r = \frac{\frac{1}{2}E^2 h_{eff}^2}{4R_{Ar}} = \frac{\frac{1}{2}E^2}{Z_o} \cdot A_r \qquad (2.27)$$

Where,

A_r …… is the effective aperture area of the rod Antenna [m^2]
Z_o …… is the impedance of free space (= 120π [Ohms])
E …… is the amplitude of the exciting electric field strength [Volt/m]

II. For the rod antenna connected to an actual Amplifier:

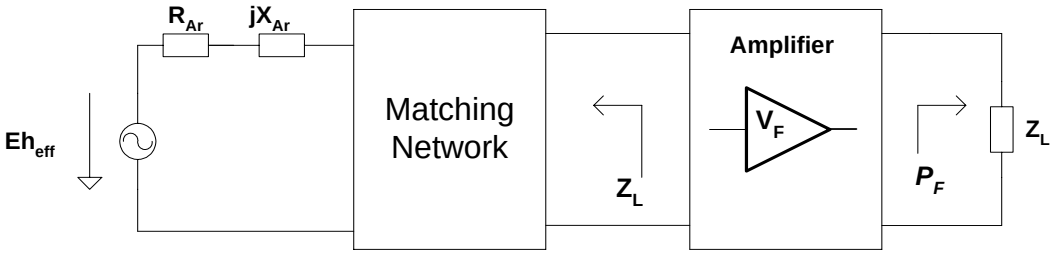

Figure 2.17: Loaded Rod Antenna Connected to an Amplifier

From Figure 2.17, define the amplifier power gain to be V_F, then the average maximum received power P_F is:

$$P_F = \frac{\frac{1}{2}E^2}{Z_o} \cdot A_r \cdot V_F \tag{2.28}$$

A typical value [8] of such an actual amplifier power amplification is $V_F = 4 \approx 6$[dB].

(B) The Car window Antenna structure under test:

I. For a Passive Load (Car Windscreen Antenna):

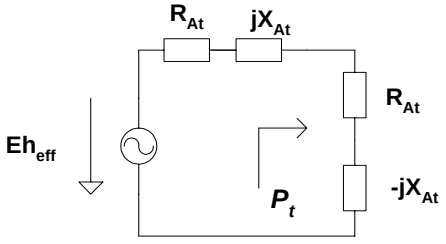

Figure 2.18: Loaded Test Antenna Model

From Figure 2.18 for a passive load, the maximum received power P_t is:

$$P_t = \frac{\frac{1}{2} E^2 h_{eff}^2}{4R_{At}} \tag{2.29}$$

Define the *aperture effective area of the window antenna structure to be* $A_{structure}$ and the azimuthally measured mean value directivity of test structure to be D_{rt}, then with a reference to the *rod antenna* case, we have:

$$A_{structure} = A_r \cdot D_{rt} \tag{2.30}$$

Accordingly, Equation (2.29) can be re-written as:

$$P_t = \frac{\frac{1}{2} E^2 h_{eff}^2}{4R_{At}} = \frac{\frac{1}{2} E^2}{Z_o} \cdot A_r \cdot D_{rt} = P_r \cdot D_{rt} \tag{2.31}$$

Typical value of D_{rt} [10] is 0.5 = -3dB.

II. For the antenna structure under test connected to an Amplifier:

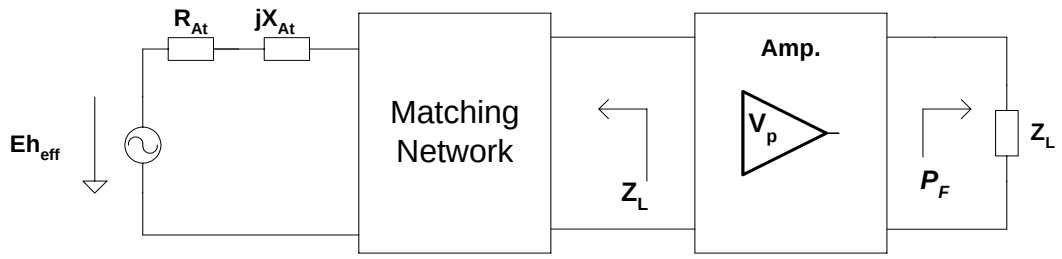

Figure 2.19: Loaded Test Antenna Structure Connected to an Amplifier

From Figure 2.19, the average maximum radiated power P_F is:

$$P_F = \frac{\frac{1}{2}E^2}{Z_o} \cdot A_r \cdot D_{rt} \cdot V_P \tag{2.32}$$

(C) The Proposed FET amplifier active antenna circuit connected to the car window Antenna structure under test:

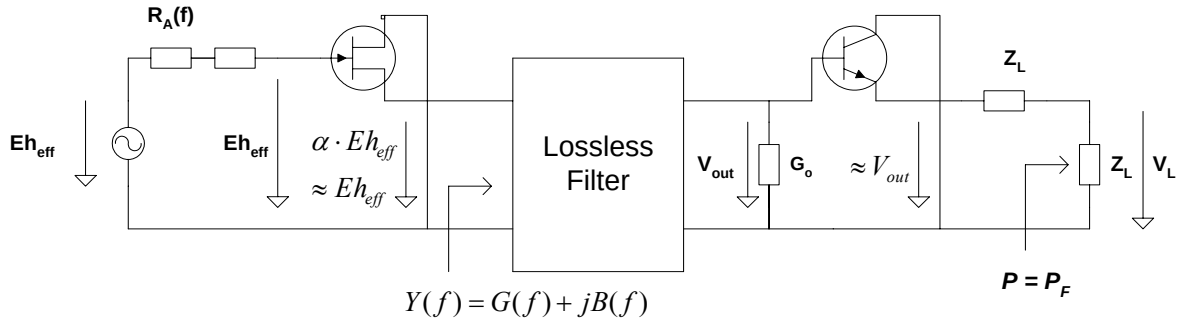

Figure 2.20: The Proposed New Active Antenna Amplifier circuit

Referring to Figure 2.20, the design goal principle can be defined to be: Output power of the circuit structure shown in Fig. 2.20 to be equal to the output power of the traditional used amplifier circuit structure shown in Figure 2.19, i.e. the goal can be formulated to be:

$$P = P_F \tag{2.33}$$

Referring to Figure 2.20, define the GaAs FET follower voltage gain to be α. The voltage across the lossless filter input frequency dependent conductance *G(f)* is equal to the voltage across the filter load G_o, so accordingly lossless filter output available power is:

$$P = \tfrac{1}{2}(\alpha \cdot E \cdot h_{eff})^2 \cdot G(f) = \tfrac{1}{2} \cdot V_{out}^2 \cdot G_o \tag{2.34}$$

From which we have

$$V_{out}^2 = (\alpha \cdot E \cdot h_{eff})^2 \cdot \frac{G(f)}{G_o} \tag{2.35}$$

But: $V_L = \tfrac{1}{2} V_{out}$, so the available power at the load will be:

$$P = \tfrac{1}{2} \cdot \frac{V_L^2}{Z_L} = \tfrac{1}{2} \cdot \frac{\tfrac{1}{4} V_{out}^2}{Z_L} \tag{2.36}$$

Combining Equations (2.35) and (2.36) leads to

$$P = \frac{\tfrac{1}{2}(E \cdot h_{eff} \cdot \alpha)^2 \cdot G(f)}{G_o} \cdot \frac{1}{4Z_L} \tag{2.37}$$

Now, the goal Equation (2.33), will be achieved by equating Eqn.(2.37) and (2.32), then we have

$$P = P_F \quad \Longrightarrow \quad \frac{\tfrac{1}{2}(\alpha \cdot E \cdot h_{eff})^2 \cdot G(f)}{G_O} \cdot \frac{1}{4 \cdot Z_L} = \frac{\tfrac{1}{2} E^2}{Z_O} \cdot A_r \cdot D_{rt} \cdot V_P \tag{2.38}$$

From (2.31), we have

$$\tfrac{1}{2}(E^2 \cdot h_{eff}^2) = 4 \cdot R_{At}(f) \cdot \frac{\tfrac{1}{2}E^2}{Z_o} \cdot A_r \cdot D_{rt} \tag{2.39}$$

Substituting from (2.39) into (2.38), we have

$$\frac{\tfrac{1}{2}E^2\alpha^2 \cdot 4 \cdot R_{At}(f) \cdot A_r \cdot D_{rt} \cdot G(f)}{4 \cdot Z_L \cdot G_o \cdot Z_o} = \frac{\tfrac{1}{2}E^2}{Z_o} \cdot A_r \cdot D_{rt} \cdot V_P \tag{2.40}$$

The frequently measured directivity of the windscreen antenna test structure as stated before is D_{rt} ($\approx 0.5 = -3$[dB]) [10] will cancel from both sides of Equation 2.40, then solving for the real part of the filter input admittance *G(f)* , we arrive to

$$G(f) = \frac{Z_L \cdot G_o}{R_{At}(f)} \cdot V_P \cdot \frac{1}{\alpha^2} \tag{2.41}$$

Normalizing the Equation (2.41) with source impedance Z_o=50[Ohm], by multiplying both sides of it by Z_o, then we have

$$Z_o \cdot G(f) = Z_o \cdot \frac{Z_L \cdot G_o}{R_{At}(f)} \cdot V_P \cdot \frac{1}{\alpha^2} = \frac{Z_L \cdot G_o}{R_{At}(f)/Z_o} \cdot V_P \cdot \frac{1}{\alpha^2} \tag{2.42}$$

Equation (2.42) can be re-written as

$$Z_o \cdot G(f) = \frac{Z_L \cdot G_o}{R_{At}(f)/Z_o} \cdot V_P \cdot \frac{1}{\alpha^2} \tag{2.43}$$

Define $G'(f) = Z_o \cdot G(f)$, and $R'_{At}(f) = R_{At}(f)/Z_o$, then we have

$$G'(f) = \frac{V_P \cdot G'_O}{R'_{At}(f)} \cdot \frac{1}{\alpha^2} \tag{2.44}$$

According to the VDA standards, the required power gain of the amplifier is $V_P = 4 \approx 6$[dB], and since, a source follower GaAsFET voltage gain $\alpha \approx 1$, so substituting from all of the above givens for V_P and α into Equation (2.44), then we have

$$G'(f) \approx \frac{4 \cdot G'_O}{R'_{At}(f)} \rightarrow G(f) \approx 4 \cdot \frac{Z_O \cdot G_O}{R_{At}(f)} \tag{2.45}$$

If this formula is satisfied, then a flat frequency response of the proposed amplifier (shown Figure 2.20) can be reached.

The Equations 2.45 shows explicitly the filter conductance dependence on the antenna impedance real part. This equation has the advantage that it can be evaluated at certain discrete frequency points as required sometimes for quick design. The results can be fed to a software optimizer to achieve the amplifier required response power gain S_{21} according to the antenna measured impedance values. In view of this equation, a variety of filter structures can be tried and used to achieve the required amplifier frequency response in condition that the filter structure admittance real part achieves Equation 2.45. Later in this chapter, a design example will be introduced based on the derived design equation.

2.2.5. II. Amplifier Frequency Response and Standard Noise Consideration

A practical active antenna amplifier design noise performance consideration, which should be taken into in view of the standard requirements of **VDA** will be introduced. In the following, an expression that relates the amplifier frequency response to the required receiver noise voltage will be derived. This expression represents an evaluation of the designed amplifier and its relation to the receiver noise consideration. Consider the proposed amplifier circuit connected to the receiver as shown in Figure 2.21.

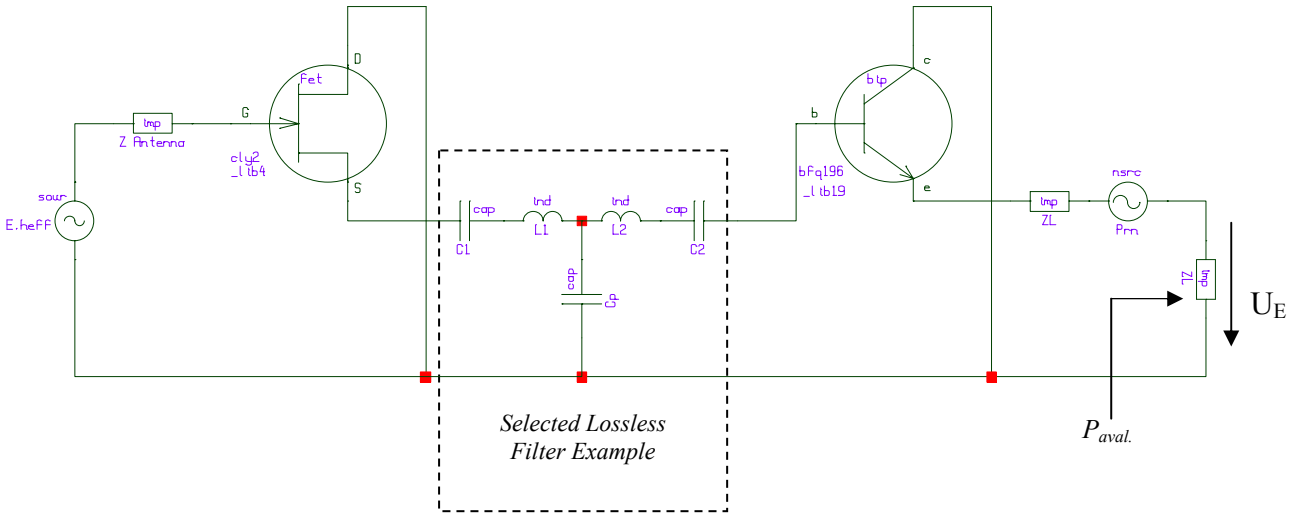

Figure 2.21: Active Antenna Amplifier Circuit connected to the Receiver

Define the circuit total noise figure (including the receiver noise) to be F_{total}. The available noise power at the Receiver input is

$$P_{aval.} = F_{total} \cdot \left|\underline{S}_{21}\right|^2 \cdot kT_oB \tag{2.46}$$

Equation (2.46) should achieve the following condition according to the allowed standard output noise voltage, so we have

$$P_{aval.} \le \frac{U_E^2}{Z_L} \tag{2.47}$$

Where, U_E is the effective value.

$$\Rightarrow F_{total} \cdot \left|S_{21}\right|^2 \cdot kT_oB \le \frac{U_E^2}{Z_L} \tag{2.48}$$

$$\Rightarrow 10\log(F_{total} \cdot \left|S_{21}\right|^2) = 10\log(\frac{U_E^2}{kT_oB \cdot Z_L}) \tag{2.49}$$

$$\Rightarrow 10\log(F) + 20\log(|S_{21}|) = 10\log\left(\frac{\left[10^{\frac{U_E dBuV}{20}} \cdot 10^{-6}\right]^2}{kT_o B \cdot Z_L}\right) \tag{2.50}$$

$$\Rightarrow F_{total}[dB] + S_{21}[dB] = 10\log(10^{\frac{U_E dBuV}{20} \cdot 2}) + 10\log\left(\frac{10^{-12}}{kT_o B \cdot Z_L}\right) \tag{2.51}$$

Substituting with: $k \cdot T_o = 4 \cdot 10^{-21}[J], B = 120[KHz], Z_L = 50[\Omega]$, We have

$$F_{total}[dB] + S_{21}[dB] = U_E[dBuV] + 16.19 \tag{2.52}$$

$$S_{21}[dB] \le U_E[dBuV] + 16.19 - F_{total}[dB] \tag{2.53}$$

From section 2.2.1 (B), by substituting into Equation (2.47) by the standard value for U_E = -7.5 dBμV assigned by the **VDA**, then we have

$$S_{21}[dB] \le 9.4 - F_{total}[dB] \tag{2.54}$$

This is the necessary evaluation equation that should be checked after designing and optimizing the proposed new amplifier structure to guarantee that the amplifier performance is within the **VDA** assigned standards. In the subsequent examples at the end of this chapter, a design check for every designed amplifier will be done using this equation.

2.2.5. III. The Active Antenna Amplifier Stability

One of the first requirements that an active antenna amplifier circuit must meet is a stable performance in the frequency range of interest. This is a particular concern when dealing with RF circuits, which tend to oscillate depending on operating frequency and termination. To the conventional analog IC designer, analysis of stability are rooted in descriptions of loop gain and phase carrying names like Routh, Nyquist, and Bode [35],[36],[37], [38], [48]. Venturing into a culture of microwave active antenna circuit design that has grown up around two-port representations, stability parameters derived from impedances or (equivalently) reflection coefficients, and Smith chart-based stability circles tends to leave a puzzling situation for which is better to use ? (The reverse situation is also true: most microwave designers are no more comfortable with phase margins than IC designers are with stability circles). An improved scenario would be to establish a comfort level in believing that these different considerations of stability are at least consistent. Rather than attempting to demonstrate mathematical equivalency, the goal here is to interpret some typical stability problems for a source follower GaAs transistor stage as it represents the first basic stage of the proposed new design, and then to try to understand why these conditions of potential instability might exist. Many good texts on microwave design provide derivations of amplifiers stability circles, Rollett factor *k*,etc., through the algebric manipulation of complex numbers [12],[13],[46],[47],[52]; though these derivations are not repeated here, however the results that will be applied trough the stability study are summarized in the following discussion. Consider a general amplifier characterized through its S-matrix at a particular DC bias point and terminated with arbitrary external terminations described by Γ_L and Γ_S as shown in Figure 2.22.

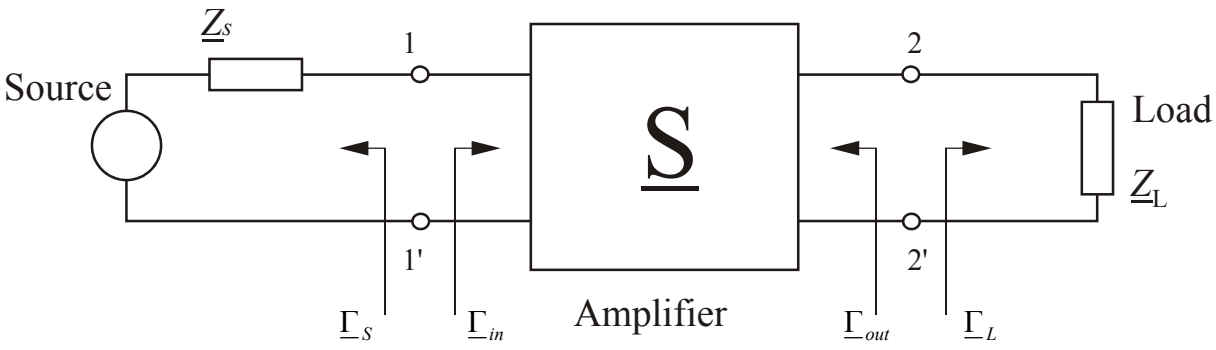

Figure 2.22: General Amplifier with Arbitrary Terminations

Stability then implies that the magnitudes of the reflection coefficients are less than unity [44], [52]. Namely,

$$\left|\underline{\Gamma}_{in}\right| = \left|\frac{\underline{S}_{11} - \underline{\Gamma}_L \Delta}{1 - \underline{S}_{22}\underline{\Gamma}_L}\right| < 1 \quad , \quad \left|\underline{\Gamma}_{Out}\right| = \left|\frac{\underline{S}_{22} - \underline{\Gamma}_S \Delta}{1 - \underline{S}_{11}\underline{\Gamma}_S}\right| < 1 \tag{2.55}$$

Where $\Delta = \underline{S}_{11}\underline{S}_{22} - \underline{S}_{12}\underline{S}_{21}$. Since the S-parameters are fixed for a particular frequency, the only factors that have a parametric effect on the stability are Γ_L and Γ_S . Unconditional stability for all frequencies is achieved if:

$$\left|\underline{\Gamma}_{in}\right| \le 1 \quad \forall \quad \left|\underline{\Gamma}_L\right| \le 1 \quad , \quad \left|\underline{\Gamma}_{Out}\right| \le 1 \quad \forall \quad \left|\underline{\Gamma}_S\right| \le 1 \tag{2.56}$$

In other words, the stability circles have to reside completely outside the $\left|\Gamma_S\right| = 1$ and $\left|\Gamma_L\right| = 1$ circles. It has been shown in [52], that conditions (2.55) and (2.56) can be expressed in terms of the stability or Rollett factor *k*:

$$k = \frac{1 - \left|\underline{S}_{11}\right|^2 - \left|\underline{S}_{22}\right|^2 + \left|\Delta\right|^2}{2\left|\underline{S}_{12}\right|\left|\underline{S}_{21}\right|} \tag{2.57}$$

Whereas

For k > 1, the amplifier circuit is unconditionally stable

For k < 1, the amplifier circuit is conditionally stable

Even though *k* can vary widely, most unstable practical designs fall into the range $0 \le k \le 1$.It would be worthy to note that oscillators target the entire Smith Chart as the unstable domain, resulting in negative values of *k*.

It is also interesting to observe that in the absence of any output to input feedback ($S_{12} = 0$) the transistor is inherently stable, since the stability factor yields $k \rightarrow \infty$. In practice, one often examines k alone without paying attention to the $|\Delta| < 1$ condition. In the following, we will introduce a simulation and experimental study done through out this work to show the basic GaAs FET CLY2 cell stability performance.

Consider the GaAs FET cell illustrated in chapter one (Figure 1.25) in a 50 Ohm system which represents the first stage in the proposed new design. This circuit has been realized in [20] for a proper work in the FM range based on the CLY2 GaAs FET with a bias conditions of $I_D = 50mA$ and $V_{DS} = 2.8V$.

Generally, the stability of a circuit should be checked from a very low frequency up to several GHz, however let the start be done with calculating the stability checking factor introduced by Equation (2.57) by simulating the circuit in the FM range (87 MHz – 108 MHz). The simulation results are shown in Figure 2.27. From these results, one can conclude that the circuit is *not unconditionally stable* ($k < 1$) but reveals a *conditional stability* in the FM range which means that the circuit might be stable or not, and sure this is depending on the circuit layout parasitic and experimental implementation topology.

Actually, after realizing a lot of samples of the circuit demonstrated in Figure 1.25 (using a GaAs follower cell), the experimental investigations in the laboratory showed oscillations, which appeared out of the FM range (starting from 400 MHz for some samples up to several GHz) and starting from 750 MHz up to several GHz) for other sample,…etc.). This reveals that the circuit experimentally has no tendency to oscillate in the low frequency spectrum including the FM range frequency of interest. *This experimental remark can be considered as a general rule, but the results can be different from layout to layout and from transistor sample to sample variation which results in a different frequency response.*

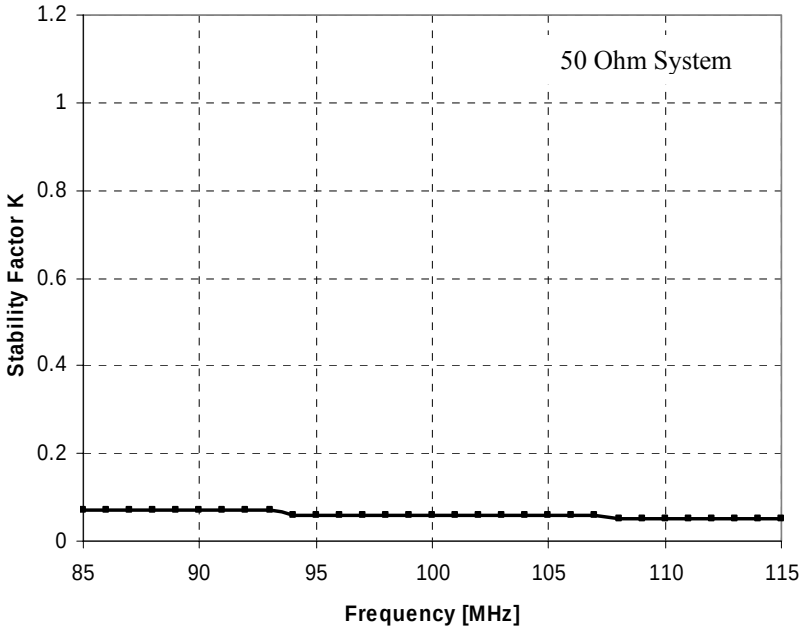

Figure 2.23: GaAs FET CLY2 Follower Amplifier Stability Factor *k* Simulation In FM Range

Now by performing the circuit simulation again starting from a frequency of 40 MHz up to 6 GHz (which is the maximum measurable capability of our laboratory spectrum analyzer from Hewlett Packard 8561A), one gets the stability *k* factor results shown in Figure 2.24. The graph shows also that $k < 1$ for high frequencies too, however an attention and comment should be given here about the negative *k* values resulted starting from a frequency of 410 MHz up to the several GHz.

In section 2.2.5. III., it has been explained that oscillators target the entire Smith Chart as the unstable domain, resulting in negative values of *k*, and from here one can conclude an experimental empirical interpretation that *a negative values of k (k<0) indicates a potential of oscillation,* and as illustrated before that for some realized GaAs FETs follower samples, an oscillation has been seen in the Laboratory spectrum analyzer, whereas the starting oscillation frequency happened at 400 MHz and in [20] too, which agrees with the simulations results of Figure 2.24 and consequently agrees with the presented interpretation of potential instability for negative *k* factor values at high frequencies.

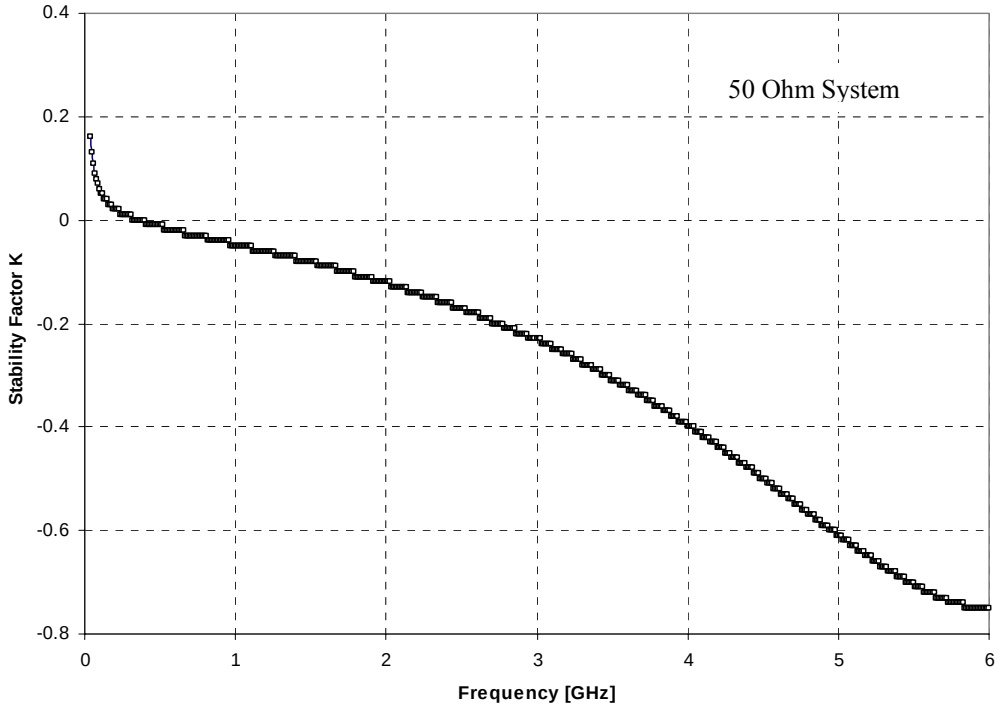

Figure 2.24: GaAs FET CLY2 Follower Amplifier Stability Factor *k* Simulation at Higher Frequencies

These results introduced for 50 Ohm source impedance, and for frequency dependent source impedance which represents the car windscreen antenna. The stability behavior has been tested of the same samples in the laboratory as shown in Figure 2.25 which represents the test procedure block diagram of the experimental setup whereas the 50 Ohm source impedance is transformed by different passive networks so that to emulate a frequency dependent source connected in front of the GaAs FET amplifier, and then the circuit output is connected to the spectrum analyzer directly once, and via a passive network to emulate a frequency dependent load too. Experimentally oscillations observed for a frequency dependent source and load too, which illustrates the basic experimental problem of active antenna amplifiers realization.

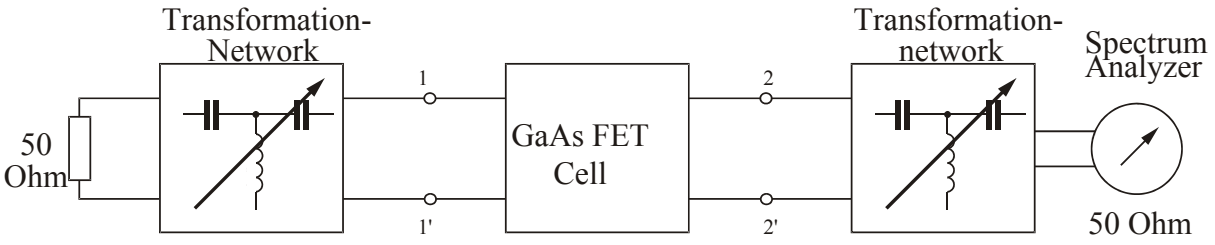

Figure 2.25: GaAs FET CLY2 Amplifier Cell Stability Experimental Test for different Source and Load Impedances

In [20], the author introduced a practical solution for avoiding these high frequency instabilities by testing and connecting a different ferrite beads in the series path of the GaAs FET gate terminal as shown in Figure 2.26.

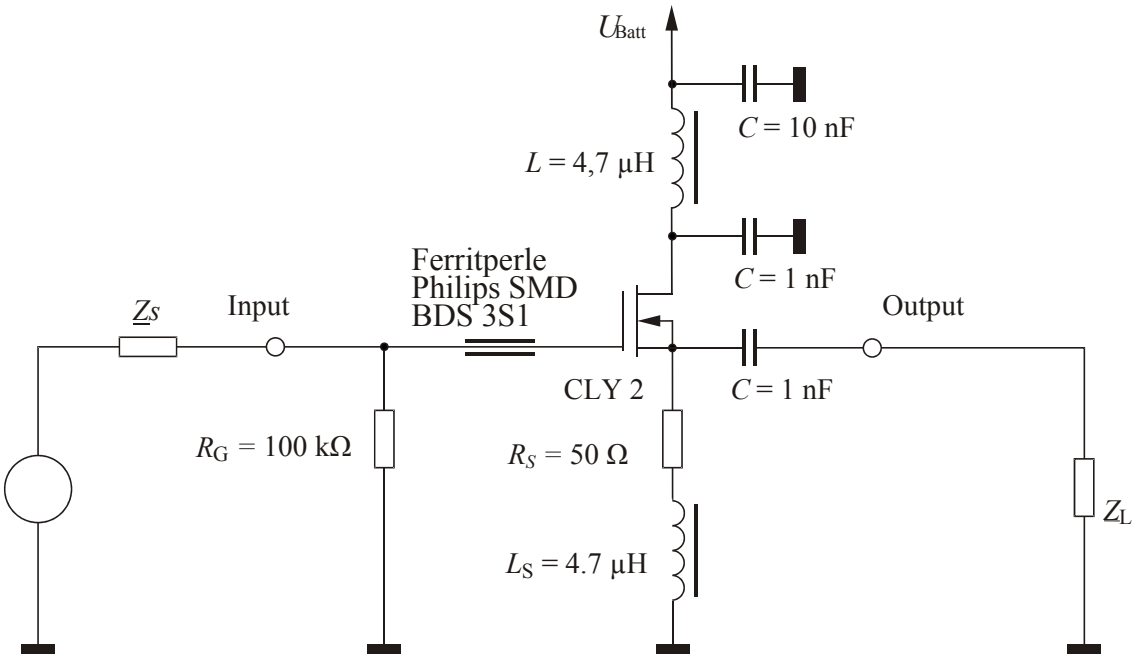

Figure 2.26: GaAs FET CLY2 Amplifier Cell Stability Using the Gate Ferrite Bead

The measured results in [20] in the 50 Ohm system are re-printed in Figure 2.27. One should pay attention first, that the simulation of the stability factor results in Figure 2.23, 2.24 agrees approximately with the measurements shown in Figure 2.28 in [20] up to an approximate frequency of 2.6 GHz which means that the discussed negative stability k - factor values instability conclusion still holds and the measurements shown can vary from sample to sample, but generally from Figure 2.27, one can conclude that the GaAs FET follower cell stability can be achieved by using different ferrite beads which led to a stability in case of 50 Ohm system, but for a complex source impedances, unfortunately instabilities appeared for some complex source impedance cases, however and still the stability solution introduced by [20] can be used to solve the cell high frequency stability problems in case of some complex source impedances which should be checked experimentally for each realized amplifier.

At first glance, a difficulty may be clear from using a ferrite bead, since from Figure 2.27, the stability factor k values changes from ferrite sample to another, and as shown for example, the Ferrite bead 4S2 from Philips achieved a better performance (better $k > 1$ values) than 3S1, which sets from the design point of view an obstacle to achieve a standard stability GaAs follower cell, even in case of 50 Ohm system.

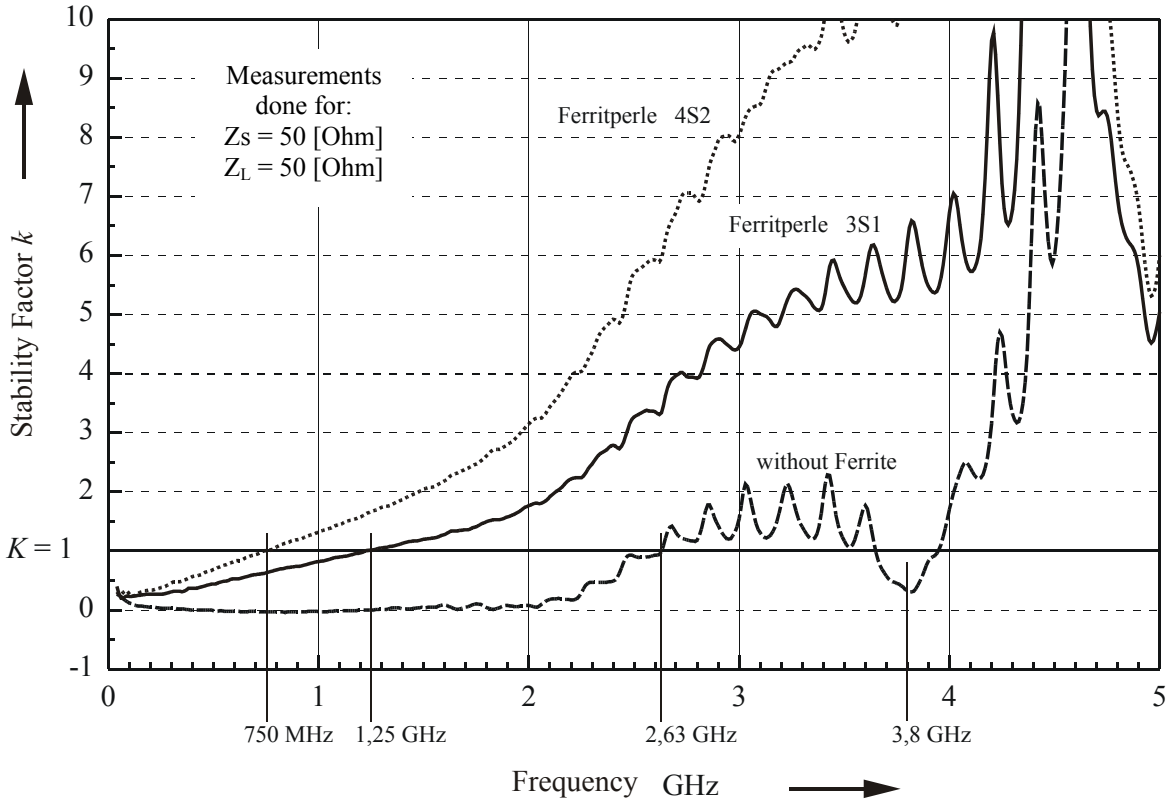

Figure 2.27: Measured [20] GaAs FET CLY2 Amplifier Cell Stability *k* - factor Using Different Gate Ferrite Beads

Although the ferrite stability technique has proven cell limited stability success (for some complex source impedance cases), however the technique has been adopted and used for the working cases whereas the ferrite samples standard variation problem has been solved by replacing it with a resistance of 10 Ohm in parallel with a coil of 12 nH.

Until now, the experimental GaAs FET follower cell stability problems has been discussed with reviewing the different solutions done in [20] and in industry too, however before adopting the presented GaAs follower cell [20] even with its limited stability performance, let us back to the design philosophy presented in the beginning of this chapter, which is the strong argue to get the initial emphasis on the follower cell noise performance, so in the present work, a trials are done to re-evaluate the cell noise figure performance with the previously reviewed stability solutions. Consider Figure 2.28, which represents the block diagram of the noise Figure setup done on the Laboratory using the new Agilent Noise Figure Analyzer (N8974A) to measure the realized GaAs FET cell using the stability technique suggested in [20], whereas a high gain and low noise figure amplifier is connected at the output of the GaAs FET cell for measuring the cell noise figure as accurate as possible. Both the GaAs FET cell and the low noise amplifier are connected and covered inside a closed chamber for preventing any external noise interference.

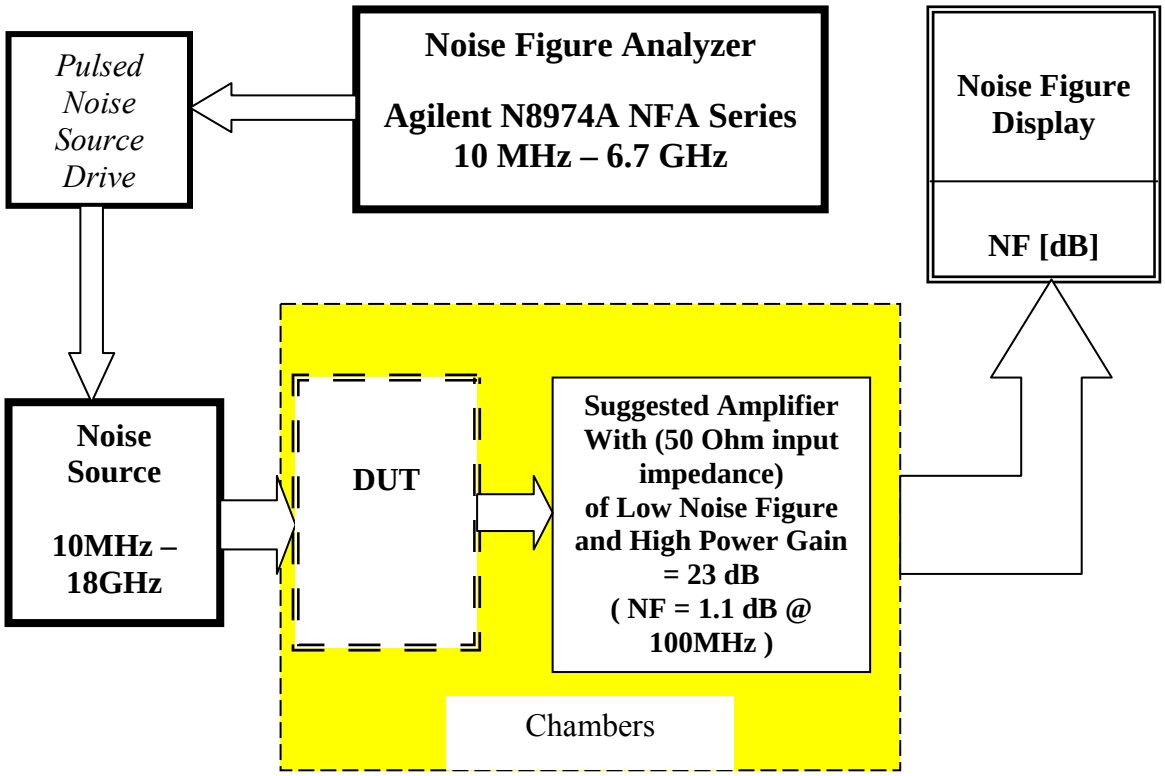

Figure 2.28: Noise Figure Measurement Setup

According to [20] stability technique of using a ferrite bead, a noise figure of 3.6 dB was measured at 100 MHz when the 4S1 ferrite bead is connected in series with the GaAs FET gate terminal (Figure 2.26), and according to the suggested technique of replacing the ferrite bead by a coil of 10nH in parallel with 10 Ohm resistor, a noise figure of 2.4 dB has been measured at 100 MHz. In both cases, the values of 3.6dB or even the 2.4 dB are still high in reference to the expected GaAs FET low noise figure capability [13], [14], [18], [21], [26], [33] and compared to a 0.9~1 dB noise figure simulated by Serenade Harmonica Software ver. 8.7 [54].

A lot of references explained that for any transistor (Bipolar, FET, ..etc.), any small inductance in series with assumed grounded transistor terminal can cause instability, and accordingly the circuit can produce a high noise figure value [30], [31],[32], [33], [40],[43] and [47]. In [13],[28], [40] and [47], a lot of biasing techniques has been introduced for common source and common gate FET amplifiers, however the source follower cell biasing has never been discussed as an amplifier due to the believe that the cell has a negative resistance and accordingly it is not stable.

In the present work, a trial has been done to re-analyze the GaAs FET follower cell bias situation in all of the above explained cases, and a start bean by adopting that the drain terminal should be grounded as directly as possible. From the measurements done on different source follower samples with the suggested biasing circuit as in Figures 1.20 and 2.26, the average noise figure values of 3.6dB or even the 2.6 dB measured at 100 MHz was not constant from sample to sample, which suggests that the grounding capacitors at the drain terminal may not be short circuit enough at the operating frequency. And since in addition, the grounding capacitors vary from sample to sample which started to set one of the reasons of the measured variable noise figure. In this work, a direct GaAs FET drain grounding has been achieved by adopting a negative supply bias circuit as shown in Figure 2.29.

In this circuit, the drain terminal of the GaAs FET is directly grounded, and since many antennas present an uncontrolled impedance environment to the GaAs FET input, a network composed of a capacitor *C* in series with a resistor *R* (or ferrite bead) is implemented between the GaAs FET gate terminal and ground to face the different antenna impedances variation. The network is connected as a shunt conductance, so that the circuit series path from the input to the output is free from any component, and accordingly negligible circuit noise figure degradation is expected as measured. Experimentally, a trimming ofthe capacitor C and/or the resistor R is suggested in this work until the oscillation disappears in case of antenna impedances (a suggested C-R network limiting values according to our measurements for low noise figure degradation are: 68 Ohm < R < 3KOhm, and 1pF < C < 11pF).

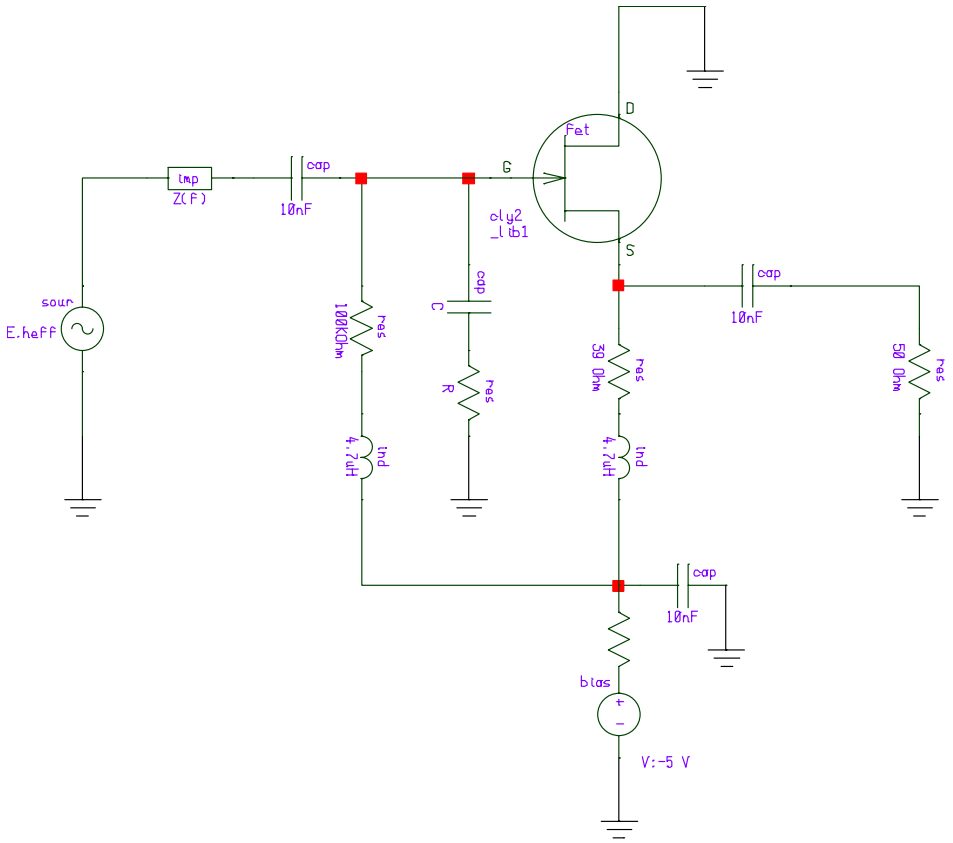

Figure 2.29: Negative Biasing of GaAs FET CLY2 Amplifier Cell

A capacitance value of C = 2.4 pF and a resistor value of R = 2 KOhm combinations has been experimentally reached whereas no oscillations appeared up to 6 GHz with different antenna impedances using the spectrum analyzer setup measurement shown in Figure 2.25 previously, however one should point out that these values arrived for a layout dimension of 3.3cm× 3cm and thickness of 0.15cm and sure these may change according to the layout that will be designed and used. Consequently a different C-R network trimming is required, also when realizing the total amplifier FM circuit, a slight trimming may be needed again to arrive to the optimum C and R values for stable circuit and system. According to the follower cell in Figure 2.29, a noise figure value of approximately 1.1~1.3dB (compared to a simulated noise figure of ~1dB) has been measured at 100MHz in a 50 Ohm system with variety of follower cell realized samples using the suggested negative bias circuitry. The GaAs FET follower cell noise figure has been measured in the laboratory according to Figure 2.28 noise figure setup block diagram.

One can conclude that the measured low noise figure of the GaAs FET follower cell biased with a negative supply is considered to be a very good experimental result, since the simulation results showed a noise figure of ~1dB, which reveals that the experimental results

are in a good agreement with the simulation results and the circuit start to behave ideally. The reason is that the follower drain terminal now has a stable ground bias condition, however the main draw back of such a negative bias suggestion is that the negative supply usually not available in different cars, whereas the positive power supplies dominates. Although that the conversion of positive supplies to negative ones is available using some known circuits, however this complicates the design and basically increases the price. Instead of using a negative bias, or even converting the positive bias to a negative one, a technique can be generalized using also a positive bias by designing a separate grounding layout for the GaAs FET follower cell when it is intended to be used with other stages or circuits. This is to guarantee a stable ground for follower cell circuit, thus the GaAs FET follower cell is away from the rest of the whole system parasitic and accordingly a low acceptable noise figure performance can be achieved with positive bias.

Figure 2.30 shows generally the new suggested layout ground topology for realizing the total FM amplifier using the GaAs FET separate ground. The topology can be used for any general application based follower GaAs FET cell. The link between the circuit ground and the GaAs follower cell ground can be achieved using capacitor of 10nF connected in parallel with a 4.7µH coil in case of FM application. The capacitor and coil values can be chosen according to the application frequency of operation.

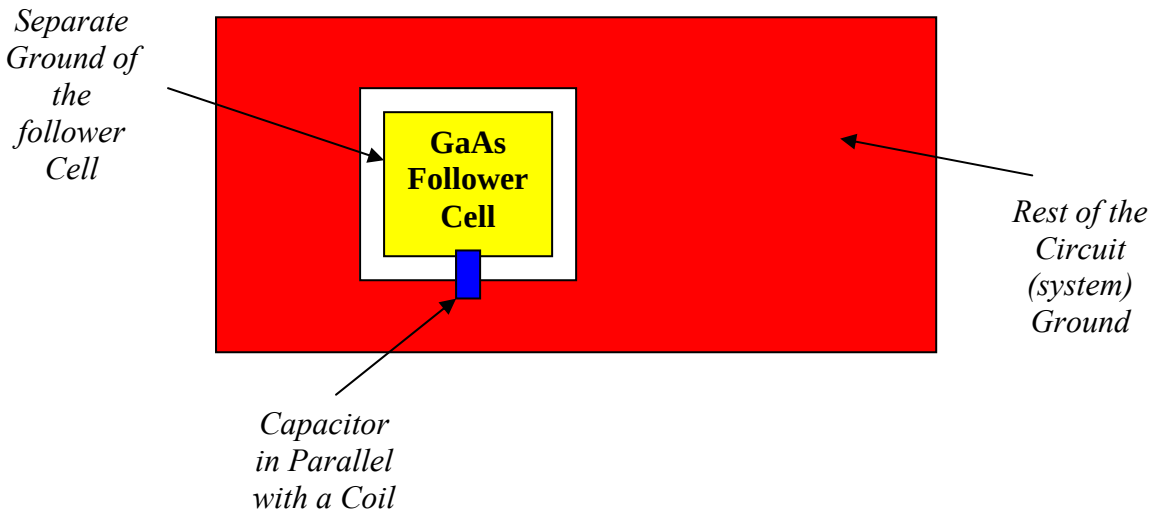

Figure 2.30: Suggested General Layout for implementing the FM amplifier based GaAs FET Follower Cell Separate Ground

The advantage of such a separate ground layout is the use of the positive bias; however the main drawback that appeared is to find an optimum dimension of such a separate grounding layout surface for minimum noise figure, which is a very complicated task, especially if the parasitic of every GaAs FET is vary from sample to sample.

The measured different realized samples using this new technique, resulted in a noise figure of1.5~1.7 dB in some cases and a 2.4~2.6dB in other cases. The problem in principle lies on finding an optimum dimension of such a separate ground as explained before.

Instead of going through the suggested separate grounding layout and its complexity, an experimental technique has been tried using the cell standard positive bias, whereas a network structure has been reached to be connected at the GaAs FET input stage. This guaranteed the stability of the cell and achieved a considerable low noise figure. *The new idea in this work to stabilize the GaAs FET follower cell depends on connecting a variable resistance in series with the GaAs FET gate terminal, and monitoring the cell output on a spectrum analyzer while changing the cell source impedance. A series gate resistance value is reached to be 3.5~5KΩ. This resistance range increased the cell Noise figure dramatically to 16 ~22dB. A coil of 100nH is used to shunt the reached series gate resistance, and accordingly a noise figure of around 1.4dB is measured.* As shown in Figure 2.31, a series combination of R and C is connected between the GaAs FET gate and ground. An empirical values of C = 1~2pF and R = 570Ω is reached experimentally in the laboratory, whereas a minimum NF is measured (order of 1.4dB) and stability against the variable source impedance is achieved and checked experimentally. The final stable cell is shown in Figure 2.31.

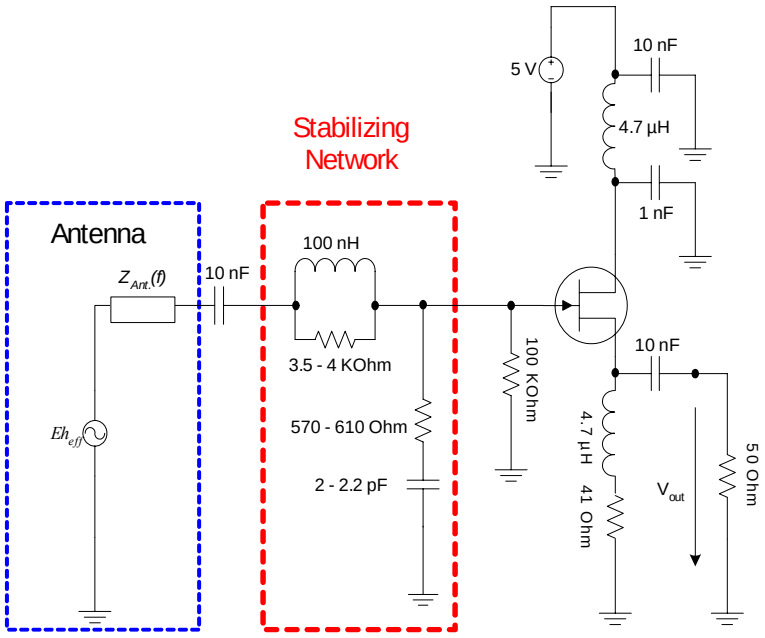

Figure 2.31: GaAs FET CLY2 Source Follower Cell Stabilizing Network

It should be noted that the stabilizing network reached with the normal available positive bias utilized the network used by the negative bias cell of using a resistance R in series with a capacitor C between the GaAs FET gate and ground. The source follower cell with the stabilizing network reached has been realized with a different layouts *of different thicknesses of 0.5,1 and 1.5mm* and tested experimentally, whereas a noise figure of 1.4 ~1.45dB has been measured which didn't vary from sample to sample, and in addition showed a stability in face of a different variable source impedances. Although that the cell measured noise figure is a little bit higher than the case of negative bias case (NF= 1.2 ~1.3dB), however the cell utilizes a positive bias with stable performance and acceptable low noise figure for FM applications. In addition that the network can be used with any source follower circuit realized by different transistors too with just choosing the right components values for the suggested stabilizing network according the application used frequency range.

Figure 2.32 summarizes the noise figure measurements done for different GaAs FET follower cells realized with the different explained stability techniques and compared to the simulation results too, whereas the circuit components losses is included (e.g.coils of quality factor Q = 10 at 100MHz has been substituted in simulation for a better noise figure real results). This low coil quality factor is typical for most RF coils available as explained earlier. In the following section, a general design examples based on the different discussed stability techniques will be introduced.

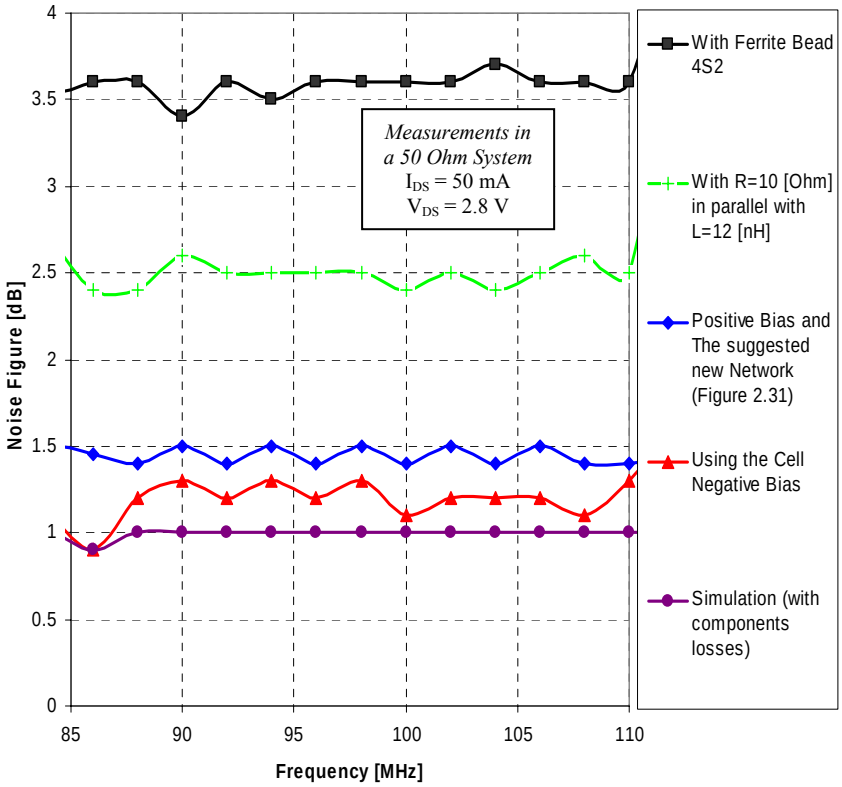

Figure 2.32: GaAs FET CLY2 Source Follower Cell Simulated and Measured Noise Figure

2.2.6 Design Examples of the Proposed Active Antenna New Amplifier

In this section, a FM active antenna amplifier design examples based on the new concept introduced in Figure 2.1 will be presented for typical antenna impedances that frequently encountered in windscreen vehicles. The windscreen antenna structure design for different impedances is not the scope of this work; however the measured impedances will be used throughout the design. The antenna impedance one port measurements will be transformed to two port as explained in chapter one (section 1.2.3 and Figure 1.10) for the necessary design and simulation. For the amplifier stability requirements, the different explained techniques demonstrated in section 2.2.5.III will be utilized in different examples for illustrative purpose. Finally, an evaluation conclusion will be presented for the different design examples. In the following sections, a type for each measured antenna impedance will be assigned, whereas type assignment is only for differentiating each antenna from the other.

2.2.6.1 Antenna Impedance Type (A)

Consider the measured windscreen antenna impedance in the FM range (87MHz – 108MHz) as shown in Figure 2.33.

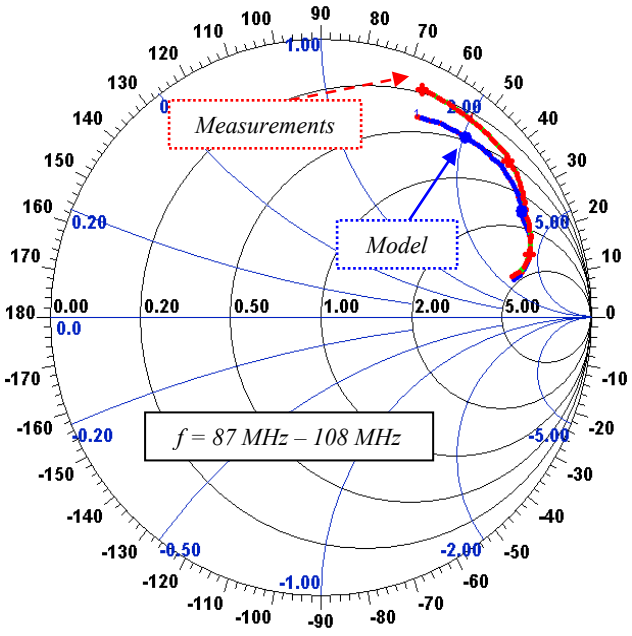

Figure 2.33: Type (A) Vehicle Windscreen Antenna Measured Impedance (Red Circles) and its Equivalent Circuit Model (Blue Circles)

As explained in section 2.2.5. I.(C), the main design goals are to achieve a power gain of *5 – 6 dB* in the FM range, evaluating the system noise figure and the third order intermodulation

distortion performances according to the **VDA** requirements as explained earlier. The complete design procedure in this example will be expalined, so that to apply it for the rest of examples.

The first step is the lossless filter structure (Figure 2.1) selection which should verify Equation 2.45. As explained in chapter one, section 1.5.2.2 that a T-filter structure can fulfill the required intermodulation distortion in the FM band [20]. The T- filter structure will be investigated followed by an evaluation of the amplifier total performance. Different filter structures will be investigated too in different examples. Finally the measurements will be compared to the simulation with the realized filter structure. The general RF circuit to be designed is shown in Figure 2.34.

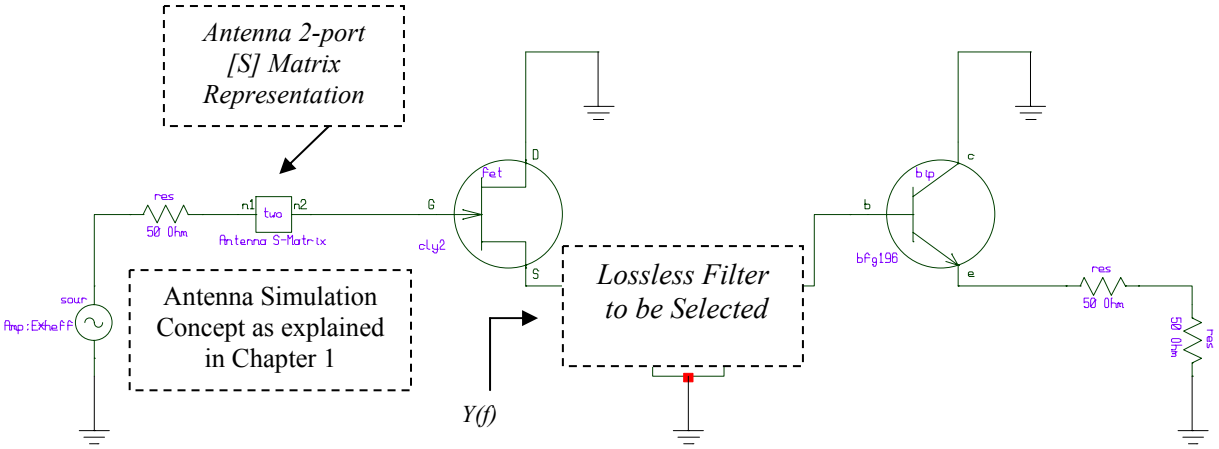

Figure 2.34: Active Antenna Amplifier for Type (A) Antenna

The chosen bias currents of the GaAs CLY2 FET and the Bipolar (BFG 196) are 50 mA and 25 mA respectively. The filter component values can be optimized according to Equation 2.45 at certain discrete frequency points or direct software optimization as required. Both ways will be presented for illustration purpose. Assuming a constant antenna directivity, and using Equation 2.45, let us choose a design value of G_o = 465µS, and selected the frequency points 87.5MHz, 96MHz and 108MHz respectively.

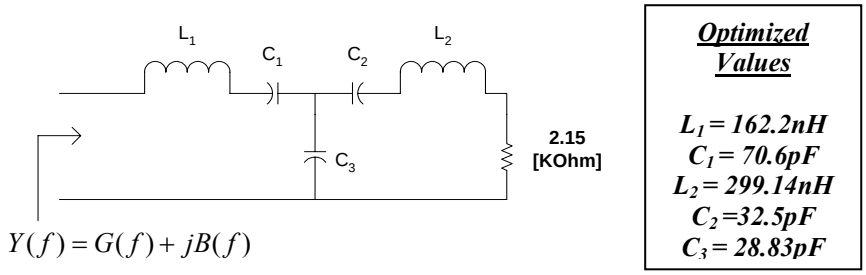

Figure 2.35: The Optimized Filter for Type (A) Antenna

As shown in Figure 2.35 evaluating the filter admittance real part at these chosen frequencies led to $G(f) = 0.075, 0.033, 0.003$ [S] respectively. Feeding these values to the software optimizer, led to the components values listed in Figure 2.35. Consequently, the Amplifier simulated Frequency response and the noise figure is shown in Figure 2.36.

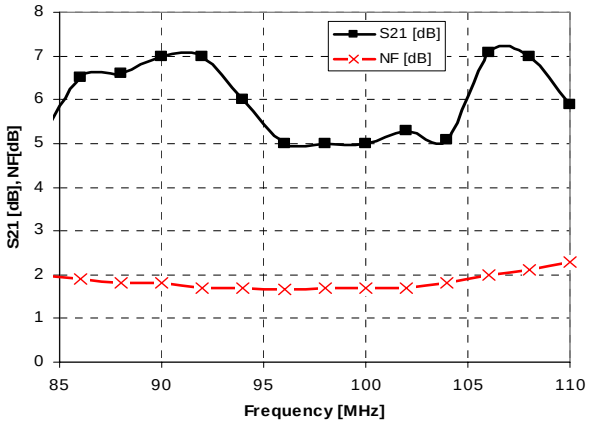

Figure 2.36: Simulated Amplifier Frequency Response Using Discrete Frequency Points

The results shown are quite satisfactory compared to the less points used during the computation. Although the computational way using Equation 2.45 may look lengthy, especially if a great accuracy is required, however it explains the required explicit condition between filter admittance and antenna impedance. A software based symbolic optimization can help and reduce the number of calculations which will lead to a satisfactory flat frequency response; however this was not available at the preparation of this work.

Now, adopting the direct software numeric optimization (*with the acceptance that the optimization results can't be actually controlled as required*), by assigning an optimization goal in the FM range to have a frequency response power gain of 5-6 dB. The new optimized filter components values obtained are: $L_1 = 100nH$, $C_1 = 330pF$, $C_2 = 220pF$, $L_2 = 470nH$ and $C_3 = 33pF$. The designed circuit shown in Figure 2.37 has been realized in the laboratory whereas the antenna has been replaced by an equivalent passive network optimized to approximately match the impedance measurements as shown in Figure 2.33 (blue circles). The measurements and simulation results of the amplifier frequency response, noise figure and third order intermodulation distortion performances are depicted in Figures 2.38 and 2.39 respectively. A good agreement has been achieved between the simulation and measured results. For stability of the designed amplifier, the stabilizing technique reached in Figure 2.31 has been used, thus a stable FM active antennas is achieved.

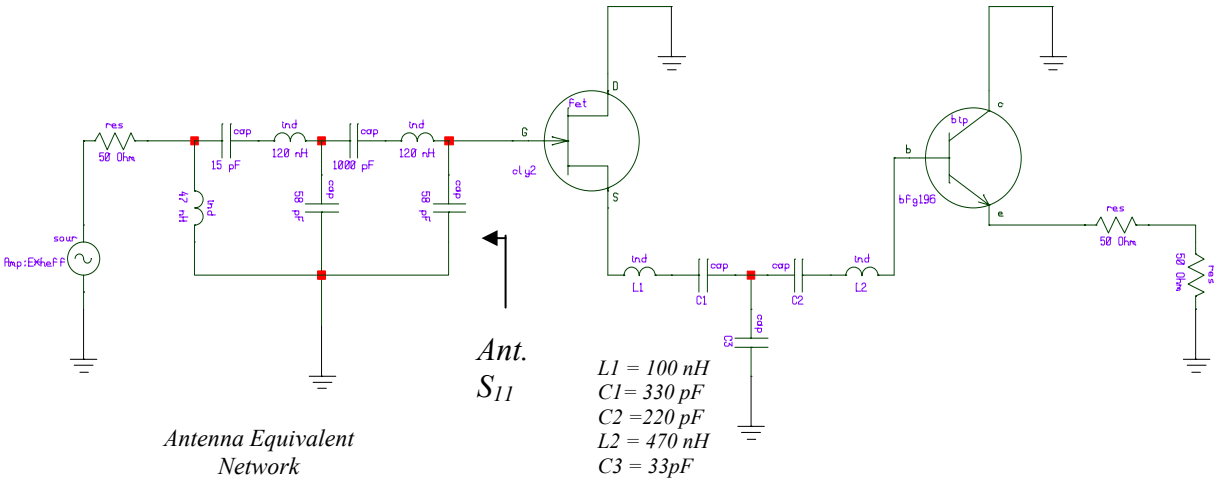

Figure 2.37: Realized Active Antenna Amplifier RF Circuit Schematic

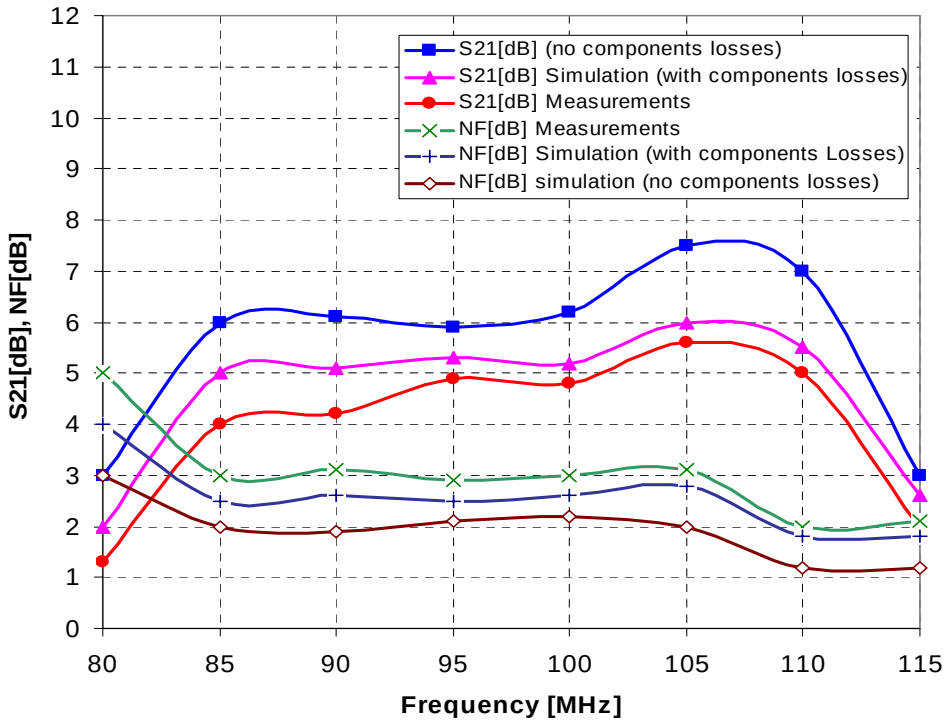

Figure 2.38: Measurements and Simulation Results of the Realized Active Antenna Amplifier

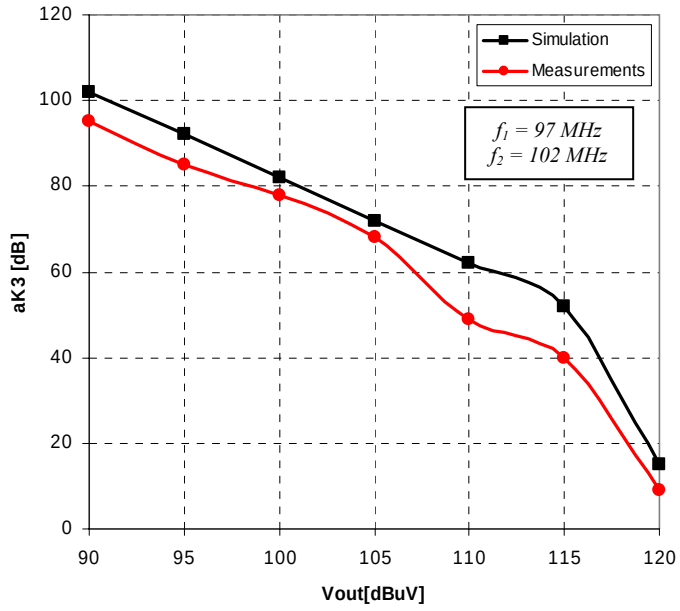

Figure 2.39: Measurements and Simulation Results of the Amplifier Third Order Intermodulation Distortion Performance

In view of the introduced evaluation Equation (2.54) in section 2.2.5.III, let us evaluate the obtained measured results regarding the power gain and the noise figure at 100MHz. The measured noise figure at 100MHz is approximately 3dB. By substituting this value in equation (2.5), we have: S_{21}[dB] ≤ 9.4-F[dB] = 9.4 – 3 = 6.4[dB], whereas the measured power gain S_{21} is approximately 4.9[dB]. Thus Equation (2.54) is satisfied according to the **VDA** standard requirements between the power gain and noise figure. From Figure 2.39, the circuit intermodulation separation a_{K3} ≈ 80 dB at the circuit output voltage of 100dBμV, which means the amplifier fulfilled the nonlinear requirements too assigned by the **VDA**.

2.2.6.2 Antenna Impedance Type (B)

Consider the windscreen antenna impedance in the FM range (87MHz – 108MHz) as shown in Figure 2.40. Figure 41 shows the realized circuit schematic. As shown in this figure, the lossless filter structure chosen is of L-Type, whereas the optimized coils values are L_1, L_2 = 39nH, and the series capacitor C_1 = 33pF and the parallel capacitor C_2 = 39 pF. The bipolar transistor input impedance will be chosen to be 300 Ohm. The circuit has been realized using a negative supply for both transistors and a stability technique of using capacitor (C= 2.2pF) in series with a resistance of 2KΩ has been adopted (as in Fig. 2.29).

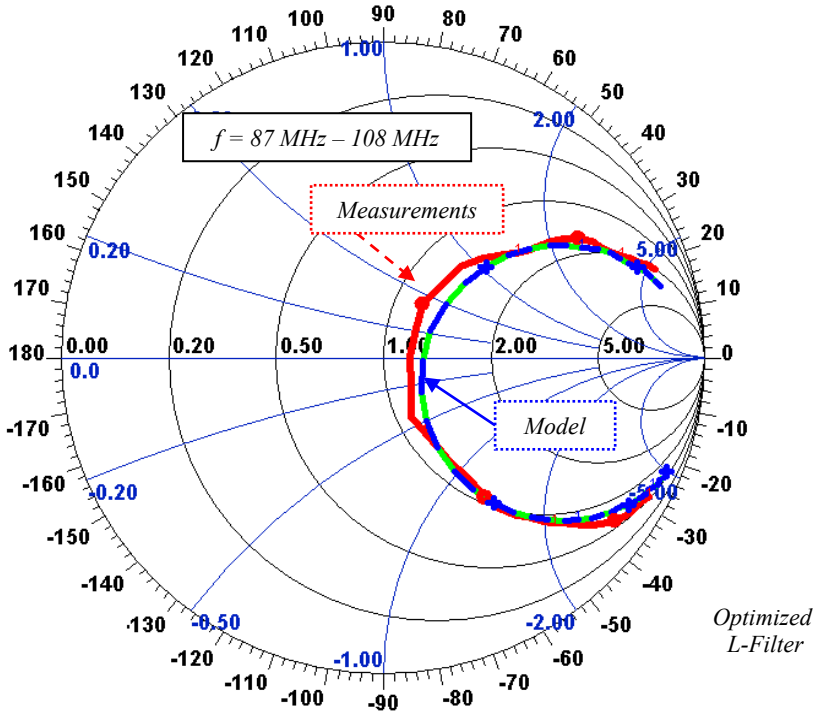

Figure 2.40: Type (B) Vehicle Windscreen Antenna Impedance (Red Circles) and its Equivalent Circuit Model (Blue Circles)

The antenna has been realized using suitable equivalent network matches approximately the measured values as shown in Figure 2.40 (blue circles). A very good agreement has been achieved between the simulated and measured values of the amplifier frequency and noise figure responses as shown in Figure 2.42.

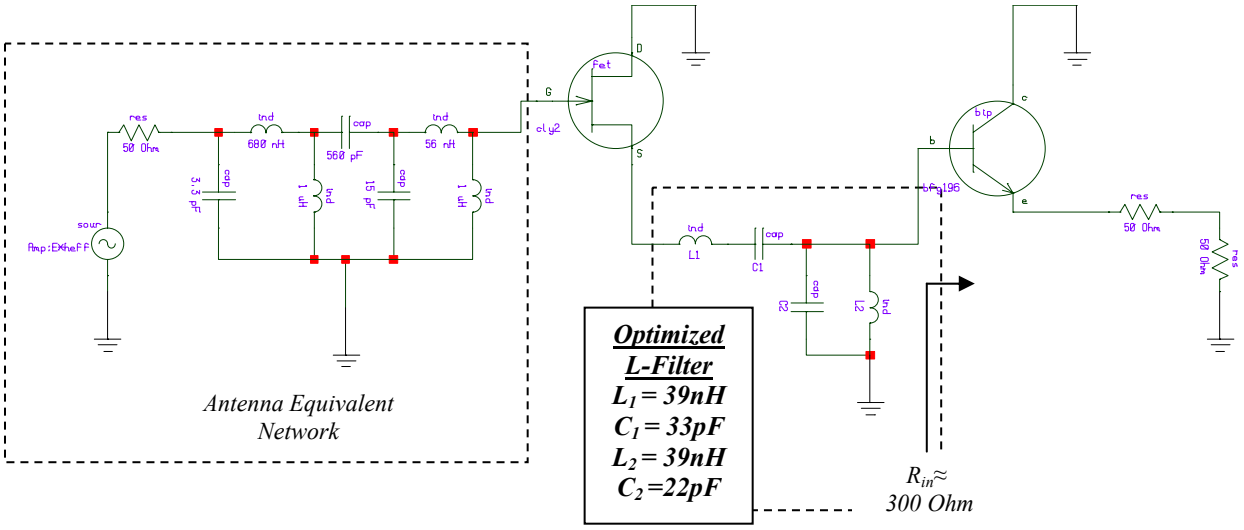

Figure 2.41: Realized Active Antenna Amplifier with Negative Supply (RF Circuit Schematic is shown)

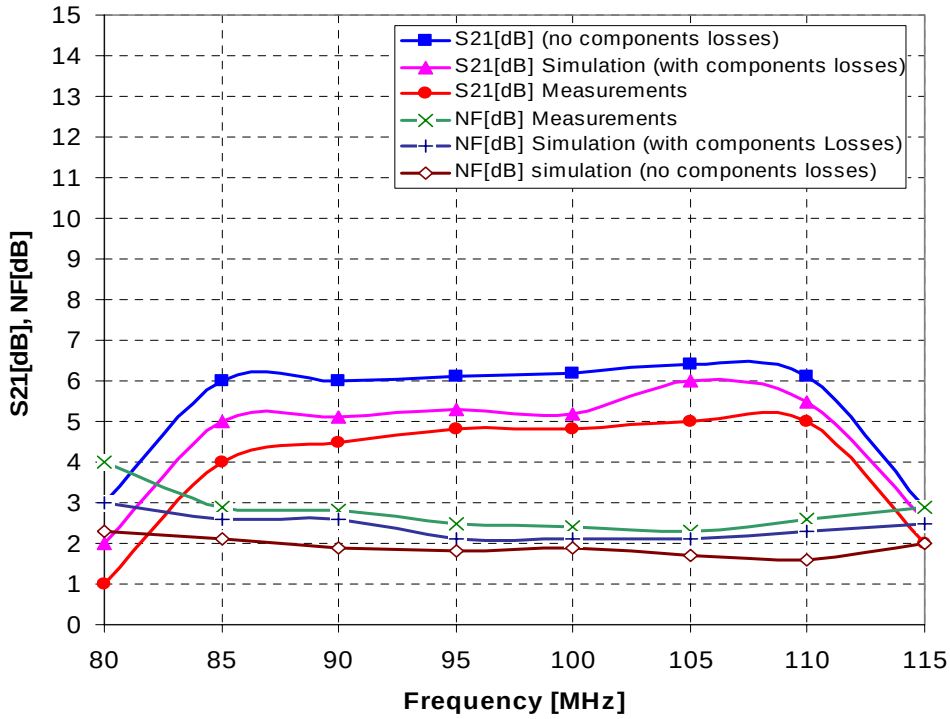

Figure 2.42: Measured and Simulated Frequency Response of the Realized Active Antenna Amplifier with negative supply

As explained in the previous section, let us re-evaluate the obtained measured results regarding the power gain and the noise figure at 100MHz for type (B) antenna impedance amplifier. The measured noise figure at 100MHz is approximately 2.4dB. By substituting this value in Equation (2.54), we get: $S_{21}[dB] \leq 9.4 - F[dB] = 9.4 - 2.4 = 7[dB]$, whereas the measure S_{21} is approximately 5[dB] and thus equation (2.54) is satisfied. Consequently the designed amplifier satisfied the **VDA** requirements.

The circuit third order intermodulation distortion has been simulated for two different GaAs FET drain current values of 180 mA and 50 mA respectively, whereas the bipolar transistor input resistance has been varied from 300 Ohm to 600 Ohm. A noticeable enhancement of the intermodulation distortion has been noticed at high drain current of 180mA with R_{in} = 600 Ohm bipolar input resistance (shown in Figure 2.41), whereas at the same current and with increasing the input resistance R_{in}, a 1.5dB enhancement has been noticed, but any extra increase of the input resistance didn't enhance the IMD. The circuit measurements done at I_{ds} = 50 mA and compared to the simulated ones as shown in figure 2.43. *(Measured $a_{K3}[dB] \approx$ 76dB compared to 80dB simulated value @ 100dBμV).*

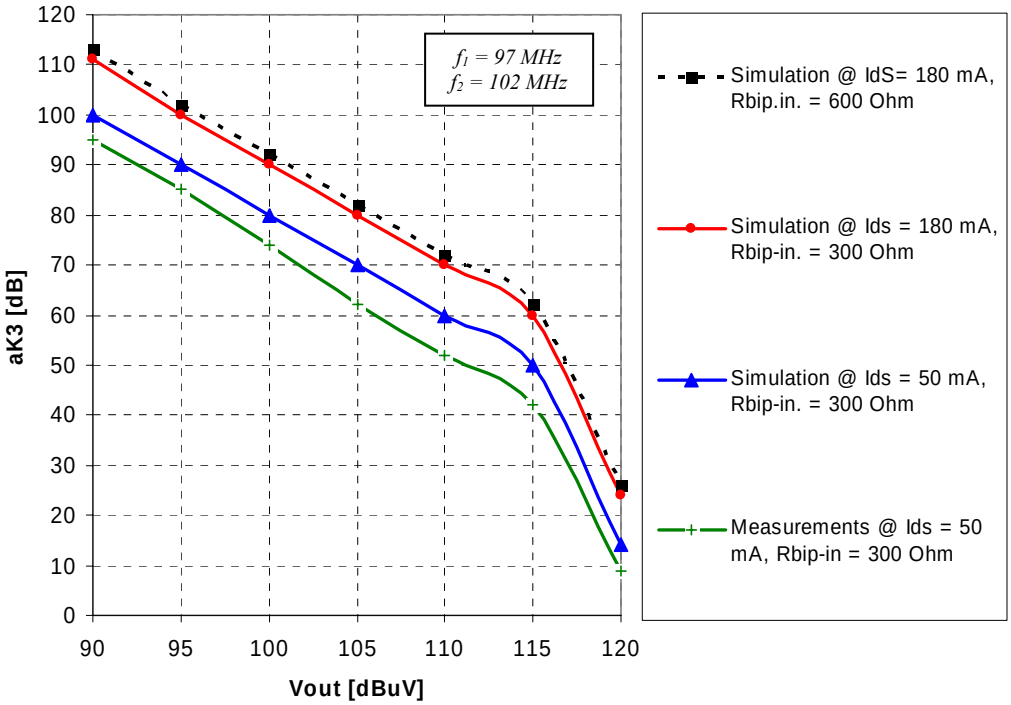

Figure 2.43: Measurements and Simulation Results of the Amplifier Third Order Intermodulation Distortion Performance

For this circuit, additional T-Filter structure (as in Figure 2.35) with a bipolar input resistance of R_{in} = 600 Ohm has been optimized for comparison purpose regarding the intermodulation distortion. The filter optimized values obtained were *L_1 = 467nH, C_1= 1332.2pF, L_2= 300.5nH, C_2 = 1271.4pF and C_3 = 79.2pF respectively.* Figure 2.44 depicts the third order intermodulation simulation results at drain current of 180mA and bipolar collector current of 25mA. It should be noted that the T-Filter structure for this circuit degrades the intermodulation distortion by around 10dB which is quite a high value. Actually the reason is not related to the filter T-structure, however to its input impedance which didn't achieve the stated condition of equation 2.45. This is only a consequence of the direct numeric optimization which succeeded to achieve a similar frequency response like that in figure 2.38 but fails to maintain the same third order intermodulation performance as depicted in figure 2.44. This can happen with some filter structures and with other not as in case of L-structure filter optimized numerically with the same numeric software optimizer. Instead of displaying both filter input impedances to see if they are high or not, let us analyze this situation physically due an important fact that these obtained filter components are optimized directly by the software optimizer used. This situation will be analyzed in some detail in view of the derived design condition of equation 2.45 which represents an important design concept as will be explained.

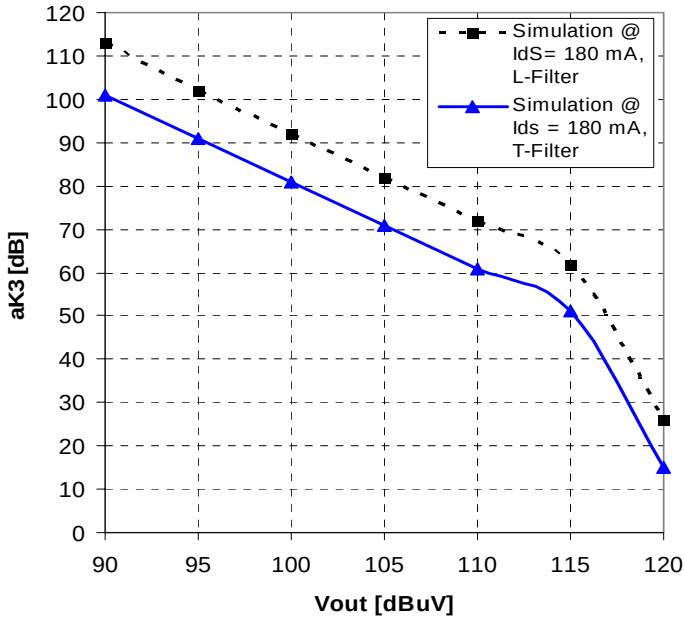

Figure 2.44: Simulation Results a_{K3} [dB] with Different Filter Structures

Figure 2.45 shows the frequency dependence of the antenna real part impedance in the FM range used in this example. Figure 2.46 shows the numerically optimized L and T filter structures and their simulated real part input admittances respectively. Both filters are directly optimized using the software optimizer.

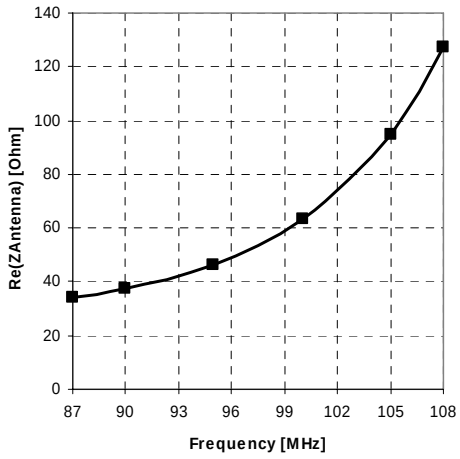

Figure 2.45: Real Part of Type (B) Antenna Impedance

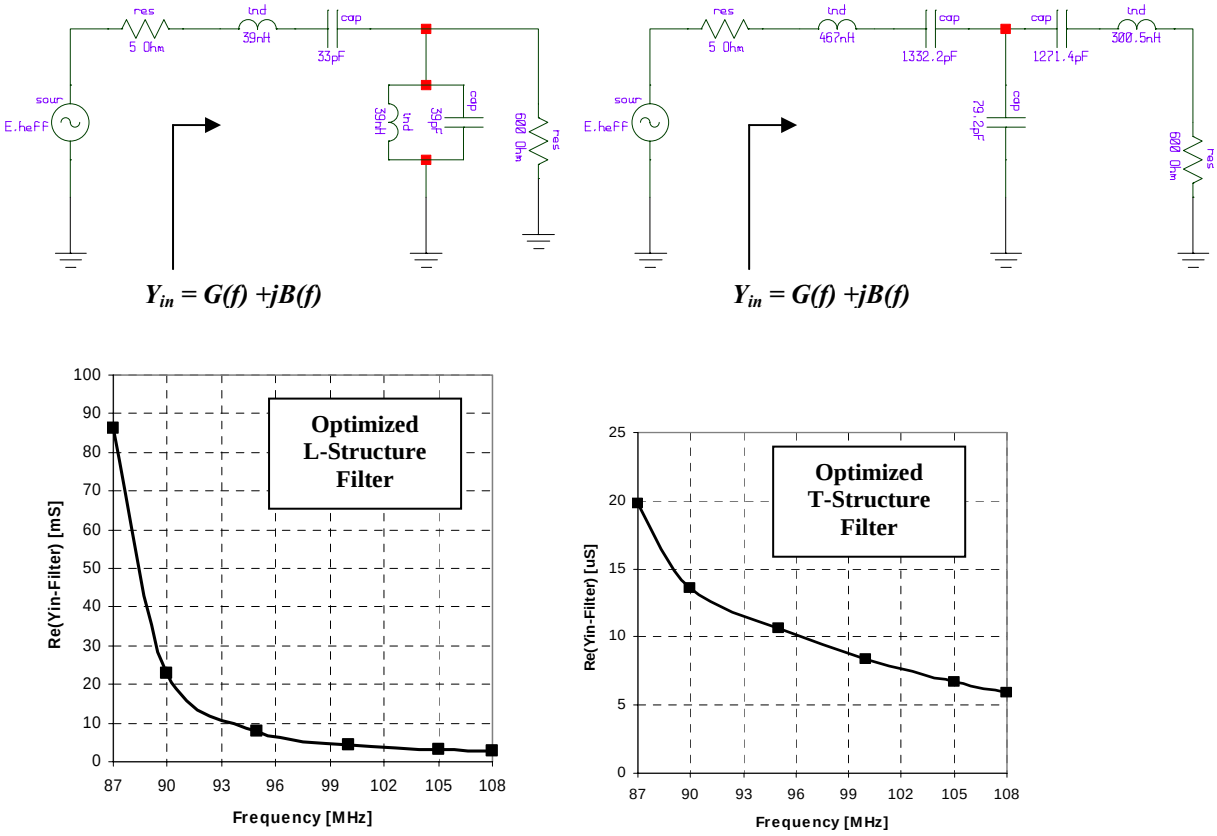

Figure 2.46: Simulated L and T filter Structures Input Admittances

From figure 2.46, for the filter structure simulation purpose, the 5 Ohm source resistance represents the the GaAs FET source terminal output low impedance whereas the 600 Ohm represents the selected bipolar input impedance. Let us check the design condition set by Equation 2.45 at a frequency of 100MHz for example. From Figure 2.42, at 100MHz, the antenna resistance is approximately 63.6 Ohm, substituting in Equation 2.45 for a 600Ohm filter load resistance (*leads to* G_o*= 1/600mS*) results in a minimum required filter real part admittance of $G_{min}(100MHz)$ = 104.8µS. By reading the real part admittance of both optimized filters in Figure 2.46, we get: $G\text{-}_{L\ filter\ structure}(100MHz)$ = 4.3mS = 4300µS, whereas $G\text{-}_{T\ filter\ structure}(100MHz)$ = 8.4µS which shows that over the minimum admittance real value has been achieved by the L structure whereas the T structure has a very poor real input admittance value and considerably lower than the required minimum value. This affects considerably the whole amplifier intermodulation distortion performance whereas the amplifier frequency response was almost the same due to the right filter input admittance design tendency which is approximately reciprocal to the antenna resistance as shown in figure 2.45 and 2.46 according to Equation (2.45). It should be clear at this stage that the directly optimized amplifier using any software optimizer can lead to such a noticed situation

and consequently the circuit can directly be optimized (without using Equation 2.45) using different filter structures until the desired goal of both good frequency response and intermodulation distortion is reached. A conclusion can be arrived here, *that not only the filter structure was the main cause of the circuit third order intermodulation distortion degradation, but also its input impedance*. This problem will be discussed in detail through this chapter in section 2.2.7.

2.2.6.3 Antenna Impedance Type (C)

Consider the windscreen antenna impedance in the FM range (87MHz – 108MHz) as shown in Figure 2.47.

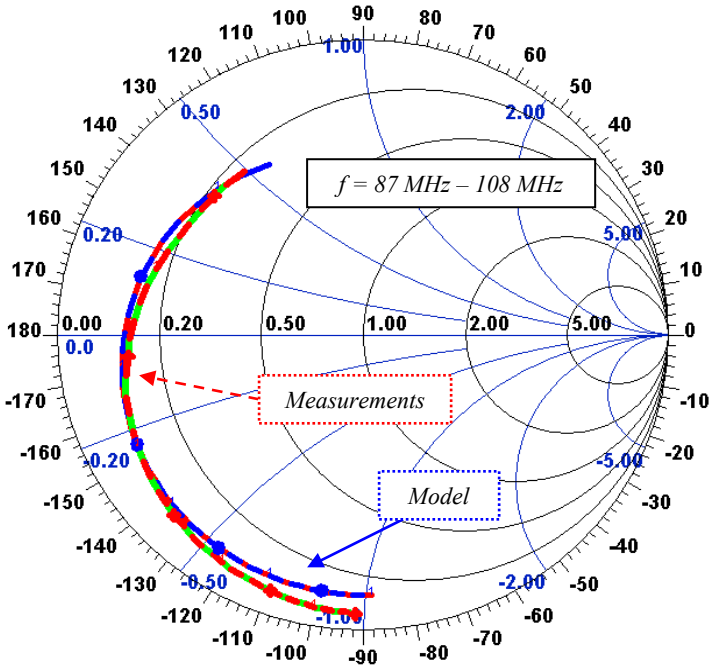

Figure 2.47: Measurements Type (C) Vehicle Windscreen Antenna Impedance (Red Circles) and its Equivalent Circuit Model (Blue Circles)

Figure 2.48 shows the implemented RF-circuit with an antenna equivalent network (optimized to approximately match the impedance measurements). The circuit is implemented with a positive power supply with selected bias currents of $I_{DS} = 50mA$, $I_C = 25mA$ respectively. The stability technique used is a ferrite bead 4S2 from Philips as shown in the schematic figure of 2.26. T-Filter structure has been chosen, whereas the direct software optimization didn't succeed to bring a satisfactory frequency response, so the numerical technique derived in section 2.2.5 is used (as explained as in the first example by evaluating equation 2.45) at discrete frequency points of 87MHz, 90MHz, 95MHz, 100MHz, 105MHz and 108MHz. The optimized filter component values are included in Figure 2.48. Figure 2.49, shows the measured and simulated results of the realized amplifier frequency and noise figure responses whereas the circuit bias currents are $I_{DS} \approx 50mA$, $I_C \approx 25mA$ respectively.

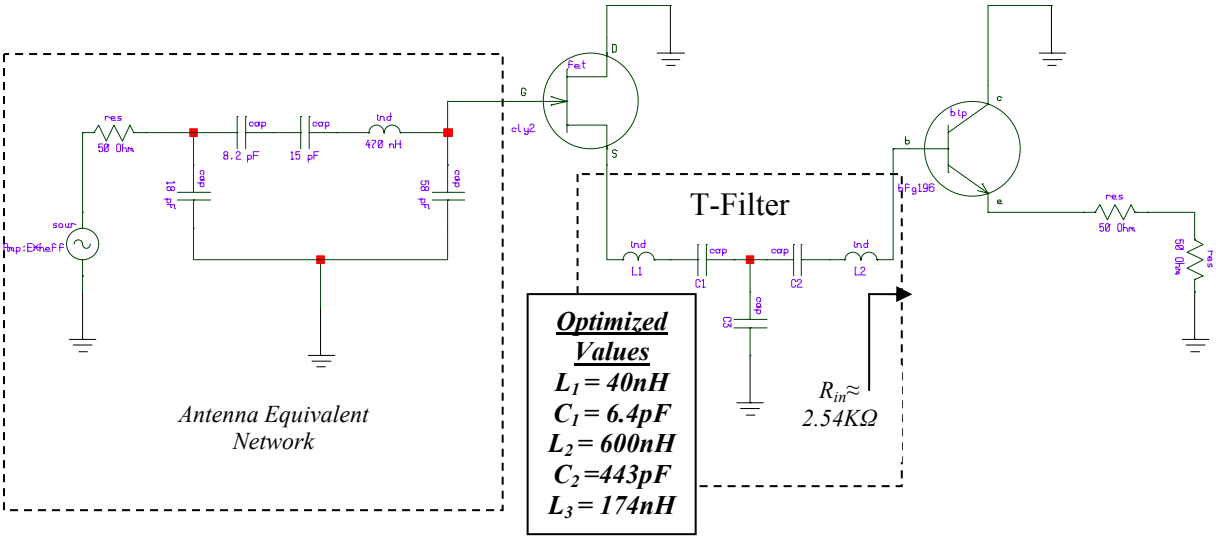

Figure 2.48: Realized Active Antenna Amplifier RF Circuit Schematic

The poor noise figure is expected as explained in section 2.2.2 (Figure 2.8) due to the fact that the measured antenna real part resistance is lower than 8 Ohm. By applying the design evaluation equation (2.54) in this case, we get: The measured noise figure at 100MHz is 15dB, then substituting in (2.54) we obtain S21≤ 9.4 – 15 = -5.1dB, whereas the measured S_{21} is 2.5dB which indicates that the inequality (2.54) is not satisfied in this amplifier. Consequently, this indicates that this amplifier with such low impedance antenna type introduces a high output noise voltage and thus, it can't be used satisfactorily.

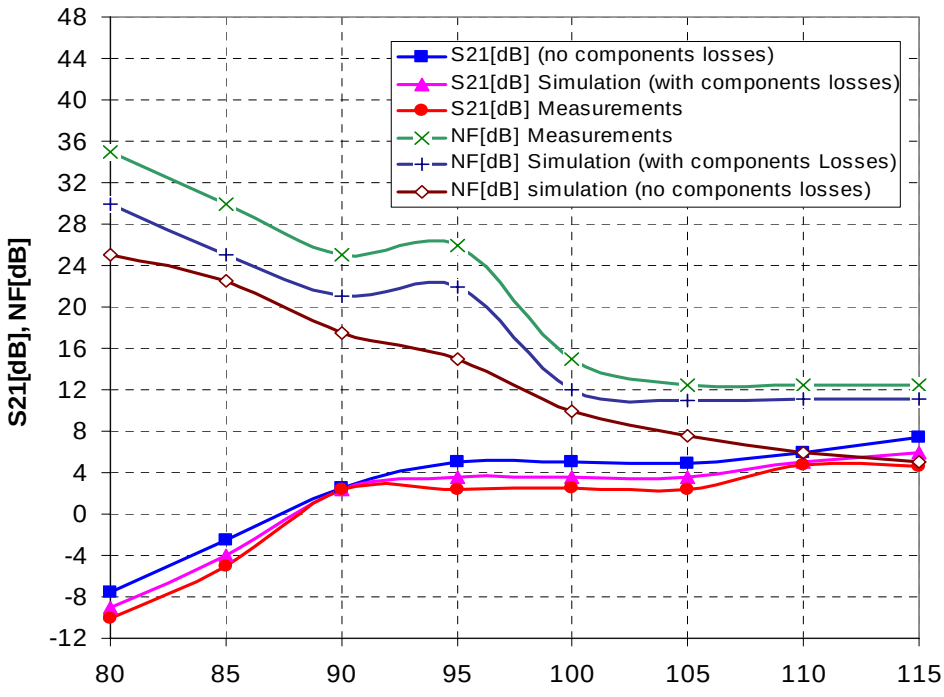

Figure 2.49: Measured and Simulated Frequency Response of the Realized Active Antenna Amplifier for Antenna Type (C) Impedance

Figure 2.50 depicts the amplifier measured and simulated third order intermodulation distortion which is quite satisfactory according to the **VDA**. As shown in this figure by simulating an increase of the GaAs FET bias current to 180mA, a 15dB enhancement is achieved of the total amplifier third order intermodulation distortion compared to the simulation results at 50mA GaAs FET bias current.

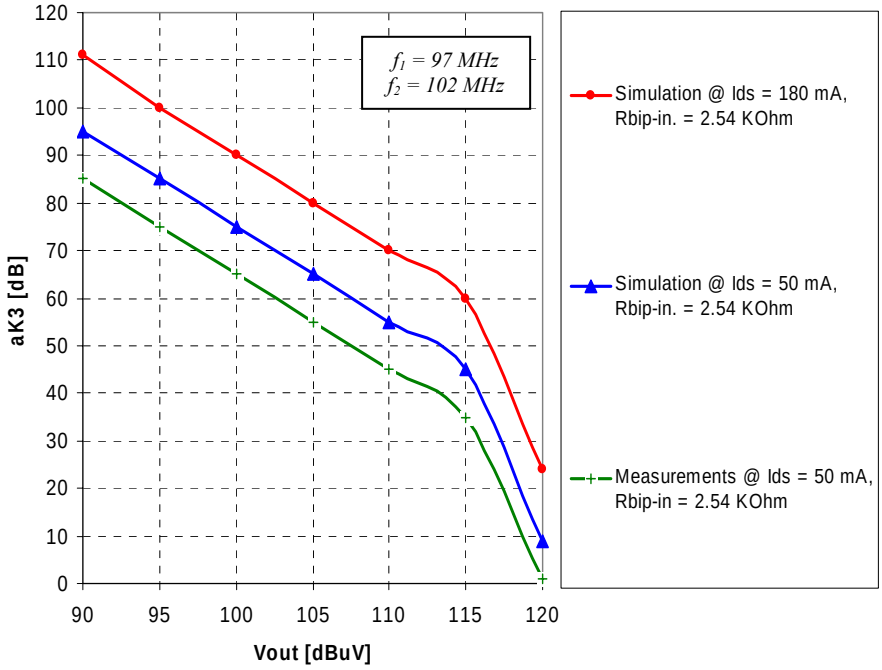

Figure 2.50: Measurements and Simulation Results of the Amplifier Third Order Intermodulation Distortion Performance

At this stage, it would be worthy to state that with such a low impedance type, a satisfactory third order intermodulation distortion can be obtained, but the high noise figure in the amplifier required frequency response may be the main obstacle to use such an amplifier with such low impedance antenna as explained and evaluated. As derived in section 2.2.2, such a low impedance antenna should be set as a forbidden region to use due to the dominance of the high noise figure. In addition, the suggested and designed active antenna amplifier in [20] set a forbidden region of such an antenna type too.

However, it should be noted that this is correct in case of direct connection between the amplifier and the antenna. But if a transformer of high turns ratio is connected between the amplifier and this low impedance antenna, a considerable reduction of the noise figure is expected. Figure 2.51, shows the simulation results (*compared to the previous case*) done by connecting an ideal transformer of turns ratio (N_2:N_1 = *10*) between the antenna and the amplifier.

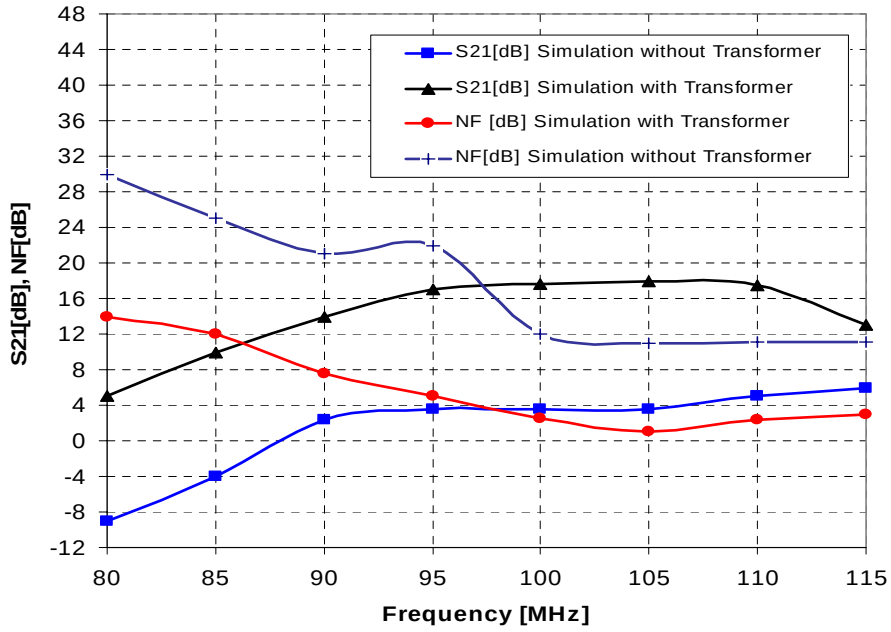

Figure 2.51: Simulated Frequency Response of the Realized Active Antenna Amplifier for Antenna Type (C) Impedance with Ideal Transformer of 10 Turns Ratio Connected Between the Antenna and the Amplifier (components losses included in the simulation)

It is clear that a considerable enhancement obtained in the whole amplifier frequency response, which sets a scientific solution that can be implemented with low impedance antennas, however using an extra transformer is not a preferable solution; since this increases the price of such a product.

2.2.7 Discussion and Design Suggestions based on the proposed examples of the Active Antenna New Amplifier

Section 2.2.6 illustrated in detail a different realized active antenna amplifier design examples. The main problem noticed is that with optimizing different filter structures, the FM amplifier third order intermodulation distortion may be degraded with some filter structures. In this section, let us pick up the case of example two of antenna type (B) explained in section 2.2.6.2. The example has been realized using two different optimized filter structures, one is L-structure and the other is T-structure.

To visualize this situation and variation of the amplifier intermodulation or degradation, let us refer to Figure 1.33, whereas the follower cell based GaAs FET intermodulation separation a_{K3} has been simulated versus the amplifier output voltage V_{out}[dBμV]. A conclusion has been reached that as the cell load resistance increases, the separation a_{K3} increases until it saturates at a certain value. One can simply approximate and portray this situation as shown in Figure 2.52 (at V_{out} = 100dBμV according to **VDA**), whereas the separation a_{K3}[dB] can be expressed as if it is proportional logarithmically to the load R_L at a certain FET drain current. Consequently as R_L increases, a_{K3}[dB] increases up to a certain maximum value. Now, the case of the filter as a load to the source follower cell, will lead to variable feedback impedance $Z_F(f)$ as depicted in Figure 2.52, and such variation is an optimizer dependent. This simply means, that when a certain filter structure is optimized and achieves the required frequency response, the follower feedback impedance $Z_F(f)$ can fall in the region where a_{K3}[dB] is low (points at $Z_{1F}(f)$ or $Z_{2F}(f)$ for example) and consequently a degraded amplifier intermodulation performance as noticed in some examples as in section 2.2.6.2. Such a pictorial visualization in Figure 2.52, suggests that if one scaled the optimized filter impedance by a factor of β for example, the probability of moving the points of $Z_{1F}(f)$, $Z_{2F}(f)$,….etc to the region where a_{K3}[dB] approaches its maximum value becomes higher.

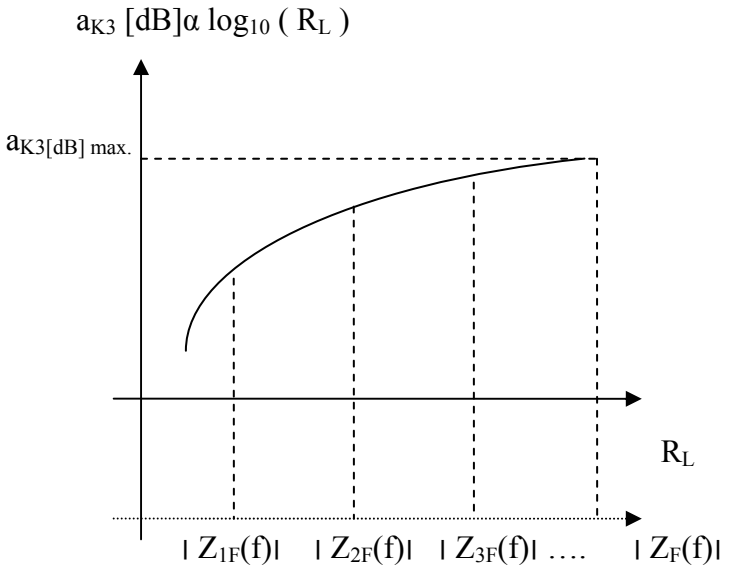

Figure 2.52: Pictorial Visualization of Source Follower Cell Intermodulation Separation a_{K3}[dB]-Load Impedance Dependence At The Circuit Output Voltage of 100dBμV

This simply means making a_{K3} *[dB] proportional to* $log_{10}(\beta \cdot |Z_F(f)|)$, *whereas* $\beta >> 1$, which can simply be a current gain of a bipolar transistor buffer amplifier for example. By such a scaling of the argument of the logarithmic function, the follower cell new feedback impedance becomes $Z'_F(f) \approx \beta \cdot Z_F(f)$**,** thus a better a_{K3} [dB] is expected as it falls in the higher values region of the logarithmic function.

Although such a suggested solution can be adopted if the intermodulation is not satisfactory with a certain optimized filter structure, however this solution can be considered to be a general technique which guarantees somehow a good intermodulation distortion separation with any filter general structure.

Let us pick up the example explained in section 2.2.6.2, in case of the optimized filter T-structure which led to a worse intermodulation distortion relative to the L-structure filter. A buffer amplifier will be connected between the GaAs FET output terminals and the optimized filter. The RF circuit is shown in Figure 2.53. It is clear that the amplifier GaAs FET first stage scaled feedback impedance $Z'_F(f)$ is now approximateley $\beta \cdot Z(f)$ whereas β is the bipolar buffer current gain and $Z(f)$ is the filter input impedance

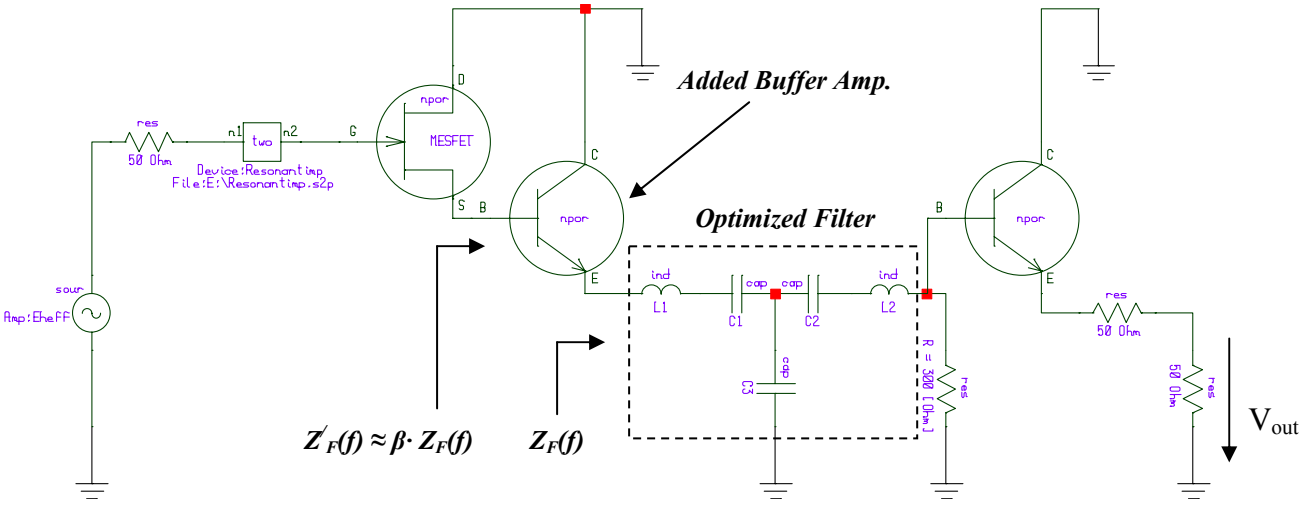

Figure 2.53: Modified Circuit in Figure 2.41 with the Suggested Added Buffer Amplifier (Design Exapmle of Antenna Type (B))

By taking the same filter component values explained in section 2.2.6.2, and operating the added buffer at a collector current of I_C = 25mA, an intermodulation separation of 90dB is reached by simulation at the circuit output voltage of 100dBµV compared to 80dB without the additional buffer. Now with the added buffer and by changing the filter structure to be the L-Filter structure as in the same example, a 95dB voltage separation is obtained by simulation compared to 80dB separation at 100dBµV output without buffer. It is quite clear that when the GaAs FET feedback impedance $Z_F(f)$ is increased from $Z(f)$ to $\beta \cdot Z(f)$, a guarantee of a high intermodulation separation is achieved as explained before.

The idea can be extended by replacing the buffer with a Darlington buffer, so that the GaAs FET feedback impedance can be greatly increased to be $\beta^2 \cdot Z(f)$. However what limits this general cascade of buffers is the total amplifier required low noise figure performance, as the noise figure is expected to increase a little bit due to the added buffer amplifier and consequently it may be degraded by a cascaded of Darlington buffers.

Adopting a single buffer transistor between the FET generally and the optimized filter can be satisfactory for different designs and it opens the thinking of replacing the total amplifier first stage GaAs FET by a cheaper JFET or even a bipolar transistor. Such thinking has been analyzed and simulated in this work generally so that to show the regions where such a replacement can be possible considering both the amplifier noise figure and intermodulation distortion behavior in case of a general antenna impedance. Section 2.2.3 (with Figure 2.9 circuit schematic) explained the general simulation procedure, whereas in the current case, the connection of buffer before the transformer will be adopted. The GaAs FET stage can be once replaced with JFET, parallel connected JFET and once with Bipolar transistor. A variety of three dimensional graphs can be obtained so that to set a condition(s) about the possible different uses of such amplifiers based JFET and Bipolar too. Let us categorize the study based on the above discussion of adding a buffer amplifier stage as follows in the following different cases of A,B,C and D as will be shown.

A- GaAs FET with Buffer Bipolar as a Feedback

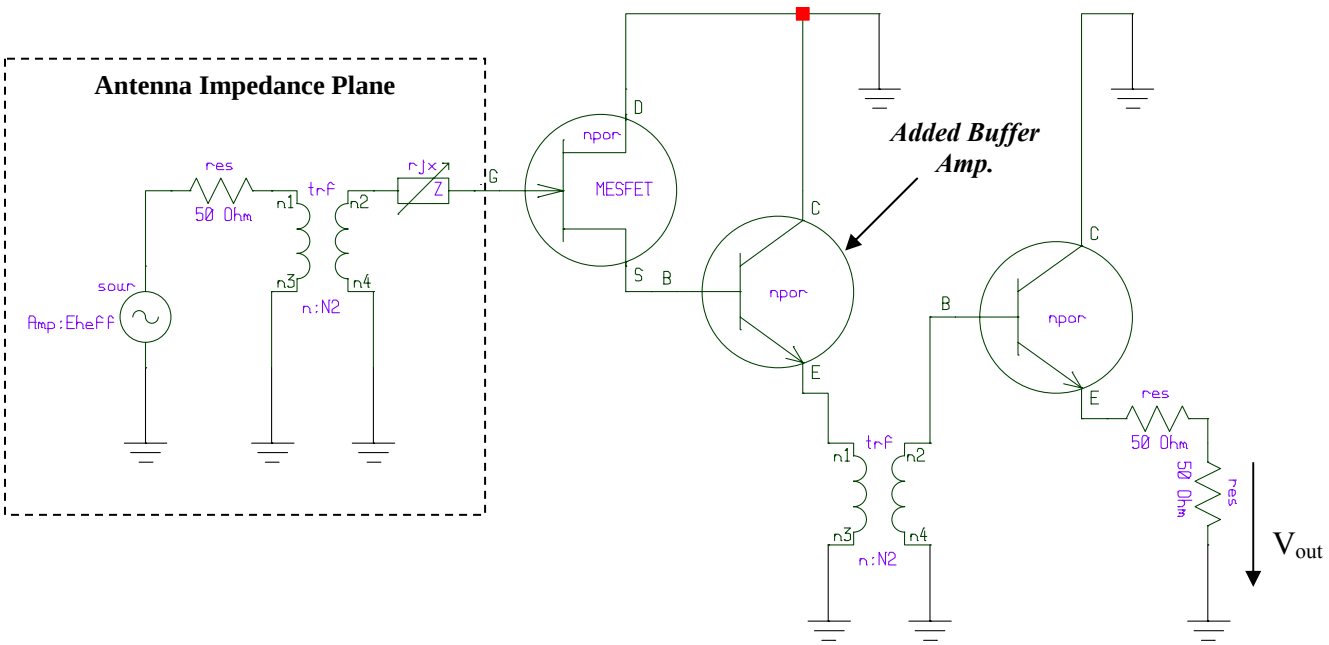

Figure 2.54: Modified Active Antenna Amplifier based GaAs FET with the additional Buffer Amplifier

Figure 2.54, shows the modified suggested active antenna amplifier with the additional buffer amplifier so that to enhance the total system intermodulation distortion.

The following intermodulation and noise figure simulation results are obtained by biasing the GaAs FET (CLY2 from Triquent) at a drain current of **I_D = 25 mA,** and both bipolar transistors (Bfq19S available from Philips) at **I_{C1} and I_{C2} of 27mA** respectively.

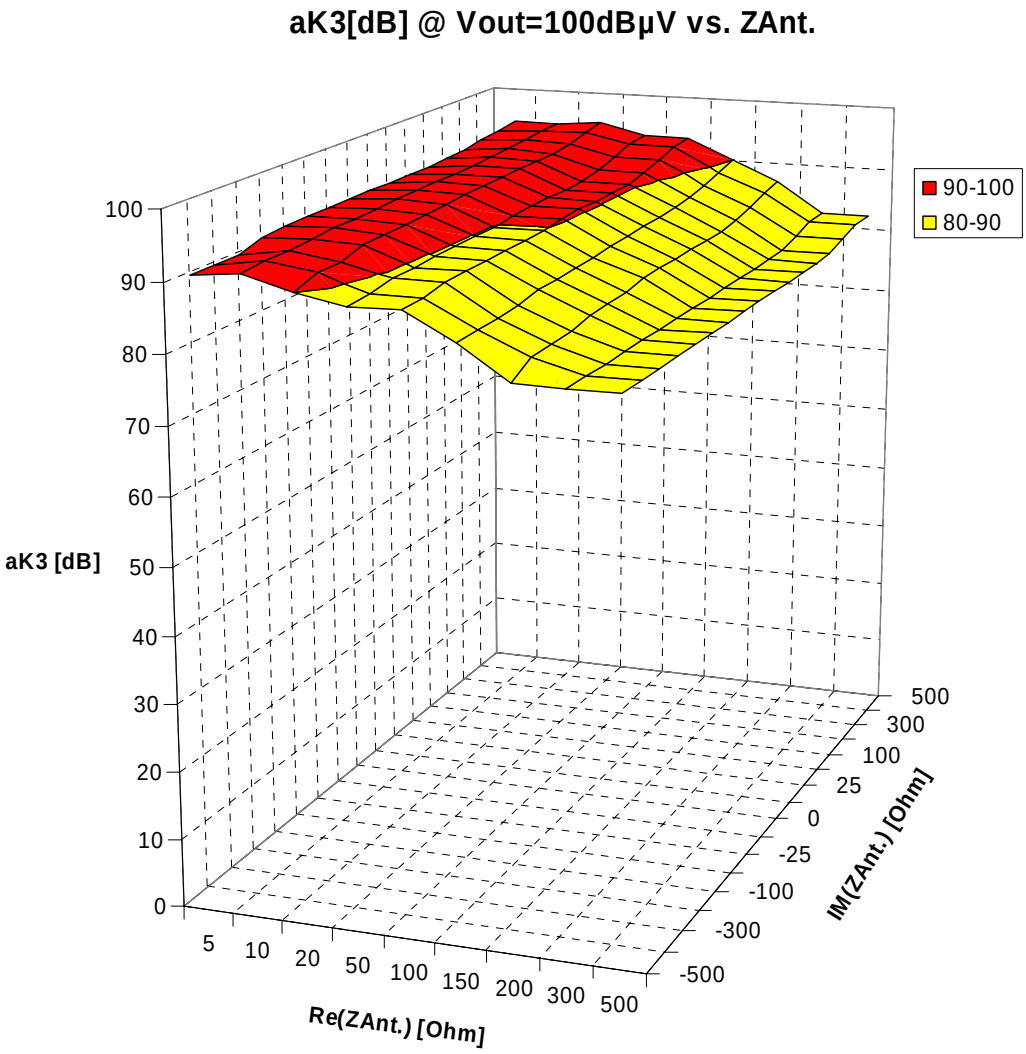

Figure 2.55: Intermodulation Distortion a_{K3}[dB] the New Active Amplifier with added buffer stage for Arbitrary Antenna Impedance

Figure 2.55, shows an important good result achieved regarding the intermodulation distortion separation at a GaAs FET low drain current of I_D = 25 mA compared to 50mA with the same results achieved in Figure 2.14 previously. This guaranteed a working of the proposed

amplifier based GaAs FET for low power applications, and this is one of the indirect effect of using the buffer amplifier as a feedback load to the GaAs FET. As seen from this figure, that the separation is still independent on the antenna impedance variation.

Figure 2.56-A, B depicts the simulated noise figure performance (A-For the three dimensional noise figure, B- For the extracted noise figure from the three dimensional graph at certain antenna reactive parts). As explained earlier, a little degradation of the noise figure happened due to the presence of the added buffer amplifier compared to Figure 2.10 illustrated in section 2.2.3, whereas the shaded red areas of low noise figure has been decreased in Figure 2.56-A. It should be noted however, that by using a better low noise bipolar transistor (like BFP460 for example from Siemens which was not available during this work), the original total system low noise behavior can still be achieved and thus using the benefit of good intermodulation distortion separation.

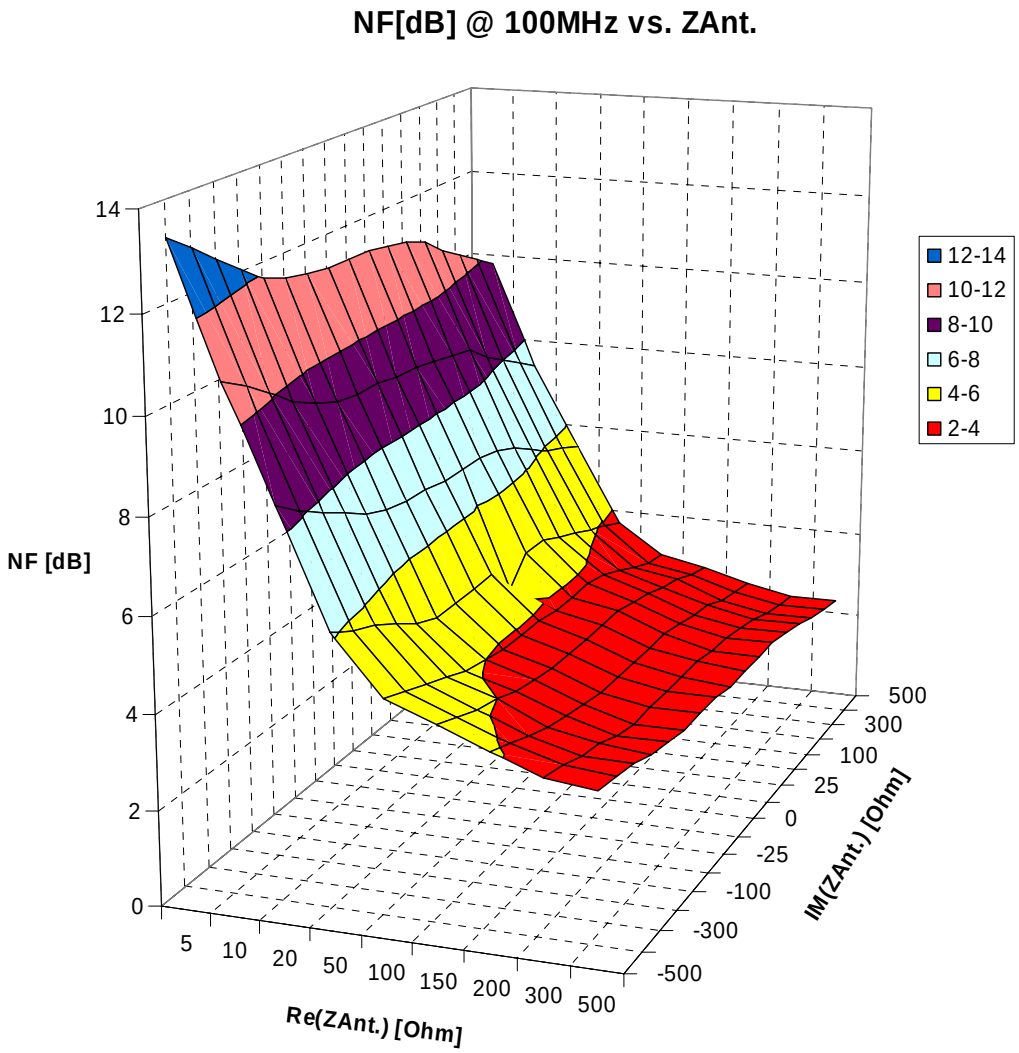

Figure 2.56-A : Noise Figure NF [dB] of the New Active Amplifier with added buffer stage for Arbitrary Antenna Impedance

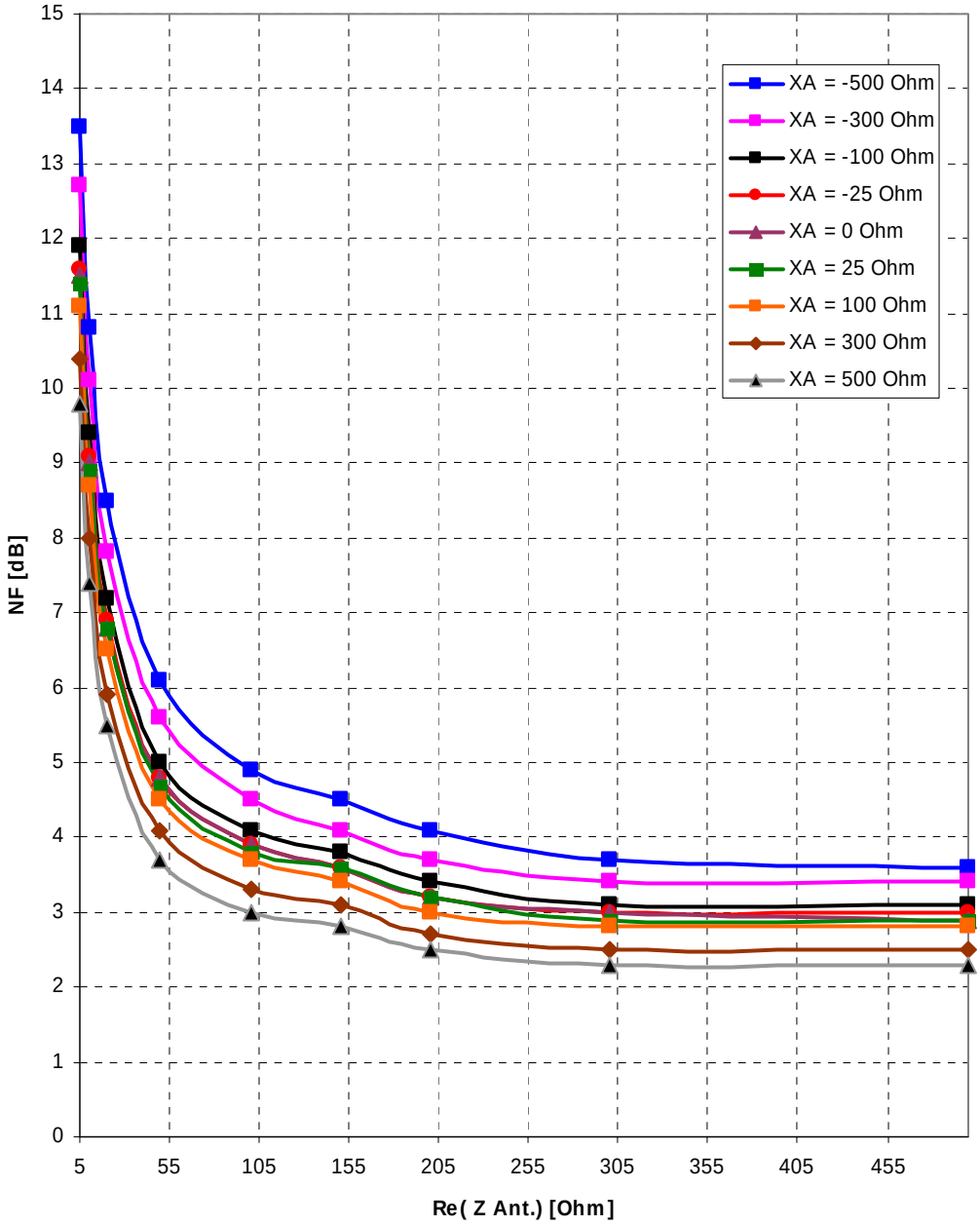

Figure 2.56-B : Noise Figure NF [dB] (extracted from the three dimensional NF graph) of the New Active Amplifier with added buffer stage versus the Antenna real part at different reactive parts

B- JFET with Buffer Bipolar as a Feedback

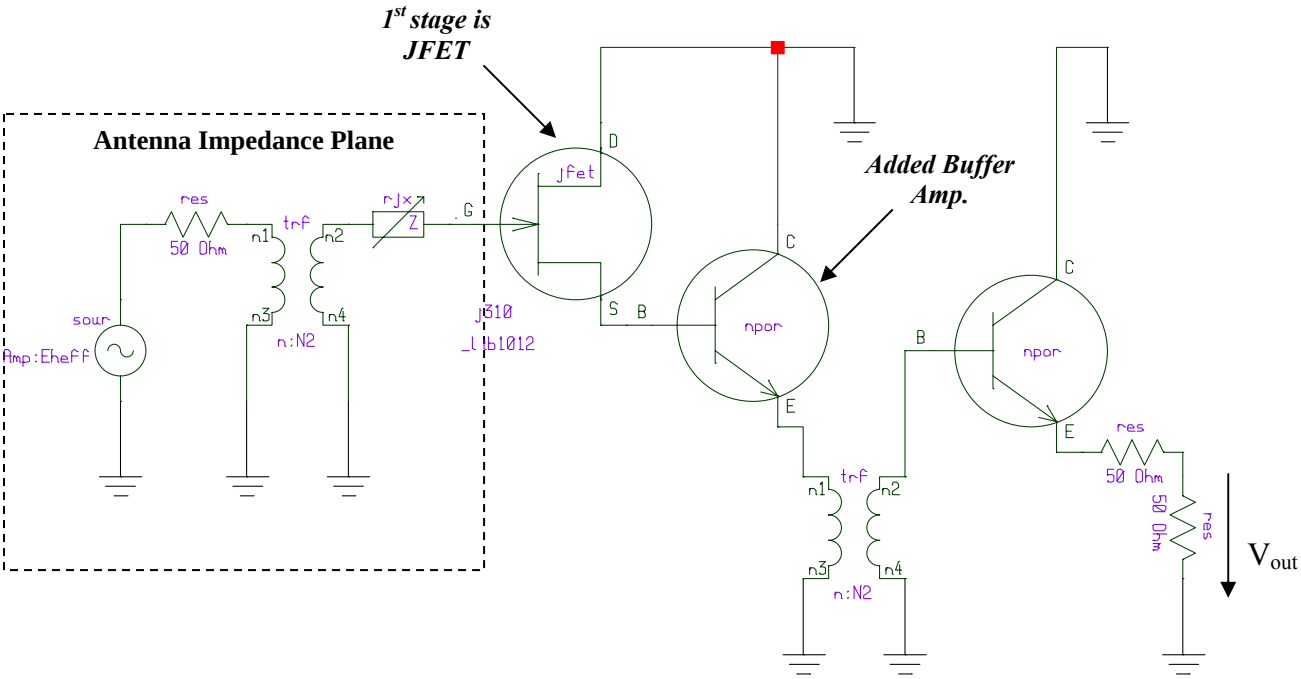

Figure 2.57: Proposed Active Antenna Amplifier based JFET in the first stage

Figure 2.57 shows the proposed active antenna amplifier based JFET in place of GaAs FET in the first stage. This proposal is a suggestion to reduce the cost using a cheap FET. The JFET SST310 from Philips has been used in the circuit investigation. According to the transistor power consumption limit, a bias drain current of 30mA has been used whereas both bipolar buffer transistors are biased at a collector current of 27mA as before. Figure 2.58 depicts the simulated results of the circuit intermodulation distortion separation. The circuit exhibits a satisfactory intermodulation distortion separation in most antenna impedance regions; however the amplifier noise figure is severely degraded in some antenna impedance other regions as shown in Figure 2.59-A,B. The possibility to adopt such an amplifier design based JFET is still existing theoretically in some antenna impedance regions as depicted in Figure 2.59-A, whereas the violet areas has quite acceptable noise figure which varies up to 5dB. Practically, one should remember that the noise figure is expected degrade more and more, even in such a low noise figure regions, whereas a noise figure of 6-7dB has been measured in some cases based JFET. Finally this depends on the application noise figure requirements.

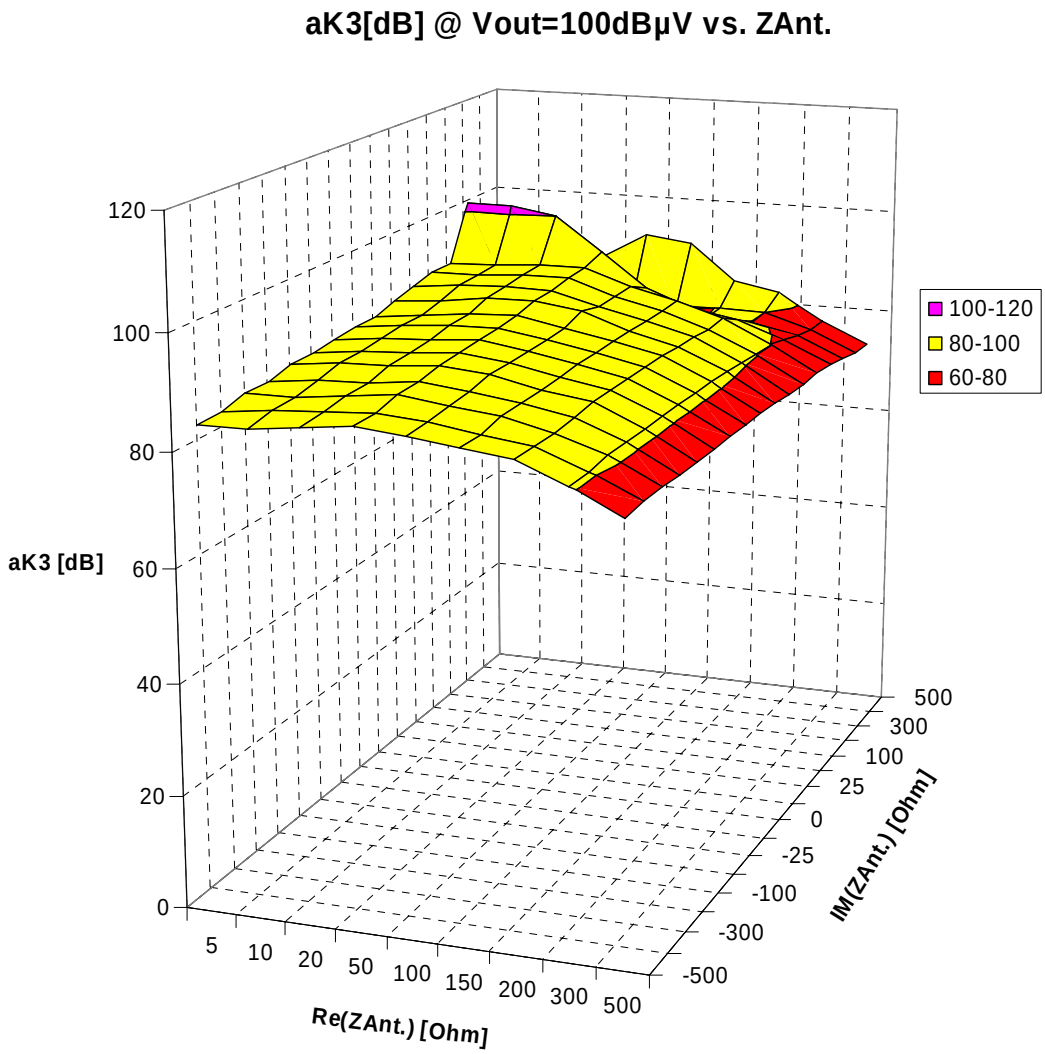

Figure 2.58: Intermodulation Distortion a_{K3}[dB] the Active Antenna Amplifier based JFET with added buffer stage for Arbitrary Antenna Impedance

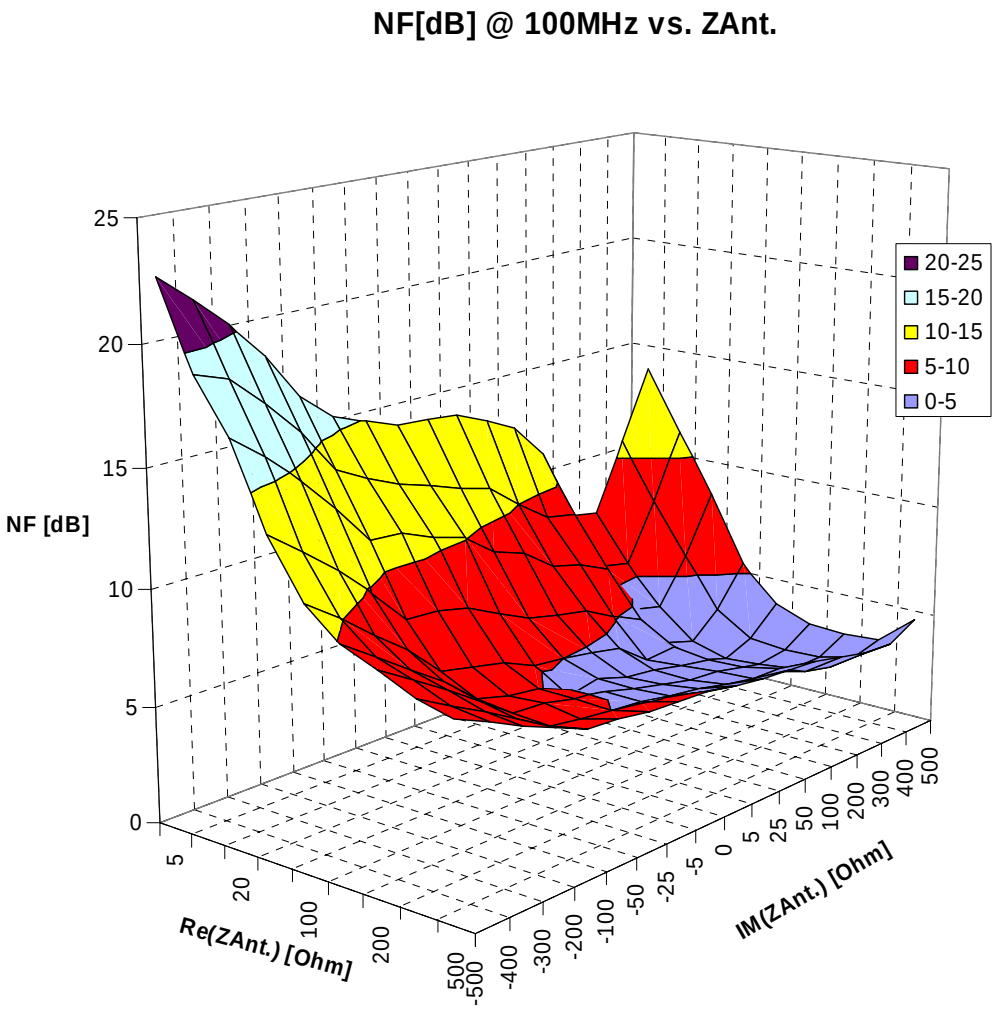

Figure 2.59-A: Noise Figure NF [dB] of the Active Antenna Amplifier based JFET with added buffer stage for Arbitrary Antenna Impedance

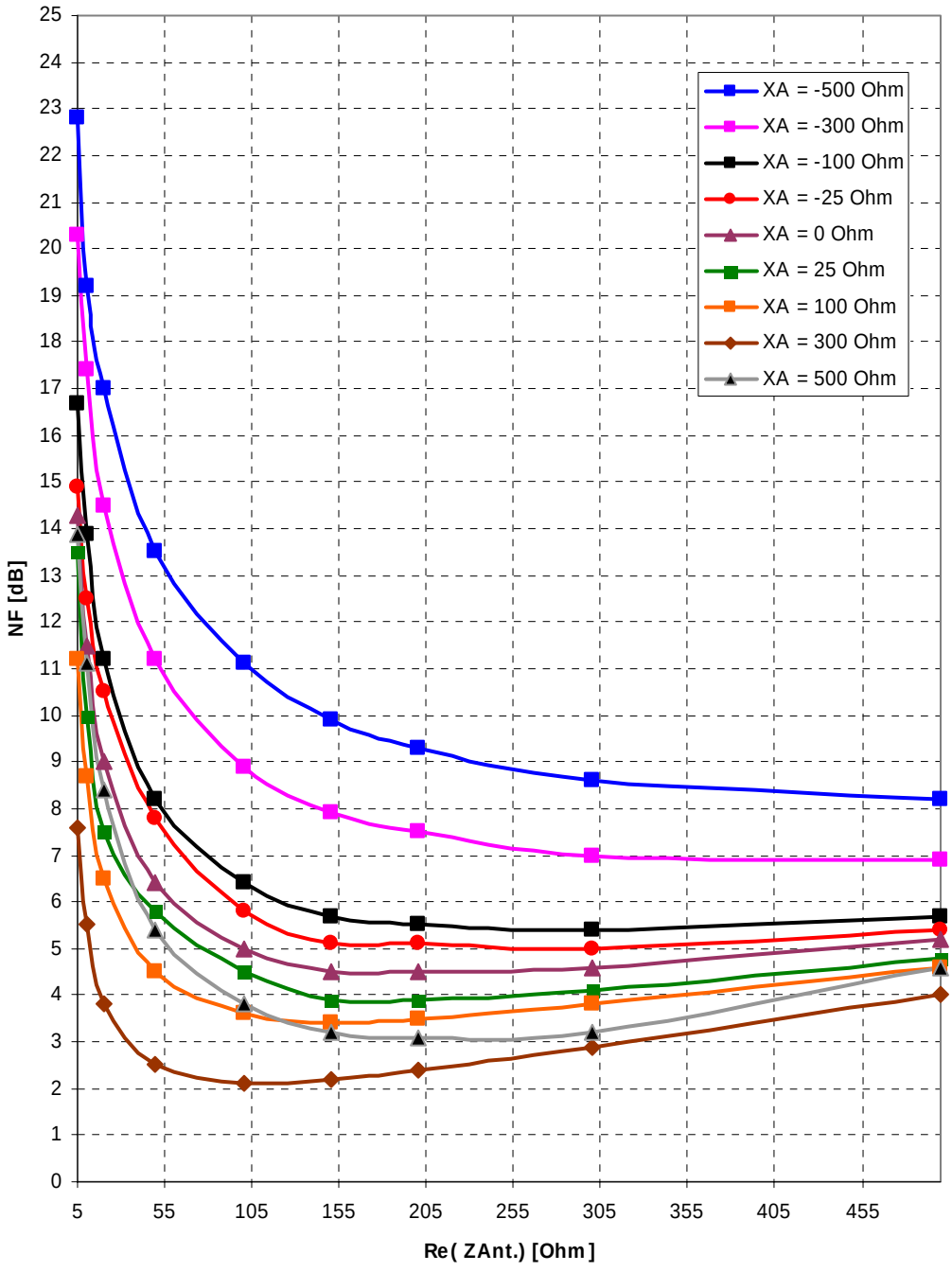

Figure 2.59-B : Noise Figure NF [dB] (extracted from the three dimensional NF graph) of the New Active Amplifier based JFET with added buffer stage versus the Antenna real part at different reactive parts

C- Parallel JFET with Buffer Bipolar as a Feedback

As explained in chapter one, that the JFET noise figure can be reduced if two JFET transistors are connected in parallel (Gate-Gate, Source-Source and Drain-Drain). Figure 2.60, depicts such a situation for a trial to enhance the circuit noise figure performance. The drain bias current for each JFET is chosen to be 15mA, whereas a 27mA collector current is used for each buffer bipolar transistor. Figure 2.61 showed that the circuit intermodulation distortion separation is almost the same, and as quite expected from the FET parallel connection, the low noise figure regions in Figure 2.62-A has been increased shown by the violet regions, which opens the possibility to use such a circuit design in some active antenna amplifier applications. Figure 2.62-B shows the extracted NF [dB] from Figure 2.62-A for different antenna reactive parts.

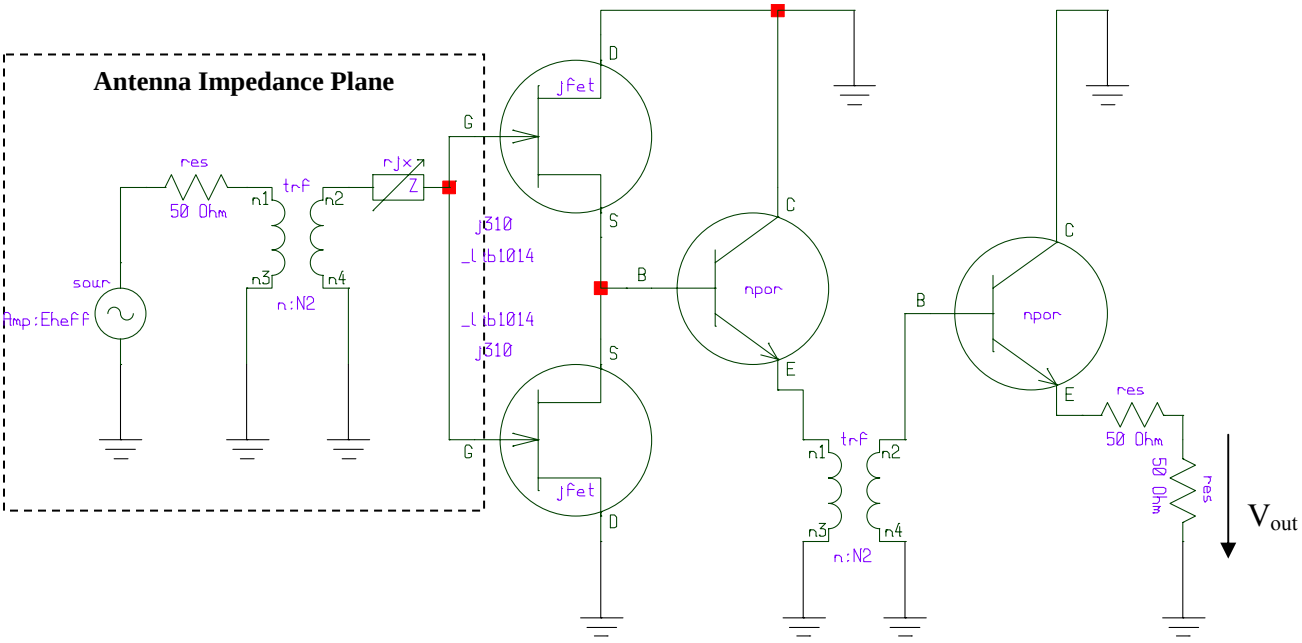

Figure 2.60: Proposed Active Antenna Amplifier based parallel JFET Transistors

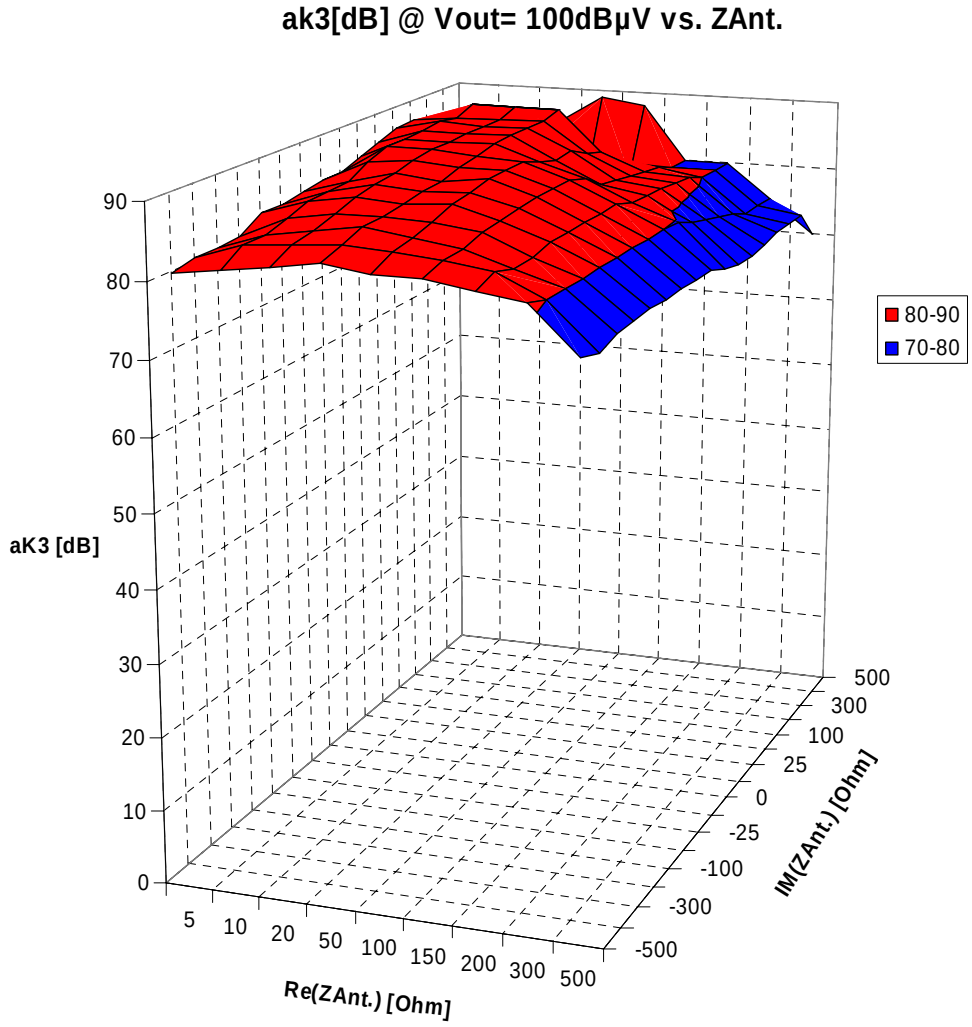

Figure 2.61: Intermodulation Distortion a_{K3}[dB] of the proposed Active Antenna Amplifier based Parallel JFET with added buffer stage for Arbitrary Antenna Impedance

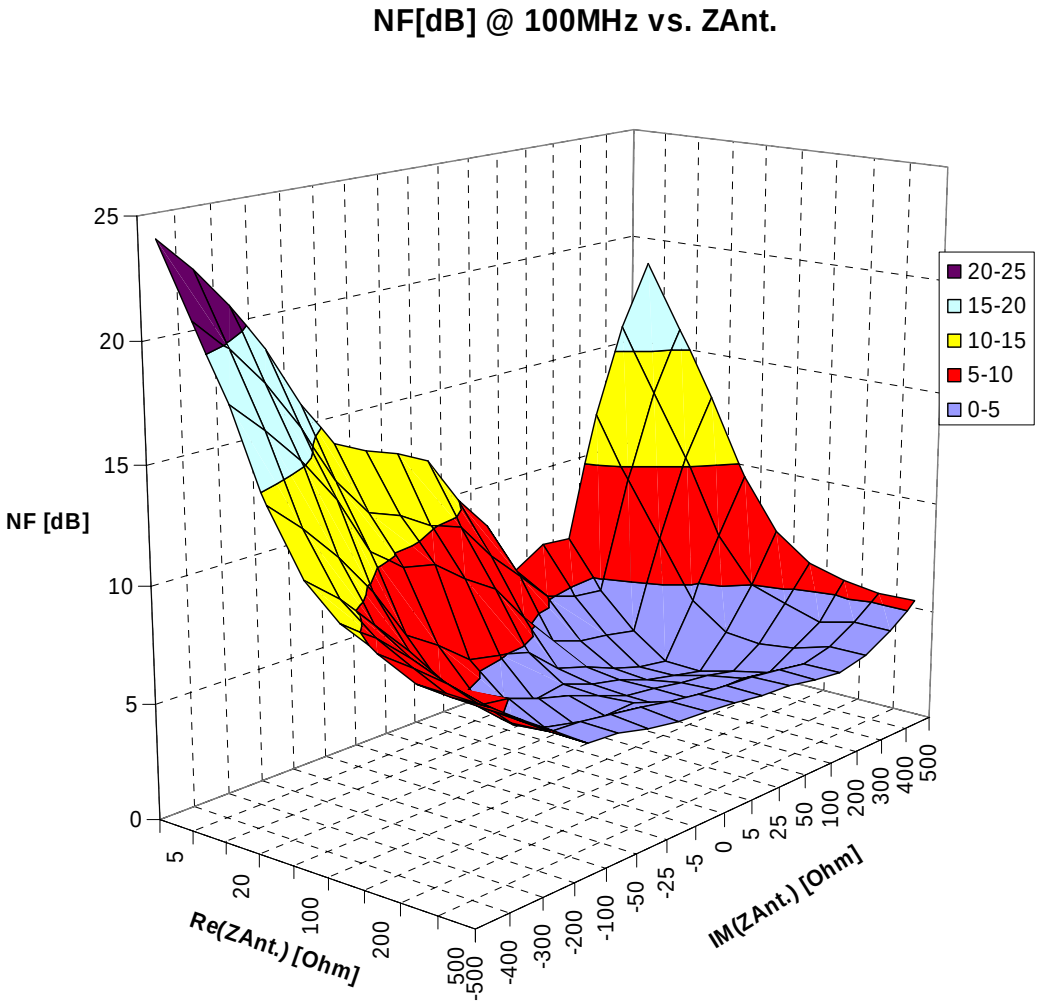

Figure 2.62-A: Noise Figure NF [dB] of the the proposed Active Antenna Amplifier based Parallel JFET with added buffer stage for Arbitrary Antenna Impedance

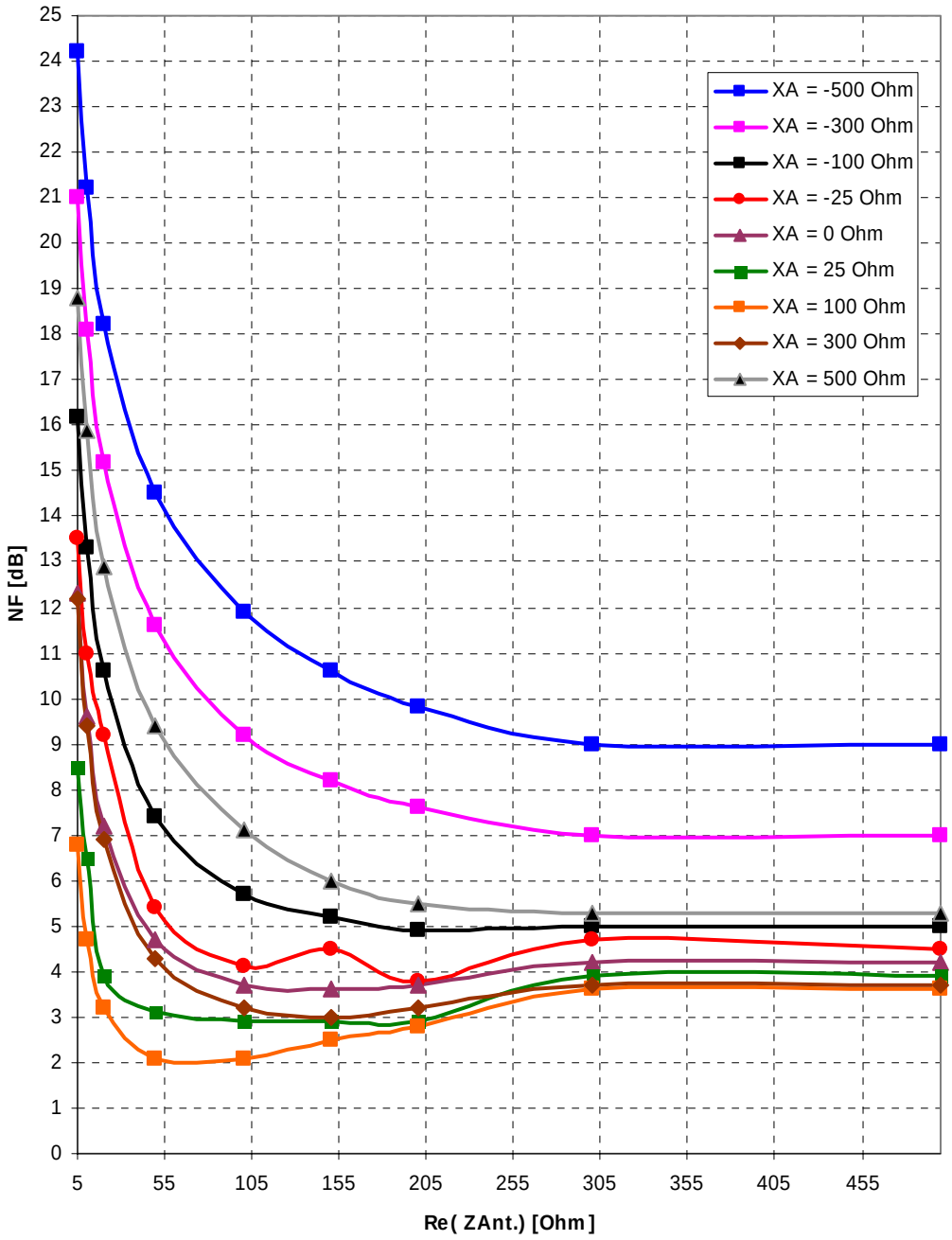

Figure 2.62-B: Noise Figure NF [dB] (extracted from the three dimensional NF graph) of the New Active Amplifier based Parallel JFET with added buffer stage versus the Antenna real part at different reactive parts

D- Bipolar with Buffer Bipolar as a Feedback

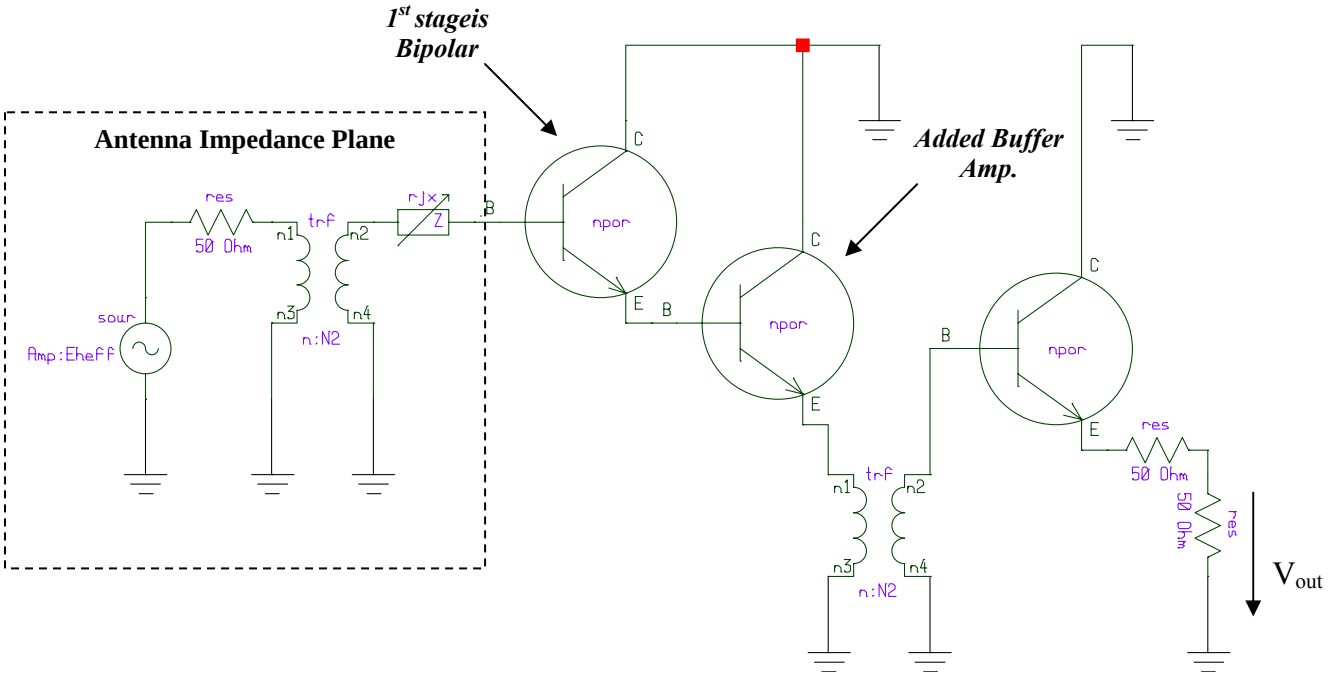

Figure 2.63: Proposed Active Antenna Amplifier based Input Stage Bipolar Transistor

Figure 2.63 illustrates a proposal of using a bipolar transistor at the input stage in place of a FET generally. It should be noted that such an emitter follower is not reported in the active antenna circuit's literature. The input stage buffer transistor bias current is chosen to be 25mA whereas the other buffer bipolar transistors are biased at a collector current of 27mA for each transistor. Figure 64 depicts the simulated intermodulation distortion performance of the proposed circuit configuration. Unfortunately, the circuit intermodulation performance is dependent on the antenna impedance, which limits the high linearity behavior for different applications. The noise figure has been simulated as shown in Figure 2.65-A, B, and although that the noise figure is quite high relative to the discussed previous cases based on JFETs, however the circuit can still find its use for a broad band source impedance of 50 Ohm, since at this region, the noise figure is quite acceptable as shown in violet regime (NF up to 5 dB).

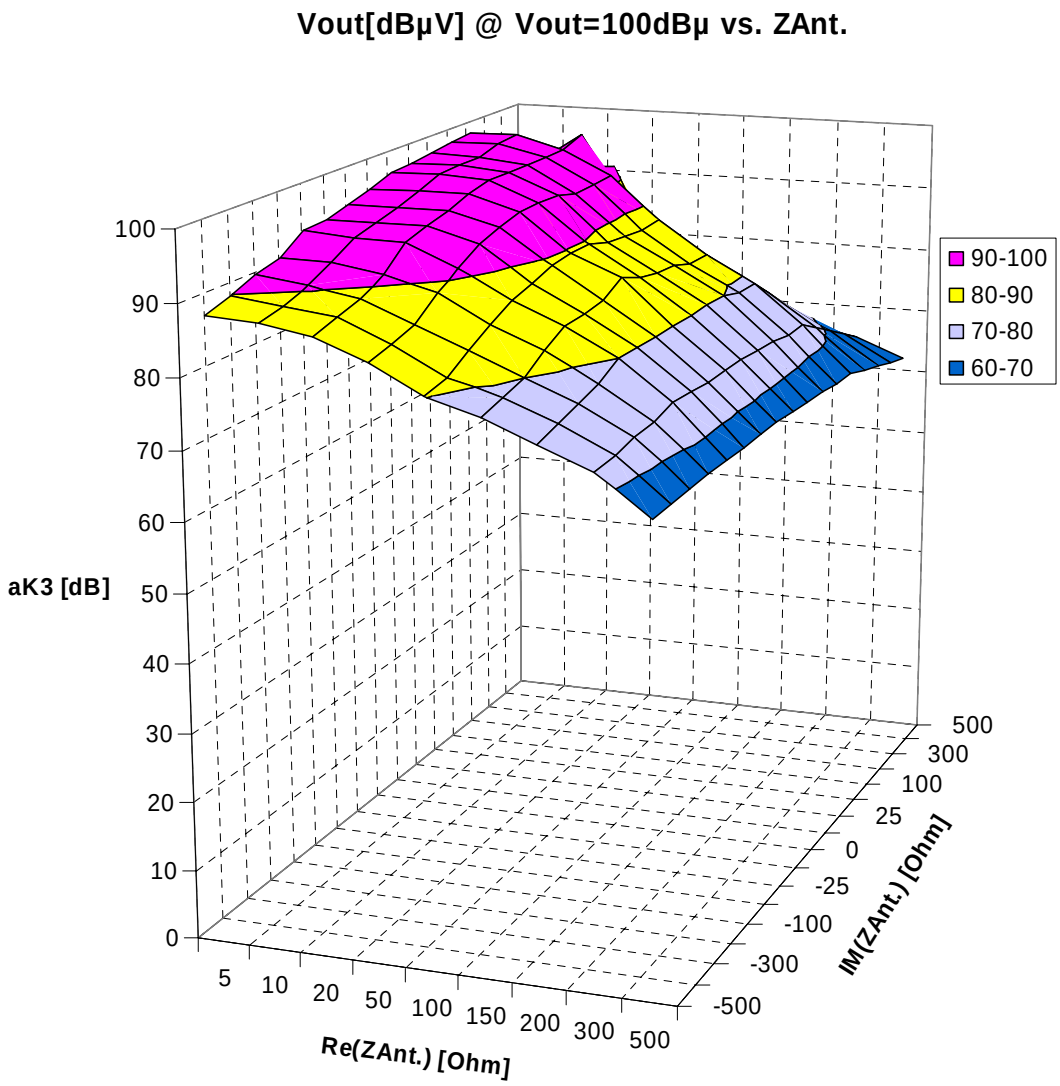

Figure 2.64: Intermodulation Distortion a_{K3}[dB] of the Active Antenna Amplifier Based Bipolar Transistor with added buffer for Arbitrary Antenna Impedance

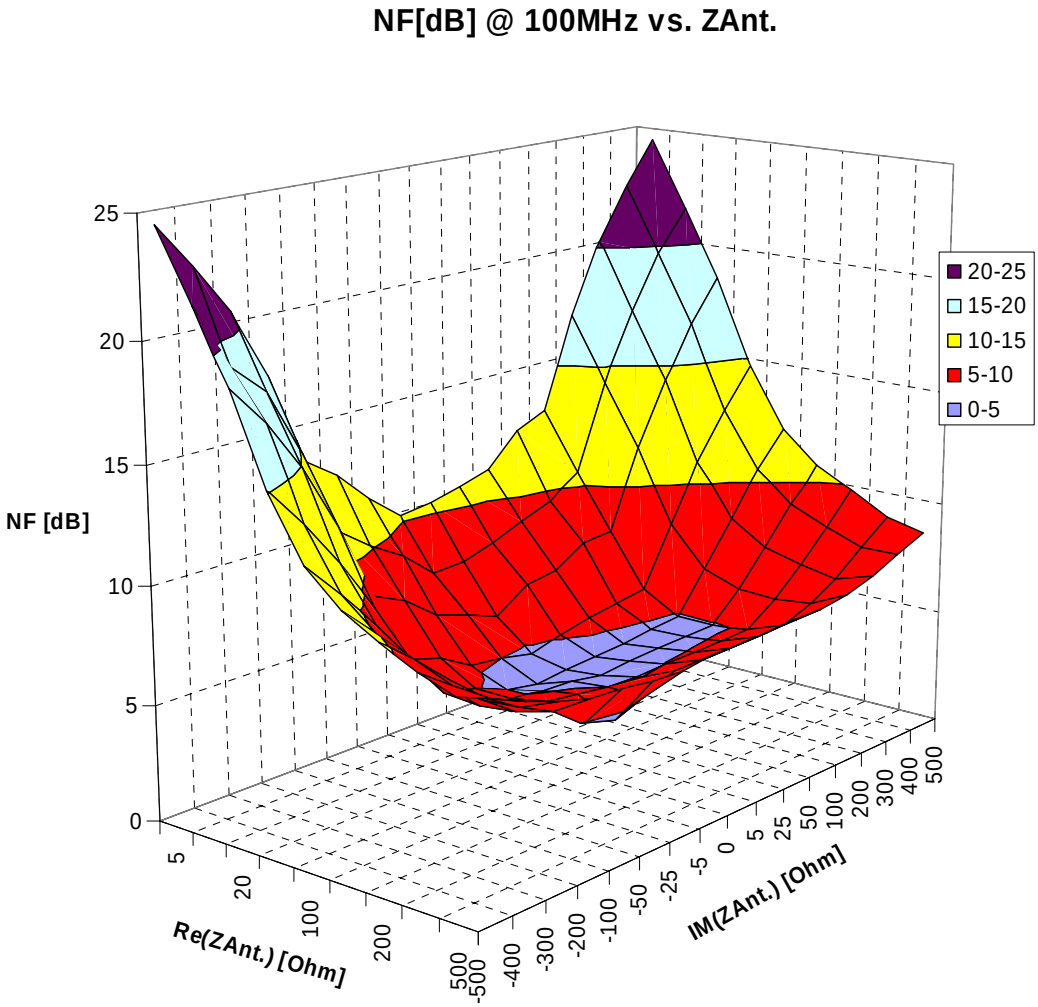

Figure 2.65-A: Noise Figure NF [dB] of the Active Antenna Amplifier Based Bipolar Transistor with added buffer for Arbitrary Antenna Impedance

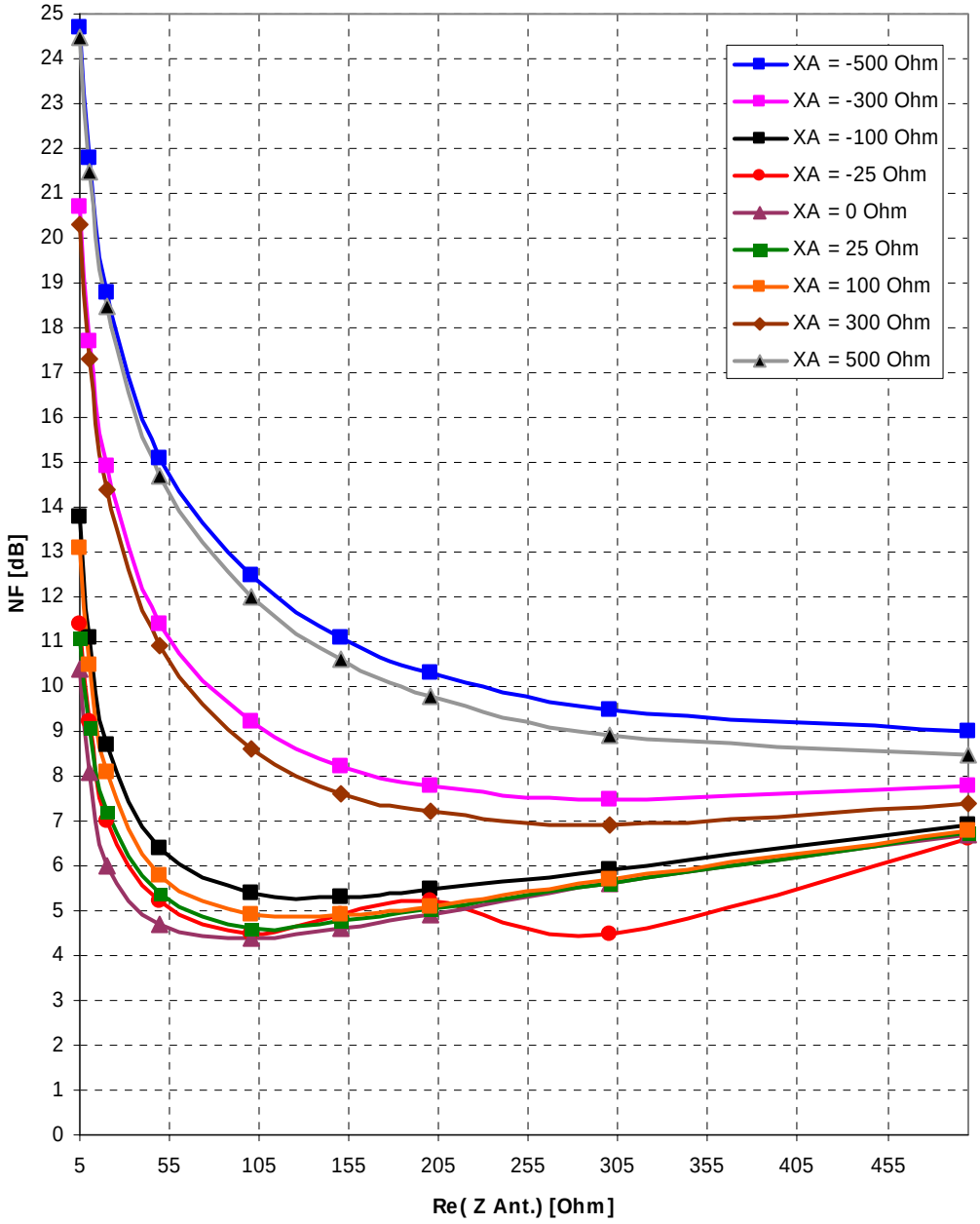

Figure 2.65-B: Noise Figure NF [dB] (extracted from the three dimensional NF graph) of the New Active Amplifier based Bipolar Transistor with added buffer stage versus the Antenna real part at different reactive parts

2.2.8 Design Example of the Proposed Modified Active Antenna New Amplifier

It is quite clear from the discussions presented in the last section that the active antenna amplifier based GaAs FET still represents the general favorable design to be selected. This was clear from the investigations done which showed that its performance is independent on the antenna impedance generally. However it has been shown that a design based JFET or even Bipolar can be accepted in case of broad band source impedance for example. In this section, an active antenna amplifier design example will be presented based on the previously modified concept introduced in the last section. The case of broadband source impedance of 50Ohm based GaAs FET will be considered by simulation and experimental realization. Finally, readout of the simulation results based JFET and Bipolar for will be introduced for comparisons purposes. Figure 2.66 shows the realized circuit using the GaAsFET at the input stage, whereas a general filter structure has been chosen and optimized without the presence of the added Buffer, and then the circuit intermodulation has been measured with and without the bipolar buffer stage. The GaAs FET bias current is chosen to be I_{DS} = 25mA at V_{DS} = 2.7V, and both bipolar buffer amplifiers biasing is chosen to be I_C = 27mA at V_{CE} = 3.2V.

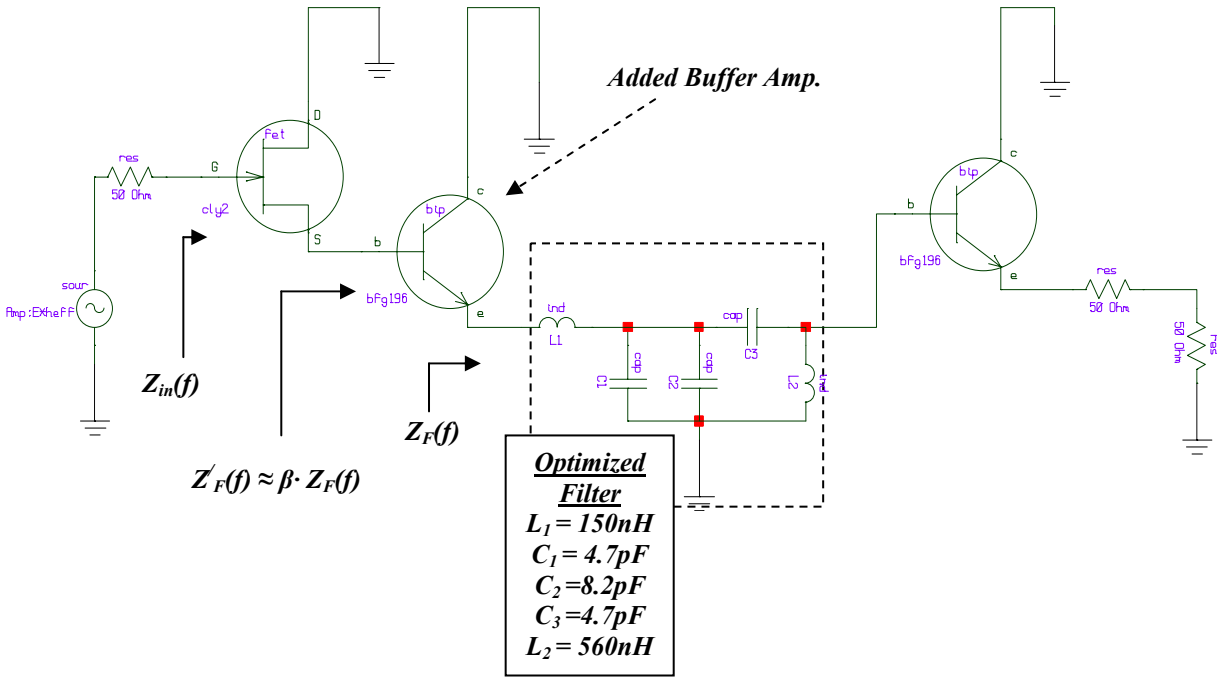

Figure 2.66: Realized Broad Band Active Antenna Amplifier RF Schematic (50Ohm)

Before proceeding with the designed circuit above, let us address the basic highlight behind the circuit possible instability which is the main disadvantage that can obstacle the working of the active antenna amplifier. A direct connection of a Buffer amplifier to the GaAs FET will compose the known Darlington connection. One of the well known basic problems of a Darlington connection in general is the increase of circuit negative input impedance which leads to the strong possible oscillations. Actually, the common drain FETs are used for oscillating circuits due to the negative input resistance exhibited by the transistor without any additional elements [72], and the connection of a buffer bipolar amplifier will present additional feedback capacitance which increases the negative resistance at the GaAs FET input. However the excellent linearity exhibited from the common drain configuration is one of the main reasons to increase the active antenna amplifier linearity. Thus a theoretical and experimental stability study should be investigated with every active antenna amplifier circuit as explained earlier in section 2.2.5. III. Consequently the stabilizing network developed in section 2.2.5. III. has been used at both input stages of the GaAs FET and Bipolar follower cells respectively, so that to change the circuit real part input negative impedance to be positive and thus guaranteeing the circuit stability as shown in Figure 2.67, whereas the circuit real input impedance is simulated in the frequency range from 80MHz up to 6GHz. As shown with the stabilizing networks, the real part of the input impedance tendency starting from 2GHz is a strong positive increasing function relative to the case without stability networks, and thus no oscillation possibility is expected. Simulation results showed that the circuit stability factor K is strongly greater than one (K reached $5 \cdot 10^9$ at 100MHz increasing function up to $25 \cdot 10^9$ at 6GHz). The circuit has been realized with a 1.5mm board thickness, and the circuit stability has been checked up to 6GHz in a 50 Ohm system and with variable source impedance environment. No oscillations appeared.

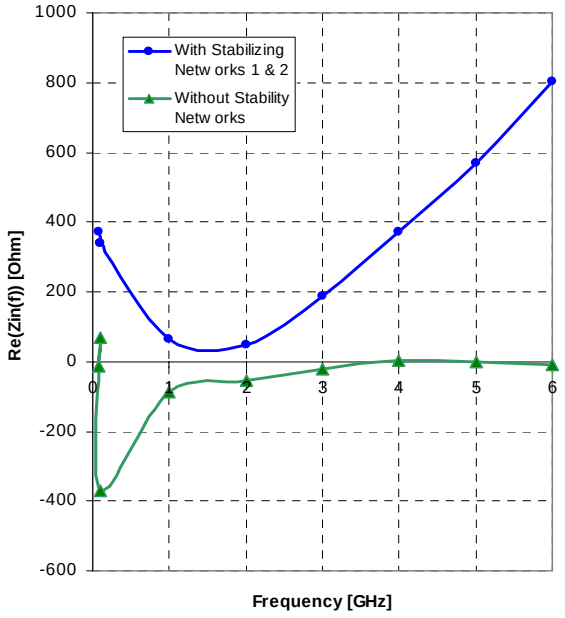

Figure 2.67: Circuit Real Input Impedance Frequency Dependence

Figure 2.68 shows the circuit simulated and measured intermodulation distortion separation with and without the additional buffer stage. With the additional buffer, a good value of a_{K3} of 80dB has been measured at 100dBμV output voltage compared to 70dB without the additional buffer stage. Figure 2.69 depicts the circuit measured frequency response. It is realized that the circuit noise figure is a little bit high due to the buffer stage, however by reducing both bipolar transistors biasing collector currents to 22mA, a noise figure of ~ 3dB has been measured at 100MHz compared to 3.4dB with both Bipolar transistors collector current of 27mA.

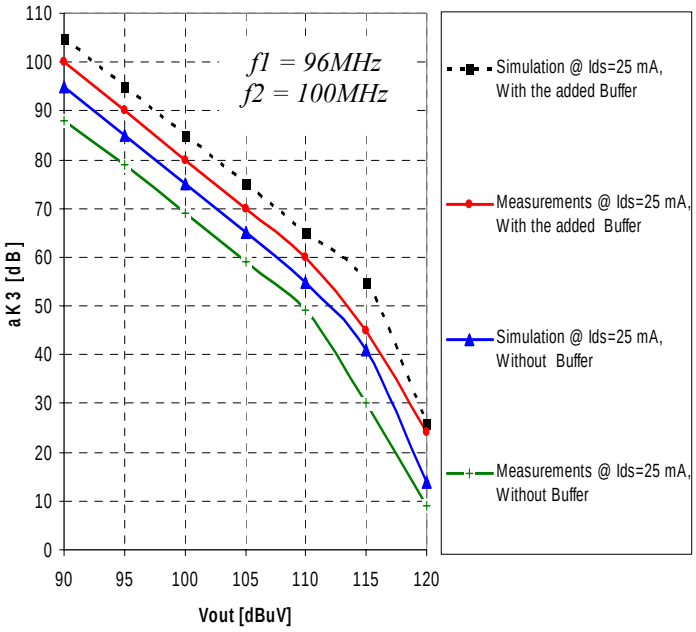

Figure 2.68: Measured and Simulated Third Order Intermodulation Separation

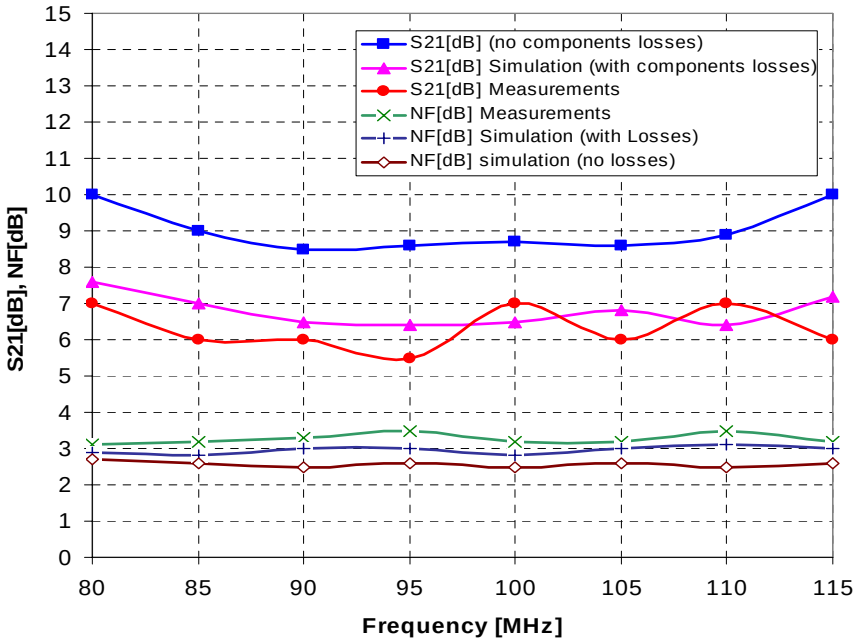

Figure 2.69: Circuit Simulated and Measured Frequency Response With the added Buffer

For the introduced circuit in Figure 2.66 and with the additional Buffer transistor, a replace of the GaAs FET with a JFET transistor has been done once and another replace with Bipolar has also been done. A simulated value of a_{K3}[dB] = 80dB has been read at 100dBμV output voltage in both cases which is 5dB lower that obtained using the GaAs FET simulation results in Figure 2.68. The noise figure read at 100 MHZ was 3.4dB by simulation. However by adopting a parallel JFET connection as shown in Figure 2.60, the noise figure read was 2.7dB at 100MHz.

From the above example and all introduced investigations with other transistors like the JFET and Bipolar, a final conclusion can be built at this stage that in case of broad band source impedance of 50[Ohm], the JFET and Bipolar transistors can replace the GaAs FET at the first stage, however the GaAs FET still introduces the general low noise high linearity device to be used with any antenna impedance as concluded in chapter one and investigated through this chapter too.

Chapter 3

Control Circuits for Enhancing the Non-linear Performance in Large Signal Environment in Active Antenna Amplifiers

INTRODUCTION

Chapter two considered the new low noise – high linearity FM active antenna amplifier concept that will be connected to the car radio receiver input. Also, a different amplifier design example for typical antenna types that may be printed on the car windscreen is introduced. To complete the active antenna amplifier design, it is necessary to avoid the radio receiver nonlinearity that may be initiated due to the presence of high input signal levels. These high levels may be received at a specific frequency within the FM band and amplified by the designed amplifier connected to the receiver. According to the **VDA** standards, an amplifier output signal range of 120 -130dBμV is a high signal that should be avoided to reach the receiver input. This simply suggests increasing the third order intermodulation separation a_{K3} at the amplifier output signal range of 120-130dBμV. A 50-60dB separation is considered to be satisfactory according to the **VDA** standards. To achieve these requirements, a certain control circuit(s) should be designed to predict the amplifier stated high signal output voltage levels, so that at these levels, the amplifier frequency response should be controlled in a way to stop amplification (i.e. introducing attenuation), thus facing these signals at the amplifier input, which means increasing the separation a_{K3} at these high output signal voltage levels. Consequently, this will avoid the high signal levels at the receiver input. In the design of such control circuit(s), three basic requirements should be considered so that not to change the active antenna high input impedance amplifier principle from the beginning. These basic design requirements can be summarized as follows:

1- Protecting the receiver from the high input signal levels (amplifier output signal voltage range of 120-130dBμV).
2- Keeping the third order intermodulation distortion of the GaAs FET performance at the input stage not affected or even changed.
3- Keeping the amplifier feeding signal source(s) to see a high input impedance in all cases for any received signal levels so that not to affect the other connected circuitry that may be connected to the GaAs FET input, i.e. keeping the high input impedance.

In this chapter, the previously introduced active antenna amplifier will be extended with connecting different developed control circuits that will be discussed. However, before proceeding with the control circuits developed, a brief discussion about the third-intermodulation distortion of active antenna amplifiers will be introduced. One of the important characteristics of a microwave high power amplifier is the so-called **gain compression**. As the input signal to the amplifier approaches the saturation region, the gain begins to fall off, or compress. The typical relationship between input and output power is shown in Figure 3.1on a log-log scale. At low drive levels, the output is proportional to the input power. However, as the power increases beyond a certain point, the gain of the transistor decreases, and eventually the output power reaches saturation. The point where the gain of the amplifier deviates from the linear or small-signal gain by **1 dB** is called the **1 dB compression point** and is used to characterize the power handling capabilities of the amplifier. The gain corresponding to the 1 dB compression point is refered to as $\mathbf{G_{1dB}}$ and is computed as $\mathbf{G_1 dB = G_o - 1\ dB}$, where $\mathbf{G_o}$ is the small-signal gain. If the output power $P_{out,1dB}$ at the 1 dB compression point is expressed in dBm, it can be related to the corresponding input power $P_{in,\,1dB}$ as

$$P_{out,1dB}(dBm) = G_{1dB}(dB) + P_{in,1dB}(dBm) = G_O(dB) - 1dB + P_{in,1dB}(dBm) \tag{3.1}$$

Another important characteristic of an amplifier is its **dynamic range** labelled d_R .

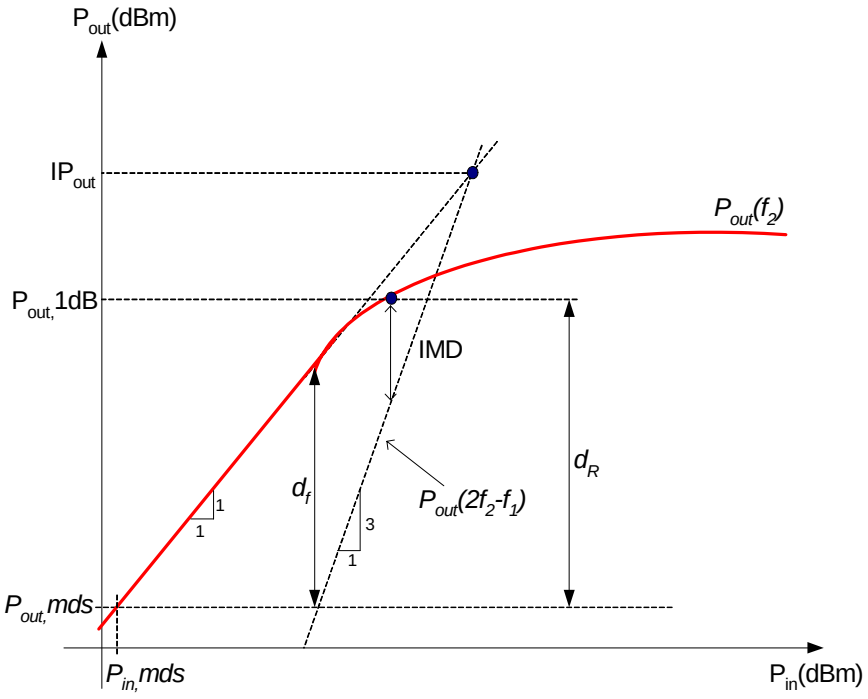

Figure 3.1: Recording of IMD Based on Input – Output Power Relation

The dynamic range signifies the region where the amplifier has a linear power gain expressed as the difference between $P_{out,\ 1dB}$ and the output power of the **minimum detectable signal** $P_{out,\ mds}$. The quantity $P_{out,mds}$ is defined as a level X dB above the output noise power of an amplifier is given as

$$P_{n,out} = KTBG_O F \tag{3.2}$$

Which, if expressed in dBm, can be cast in the form

$$P_{n,out}(dBm) = 10\log(KT) + 10\log B + G_O(dB) + F(dB) \tag{3.3}$$

Where 10log (KT) = -173.8 dBm at T= 290^{o}K, F is the noise figure and B is the bandwidth. As with any nonlinear circuit, high-power amplifiers create harmonic distortions (multiples of the fundamental frequency). They appear as a power loss in the fundamental frequency. As discussed and explained in chapter two, the third order intermodulation distortion is an undesirable property of power amplifiers generally and for FM active antennas specifically. Although present in any amplifier (like harmonic distortion) it is most prominent in the high-power region of an active device where the nonlinear behaviour has to be taken into account. Unlike harmonic distortions, intermodulation distortion is the result of applying two un-modulated harmonic signals of slightly different frequencies to the input of an amplifier and observing the output, as shown in chapter one in Figure 1.23. Due to third-order nonlinearities of an amplifier, the input signals $P_{in}(f_1)$ and $P_{in}(f_2)$ create, besides the expected output signals $P_{out}(f_1)$ and $P_{out}(f_2)$, additional frequencies $P_{out}(2f_1- f_2)$ and $P_{out}(2f_2-f_1)$. The additional frequency components can serve a desirable purpose when dealing with mixer circuits [43]. However, for an amplifier one would like to see these contributions to be as small as possible. As explained in chapter one, the difference between the desired and undesired power level at the amplifier output port is typically defined as **IMD** (**a_{K3}[dB])**. In figure 3.1 the output powers $P_{out}(f_2)$ and $P_{out}(2f_2-f_1)$ are plotted versus the input power $P_{in}(f2)$ on a log-log scale. In the region of linear amplification, the output power $P_{out}(f_2)$ increases proportionally to the input power $P_{in}(f_2)$, let us say $P_{out}(f_2) = \alpha P_{in}(f_2)$. However, the third order product $P_{out}(2f_2-f_1)$increases proportional to the third power [i.e., $P_{out}(2f_2-f_1)= \alpha^3 P_{in}(f_2)$]. Thus, the **IMD** is reduced in proportion to the inverse square of the input power. Projecting the linear region of $P_{out}(f_2)$ and $P_{out}(2f_2-f_1)$ results in a fictitious point called the **intercept point** (**IP**). In practice, if higher than third order products can be neglected, the **IP** becomes a fixed point, independent of the particular power gain of the amplifier. This allows us to use the IP as a single number to quantify the **IMD** behaviour. Also shown in Figure 3.1 is a quantity called spurious free dynamic range, d_f, which is defines as

$$d_f(dB) = \frac{2}{3}\left[IP(dBm) - G_O(dB) - P_{in,mds}(dBm)\right] \quad (3.4)$$

In the following sections, the previously introduced new active antenna amplifier will be extended with connecting different developed control circuits that will be discussed. The different measurements done in the laboratory will be displayed and compared. The goal of this chapter in addition is to show that the control circuits can be used while the amplifier introduced design technique and linear performance remains the same.

3.1 Active Antenna Amplifier Series Control

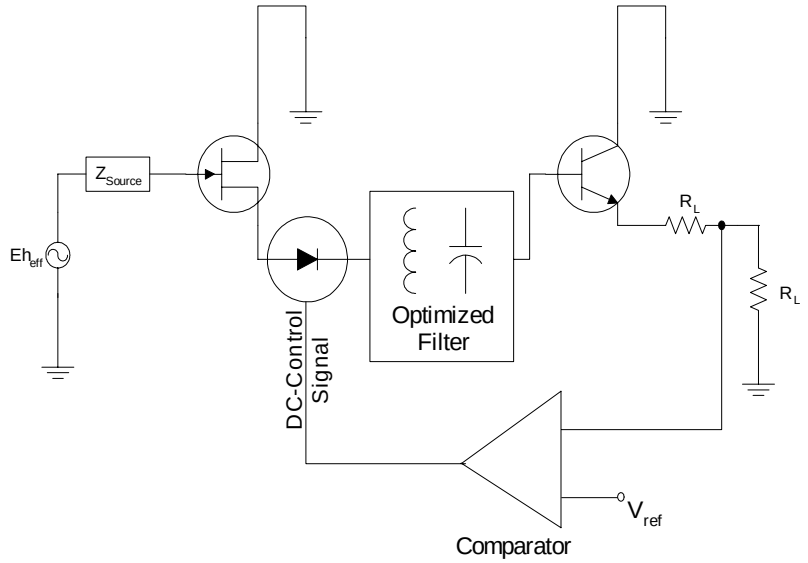

Figure 3.2: The FM Active Antenna Amplifier with Series Control Circuit Concept

As shown in Figure 3.2, the series control concept depends on connecting a nonlinear element in the series path between the GaAs FET output and the bipolar transistor input. In this case a diode is used whereas its forward and reverse operation can be controlled via a comparator output level. In principle, in low signal output levels region at the amplifier output (Load or the receiver input), the comparator output level is at its high level switching on the series diode thus introducing a forward resistance (≈ 0.6Ω different from diode to diode) which has negligible effect on the amplifier amplification S_{21}. When the amplifier output large signal (120-130dBμV) at the load (received input) is reached, the comparator output level is switched to a low level state and accordingly switching the series diode off, which means a high series resistance (> 1MΩ), thus introducing a high attenuation of the input signals which caused that high output levels. The principle of the expected modified Input-Output characteristic of the amplifier with series control is shown in Figure 3.3.

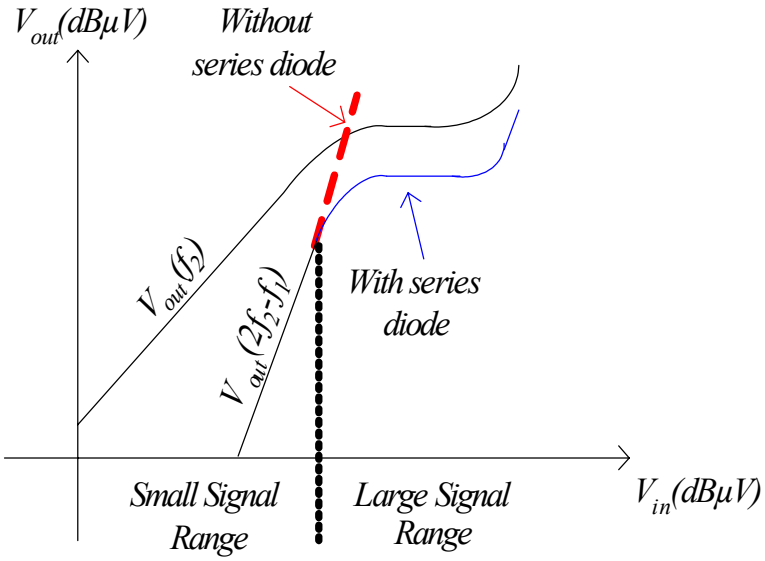

Figure 3.3: Amplifier Input-Output Characteristic with and without the Control Diode

Figure 3.4 illustrates a realized active antenna amplifier (series control diode) schematic circuit diagram example with the implemented proposed feedback control shown in Figure 3.2. The example is shown in case of broad band source impedance of 50 Ohm.

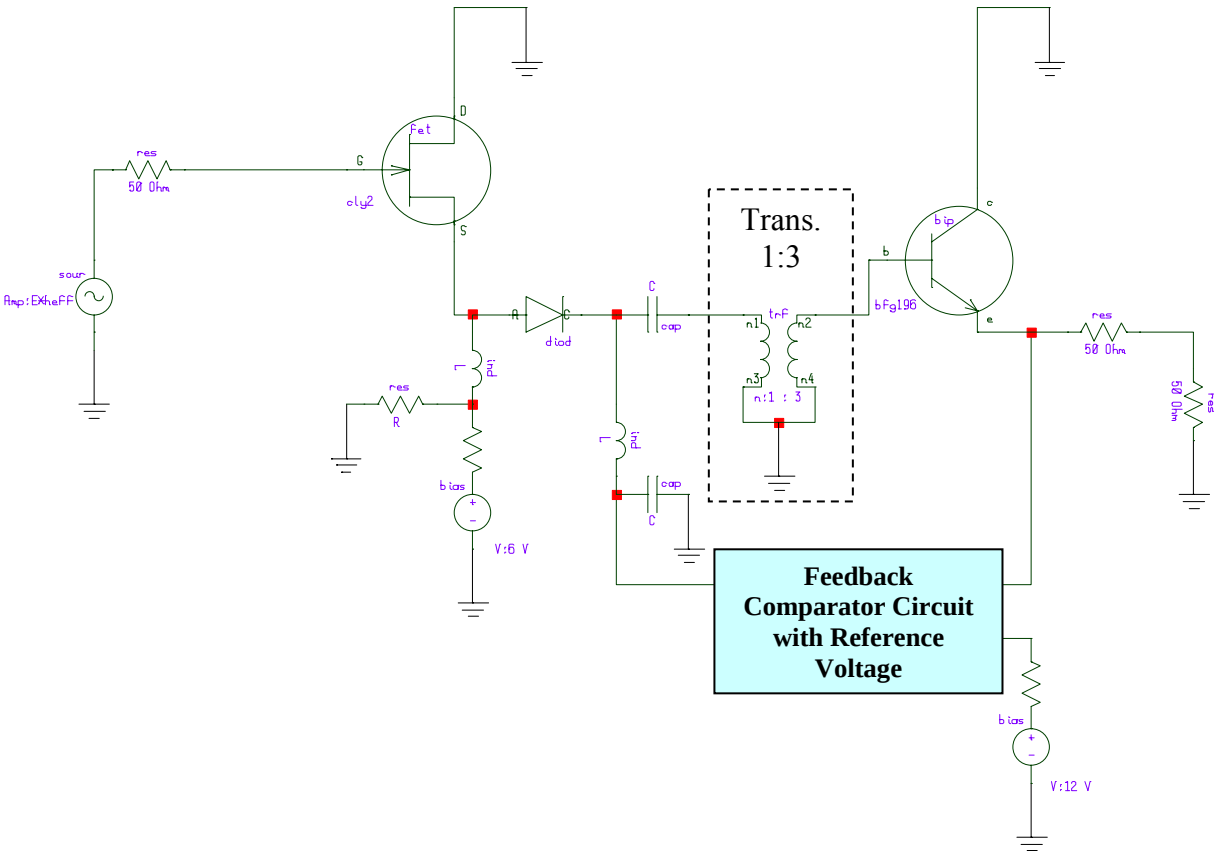

Figure 3.4: Active Antenna Amplifier Example (RF Circuit)

Figure 3.5 shows the realized amplifier measured input-output characteristic, whereas a biasing condition of I_{DS} = 50 [mA], V_{DS} = 2.6 [V], and I_C = 25 [mA], V_{CE} = 3.8 [V] has been utilized. The effect of the diode conduction action for large signal input range is realized by the output characteristic saturation which brought the output level lower than the undesired high voltage levels 120-130dBμV in the FM range.

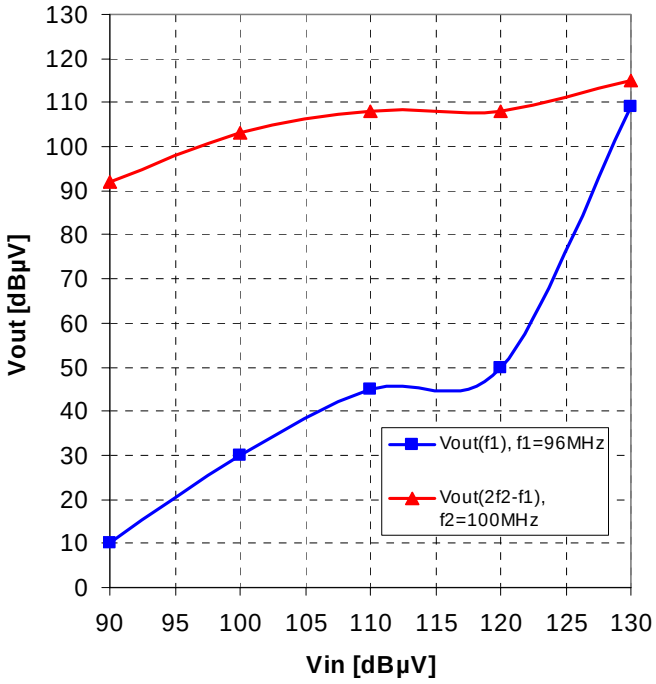

Figure 3.5: Measured Amplifier Input-Output Characteristic (Series Control)

In addition, Figure 3.5 depicts that the amplifier achieved an acceptable value of $a_{K3} \approx 78$[dB] at output voltage of 100dBμV, however still at the higher output voltage levels, the achieved value is quite low ($a_{K3} \approx 58$[dB] at input voltage of 120dBμV), which is still suggests thinking of another control technique to increase the a_{K3} separation at higher input levels. It should be realized that a basic disadvantage of using such a kind of amplifier control is the series diode, which degrades the total amplifier noise figure performance (NF [dB] may increases by around 0.3-0.7 dB as measured in some situations). For this reason, in the next section, a different control technique has been realized and measured, whereas the control diode is connected in parallel to the GaAs FET high input impedance, thus no actual noise figure degradation effect can be noticed and additionally enhancing the input output characteristics for higher output voltage levels.

3.2 Active Antenna Amplifier Parallel Control

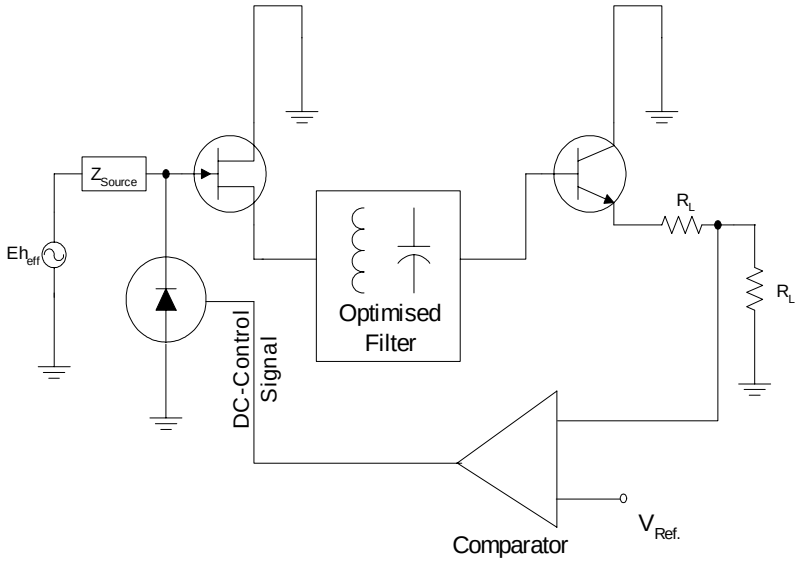

Figure 3.6: The FM Active Antenna Amplifier with Parallel Control Circuit Concept

Figure 3.6 shows the block diagram of the active antenna parallel control concept, whereas a diode is connected in parallel to the GaAs FET input. The comparator circuit is designed, so that in low signal output levels region at the amplifier output, the comparator output level is high, so that the diode is not conducting, thus presenting a high reverse resistance, which means that the high input impedance concept is not affected, thus all source antenna sees the same high input impedance. When the amplifier output large signal (120-130dBμV) at the load is reached, the comparator output level is switched to a low level state, thus the diode is conducting and forcing the circuit to introduce attenuation to the corresponding input signals which caused the amplifier high output signal voltage levels. Figure 3.7 shows a realized active antenna amplifier with parallel control diode, whereas a transformer (N2:N1 = 1:3) is connected between the GaAs FET output and the Bipolar input. The reason of using a linear broad transformer comes from the fact that this procedure will be tested with a broad band source impedance of 50Ω. Figure 3.8 shows the measured input-output characteristic of the implemented amplifier circuit in case of broad band source impedance. The intermodulation distortion separation enhancement is achieved at the higher output levels (whereas more than 50dB intermodulation separation is achieved for higher input voltage levels).

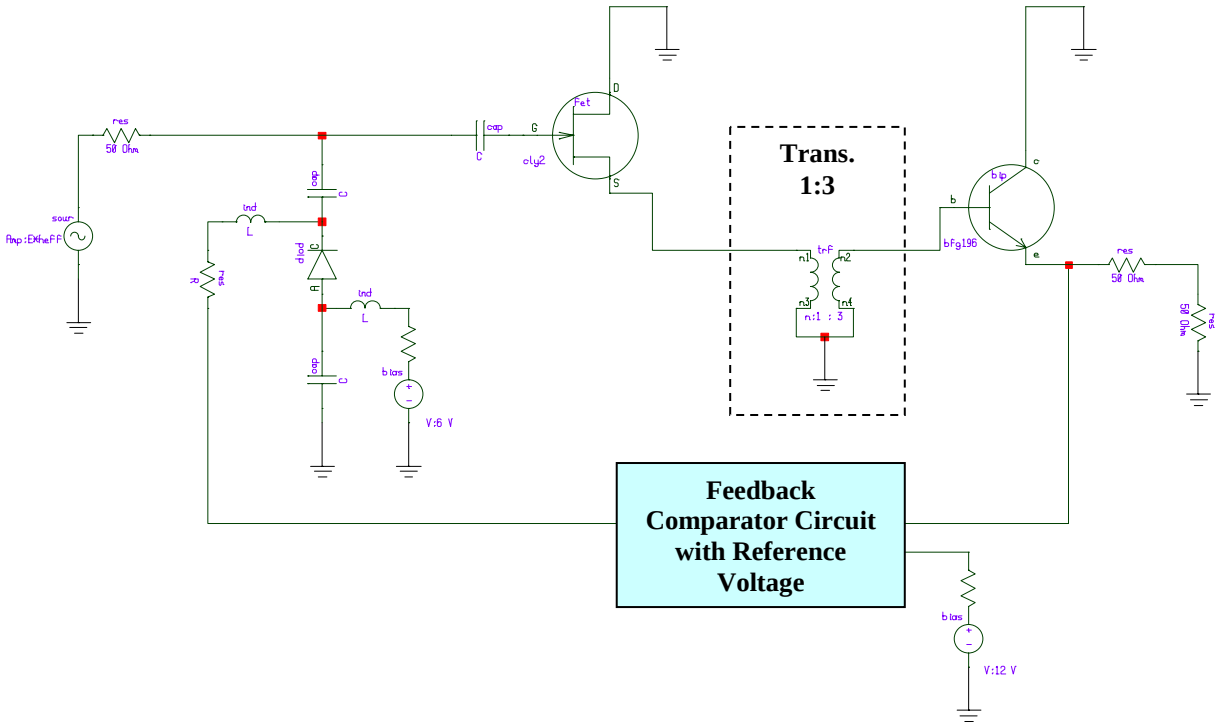

Figure 3.7: The FM Active Antenna Amplifier (RF Circuit) with Parallel Control Circuit

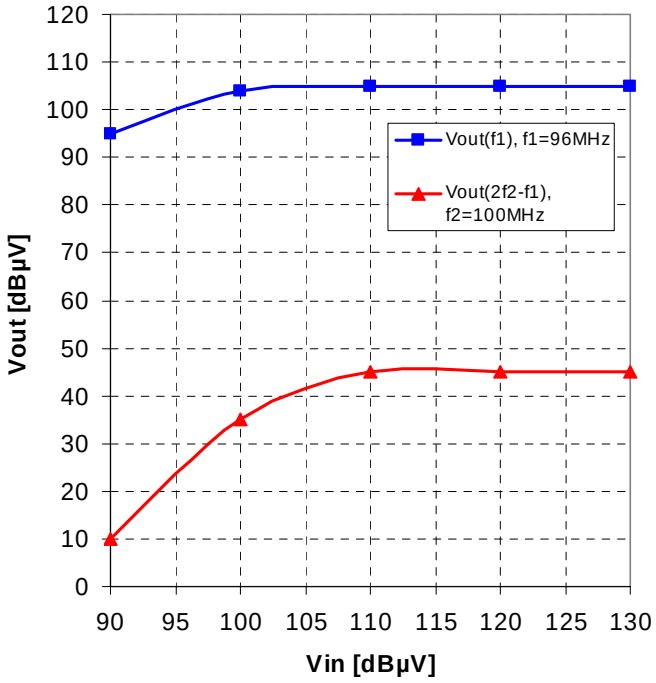

Figure 3.8: Measured Amplifier Input-Output Characteristic (Parallel Control)

3.3 Active Antenna Amplifier Control with AGC at the input including High Input Impedance

One drawback of the former introduced parallel control circuit is that the high input impedance feature of the amplifier is not always satisfied, and depends on the input PIN diode conduction condition. Figure 3.9 shows a modified circuit design which includes two diodes at the input port of the GaAs FET, thus achieving constant high input impedance in both conduction states of each PIN diode. The feedback control circuit is the same as before, so it is not repeated in Figure 3.9. An important design concept in the shown circuit is that it utilizes the use of a buffer after the GaAs FET stage as explained in section 2.2.4, so that to provide the highest feedback impedance to the GaAs FET, which increases the intermodulation separation at higher input signal levels as required. The bias current of GaAs FET used here is I_{DS} = 50mA, whereas for both bipolar transistors, a collector bias current of $I_{C1} = I_{C2}$ = 22mA has been used.

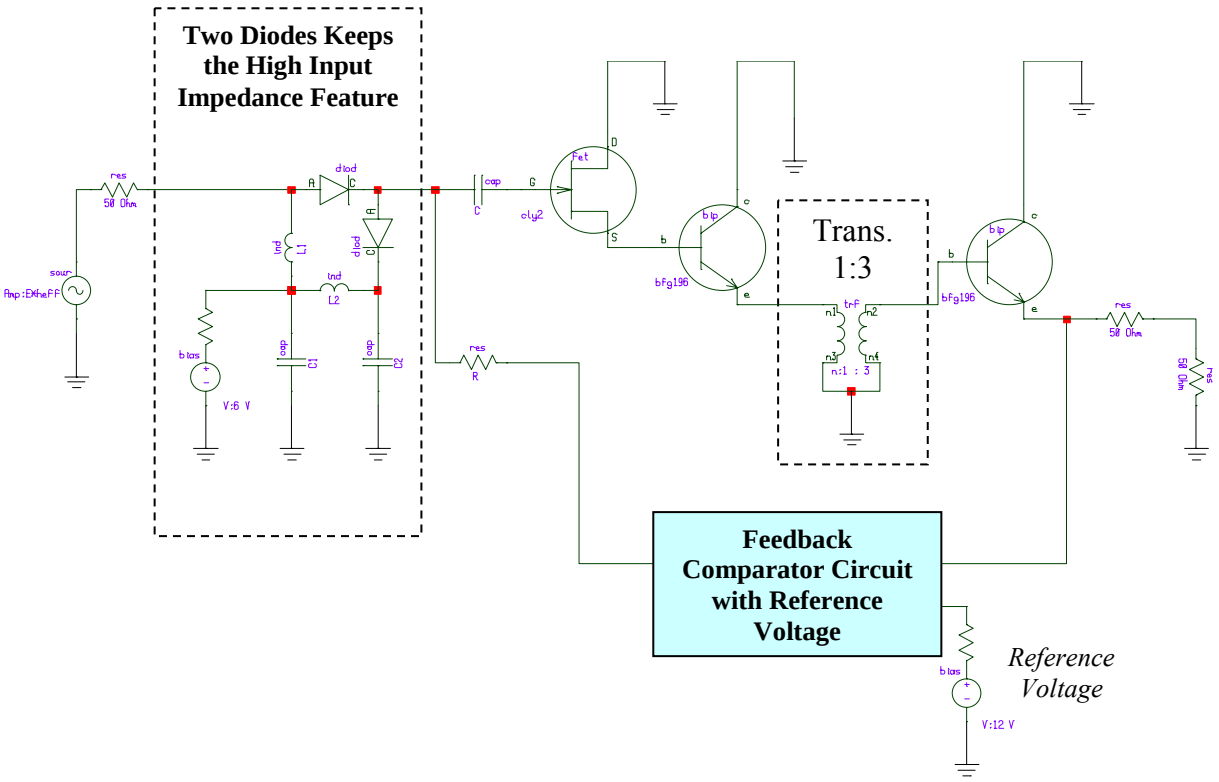

Figure 3.9: The FM Active Antenna Amplifier (RF Circuit) with AGC at the input including High Input Impedance

Figure 3.10, shows the circuit measured input-output characteristics. The required high separation at the circuit output voltage of 100dBμV is achieved (a_{K3} = 88dB), and additionally at the higher input signal levels of 120dBμV, a more than 80dB of a_{K3} separation is reached compared to 60dB in case of parallel control case (Figure 3.9). It should be noted finally that due to the input diode at the GaAs FET stage in Figure 3.9, a little increase in the total noise figure is measured ~3.4dB compared to 3.2dB without the input stage diode, which is still acceptable.

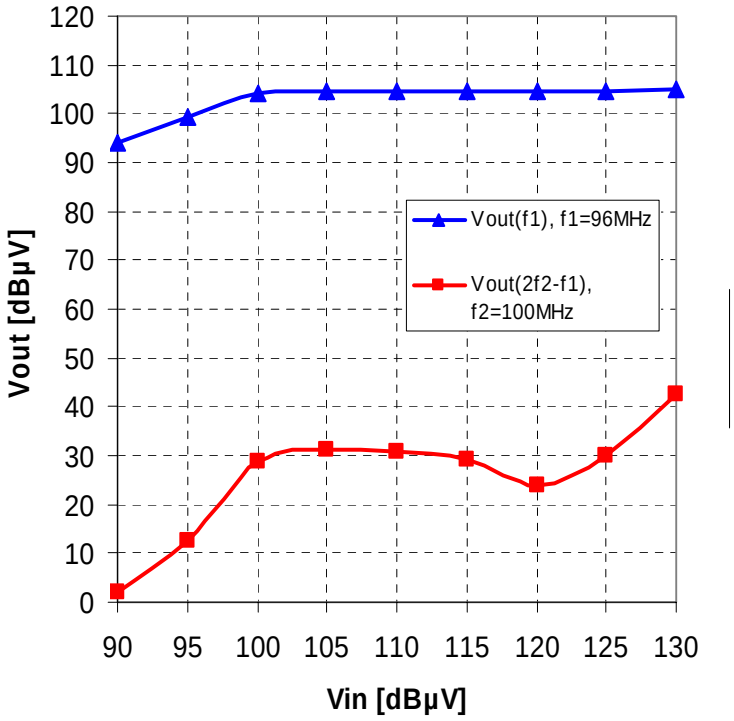

Figure 3.10: Measured Amplifier Input-Output modified Characteristic

Chapter 4

Conclusions and Future Directions

This dissertation described a new realized concept of FM active antenna amplifier. The new concept utilizes the GaAs FET technology. The advantages obtained with this new active antenna concept based GaAs FET connected directly to the windscreen antenna can be summarized as follows:

- No RF power extracted from the windscreen, thus no RF losses.
- The input GaAs FET acts as a probe.
- Switching in front of the active element is also possible.
- Frequency separation for FM and TV application is possible after the GaAs FET amplifier input stage.
- Switching for FM has no effect on TV and vice versa.
- For any antenna structure, the design rules available in situation of any amplifier realization.

A general matrix approach to represent and simulate any antenna measured impedance is introduced and discussed in detail. Such matrix approach facilitates the active antenna amplifier design in presence of any antenna measured impedance.

The thesis in addition introduced a general study procedure about the possibility to use HEMT, JFET and Bipolar transistors for active antennas. A conclusion has been arrived that JFET and Bipolar transistors can replace the GaAs FET in a 50 system, which gives the possibility to design a FM active antenna using cheap devices in broad band source cases.

However, it should be importantly noted that the thesis showed that the GaAs FET enjoys a stable non linear performance in face of variable source impedance compared to a variable non linear performance of JFET transistors as showed in chapter one (Figure 1.29 and Figure 1.31), which reveals that the GaAs FET introduces the general attractive solution fot FM active antenna amplifiers, in addition to their superior low noise performance.

The effect of a typical antenna impedances on the new presented FM amplifier concept based GaAs FET has been studied in detail in chapter two, whereas a conclusion has been reached regarding the necessary antenna impedance real part value that should be used with the presented design to fulfil the **VDA** requirements of active antenna amplifier additional noise figure.

Such a condition has been formulated as discussed in section 2.2.2 ended with the following condition,

$$For \quad F_{Zzakt.VDA-s\tan dard} < 6.3dB \rightarrow \quad The\ antenna\ real\ part\ should\ be: \left|R_A\right|_{\min} \geq 8\Omega$$

This condition sets the limitation on using the presented amplifier regarding the minimum value of the antenna real part that should be used with the presented new FM amplifier concept. If such a condition is not followed, noise will mask the amplifier frequency response as shown in section 2.2.6.3 of a typical antenna impedance type (C) and Figure 2.49.

Different control circuits are discussed for controlling the active antenna amplifier intermodulation performance for facing undesirable high level output signal values.

Finally it should be noted that this dissertation introduced a general simulation and design procedure for active antenna amplifiers. It should be remarked that a lot of GaAs FET transistors are existing in most Software libraries; however what is more important is what is available in the transistor market. During the development of all circuits in this dissertation, the GaAs FET CLY2 was available from TriQuint which was the base transistor in this dissertation, however, recently in the mid of 2004, another low noise GaAs FET was released from NEC. Its type is NE2700. During the writing of this work, this transistor was not available in the market, but the model was released which allows a simulation of such a transistor.

Figure 4.1 and 4.2 compares the frequency response and intermodulation separation performances of the new released GaAs FET NE2700 from NEC and the used CLY2 from Triquint. Both transistors are biased at a drain current of I_{DS} = 50[mA].

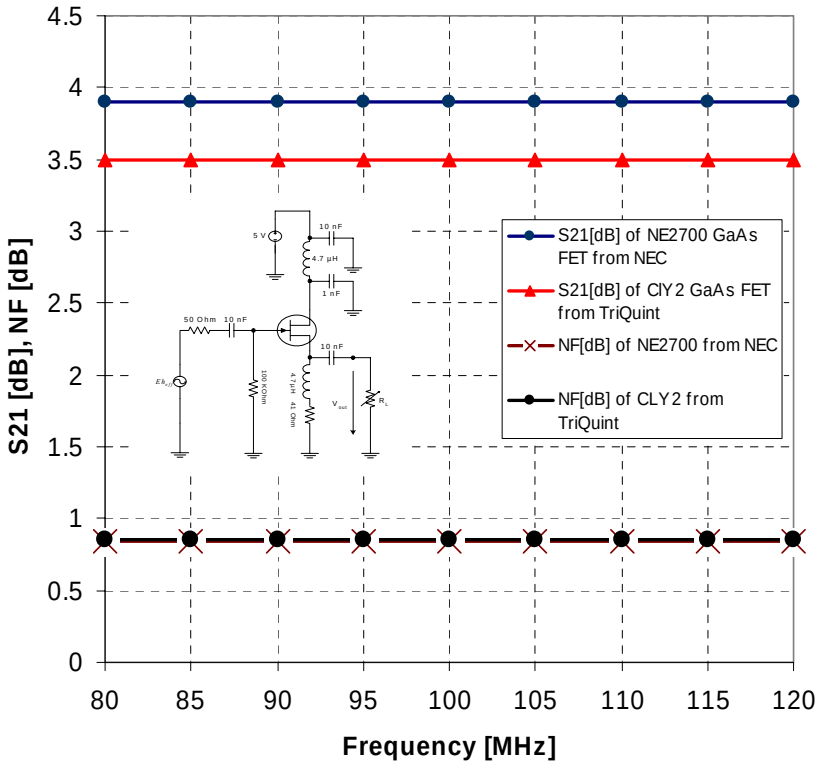

Figure 4.1: Frequency Response Simulation Comparison (50 Ohm System) between CLY2 and NE2700 GaAs FETs Follower Cells

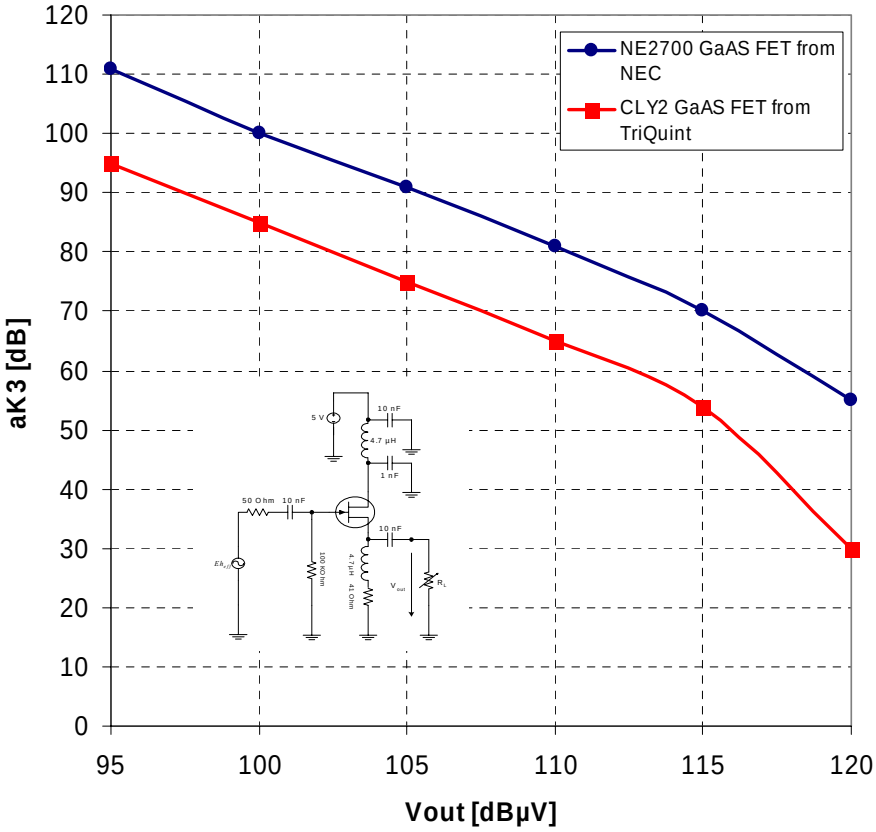

Figure 4.2: Intermodulation Separation Simulation Comparison (50 Ohm System) between CLY2 and NE2700 GaAs FETs Follower Cells

The results in Figure 4.1 and 4.2 predicts that a better performance can be achieved using the GaAs FET NE2700 from NEC. Although from Figure 4.1, both transistors enjoys similar noise figure performance, but the GaAs FET NE2700 achieves a better power gain of 3.8dB compared to 3.5 dB using CLY2. Figure 4.2 depicts that the intermodulation separation at output voltage of 100dBµV achieved by NE2700 is around 100dB compared to 85dB using CLY2. However it should be noted that the transistor NE2700 performance is not measured during this work due to the stated reasons of unavailability of its samples, but the simulation results predicts a better performance using the new NE2700 GaAs FET which show a future work that may be based on this new GaAs FET transistor.

A conclusion can be reached that whenever a better GaAs FET will be available, an expected highly linear active antenna amplifier can be realized. This dissertation introduced a general set of rules to study any FET and its integration with the antenna via simulation of the whole system.

Appendix A

Acronyms

VDA Verband der Automobilindustrie (German Association of the Automotive Industry)

LNAs Low Noise Amplifiers

RF Radio Frequency

FM Frequency Modulation

JFET Junction Field Effect Transistor

GaAs FET Gallium Arsenide Field Effect Transistor

HEMT High Electron Mobility Transistor

AGC Automatic Gain Control

LPF Low Pass Filter

SAS Switching Antenna System

Appendix B

Important Variables Definitions

a_{K3}	Third Order Intermodulation Separation
V_{out}	Voltage at the active antenna amplifier output
I_{DS}	FET Drain to Source DC Bias Current
V_{DS}	FET Drain to Source Voltage
Z_A	Antenna Impedance [Ω]
Y_A	Antenna Admittance [mho]
Z_L	Load Impedance [Ω]
E	The Electric Field Strenth [Volt/m]
h_{eff}	Effective Heiht of the Antenna [m]
V_T	The Voltage that Drives the GaAs FET
F	Noise Factor of the System
NF	Noise Figure of the System
V_{nscr}	Receiver Noise Source Voltage
D_{rt}	Azimuth Directivity of the Car Windscreen test Structure
A_r	Effective Aperture Area of the Rod Antenna [m^2]
Z_O	Free Space Impedance (= 120π [Ohms])
SNR	Signal to Noise Ratio

Bibliography

[1] H.H. Meinke,in German "Aktive Antennen", Nachrichten Technische Zeitschrift NTZ, Jahrgang 19,Heft 12, December 1966, pp. 697-705.

[2] H.K. Lindenmeier,in German „Kurtze Aktive Empfangsantennen", Dr.-Ing. Dissertaion, Technical University Muenchen,TUM, 1967.

[3] H. Lindenmeier,in German „Einige Beispiele rauscharmer transistorierter Empfangsantennen", Nachrichtentechnische Zeitschrift, Heft 7, pp. 381-389,1969.

[4] H. Lindenmeier and H. Meinke,in German,, *Aktive Autoantenna*", funkschau 41, pp.569-571 and 813-815, 1969.

[5] Dr.-Ing. Heinz Lindenmeier,in German " Rauschen und Linearität transistorierter Empfangsantennen", Habilitationsschrift, 1971.

[6] Heinz Lindenmeier, „ Optimum Bandwidth of Signal-to-Noise Ratio of Receiving Systems with Small Antennas", AEÜ 1976.

[7] Lindenmeier H., Meinke H.,in German " Aktive Antennen ", Technische Universität München, 1977.

[8] Heinz Lindenmeier, *in German*: "Grundzüge der Dimensionsionierung des Übertragungsfaktors ü des Filters in einem Verstärker mit hochohmigem Eingang unter Einhaltung der maximal tolerierbaren Ausgangsrauschleistung in Abhängigkeit vom Realteil der Antennenimpedence einer Antennenstruktur", new not published notes 2004.

[9] H.K. Lindenmeier, L. Reiter, J. Hopf, K. Fujimoto, and K. Hirasawa, *" Land Mobile Antenna Systems III: Cars, Trains, Buses "* , Mobile Antenna Systems Handbook, 1994.

[10] Reiter, Leopold,in German, *"Mobile Rundfunkempfangestechnik"*, Habilitationsschrift zur Erteilung der Lehrbefugnis in der Fakultät für Elektrotechnik der Universität der Bundeswehr München, February 1995.

[11] J.Brose, in German: Berechnungen an Fahrzeugantennen; Unveröffentlichter Bericht am Institut für Hoch-und Höchfrequenztechnik der Univ. der Bundeswehr München.

[12] Carson, S. Ralf, *"Radio Concepts, Analog"*, John Wiley & Sins, Inc. 1990.

[13] Ulrich L. Rohde, David P. Newkirk, *"RF/Microwave Circuit Design for Wireless Applications"*, John Wiley & Sins, Inc. 2000.

[14] Chris Diorio, Todd Humes, Johannes K. Notthoff, *"A Low-Noise, GaAs/AlGaAs, Microwave Frequency-Synthesizer IC"*, IEEE Journal of Solid-State Circuits, Vol. 33, No. 9, September 1998.

[15] Chung-Yu Wu, Shu-Yan Hsiao, *"The Design of a 3-V 900-MHz CMOS Bandpass Amplifier"*, IEEE Journal of Solid-State Circuits, Vol. 32, No. 2, February 1997,pp. 159-168.

[16] J.F. Hopf, H. K. Lindenmeier, L.M. Reiter, *"Mobile Multimedia Antenna Systems for Stations Wagons and the Achievable Diversity Effectiveness Obtained By Analysis of Virtual Test Drives"*, International Conference of Radio Science – Germany-2001.

[17] T.S.M. Maclean and G. Morris, *"Short Range Active Transmitting Antenna with Very Large Height Reduction"*, IEEE Transactions on Antennas and Propagation, March 1975,pp. 286-289.

[18] J. A. García, A. Tazón, A. Mediavilla, I. Santamaría, M. Lázaro, C. Pantaleón, J. C. Pedro, *"Modeling MESFETs and HEMTs Intermodulation Distortion Behavior Using a Generalized Radial Basis Function Network"*, International Journal of RF and Microwave Computer-Aided Design, vol. 9, pp. 261-276, 1999.

[19] H.H. Meinke, *"Tunnel Diodes Integrated with Microwave Antenna Systems"*, The Radio and Electronic Engineer Proceedings, February 1966,pp. 76-79.

[20] Thomas F.Bechteler, *"Hochlineare breitbandige Antennenverstärker mit Feldeffekttransistoren"*, PhD Thesis University der Bundeswehr Munich – Germany,27 March 2001.

[21] Jakub J. Kucera and Urs Lott, *"A 1.8dB Noise Figure Low DC Power MMIC LNA for C-Band"*, IEEE GaAs IC Sysmposium 1998, pp. 1-4.

[22] A.E. Parker and J.B. Scott, *"Intermodulation nulling in GaAs MESFETs",* Electronics Letters, 28th October 1993, Vol.29, No.22, pp. 1961-1962.

[23] Don G. Peterson, *"Noise Performance of Transistors"*, IRE Transactions on Electron Devices, May 1962, pp. 296-303.

[24] K. Kurokawa, *"Power Waves and the Scattering Matrix"*, IEEE Transactions On Microwave Theory And Techniques, Vol.MTT-13, No.2, March, 1965, pp.194-202.

[25] Ryan Y. Miyamoto, Kevin M. K. H. Leong, Seong-Sik Jeon, Yuanxun Wang, Yongxi Qian and Tastsuo Itoh, *"Digital Wireless Sensor Server Using an Adaptive Smart-Antenna/Retrodirective Array"*, IEEE Transactions On Vehicular Technology, Vol. 52, No. 5, September 2003, pp. 11811188.

[26] Kohei Fujit, Yasuhiko Hara, Fadhel M. Ghannouchi, Toshiyuki Yakabe and Hatsuo Yabe, *"A Nonlinear GaAs FET Model Suitable for Active and Passive MM-Wave Applications"*, IEICE Trans. Fundamentals, Vol.E83-A, NO.2 February 200, pp. 228-235.

[27] Frank Ellinger, Jakub Kucera and Werner Baechtold,*"Improvements on a GaAs MESFET Model for Nonlinear RF Simulations"*, IEEE MTT International Microwave Symposium, 1998, pp. 1623-1626.

[28] Fred Bonn, *"Biasing N-Channel GaAs MESFETs"*, Microwaves and RF, Septemeber 2000, pp. 81-95.

[29] Gerard Wevers, "A High IIP3 Low Noise Amplifier for 1900 MHz Applications Using the SiGe BFP620 Transistor ", Applied Microwave and Wireless, July 2000, pp. 64-80.

[30] S.C. Peacock, M.A. Stauffer, A.M. Van Slyke, and E.S. Ferre-Pikal, *"Study of Flicker Phase Modulation and Amplitude Modulation Noise in Field Effect Transistor Amplifiers"*, IEEE International Frequency Control Symposium and PDA Exhibition, 2001, pp. 200-204.

[31] V.N. Kuleshov, T.I. Boldyreva, and A.A. Krylov, *"PM and AM Noise of Common Collector and Darlington Amplifiers"*, IEEE International Frequency Control Symposium and PDA Exhibition, 2001, pp. 192-199.

[32] Tatiana I. Boldyreva, *"Reduction of 1/f PM Noise in BJT Amplifiers with Emitter Feedback Using Compensation Effects"*, IEEE International Frequency Control Symposium and PDA Exhibition, 2001, pp. 183-191.

[33] Dimitris Pavlidis, *"HBT vs. PHEMT vs. MESFET: What's best and Why"*, GaAs MANTECH International Conference on Compound Semiconductor Manufacturing Technology, 1999.

[34] Francisco E. Rangel Patino and J. Rodrigo Camacho Perez, Ave. Hermanos Escobar, *" Modeling and Simulation of Pseudomorphic HEMT's for Analog Circuit Design and Analysis"*, Instituto Technologico de Chihuahua, ELECTRO 2001, pp.277-282.

[35] David Vye, *"Using Nyquist Stability Analysis to Verify Stability of Wireless Circuits"*, Applied Microwave and Wireless Mag., 2001, pp.62-68.

[36] J.M. Rollet, *"Stability and Poer-Gain Invariants of Linear Two-Ports"*, IRE Transactions on Circuit Theory, Vol. CT-9, March 1962, pp. 29-32.

[37] A. Platzker, W. Struble and K. Hetzler, *"Instabilities Diagnosis and the Role of K in Microwave Circuits"*, IEEE MTT-S International Microwave Symposium Digest, 1993, pp. 1185-1188.

[38] Nyquist, *"Regeneration Theory"*, Bell System Technical Journal, Vol. 11, January 1932.

[39] W. Struble and A. Platzker, *"A Rigorous Yet Simple Method for Determining Stability of Linear N-Port Networks"* , GaAs IC Symposium Digest, 1993.

[40] Agilent Technologies Application Note 944-1, *"Microwave Transistor Bias Considerations"*, 2000.

[41] GH. Cartianu, D. Poenaru, *"Variation of Transfer Functions with the Modification of Pole Location"*, IRE Transactions on Circuit Theory,1962, pp. 98-99.

[42] J. O. Scanlan, and J. S. Singleton, *"The Gain and Stability of Linear Two-Port Amplifiers"*, IRE Transactions on Circuit Theory, 1962, pp. 240-246.

[43] Peter Vizmuller, *"RF Design Guide Systems,Circuits, and Equations"*, Artech House Publishers, 1995.

[44] Reinhold Ludwig, Pavel Bretchko, *"RF Circuit Design Theory and Applications"*, Prentice-Hall, Inc., 2000.

[45] Richard A. Williams, *"Communication Systems Analysis and Design A Systems Approach"*, Prentice-Hall, Inc., 1987.

[46] Samuel Y. Liao, *"Microwave Solid-State Devices"*, Prentice-Hall, Inc., 1985.

[47] George D. Vendelin, Anthony M. Pavio, Ulrich L. Rohde,*"Microwave Circuit Design Using Linear and Nonlinear Techniques"*, John Wiley & Sons, Inc. 1990.

[48] Norman S. Nise, *"Control Systems Engineering"*, Addison-Wesley Publishing, Second Edition, 1995.

[49] C.D. Motchienbacher, F. C. Fitchen, *"Low-Noise Electronic Design"*, John Wiley & Sons, Inc. 1973.

[50] Jack Smith, *"Modern Communication Circuits"*, Mc Graw-Hill, Inc. 1986.

[51] International Telecommunication Union CCIR, *"Recommendations and Reports of the CCIR, 1982"*, Volume I, Geneva 1982.

[52] Guillermo Gonzalez, *"Microwave Transistor Amplifiers"*, Prentice-Hall, Inc. Second Edition 1997.

[53] MACOM Application Note S2079, *"Drivers for GaAs FET Switches and Digital Attenuators"*, 2001.

[54] Super-Compact, Serenade Microwave Harmonica , "*Elements Library Version 8.7"*, Hand Book 2002.

[55] Lindenmeier H., Reiter L., Hopf J. , Kronberger R. , *"Electronic Systems for Vechicles",*VDI Berichte Nr. 1547, 2000.

[56] Raoul Pettai, " *Noise In Receiving Systems"*, John Wiley and Sons, Inc. 1984.

[57] K. Fujimoto, and J. R. James, *" Mobile Antenna Systems Handbook "* , Artech House, INC., 1994.

[58] Julio A. Navarro and Kai Chang, *"Integrated Active Antennas and Spatial Power Combining"*, John Wiley & Sons, INC., 1996.

[59] J. Copeland and W. Robertson, *"Antenna-verters and antennafiers" ,* Electronics, pp. 68-71, Oct. 1961.

[60] H. Meinke and F. Landstorfer, *" Noise and Bandwidth Limitations with Transistorized Antennas "* IEEE Antennas and Propagat. Symp., Boston, Sep. 1968.

[61] P. Ramsdale and T. Maclean, " Active loop-Dipole Aerials ", Proc. IEE, vol. 118, no.12, pp. 1698-1710, Dec. 1971.

[62] H.Thomas, D. Fudge, and G. Morris, " *Gunn source integrated with a microstrip patch "*, Microwaves and RF, vol.24, no. 2, pp. 87-89, Feb. 1985.

[63] A. Al-Ani, A. Cullen, and J. Forrest, " *A Phase Locking Method for Beam Steering in Active Array Antennas "*, IEEE Trans. Microwave Theory and Tech., vol. MTT-22, pp. 698-703, June 1974.

[64] R. York, Z. Popovic, "*Active and Quasi-Otical Arrays for Solid-State Power Combining"*, Wiley, New York, 1997.

[65] S. Chew and T. Itoh, " *A 2×2 Beam-Switching Active Antenna Array* ", IEEE MTTT-S Int. Microwave symp. Dig., pp. 925-928, 1995.

[66] S. Ortiz, J. Hubert, L. Mirth, E. Schlecht, and A. Mortazawi, „ A 25 Watt and 50 Watt Ka-Band Quasi-Optical Amplifier „, IEEE MTTT-S Int. Microwave Aymp. Dig., pp. 797-800, 2000.

[67] H. Lindenmeier and H. Meinke,in German„ *Elektronische Autoantennen heute*", funkschau 48, pp.587-580 , 1976.

[68] Kronberger R., in German *" Ein Verfahren zur Gestaltung von Gruppenantennen auf Fahrzeugen unter Einbeziehung des Strahlungsverhaltens des Fahrzeugkörpers"* . Dissertation, Universität der Bundeswehr München, 1996.

[69] Lindenmeier H., J. Hopf, L. Reiter and B. Leinwetter " Integrated Backlite Antenna System for AM/FM and TV Broadcast Reception and for Mobile Telephone ", SAE Technical Paper, Detroit Michigan, USA , Feb.28, 1994..

[70] Lindenmeier H., J. Hopf, and L. Reiter "Active Window Antennas for Radio Reception in Cars for Single Antenna and for Antenna Diversity Applications", JINA 1986, Nice, France.

[71] VDA-Spezifikation für Fahrzeug-Antennen Stand 31. Juli 2002, Version 1.

[72] A. Megej, K. Beilenhoff, B. Mottet and A. Mier, "Design and Simulation of Fully Integrated Broadband PHEMT Voltage Controlled Oscillators", Annual Report of Darmstadt Technical University TUD, 1998.

[73] German standards: „ Frequenzbereichszuweisungen an Funkdienste im Frequenzbereich von 9 KHz bis 300 MHz".